SARs for the Antiparasitic Plant Metabolite Pulchrol

SARs for the Antiparasitic Plant Metabolite Pulchrol

Paola Terrazas

LUND
UNIVERSITY

DOCTORAL DISSERTATION
by due permission of the Faculty of Science, Lund University, Sweden.
To be defended in lecture hall C, Kemicentrum, on Thursday 17th of June 2021 at 14:00

Faculty opponent
Professor Patricia Mollinedo
Chemistry Research Institute, San Andres University, Bolivia

Organization LUND UNIVERSITY Centre of Analysis and Synthesis Department of Chemistry Author(s) Paola Terrazas	**Document name** Doctoral Thesis
	Date of issue
	Sponsoring organization Swedish International Development Cooperation Agency (SIDA)

Title and subtitle
Sars for the antiparasitic plant metabolite pulchrol.

Abstract

Pulchrol, a natural compound isolated from the roots of the vegetal specie *Bourreria pulchra* has been shown to possess potential antiparasitic activity toward Trypanosomatids, particularly against *Trypanozoma cruzi,* which causes the Chagas disease; and moderately against *Leishmania* species, responsible for Leishmaniasis. In this investigation, several pulchrol analogues were prepared and assayed toward *T. cruzi* epimastigotes, and *L. braziliensis* and *L. amazonensis* promastigotes, to develop structure activity relationship studies (SARs).

Analogues with transformations in the three rings of the pulchrol's scaffold were prepared. Initially, compounds with transformations at the benzylic position in the A-ring were assayed to evaluate the role of the benzylic alcohol in pulchrol. The results showed that an hydrogen bond acceptor group is important for the antitrypanosomatid activity and that ester groups with bulky alkyl substituents increase the potency toward all parasites. Analogues with transformations in the B- and C-rings, were focused on the variation of lipophilicity. In the B-ring, the methyl substituents placed at position 6 in pulchrol were replaced for two hydrogen atoms, just one methyl substituent, or two longer alkyl substituents. The biological activity results showed that longer chains with less than four carbon atoms are benefitial for the activity. A methoxy subtituent is placed at position 2 in pulchrol's C-ring, in this study, analogues with the methoxy subtituent placed in different positions or replaced with alkyl subtituents were prepared, the results showed that compounds with hydrophobic groups in the C-ring incresed the potency.

Several analogues with more than one modification in different rings were also prepared. The combination of carbonyl groups in the A-ring with bulky alkyl groups in the C-ring was the most benefitial for the activity. In contrast, esters subtituted with a hydrophobic group in the A-ring and bulky alkyl groups in the C-ring hampered the activity. A hydrogen bond acceptor at the benzylic position in the A-ring, as well as an additional hydroxyl group at position 1 in the C-ring (as in cannabinol) appeared to be important for the activity. The combination of different functionalities also seemed to have and effect in the orientation of the molecule inside the target protein.

Our results showed that differences between the active sites for the different parasites may exist, however, preliminary pharmacophore hypotheses based on our biological results showed that the main pharmacophoric features are two hydrogen bond acceptor groups (one at the benzylic position and one on the B-ring's oxigen) and three hydrophobic features (two in the B-ring at position 6, and one in the C-ring at position 2 or 3).

A qualitative evaluation of ADMET-descriptors calculated *in silico*, showed that most of the molecules have potential as orally administered substances, however, further studies focused on the development of compounds with more potency and focused on the optimization of the ADME characteristics are recommended.

Key words pulchrol, pulchral, SARs, antiparasitic, *Leishmania braziliensis*, *L. amazoniensis*, *Trypanozoma cruzi*, *Bourreria pulchra*, leishmaniasis, Chagas disease, synthesis, pharmacophore ADMET.

Classification system and/or index terms (if any)

Supplementary bibliographical information		**Language** English
ISSN and key title		**ISBN** 978-91-7422-816-8 978-91-7422-817-5
Recipient's notes	**Number of pages**	Price
	Security classification	

SARs for the Antiparasitic Plant Metabolite Pulchrol

Paola Terrazas

LUND
UNIVERSITY

Coverphoto by Paola Terrazas

Faculty of Science
Department of Chemistry
Centre for Analysis and Synthesis

ISBN 978-91-7422-816-8 (printed version)
978-91-7422-817-5 (digital version)

Printed in Sweden by Media-Tryck, Lund University
Lund 2021

To my Mom, my Dad, my Sister and my beloved David

Table of Contents

Popular summary

Leishmaniasis and Chagas are neglected diseases caused by trypanosomatid parasites from the genus *Leishmania* and *Trypanosoma*, respectively. These diseases occur primarily in tropical and subtropical regions, affecting mainly people from underdeveloped countries that live in distant rural places with insufficient access to medical care. The development of appropriate treatments has been overlooked by the big pharmaceutical companies, and current treatments mostly come from repurpose drug studies, presenting several disadvantages such as unwanted side effects, and the need for parenteral administration that may require hospitalization in some cases.

The complex life cycles of the *Leishmania* and *Trypanosoma* parasites makes it difficult to understand their infection mechanisms, making the development of new drugs challenging. However, empirical knowledge obtained from traditional medicine, may contribute to the isolation and identification of new natural products with potential antiparasitic activity. Such is the case of natural product pulchrol, isolated from the roots of the vegetal specie *Bourreria pulchra*, traditionally used to treat cutaneous diseases, infections and fevers in Yucatan, Mexico. After its isolation, pulchrol has been shown to possess interesting activity toward *T. cruzi*, and several *Leishmania* species.

In this investigation, several pulchrol analogues systematically modified were prepared to be used in structure-activity relationship studies. The effects that transformations of pulchrol's substituents produced in the antiparasitic activity were evaluated. A hydrogen bond acceptor at the benzylic position in pulchrol's A-ring, ethyl substituents in the B-ring, and isopropyl substituents in the C-ring were found to be important for the activity. A pharmacophore hypothesis developed for *T. cruzi* agreed with the observations made during the SAR studies.

The absorption, distribution, metabolism, excretion and toxicity (ADMET) potential of pulchrol's derivatives was evaluated qualitatively. Most of them were able to be absorbed orally, and therefore had potential as orally administered drugs.

List of papers

This thesis summarizes and supplements the following papers.

Paper 1

Terrazas, P.; Salamanca, E.; Dávila, M.; Manner, S.; Giménez, A.; Sterner, O. SAR:s for the Antiparasitic Plant Metabolite Pulchrol. 1. The benzyl alcohol functionality. *Molecules*. **2020**, 25, 3058.

Contribution: Performed all the synthetic work, contributed to the formulation of the research problem, the interpretation of the data, and to writing the manuscript.

Paper 2

Terrazas, P.; Salamanca, E.; Dávila, M.; Manner, S.; Giménez, A.; Sterner, O. SAR:s for the Antiparasitic Plant Metabolite Pulchrol. 2. B- and C-ring substituents. *Molecules*. **2020**, 25, 4510.

Contribution: Performed all the synthetic work, contributed to the formulation of the research problem, the interpretation of the data, and to writing the manuscript.

Paper 3

Terrazas, P.; Salamanca, E.; Dávila, M.; Manner, S.; Giménez, A.; Sterner, O. SAR:s for the Antiparasitic Plant Metabolite Pulchrol. 3. New substituents in A/B-rings and A/C-rings. *In manuscript*.

Contribution: Performed all the synthetic work, contributed to the formulation of the research problem, the interpretation of the data, and to writing the manuscript.

Paper 4

Terrazas, P.; Dávila, M.; Manner, S.; Sterner, O. SAR:s for the Antiparasitic Plant Metabolite Pulchrol. 4. Pharmacophore design hypothesis and qualitative assessment of predicted pharmacokinetic properties. *In manuscript*.

Contribution: Performed all the computational work, contributed to the formulation of the research problem, the interpretation of the data, and to writing the manuscript.

Abbreviations

A375	Human malignant melanoma cells
A546	Human lung carcinoma cells
ADMET	Absorption, distribution, metabolism, excretion and toxicity
BEDROC	Boltzmann-Enhanced Discrimination of Receiver Operating Characteristics
Caco-2	Human colorectal adenocarcinoma cells
CB1	Cannabinoid receptor type 1
CB2	Cannabinoid receptor type 2
CNS	Central nervous system
DIBALH	Diisobutylaluminum hydride
DME	1,2-Dimethoxyethane
DMF	Dimethylformamide
ERβ	Estrogen receptor beta
HCT116	Human colon carcinoma cells
HBA	Hydrogen bond acceptor
HBD	Hydrogen bond donor
HegG-2	Human hepatoma cells
HERG	Human ether-à-go-go related gene
IC_{50}	Half maximal inhibitory concentration
P	Partition coefficient
MCF7	Human Caucasian breast adenocarcinoma
MeCN	Acetonitrile
MeLi	Methyllithium

MeMgBr	Methyl magnesium bromide
MW	Molecular weight
NaSEt	Ethanethiolate
NCE	New chemical entity
NTD	Neglected tropical diseases
PSA	Polar surface area
QPlogBB	Predicted brain/blood partition coefficient
QPlogHERG	Predicted IC_{50} value for blockage of HERG K^+ channels
QPlogKhsa	Prediction of binding to human serum albumin
QPlogPo/w	Predicted octanol/water partition coefficient
QPlogS	Predicted aqueous solubility
QPPCaco	Predicted apparent Caco-2 cell permeability
QPpolarz	Predicted polarizability
RAW	Mouse monocyte macrophage
RMSD	root-mean-square deviation
SARs	Structure activity Relationship studies
SASA	Total solvent accessible surface area
SI	Selectivity index
SW1116	Human colorectal adenocarcinoma cells
THC	Δ^9-Tetrahydrocannabinol
TBAF	Tetrabutylammonium fluoride
TBDPSCl	*Tert*-Butyldiphenylsilane
THF	Tetrahydrofuran

1 Introduction

1.1 Natural products and their uses

Natural products are compounds generated by living organisms. The secondary metabolism transforms primary metabolites to produce secondary metabolites, also known as natural products [1].

Primary metabolites are compounds essential for life, and most of them and their biosynthetic pathways are common for all organisms. Secondary metabolites, on the other hand, are specific for different groups of organisms, their purposes are in general not understood but they appear to interact with the external environment, for example attracting other species or repelling predators as a defence mechanism [1-3]. These metabolites are produced as a result of millions of years of evolution in which organisms have adapted to various abiotic and biotic stresses [2-5].

Humans have found practical uses for many secondary metabolites, traditionally from plants, but recently also from microorganisms. We have used natural products as pesticides, flavouring agents, fragrances, and especially as drugs to treat different illnesses [2]. Knowledge on the traditional therapeutic use of plants was obtained on an empirical basis from rather early in history, reports found in Mesopotamia approximately 2400 BC, a compendium of traditional medicine (Ebers Papyrus) written around 1500 BC in Egypt [4, 6], and all the documents from the traditional Chinese medicine that have been recorded for thousands of years [6, 7] evidence the existence of this knowledge.

So far, traditional medicine has served as a starting point for rational drug discovery. One example is opium and its traditional use as analgesic, which afterward led to the isolation of morphine [8, 9]. Likewise, various compounds such as taxol isolated from the pacific yew (*Taxus brevifolia*) [10]; camphotecin isolated from the Chinese plant *Camptotheca acuminata* [11]; and the vinca alkaloids obtained from the Madagascar periwinkle (*Cantharanthus roseus*) [12], are used to treat various forms of cancer [13, 14]. In addition, we can mention examples of anti-parasitic drugs found in nature, like quinine, isolated from the bark of the Cinchona trees (e.g., *Cinchona officinalis*), which were traditionally used to counteract shivering caused by low temperatures or fever in South America [15]. Similarly, the natural product artemisinin isolated from the sweet wormwood (*Artemisia annua*), was used in Chinese traditional medicine to treat fever, inflammation and malaria

(see Figure 1) [16, 17]. Both the abovementioned compounds have been important for treating patients with malaria.

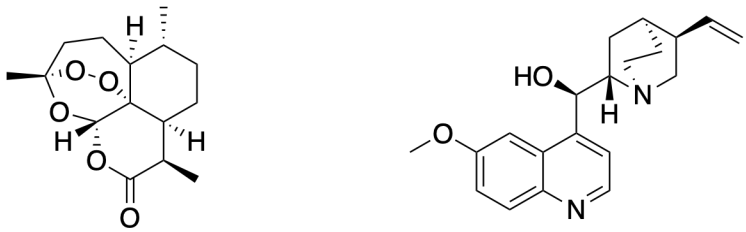

artemisinin (**1**) quinine (**2**)

Figure 1
Antimalarial natural products artemisinin and quinine

Ethnopharmacology based on the world's almost inapprehensible biodiversity provides an extremely valuable tool for drug discovery; nevertheless, ethnic traditional knowledge and natural habitats are endangered, and may decline or disappear, with all of their valuable information, due to the growth of urban and farm areas [6, 18]. Besides the environmental factors, there are also other challenges for natural product discovery: the composition, altitude, process, and storage conditions; are factors that need to be controlled during the harvesting process [4, 6]. The isolation and purification processes are also expensive, time consuming and often impractical to scale up; on top of that, the amounts of secondary metabolites obtained are in general small and may be insufficient for the testing of a wider range of biological activities [4-6].

Due to the challenges described above, the interest in natural product-based drug discovery has declined, leaving natural product research to a major extent to universities and start-up companies [6].

1.2 Synthetic natural products

Synthetic chemists have solved the problem of insufficient amounts of metabolites isolated from natural sources by designing synthetic routes to prepare them in the laboratory. This solution made possible to test natural products more extensively in various biological assays. Once a biologically active compound would have been found, it was possible to prepare derivatives and analogues based on its structure, looking for improvements in the activity or therapeutic properties that may lead to a potential drug [5, 19].

Natural product synthesis also enriched the chemical variety of prior purely synthetic compounds, providing privileged scaffolds belonging to biologically active pharmacophores [4, 5, 19, 20]. The first natural product synthesized as a drug was salicylic acid, a natural oxidation product of the glucoside salicin that was isolated from the bark of the white willow (*Salix alba*). Salicylic acid was developed to the less irritating prodrug Aspirin by acetylation. Later other drugs such as Chloroquine and Mefloquine were produced inspired by quinine, to be used to combat malaria (for the structures see Figure 2) [6].

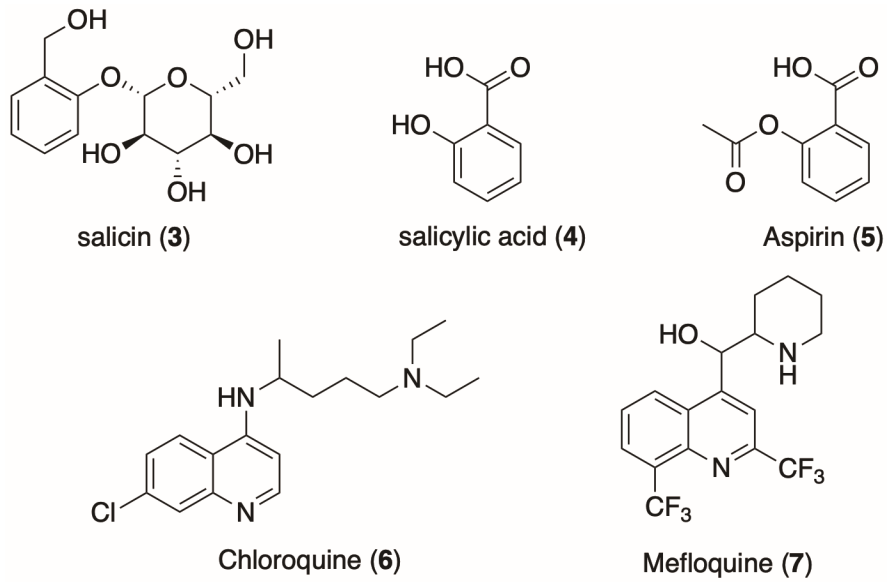

Figure 2
Above, natural products salicin, salicylic acid and its synthetic derivative Aspirin. Below, synthetic derivatives Chloroquine and Mefloquie

Ultimately, natural product's synthetic derivatives have prevailed over natural products as a result of the advantages of the synthetic process. Before 1940, unmodified natural products and their derivatives represented 43% and 14%, respectively, of all new chemical entities (NCEs) approved as drugs. Since then, until 2000, unmodified natural products and their derivatives represented 5.3% and 28% respectively [21].

Nevertheless, true natural products continue to be an important source of new molecular scaffolds, which could lead to the development of novel drug candidates after conducting structure-activity relationship studies based on synthetic analogues [5]. Nowadays, the definition for therapeutic natural products has broadened to include chemically modified natural compounds and purely synthetic medicinal compounds inspired by them [21].

1.3 Natural products as a source of new drugs

Apart from its chemical diversity, natural products may possess potential selectivity, since they are in contact with natural macromolecules during the complete development of their biosynthetic pathways. As many of those biochemical building blocks are common to all living organisms, natural compounds could possess an inherent selectivity for binding macromolecules in the human body [4, 6].

Another advantage is the vast biodiversity that can produce bioactive compounds with different chemical scaffolds. Only approximately 6% of the existing plant species have been investigated pharmacologically, and just about 15% phytochemically, so there remains a huge number of new plant metabolites that can be found in the approximately 310 000 plant species described so far [6].

Despite the advantages, the pharmaceutical industry is not investing as much in natural products as in synthetic molecules, mainly because of the high costs for the isolation and characterization of substances [21]. However, among the drugs approved between 1981 and 2019, it can be noted that natural products and natural inspired products still play an important role in drug discovery (Figure 3). From the 1603 drugs approved during this period, 588 were synthetic drugs, 286 natural derivatives, 254 natural inspired synthetic drugs, and 69 natural products [22].

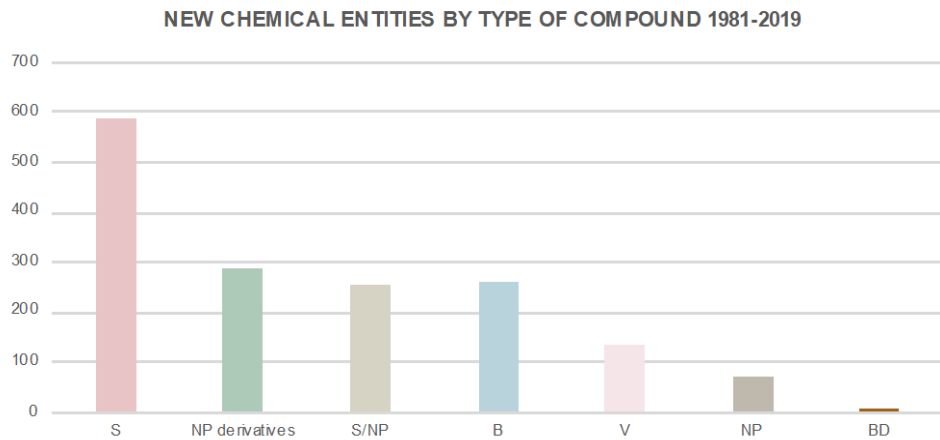

Figure 3
New chemical entities approved between 1981-2019. S (Synthetic compounds), NP (Natural products), S/NP (Synthetic compounds with natural product pharmacophore), B (Biological macromolecule), V (Vaccine), BD (Botanical drug) [22]

As can be seen, natural products still play a highly significant role in drug discovery as sources of bioactive chemical leads, and traditional medicine is still an important pool for the identification of new pharmacophores [5, 19, 20, 22].

1.4 Drug discovery approaches

The advantages of the structural singularity shown by natural bioactive products also carry some difficulties, when knowledge about the mode of action or the molecular target involved in their biological activity is lacking [23, 24]. Still, drug discovery research can be performed on cells or whole organisms without detailed knowledge of the target [23, 25, 26].

Phenotypic studies can be applied for diseases in which the mechanism or the drug target is unknown, which is the case in many understudied illnesses such as the neglected parasitic diseases [25, 27, 28]. In contrast, target-based studies may be more favourable for chemical lead optimization, but a mistaken selection of the target may result in undesirable outcomes [25, 26]. In order to perform target-based studies on parasitic diseases like Leishmaniasis, essential targets for its survival should be known and those must differ from human targets. Nonetheless, not many parasitic targets have been validated, therefore, phenotypic screening might work better for parasitic diseases in the first stages of research [29].

Another advantage for the phenotypic studies, regarding cell permeability is that the biological assays are usually performed over complex biological systems, as cells or living organisms, making the results more physiologically relevant [23, 25, 27]. Contrarily, in target-based studies the assays are performed directly in the target, and it may be uncertain if the molecule will work in more complex systems [6, 23, 25].

When a lead compound is found, a structure-activity relationship (SAR) study can be conducted and for this purpose analogues are synthesized and tested on a determined biological system, the correlations obtained between the biological activity and the structural variations can then be analysed [23, 30]. SAR studies are usually developed under the hypothesis that just one target is involved, albeit, this assumption may be false and multi-target binding can occur. After SAR studies, it is still desirable to identify the target that the lead compound is interacting with, especially for the subsequent stages on drug development [30].

In this context, the phenotypic approach has as the main purpose to discover new biologically active compounds [23]. Over the years, phenotypic studies have been shown to be more effective for the identification of first-in-class drugs, while target-based studies are more efficient to produce follower drugs [26]. During the last years, investment in drug discovery has increased, although an attrition rate on the identification of first-in-class drugs has been observed, difficulties during the selection of the target and decrease on phenotypic research are considered some of the factors [24]. However, both approaches may provide better results working together, as this may reduce attrition rates on first-in-class drug identification and improve subsequent drug optimization, which may also be beneficial in the discovery of new treatments for understudied diseases [23, 31].

1.5 Neglected tropical diseases

Neglected tropical diseases (NTDs) are a group of 17 infectious diseases, native from tropical and subtropical regions that affect around 1 billion people belonging to underprivileged populations in 149 countries [32]. NTDs may lead to death, disabilities and deformities that may produce psychological, social and economic damage [28, 33, 34], yet they have not received enough attention and their nonexistence in developed countries has made them invisible for industry and research [33, 35, 36]. Currently, some pharmaceutical industries have opened their compound libraries to find new repurpose drugs, nevertheless, investments in research for the identification of new lead compounds are still necessary [37, 38, 27].

Drug discovery for NTDs has been shown to be more successful using a phenotypic approach [24], mainly because there are few validated targets to perform target-based studies, and a little understanding of the complex life cycle of these pathogens [28].

Within the 1556 new drugs developed between 1975 and 2004, only 21 (representing approximately 1%) were aimed for NTDs [38]. From 1981 to 2019, 402 anti-infective drugs were approved, between them: 162 were antibacterial compounds, 186 antiviral compounds, 34 antifungal compounds and just 20 antiparasitic compounds. Among those, 2 were natural products, 7 natural product derivatives, 6 synthetic compounds, 3 synthetic compounds with natural product pharmacophore and 2 were vaccines (See Figure 4) [27, 22].

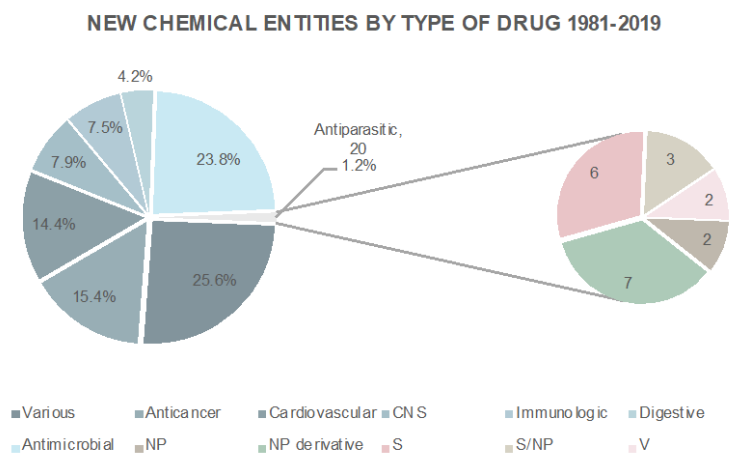

Figure 4

New chemical entities approved between 1981-2014 by type of drug and type of compounds approved as antiparasitic agents. S (Synthetic compounds), NP (Natural products), S/NP (Synthetic compounds with natural product pharmacophore), B (Biological macromolecule), V (Vaccine), BD (Botanical drug) [22]

1.6 Trypanosomatid diseases

Protozoan parasites from the genera *Trypanosoma* and *Leishmania* are members of the Trypanosomatidae family and the order Kinetoplastida. Some species belonging to those two genera are responsible for several neglected diseases, among them, *Trypanosoma cruzi*, which causes the Chagas disease, and several *Leishmania* species responsible for Leishmaniasis (See Figure 5) [39, 40].

Trypanosomatids from the genera *Trypanosoma* and *Leishmania* are dixenous parasites transmitted by hematophagous insects. During their life cycle, they are subjected to changes in morphology, cell biology and biochemistry, which make the understanding of their infectious processes challenging [37, 39, 40]. Nevertheless, some similarities observed in the molecular mechanisms and metabolic pathways of species from the genera *Trypanosoma* and *Leishmania* have made trypanosomatid-specific active sites a reasonable alternative to use in targets-based studies [39].

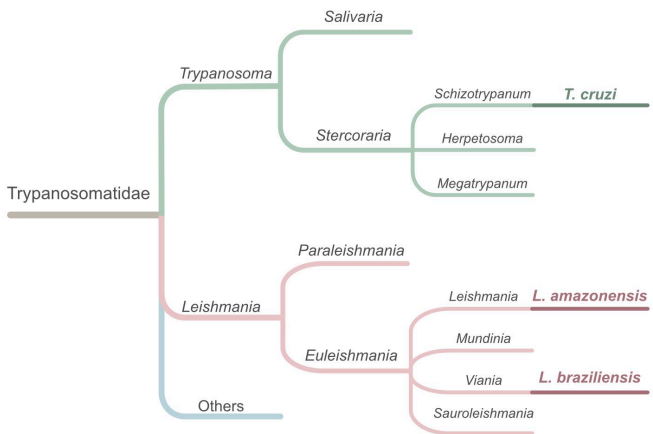

Figure 5
Taxonomic classification of the species under study *T. cruzi*, *L. brasiliensis* and *L. amazoniensis*

1.6.1 The Chagas disease

The Chagas disease, also known as American Trypanosomiasis, was discovered by Doctor Carlos Justiniano Chagas in Brazil at the beginning of the 20th Century. The protozoan parasite *Trypanosoma cruzi* causes the Chagas disease, which is transmitted by Triatomine bugs [41], these bugs live in the cracks of walls and bite their victims on exposed skin during the night. After the bite, they excrete *T. cruzi* trypomastigotes near the biting site making the victim to scratch the contaminated area, as a consequence, the disease is contracted [40, 41].

Chagas disease is endemic in 21 Latin American countries but nowadays it can be found in other continents (See Figure 6); most of the cases have been observed in Argentina, Brazil and Mexico [41]. This disease mostly affects people belonging to the lowest socioeconomic classes who may not have access to a proper social healthcare system nor have the resources to afford treatment privately [42, 43].

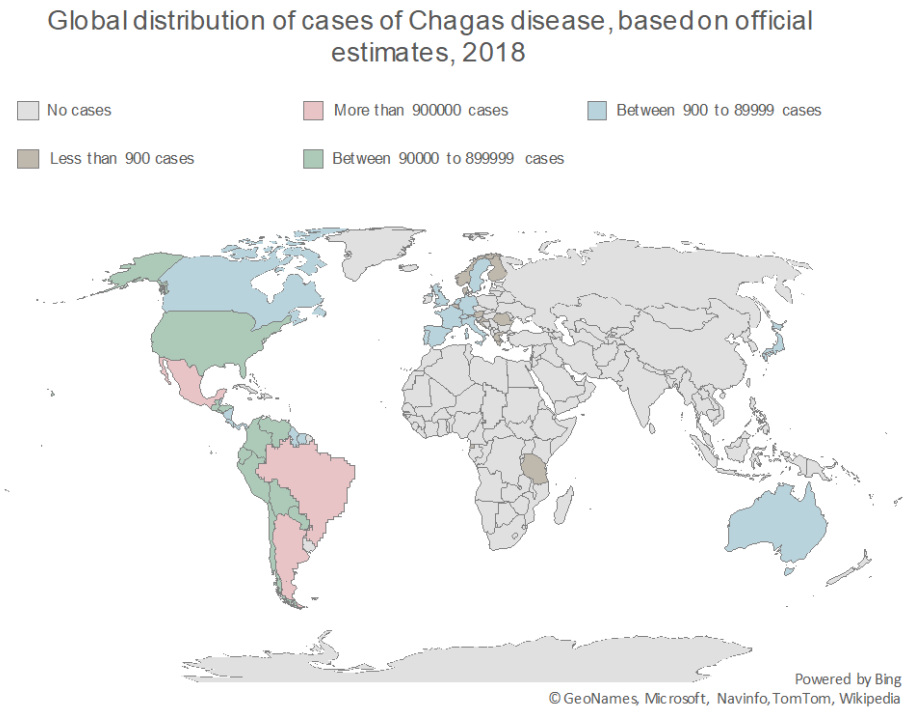

Figure 6
Chagas disease global distribution map based on official estimates for 2018 [44]

Currently around 6 to 7 million people are infected, 75 million people are at risk, and up to 30% of the chronically infected develop cardiac alterations [41].

The Chagas disease is developed in 2 phases: The acute phase and the chronic phase. During the acute phase, *T. cruzi* metacyclic trypomastigotes infect various cell types around the Triatomine bug bite, once inside the cell, they transform into amastigotes and multiply by binary fission. This process takes approximately 1 week, then the host cell ruptures and the amastigotes differentiate into motile trypomastigotes, which are released into the bloodstream and distributed throughout the body [45].

The acute phase continues until the immune system control the replication process, which takes around 2 months [45, 46]. Before that, another Triatomine bug

can ingest metacyclic trypomastigotes in a blood meal, to subsequently transform them into epimastigotes, which replicate in their midgut. Afterward, the epimastigotes move to the hindgut, where they differentiate into metacyclic trypomastigotes, closing the life cycle of the parasite (See Figure 7) [40].

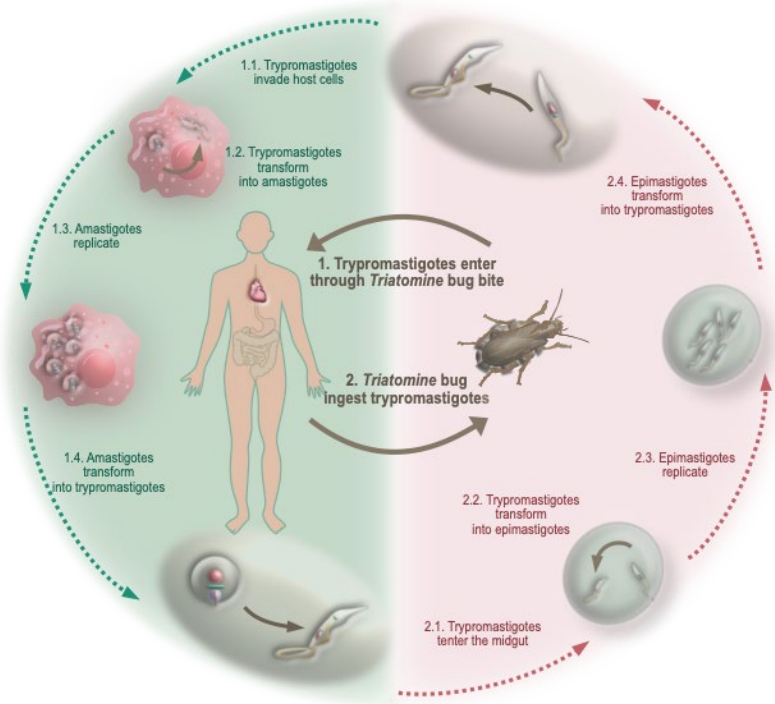

Figure 7
Life cycle of *T. cruzi*

During the acute phase, more than 50% of the infected does not show any symptoms, the rest may show a skin lesion around the bite site, eye swelling, fever, headache, enlarged lymph glands, pallor, muscle pain, difficulty in breathing, and abdominal pain as a result of the activation of the immune system [41, 46].

During the chronic phase, parasites may be hidden in different tissues for decades, producing eventually a chronic inflammatory response, which can predominantly lead to cardiomyopathy induced by the damage produced in the heart tissue [41, 46]. It is thought that *T. cruzi* is also present in the adipose tissue, where the parasite can hide for a long time, as a result of nutrient availability and longevity (approximately 10 years) of adipose cells [47].

Approximately 30% of the infected develop cardiac problems and 10% gastrointestinal problems [41], an early diagnosis is essential for the treatment [41,

42], which may take between 30 to 60 days and involves the nitro-heterocyclic drugs, benznidazole or nifurtimox, which nevertheless, have produced adverse effects in 40% of the patients [43, 48, 49].

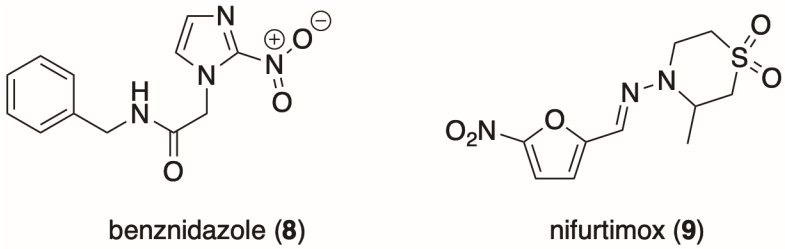

Figure 8
Benznidazole y nifurtimox

Benznidazole is the least effective during the chronic face and high-dose treatment has been observed to produce, occasionally, hypersensitivity, digestive intolerance, anorexia, asthenia, headache and sleeping disorders [46, 49].

1.6.2 Leishmaniasis

Leishmaniasis, also caused by trypanosomatid parasites, is transmitted by the bite of an infected female *Phlebotomine* sandfly [50]. Leishmaniasis can be found in three forms: cutaneous, mucocutaneous and visceral, and several *Leishmania* species can produce them (See Figure 9).

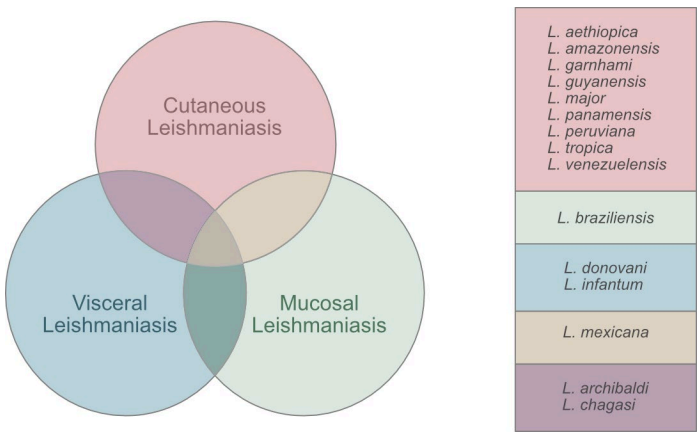

Figure 9
The three main types of Leishmaniasis and the species that produce them [50]

The development of localized lesions in the skin that heal spontaneously, is the characteristic of cutaneous leishmaniasis, nevertheless some cases require treatment to heal the wounds: When *L. amazonensis* causes the infection, ulcers spread via lymphatics (diffuse form); and when *L. tropica* causes it, lesions around the edges of healed ulcers develop (recidivans form) [51, 52].

Mucosal leishmaniasis, which is mainly produced by *L. braziliensis* causes the destructive inflammation of mucous membranes, generating non-self-heling wounds in the nose, mouth, pharynx and larynx [50-52].

Visceral leishmaniasis caused by *L. donovani* and *L. infantum* is the only fatal form of the disease, producing fever, weight loss and enlargement of the spleen and liver [50, 52, 53].

All Leishmaniasis forms may remain asymptomatic for long periods, and around 700 000 to 1 million new cases are registered mainly in the poorest regions of Africa, Latin America and East Asia. The infected also face socio-economic stigmas in different regions, which have damaging effects on their mental health [50, 54].

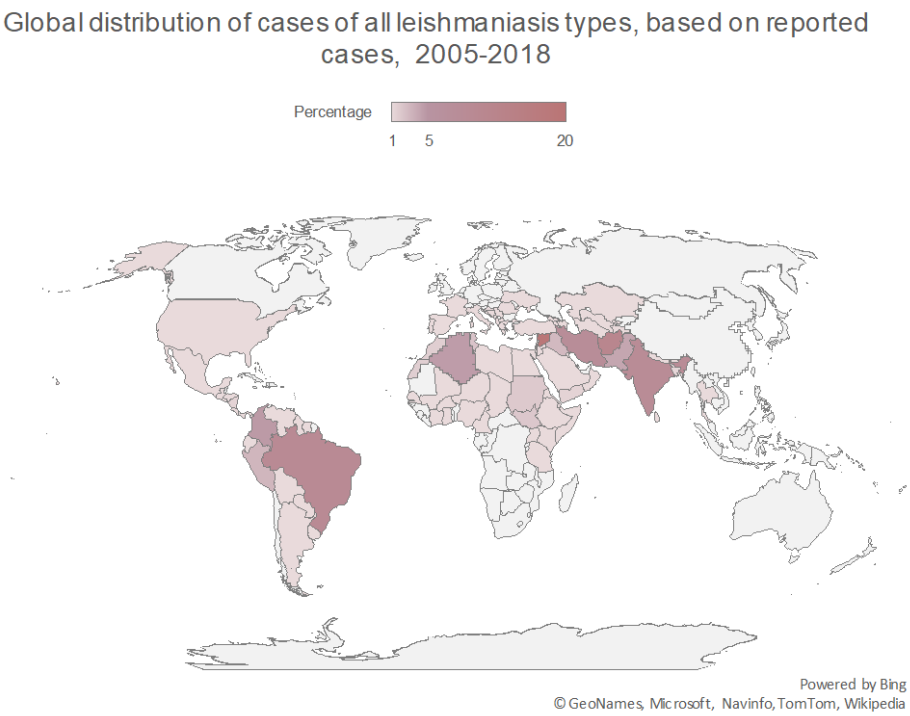

Figure 10
Leishmaniasis global distribution map based on reported cases during 2005 to 2018 [55]

Leishmania parasites life cycle begins with the bite of an infected female *Phlebotomine* sandfly, through which *Leishmania* promastigotes are transferred to the human host. The host's macrophages phagocytize the promastigotes, which differentiate into amastigotes that replicate until the cell breaks. The amastigotes are then spread throughout the body, now, another sandfly can ingest them during a blood meal. Inside the sandfly, the amastigotes travel to its gut, where they are transformed into promastigotes, and replicate to later migrate to the hypostome in order to infect another vertebrate host [51].

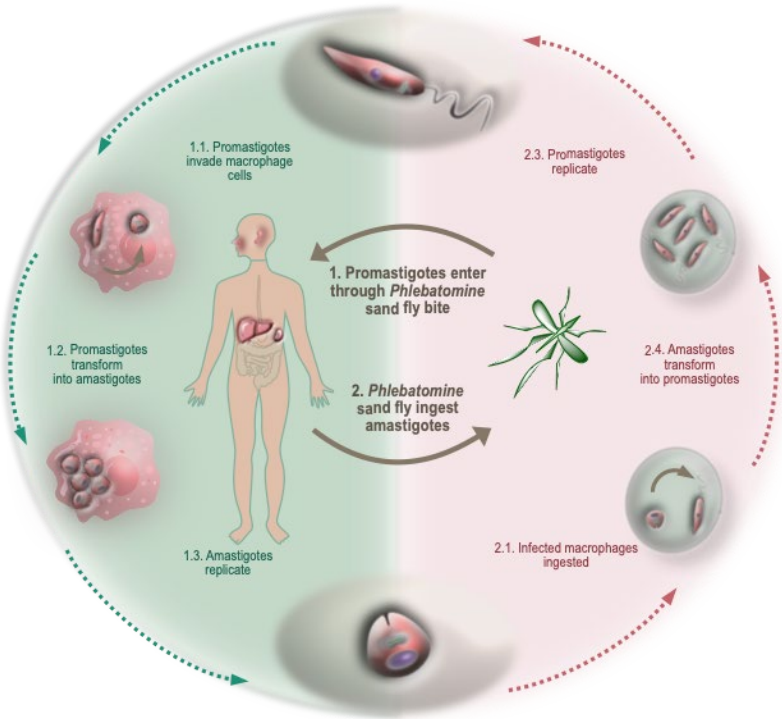

Figure 11
Life cycle of *Leishmania spp.*

Leishmania promastigotes get into the host without alarming the immune system, by naturally dying inside the sandfly generating apoptotic-like promastigotes, which are injected mixed with the living parasites, producing a non-aggressive activation of the immune system [56, 57]. It is still unknown how the parasites survive inside the macrophage, how they are distributed in the body, and how the immune response is modulated. However, proteins related to the immune system appear to be important [53, 57]. Different proteins are expressed by different *Leishmania* parasites, as well as in their different morphological forms (promastigote and

amastigote), which produce difficulties in the identification of potentially useful molecular target [53].

As Leishmaniasis infective process is not well understood, there are no specific treatment yet. Some of the currently used drugs have been discovered in repurpose studies, and not all information about their mode of action is known [52]. Pentavalent antimonials, for example, act through reduced Sb^{III}, however the mechanism is not understood [51, 58, 59]. Amphotericin B has been used before as antifungal and seems to act on the parasites by inhibiting ergosterol biosynthesis, however; the adverse effects observed and the need of hospitalization are inconvenient factors [59]. Miltefosine is the only drug that can be taken orally, but serious side effects have been reported; in addition, *L. braziliensis* have not shown sensitivity to this drug [59].

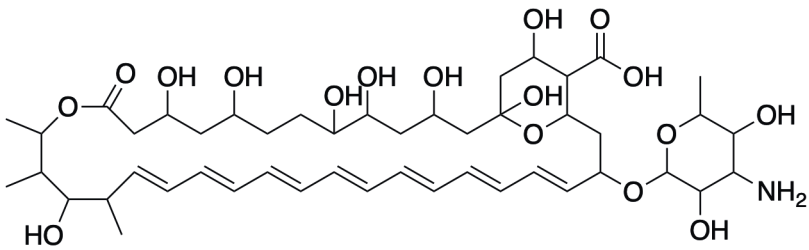

Amphotericin (**10**)

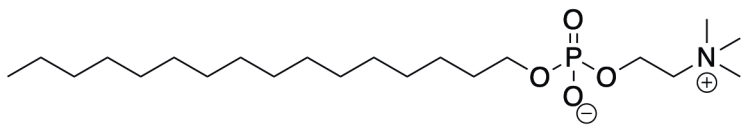

Miltefosine (**11**)

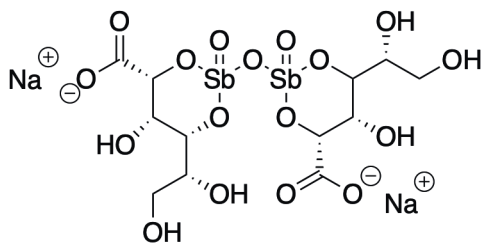

Sodium stiboglucanate (**12**)

Figure 12
Amphotericin B, Miltefosine and sodium stibogluconate

Currently new compounds which possess immunomodulatory and antileishmanial activity are being studied. Leishmaniasis is known to compromise the immune response, therefore it might be convenient to also identify such immunomodulatory substances as potential drug candidates [60].

1.7 Secondary metabolites from *Bourreria pulchra*

Pulchrol and pulchral are natural benzo[*c*]chromenes isolated from the heptane fraction of *Bourreria pulchra*'s roots [61]. This plant, also known as "Bakalche" is native from the Yucatan province in Mexico, where is traditionally used to treat cutaneous diseases, injuries, viral infections and fevers [62, 63]. Antiparasitic studies on *B. pulchra* have also been developed, and showed that the ethanolic extract obtained from its leaves possess potent activity against *T. cruzi* [64].

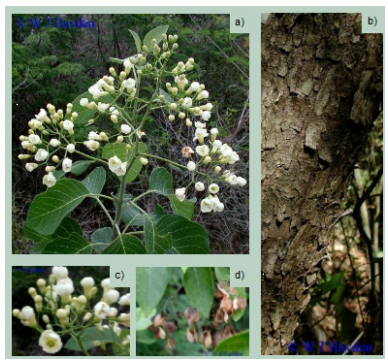

Figure 13
a) *Bourreria Pulchra*, b) Bark, c) Flowers, d) Fruits [65]

Further antiparasitic studies on the compounds isolated from *B. pulchra* (pulchrol and its analogue pulchral, Figure 14) have reported potential toxicity against several *Leishmania* species (*L. braziliensis*, *L. amazonensis*, *L. mexicana*) and particularly against *T. cruzi* [61]. Pulchrol's possible potential as antiparasitic compound, and the low yields in which it was obtained during the isolation process, have led to the development of a synthetic route which was reported earlier [66, 67].

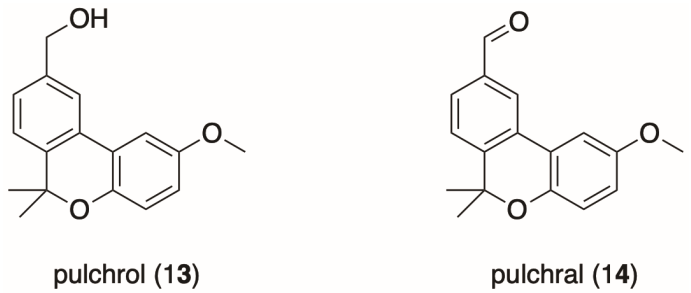

Figure 14
Structures of pulchrol and pulchral

1.8 Aim of the thesis

The objective of this thesis is to find the structure-activity relationships (SARs) for pulchrol and its synthetic analogues relative to their bioactivity measured toward various trypanosomatids. From this analysis, we expect to grasp on the possible role that different functionalities play in the antiparasitic activity presented here, additionally we will depict a preliminary view of the space surrounding pulchrol in a possible active site by presenting a pharmacophore hypothesis. As a consequence of our findings, we hope to contribute to the knowledge on antiparasitic compounds with potential to treat NTDs, particularly Leishmaniasis and the Chagas disease, we also expect our results will be of good use, for developing further studies on the pulchrol scaffold.

For this investigation, several synthetic pulchrol analogues were prepared with systematic modifications in different positions of the benzo[*c*]chromene scaffold. Each one of the prepared analogues was assayed *in vitro* against *T. cruzi* epimastigotes, *L. braziliensis* promastigotes and *L. amazonensis* promastigotes. Additionally, their cytotoxicity was measured in murine macrophage cell lines (RAW) to calculate their selectivity indexes as the ratio between the cytotoxicity and the antiparasitic activity.

Initially, some improvements in the previously published pulchrol synthetic route that are implemented here are presented in Chapter 2, in addition SARs for the analogues with transformations on the benzyl alcohol in the A-ring are discussed. In Chapter 3 the synthesis of analogues with modifications on the B- and C-rings are described and their SARs discussed. In Chapter 4 analogues with more than one modification are presented, among those the natural compounds didehydroconicol and cannabinol, their SARs are discussed in Chapter 4. Finally, Chapter 5 summarizes the antiparasitic activity in a pharmacophore hypothesis, and a qualitative analysis of the ADMET properties for the compounds is presented.

2 Modifications in the A-Ring

2.1 Background

2.1.1 Benzochromenes

Compounds belonging to the benzochromene type of molecule are often found in nature, and many of them have been isolated from endophytic fungi, lichens, vegetal and marine species [61, 68-74], benzochromenes with different substitution patterns have also been prepared synthetically [75-81]. Many natural and synthetic benzochromenes possess a wide range of bioactivities and they might be promising molecules for developing lead compounds with therapeutic applications [82].

Benzochromenes are polycyclic aromatic compounds characterized for the presence of a chromene moiety as part of their structure. The chromene structural form, features an oxygen heterocycle and appears to be an important component in several biologically active compounds. This molecular scaffold is formed by the fusion of a benzene ring with a pyran ring system. In turn, the fusion of a second benzene ring with the chromene moiety generate the benzochromene scaffold, which can be classified into four categories according to the position where the benzene ring is placed: benzo[*c*]chromenes, benzo[*f*]chromenes, benzo[*g*]chromenes and benzo[*h*]chromenes [82], their basic structural forms can be observed in Figure 15.

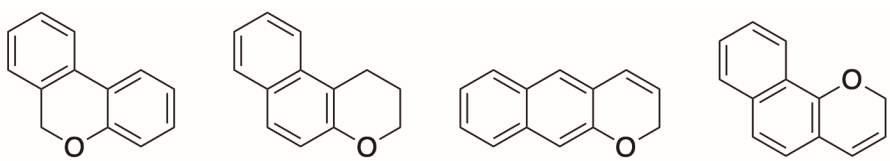

(**15**) (**16**) (**17**) (**18**)

Figure 15
Different types of benzochromenes : (**15**) benzo[*c*]chromene, (**16**) Benzo[*f*]chromene, (**17**) Benzo[*g*]chromene, (**18**) Benzo[*h*]chromene [82]

2.1.2 Bioactive benzochromenes

Compounds bearing an angular benzochromene scaffold have been isolated from natural sources or prepared in the laboratory synthetically and they have been shown to possess activity toward diverse biological systems. For instance, the natural benzo[*f*]chromene **19** was isolated from the roots of *Pentas bussei*, a plant known also as Mdobe in Kenya, where is traditionally used to treat gonorrhoea, syphilis and dysentery [73]. Natural benzo[*c*]chromene, didehydroconicol (**20**), was also isolated from the marine ascidian *Aplidium aff. Densum* and showed to possess an effect as bacteriostatic [74]. Another natural benzo[*c*]chromene, cannabinol (**21**), is one of the constituents of the leaves of *Cannabis sativa* [83], and it possesses binding affinity with the endocannabinoid receptor CB2 [84, 85] and with biological targets related to the immune system [86, 87]. Additionally, benzo[*c*]chromene-6-ones, known as graphislactones (structural type **22**), have been isolated from lichens belonging to the *Graphis* genus and different endophytic fungus species [68-72]. Some of those natural compounds are active toward the colorectal adenocarcinoma cell line SW1116 [71]. Further studies on graphislactones have also led to the development of a synthetic route to obtain them in the laboratory [75].

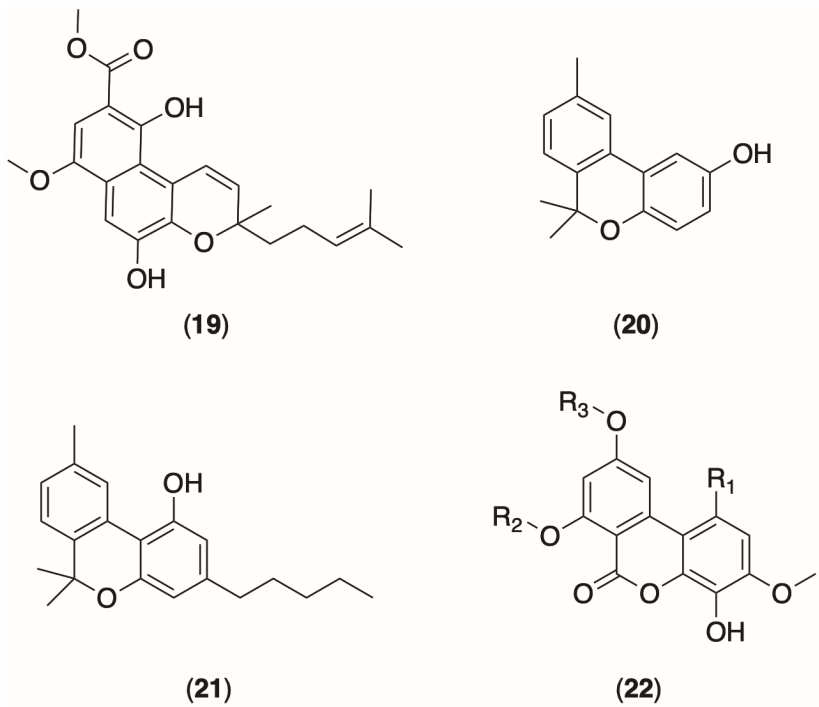

Figure 16
Natural bioactive benzo[*c*]chromenes

Benzo[*f*]chromene derivatives with structural forms **23** and **24**, have been prepared synthetically and have been found to possess antibacterial and antifungal activity respectively [76, 78]. Derivatives bearing the benzo[*f*]chromen-3-one skeleton (**25**) have been shown to be active toward cancer cell lines A546 (lung carcinoma), MCF7 (breast cancer) and A375 (melanoma), when they are substituted with alkyl groups [77]. Similarly, synthetic benzo[*h*]chromenes with alkyl substituents (generic structure **26**), have been found to possess anticancer activity toward cell lines MCF7, HCT116 (colon carcinoma) and HepG-2 (hepatocyte carcinoma) [79]. Besides, synthetic hydroxylated derivatives of natural benzo[*c*]chromen-6-one, urolithin (**27**), have been shown to possess potential as treatment of Alzheimer disease, since they have been shown to inhibit acetyl- and butyryl-cholinesterase enzymes [80]. Moreover, benzo[*c*]chromenes and benzo[*c*]chromen-6-ones, **28** and **29,** have been found to be selective ligands for the estrogen receptor ERβ [81].

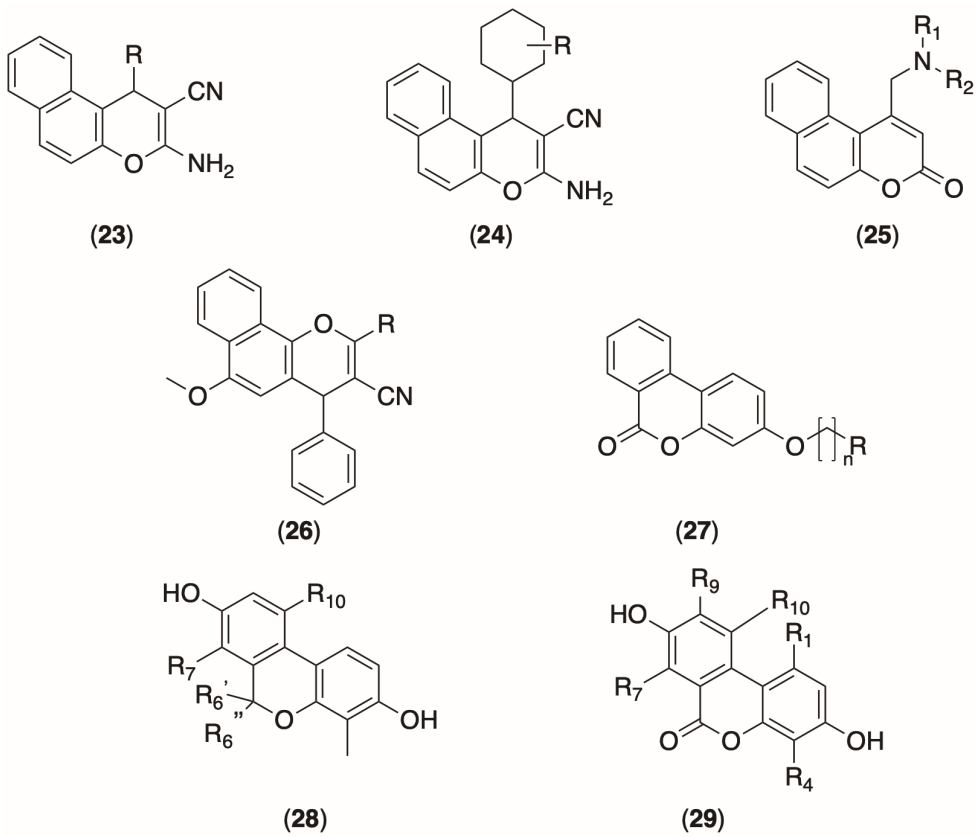

Figure 17
Synthetic bioactive benzochromenes

2.1.3 Synthesis of benzo[*c*]chromenes

There are primarily two synthetic strategies used to prepare benzo[*c*]chromenes: One way is by intramolecular biaryl formation from phenylbenzyl ethers through functionalization of C-H aromatic bonds (path A, Figure 18) and subsequent cyclization. This strategy can be developed either by transition-metal catalysed reactions using palladium [88, 89] or in the absence of transition-metals using potassium *tert*-butoxide to promote the biaryl formation via a single electron transfer [90-92]. Another important synthetic strategy to prepare the biaryl intermediate is by metal catalysed Suzuki-Miyaura cross-coupling reaction between an *o*-halo-benzoic acid and a 2-methoxyphenylboronic acid, followed by cyclization (path B, Figure 18) [93, 94].

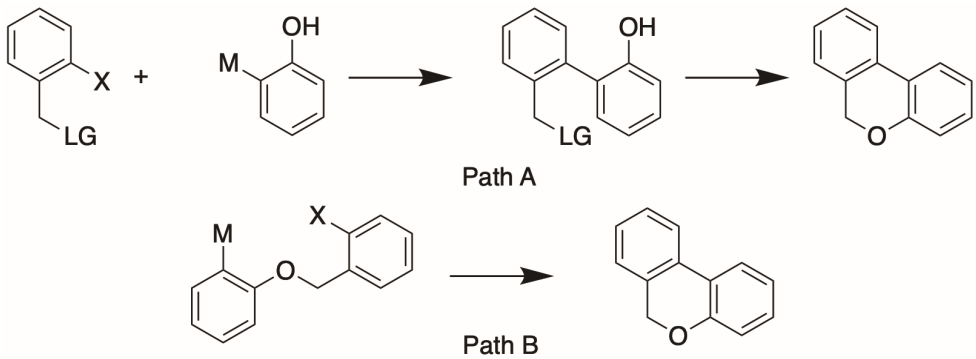

Figure 18
Main strategies for the synthesis of benzo[*c*]chromenes

Other synthetic routs to obtain the biaryl intermediate are by dicarbonyl cycloaddition to chromenes [95] or through Diels-Alder cyclo-addition reaction under high pressure [96, 97].

2.2 Pulchrol synthesis

The synthesis of the natural benzo[*c*]chromene pulchrol (**13**) was previously developed in our group and was first reported in 2014. In order to prepare the biaryl intermediate **33**, which is crucial in the synthesis of pulchrol (**13**), a Suzuki-Miyaura coupling reaction was performed between a 2-methoxyphenylboronic acid and a halogenated ester. Subsequently, the biaryl intermediate **33** was cyclised by acid catalysis, after being subjected to double alkyl addition to the ester group to form a tertiary alcohol (**34**) [66].

In this investigation we prepared pulchrol based on this synthetic route, however, in order to increase the yield and improve the reaction conditions, some modifications were introduced (see Figure 19).

In a similar way as in the synthetic route reported in 2014 [66], we have used the commercially available 3-iodo-4-(methoxycarbonyl)benzoic acid (**30**) as the starting material. In accordance with the previously published procedure, the starting material was reduced to the corresponding benzyl alcohol (methyl 4-(hydroxymethyl)-2-iodobenzoate (**31**), using a borane-tetrahydrofuran complex in THF as solvent, at 0 °C (step a). Afterward, the benzylic hydroxyl group was protected with *tert*-butyldiphenylchorosilane (TBDPSCl) using pyridine as solvent (step b) to obtain intermediate **32**.

To obtain the biaryl intermediate (**33**), a Suzuki-Miyaura coupling reaction between 2,5-dimethoxyphenylboronic acid and the intermediate **32** was conducted using palladium-tetrakis(triphenylphosphine) ($Pd(PPh_3)_4$) as catalyst and K_2CO_3 as base in dimethoxyethane (DME)/H_2O 4:1 as solvent (step c). In the investigation published in 2014, this reaction was reported to work successfully at 120 °C yielding 83% of the biaryl intermediate **33**, yet 14 h were required for the reaction to be completed [66]. Here, we performed this reaction by microwave-assisted Suzuki-Miyaura coupling, which has been reported to reduce the reaction times and increase the yields [98]. As a result, we obtained 85%-90% yield of the biaryl intermediate (**33)** in 30 min, executing the reaction at 100 °C in a microwave reactor.

For the synthesis of the intermediate **34**, the ester group in **33** was transformed into a tertiary alcohol by a double alkyl addition using two equivalents of methyllithium (MeLi) in THF at 0 °C (step d) instead of MeMgBr in THF at 40 °C [66]. As a result, the reaction time decreased from 18 h [66] to 8 h. Furthermore, due to the milder conditions in which the reaction was conducted, a cleaner product that was considerably easier to purify was obtained and the yield of the product (**34**) was comparable to that reported before [66].

Finally, during the cyclization step (step e) a larger excess of hydroiodic acid (HI) (10 equiv) was used to obtain pulchrol (**13**), this made possible to avoid the formation of cannabidiol-type biaryl by-products and to obtain the deprotected product directly, in Figure 17 the scheme for the synthetic route used to prepare pulchrol is shown.

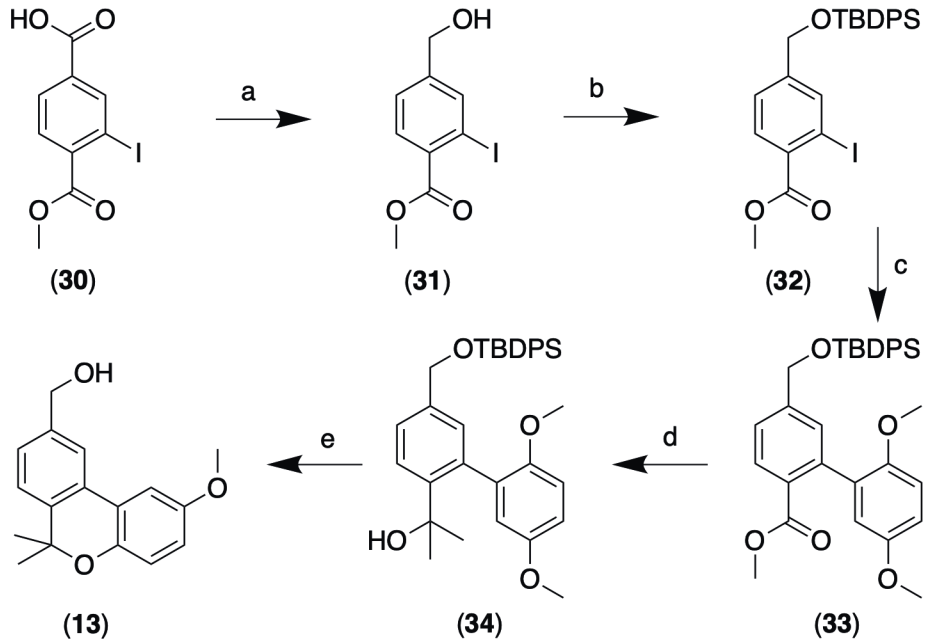

Figure 19
Synthetic route to prepare pulchrol. Reagents and conditions: (i) Borane-THF complex, dry THF, 0°C (ii) TBDPSCl, pyridine (iii) Microwave reaction: 2,5-dimethoxyphenylboronic acid, K_2CO_3, tetrakis(triphenylphosphine)palladium(0) in DME/Water 4:1, 30 min, 100 °C (iv) MeLi, dry THF, 0 °C (v) HI 55% wt, MeCN.

2.3 Transformations of the benzyl alcohol functionality

The focus in this part of our investigation is to understand the importance of the benzyl alcohol functionality for the antiparasitic activity. With that in mind, we have prepared several analogues with systematic variations in the benzyl alcohol region (the A-ring), using pulchrol as starting material (See Figure 20 for the structural types). A reduced pulchrol analogue was used to evaluate the importance of the hydroxyl group for the bioactivity, and various transformations on the benzyl alcohol were performed to determine its role, either as hydrogen bond donor or hydrogen bond acceptor. We have also prepared analogues with substituents of different bulk and size to explore the space availability, and to evaluate possible Van der Waals interactions around the benzyl alcohol region (See the experimental part in Paper 1 for details).

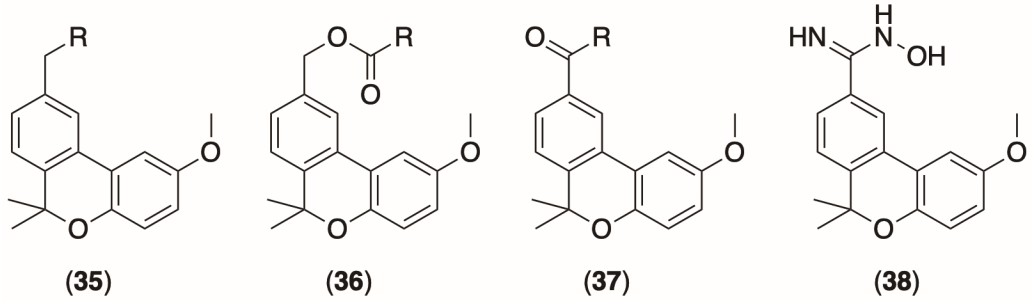

Figure 20

Pulchrol's analogues structural. **35a** R = H; **35b** R = Cl; **35c** R = methoxy; **35d** R = isopropyloxy; **35e** R = 4-methylpentyloxy; **35f** R = isopropylamino; **35g** R = isobutylamino; **35h** R = isopentylamino; **36a** R = Me; **36b** R = isopropyl; **36c** R = *tert*-butyl; **36d** R = propyl; **36e** R = isobutyl; **36f** R = neopentyl; **36g** R = pentyl; **36h** R = 2-cyclopentylethyl; **36i** R = vinyl; **36j** R = 2-furanyl; **36k** R = phenyl; **36l** R = cyclohexyl; **37a** R = H; **37b** R = Me; **37c** R = OH; **37d** R = methoxy; **38** R = NH_2. See Experimental part for synthetic details.

Table 1 contains the bioactivity results obtained from the *in vitro* assays toward *T. cruzi*, *L. braziliensis* and *L. amazonensis*. Additionally, the cytotoxicity measured on the murine macrophage cell line (RAW) is presented alongside the selectivity index, which was calculated as the ratio between the cytotoxicity and the antiparasitic activity for each one of the analogues.

Table 1

Antileishmanial, antitrypanozomal and cytotoxic activity of the pulchrol analogues, compared to the positive controls Benznidazole and Miltefosine. See Paper 1 for the experimental details.

Mol.	R	*T. cruzi*		*L. brasiliensis*		*L. amazoniensis*		Cytotoxicity[a]
		IC_{50} (μM)	SI[b]	IC_{50} (μM)	SI[b]	IC_{50} (μM)	SI[b]	IC_{50} (μM)
13		18.5 ± 9.6	1.7	59.2 ± 11.8	0.5	77.7 ± 5.6	0.4	30.7 ± 1.1
35a		51.1 ± 17.7	2.0	69.6 ± 5.9	1.4	85.3 ± 5.9	1.2	99.5 ± 22.0

35b		38.1 ± 0.4	1.6	17.1 ± 0.1	3.5	35.0 ± 2.8	1.7	59.2 ± 14.5
35c		24.6 ± 3.5	1.3	49.2 ± 15.8	0.7	56.3 ± 12.0	0.6	33.1 ± 2.1
35d		12.9 ± 0.3	2.5	35.2 ± 3.2	0.9	35.2 ± 3.8	0.9	32.0 ± 0.3
35e	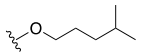	9.0 ± 0.6	3.5	127.2 ± 11.3	0.3	28.2 ± 8.5	1.1	31.6 ± 5.6
35f		70.6 ± 9.6	0.4	83.5 ± 32.1	0.4	67.8 ± 13.8	0.4	29.5 ± 9.6
35g	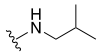	15.4 ± 4.0	0.8	25.8 ± 6.2	0.5	15.4 ± 3.1	0.8	12.3 ± 1.2
35h	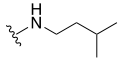	5.9 ± 1.2	1.3	15.9 ± 0.9	0.5	17.7 ± 7.4	0.4	7.4 ± 2.4
36a		14.4 ± 1.6	2.3	28.8 ± 0.3	1.1	26.9 ± 0.6	1.2	32.7 ± 22.4
36b		8.8 ± 0.9	3.0	17.6 ± 0.9	1.5	26.7 ± 2.4	1.0	26.4 ± 5.9
36c		6.4 ± 0.1	3.0	17.4 ± 1.7	1.1	20.5 ± 0.6	1.0	19.8 ± 0.9
36d		16.2 ± 3.2	6.4	57.8 ± 2.4	1.8	79.3 ± 9.4	1.3	102.8 ± 35.3
36e		4.2 ± 1.1	6.7	13.1 ± 0.4	2.2	14.5 ± 0.1	1.9	28.2 ± 9.0
36f		5.7 ± 0.3	3.3	20.0 ± 4.2	1.0	19.5 ± 0.8	1.0	19.0 ± 3.0
36g	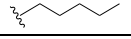	22.8 ± 5.7	2.3	27.7 ± 0.3	1.9	42.3 ± 8.7	1.2	52.1 ± 8.1
36h	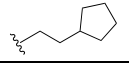	8.4 ± 3.3	6.1	122.4 ± 27.9	0.4	30.9 ± 3.0	1.6	50.7 ± 17.7
36i		13.1 ± 0.5	3.9	24.3 ± 0.8	2.1	40.5 ± 8.7	1.3	51.3 ± 8.2
36j		7.4 ± 0.9	5.4	5.7 ± 0.5	7.0	6.9 ± 1.7	5.8	40.1 ± 12.6

36k		3.8 ± 0.3	7.9	12.8 ± 0.1	2.4	12.8 ± 1.8	2.4	30.5 ± 3.6
36l		5.9 ± 0.5	4.7	21.0 ± 4.3	1.3	21.9 ± 7.7	1.3	27.8 ± 10.7
37a		24.2 ± 4.1	1.6	24.2 ± 7.5	1.6	29.8 ± 11.2	1.3	38.8 ± 3.7
37b		21.2 ± 9.2	1.5	28.3 ± 7.1	1.1	43.2 ± 8.2	0.7	31.9 ± 7.1
37c		56.3	4.4	65.1 ±16.5	3.8	198.7	1.2	246.2 ± 24.6
37d		31.8 ± 2.4	1.2	18.4 ± 5.7	2.1	59.0 ± 1.3	0.7	38.2 ± 2.7
37e		134.5 ± 38.8	0.4	144.7 ± 43.1	0.3	120.7 ± 21.2	0.4	49.8 ± 17.7
38	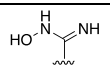	33.4 ± 14.9	0.8	52.0 ± 18.6	0.5	52.0 ± 16 .7	0.5	26.4 ± 1.5
	Benznidazole	19.2 ± 7.7	3.9					74.7 ± 9.1
	Miltefosine			13.0 ± 1.2	5.9	10.8 ± 1.5	7.1	76.6 ± 3.2

[a] Toxicity was measured on RAW cells, see Experimental for details, [b] SI, selectivity index (cytotoxicity/anti-protozoal activity).

2.4 Antiparasitic activity

Previous investigations have reported that natural product pulchrol (**13**) is toxic toward some trypanosomatid parasites [61]. In this investigation, the antiparasitic activity of pulchrol (**13**) is measured toward *T. cruzi*, *L. braziliensis* and *L. amazonensis* (See Table 1). Pulchrol was found to have potent antiparasitic activity toward *T. cruzi* epimastigotes (IC_{50} = 18.5 μM), which is comparable to the bioactivity measured for the positive control, benznidazole (IC_{50} = 19.2 μM), currently used to treat the Chagas disease. In addition, biological assays showed that pulchrol is moderately toxic toward *L. braziliensis* and *L. amazonensis* (IC_{50} values: 59.2 μM and 77.7 μM respectively). Other *Leishmania* species, like *L. mexicana* (not included here) have also been found to be more sensitive to pulchrol (IC_{50} = 17 μM) in previously reported studies [61].

Since pulchrol structure (**13**) does not contain functionalities that are associated with reactivity or unspecific biological activity, we were motivated to synthesize and assay analogues of **13**. For this study, the natural products pulchrol and pulchral (**13** and 3**5a**), together with 25 analogues were prepared and assayed against the abovementioned parasites. Their cytotoxicity was measured in a mammalian murine macrophage RAW cell line in order to get an impression of the compound's selectivity. The biological results are presented in Table 1.

2.4.1 Antiparasitic activity toward *T. cruzi*

Our initial aim was to evaluate the importance of the hydroxyl group for pulchrol's activity, to achieve this objective, pulchrol (**13**) was reduced to the 9-methyl analogue **35a**. This analogue showed to be considerably less active (IC_{50} = 51.1 μM) compared to **13**, consequently evidencing the relevance of the benzyl alcohol.

To mimic possible Van der Waals interactions around the benzylic carbon, the hydroxyl group in pulchrol (**13**) was replaced with a chlorine atom (**35b**). However, the bioactivity measured for **35b** (IC_{50} = 38.1 μM) was found to be inferior compared to that shown by **13**, suggesting that the biological activity is favoured by interactions involving the oxygen atom in the benzylic position.

The benzyl alcohol possible participation in binding interactions within the active site drove us to evaluate its role as either hydrogen bond donor or hydrogen bond acceptor. To determine its hydrogen bond donor capacity, methyl ether **35c** was prepared and assayed. Analogue **35c** showed to be slightly less active (IC_{50} = 24.6 μM) than **13**, indicating that the hydroxyl group acts more as a hydrogen bond acceptor. Bulkier ethers **35d** and **35e** were also prepared, however, contrary to the

bioactivity results reported for the methyl ether **35c**, they were more potent than **13** (IC_{50} = 12.9 and 9.0 μM, respectively), suggesting that lipophilic interactions occur in a hydrophobic pocket placed near the benzyl alcohol oxygen in the target protein. The bulkier ethers also showed better selectivity compared to pulchrol and the methyl ether analogue (**13** and **35c**, respectively). Substituted amines bearing bulky alkyl groups were also prepared (**35f**, **35g**, and **35h**), somewhat surprisingly, the isopropylamino analogue **35f** was found to be considerably less potent and selective than the isopropyl ether **35d**. On the other hand, the larger isobutyl and isopentyl amine analogues **35g** and **35h** (IC_{50} = 15.4 and 5.9 μM, respectively) were as potent as **35e** (the pulchrol ether with the largest substituent).

Pulchrol esters **36a** to **36l** were also prepared and assayed. The results of the antitrypanosomal assays showed that most of the esters were more potent and selective compared to pulchrol (**13**). Amongst them, saturated esters **36a** to **36i**, showed good antitrypanosomal activity, particularly those prepared from acids with branched alkyl groups. Notably, the 3-methylbutanoic acid ester **36e** showed the highest potency and selectivity within this group (IC_{50} = 4.2 μM and SI = 6.7). Similarly, all unsaturated esters (**36j**-**36l**) showed potent antitrypanosomal activity and high selectivity, indicating that π-π interactions with the binding pocket are favourable. The most potent and selective analogue between the unsaturated esters was found to be the furan-2-carboxylic acid ester **36k** (IC_{50} = 3.8 μM, SI = 7.9), which also showed the best results within all the analogues prepared in this part of the investigation. Furthermore, **36k** showed to be considerably more potent and even two times more selective than the positive control Benznidazole.

The benzyl alcohol in pulchrol (**13**) was also partially and totally oxidized to obtain the 1'-carbonyl analogues (**37a** - **37e**) included in this study. The aldehyde **37a** and the methyl ketone **37b** were found to be equipotent compared to **13**, and similar selectivity indexes to pulchrol's were calculated for both analogues. In contrast, the carboxylic acid **37c** and the ester **37d** were less potent and less selective than pulchrol (**13**). However, it was the amide **37e**, which showed the lower toxicity toward *T. cruzi* and the highest cytotoxicity among all analogues in this study.

Finally, analogue *N*-hydroxy-9-carboximidamide **38**, which was obtained as a by-product was also assayed toward *T. cruzi*. It was found to possess considerably low potency, although, it was still more potent than the 9-carboxamide **37e**. The low antitrypanosomal activity measured for analogue **38** evidence the importance of lipophilic substituents around the benzylic position for the biological activity.

2.4.2 Antiparasitic activity toward *L. braziliensis*

To begin evaluating the importance of the benzyl alcohol in the antiparasitic activity toward *L. braziliensis*, the hydroxyl group was reduced to a methyl group (**35a**). Similar to the results obtained with *T. cruzi*, analogue **35a** was found to be slightly less potent than **13**, evidencing the importance of the benzyl alcohol. However, the benzyl chloride (**35b**) showed an interesting potency (IC_{50} = 17.1 μM) and selectivity (SI = 3.5) toward *L. braziliensis*, in contrast to *T. cruzi*. Therefore, the presence of an oxygen atom in the benzylic position may not be as important for *L. braziliensis* as it is for *T. cruzi*. These differences in the antiparasitic effects showed by **35b** indicate that the molecular targets in the two species are different.

Ethers **35c** to **35e** were also prepared and assayed. Two of them, one substituted with a methyl group (**35a**) and the other with an isopropyl group (**35b**) were slightly more potent than **13**, while the 4-methylpentyl ether **35e** showed to be considerably less potent, meaning that ethers with bulky substituents are not as favourable for the activity against *L. braziliensis* as they are for *T. cruzi.* Alternatively, the secondary amines **35f** to **35h** showed and identical trend in relation to *T. cruzi*, and the isopentylamino analogue **35h** (IC_{50} = 15.9 μM) was one of the most potent analogues against *L. braziliensis*.

Most of the esters (**36a**-**36l**) showed to be more potent than pulchrol (**13**) toward *L. braziliensis*, except the 3-cyclopentylpropanoate acid ester **36h.** As for *T. cruzi,* the saturated esters showed that bulky substituents are better for the bioactivity than straight alkyl chains. Similarly, all unsaturated esters (**36k**-**36l**) were more potent than pulchrol (**13**). However, unlike the results observed with *T. cruzi*, the selectivity showed by analogue **36k** was not as favourable, and its bioactivity was just as good as that of the positive control. Instead, the vinyl ester **36j** was the analogue that showed the highest potency and selectivity toward *L. braziliensis* (IC_{50} = 5.7 μM and SI = 7.0), which were also better than those of the positive control.

Within the 1'-carbonyl analogues, it was observed that the aldehyde **37a**, the methyl ketone **37b** and especially the methyl ester **37d** were more potent, while the carboxylic acid **37c** and the *N*-hydroxy-9-carboximidamide (**38**) were just as good as **13**. Finally, the carboxamide **37e** was the least potent of all analogues.

2.4.3 Antiparasitic activity toward *L. amazonensis*

In the same way as before, the benzyl alcohol in pulchrol (**13**) was replaced for a methyl group to obtain analogue **35a**. Similar to the other parasites, no improvements in the antiparasitic activity were observed against *L. amazonensis*. The bioactivity observed for the chlorinated analogue (**35b**) was two times more potent compared to pulchrol's, following the same trend observed with *L. braziliensis*. All the ethers (**35c**-**35e**) prepared in this investigation were more potent than pulchrol (**13**). The bioactivity observed for the methyl and isopropyl ethers (**35c** and **35d**) was not as significant as the potency showed by the 4-methylpentyl

ether **35e**, although **35e** was found to possess a low activity toward *L. braziliensis.* For the secondary amines the observed bioactivity followed the same trend observed with *T. cruzi* and *L. braziliensis*. the isopropylamino analogues **35f** showed lower potency than the isobutyl- and isopentylamino analogues **35g** and **35h**. For the esters **36a** to **36l**, the results obtained were closely related to those observed with *L. braziliensis*, except for the 3-cyclopentylpropanoic acid ester **36h**, which was potent against *L amazonensis*. As with *L. braziliensis*, the vinyl ester **36j** was the most potent among all compounds assayed in this part of the investigation, and its SI value (5.8) makes it the most selective compound.

Finally, the 9-carbonyl analogues were prepared and assayed toward *L. amazonensis*. The aldehyde and the methyl ketone (**37a**-**37b**) were more potent than **13**, while the increase in activity showed by the methyl ester **37d** and the *N*-hydroxy-9-carboximidamide **38** were minor. Following the results discussed for the other parasites, the carboxylic acid **37c** and the carboxamide **37e** were considerably less potent against *L. amazonensis* compared to **13.**

2.5 Conclusions

In this part of our investigation, we developed a more efficient synthetic protocol to prepare the natural products pulchrol and pulchral (**13** and **35a**), which were used as starting material for the preparation of 25 analogues with modifications on the benzylic alcohol functionality. The antiparasitic activity of all analogues, as well as the natural compounds **13** and **35a** was tested towards *T. cruzi* epimastigotes, as well as *L. braziliensis* and *L. amazonensis* promastigotes. However, the modifications were focused in just one part of the molecule, which prevented us from getting a full perspective of the structure activity relationships for pulchrol. For that reason, we present just general suggestions on the bioactivity trends in this part of the investigation.

Some other factors to consider are the complex biology of the trypanosomatid parasites under study, the lack of knowledge about the molecular targets in which pulchrol (**13**) and its analogues bind, and the differences that may exist in the binding sites between the parasites. Besides, variations in properties related to the structural diversity of the analogues could be responsible for the differences measured in the bioactivity and selectivity, for instance, the solubility may be responsible for the inability of a ligand to cross the cell membrane, and then, reach the target, producing a loss in the activity.

Having said that, we can understand from our biological results that the benzylic oxygen in pulchrol is important for the anti-parasitic activity against all parasites studied. However, the hydroxyl functionality was found to act more as a hydrogen bond acceptor than a hydrogen bond donor.

Most of the ethers and esters were more potent than pulchrol (**13**), particularly those substituted with branched alkyl groups. This indicates that a lipophilic pocket exists in the binding site; nevertheless, the shape and size of this pocket may differ between the parasites. The lipophilic pocket in *L. braziliensis* appears to have a limit on the space for approximately five carbons in the region in which the ester substituent is placed. On the other hand, *T. cruzi* and *L. amazonensis* targets seems to feature flat hydrophobic regions, in which the aromatic and planar substituents interact, increasing the activity as a result.

The analogue that showed the best potential as antiparasitic was the vinyl ester **36j**, which was more potent than pulchrol, most of the other analogues, and our positive controls (benznidazole and nifurtimox). Besides, its selectivity indexes were above 5 for all three organisms. Acrylic esters like **36j** react as Michael acceptors with highly reactive nucleophiles present in the active site. Thus, the enhanced potency and selectivity shown by **36j** may be due to a role as Michael acceptor, if this would be true, analogues from **36j** could be used to fish out molecular targets for trypanosomatid parasites.

3 Modifications in the B- and C-ring

In the last chapter, the importance of the benzyl alcohol for the antiparasitic activity of our lead compound pulchrol was determined, and how transformations of this functionality affect the biological activity was discussed [99]. In this part of the work, we wanted to study how substituents and combinations of substituents in the B- and C-rings affect the antiparasitic activity of pulchrol. To prepare the synthetic analogues for this part of the study, some modifications to the synthetic strategy used to prepare the compounds described in Chapter 2 were added. Some intermediates obtained previously were used as precursors for the synthesis of the compounds studied here.

From pulchrol's structure, we can see that there is only one position available for modification in the B-ring (position 6). To evaluate the effect that different substituents may have on the biological activity, the methyl substituents were replaced with longer alkyl groups, with one alkyl group and a hydrogen atom, and with two hydrogen atoms. Additionally, we intended to investigate the effect that transformations in the C-ring may produce, thus we have prepared analogues with different substitution patterns in three of the four available positions of the C-ring. Analogues with a methoxy group in positions different from C-2 (as in pulchrol), and compounds in which the methoxy group was replaced for alkyl substituents, were prepared. Finally, an analogue with no substituents in the C-ring was prepared, to evaluate the importance of the 2-methoxy substituent in pulchrol. Altogether we prepared 16 new analogues (**8a**-**8g**, **10a**-**10h**) with differences in the substituents and substitution pattern in the B- and C-rings. All of them were tested toward *T. cruzi* epimastigotes, as well as *L. amazonensis,* and *L. braziliensis* promastigotes. Their cytotoxicity was measured in murine macrophage cells (RAW), and a selectivity index was calculated for each compound as the ratio between the cytotoxicity and the antiparasitic activity.

3.1 Modification in the B-ring

To prepare the analogues with modifications in the B-ring, a synthetic approach partially based on the previously published synthetic route to obtain pulchrol [66] was used, and the common intermediate **33** was the starting point for the preparation of the B-ring derivatives (see Figure 21).

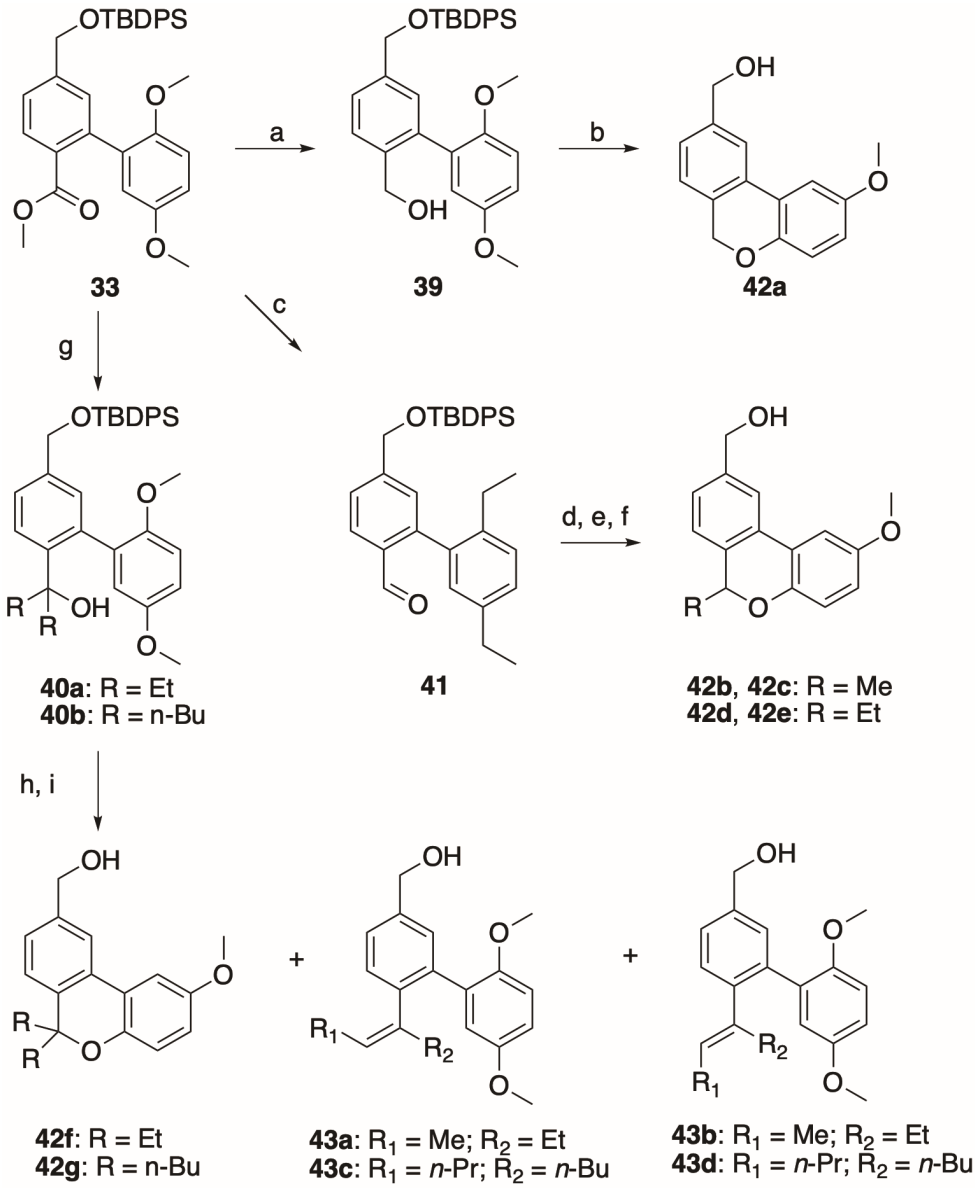

Figure 21

Synthetic route to prepare the B-ring analogues. Reagents and conditions: a) **33** (1 equiv), DIBALH (2.4 equiv), dry toluene, -78 °C; b) **39** (1 equiv), NaSEt (4 equiv), dry DMF, 110 °C; c) **33** (1 equiv), morpholine (2 equiv), DIBALH (1 equiv), dry THF, 0 °C; d) **41** (1 equiv), corresponding organolithic reagent (2 equiv), dry THF, 0 °C or -78°C depending on the organolithic reagent; e) PBr_3 (0.34 equiv), LiI (3 equiv), dry CH_2Cl_2, rt; f) TBAF (2 equiv), THF, rt; g) **33** (1 equiv), organolithic reagent (4 equiv), dry THF, 0°C or -78°C depending on the organolithic reagent; h) **40** (1 equiv), HI (10 equiv), MeCN, rt; i) TBAF (1.1 equiv), THF, rt.

Initially compound **42a** substituted with two hydrogen atoms at position 6 was prepared to evaluate the importance of the alkyl substituents in the B-ring. To prepare **42a**, intermediate **33** was expected to react with NaSEt in dry DMF at 110 °C to yield the *ortho*-demethylated phenol **39** as intermediate, but instead we obtained the cyclized and deprotected 6,6-didemethylated compound (**42a**). It was the main product, but was obtained in low yields (7%). We also prepared the monosubstituted analogues **42b** – **42e** to evaluate the effect that just one alkyl substituent at C-6 may have in the antiparasitic activity. Compounds **42b** to **42e** were prepared by partially reducing the ester intermediate **33** to aldehyde **41**, which after organometallic alkyl addition was cyclized using PBr_3 in the presence of LiI [100]. The product of the reaction was a racemic mixture from which the enantiomers were separated by high-pressure liquid chromatography (HPLC) using a normal phase semipreparative chiral column. The pure enantiomers **42b** - **42e** were obtained in low yields (below 10%). Their absolute configuration was not determined, since all the enantiomers showed to possess equipotent antiparasitic activity (see Section 3.3).

To get some understanding of the space availability around the B-ring, longer alkyl groups were inserted at position 6. Intermediate **33** was used as the starting material to obtain intermediates **40a** and **40b** after double alkyl addition to the ester group using ethyllithium and butyllithium, respectively. Subsequently, intermediates **40a** and **40b** were cyclized following the procedure used to obtain pulchrol [99], the resulting products were the 6.6-diethyl and 6.6-dibutyl analogues **42f** and **42g**. However, the excess in hydroiodic acid used to avoid the formation of the cannabidiol byproducts during pulchrol synthesis [99], was not favourable during the preparation of **42f** and **42g**, and the cannabidiol-like compounds **43a** and **43b** were obtained together with **42f**, while **43c** and **43d** were formed together with **42g**. The mixtures were separated by semipreparative HPLC and the desired products were obtained in moderate yields (**42f**, 30%; **42g**, 56%).

3.2 Modifications in the C-ring

For the analogues with modification in the C-ring, the same procedure used for pulchrol was applied [99]. However, during the Suzuki-Miyaura coupling, different 2-methoxyphenylboronic acids were used, and the reaction time was increased from 30 to 60 min, resulting in the obtention of intermediates **44a**-**44h** in good yields (75%-92%). The procedure was then followed by the approach used for the synthesis of pulchrol, and after cyclization it was noted that most of the analogues substituted with alkyl groups in the C-ring were obtained in higher yields (72%-85%) than those substituted with methoxy groups.

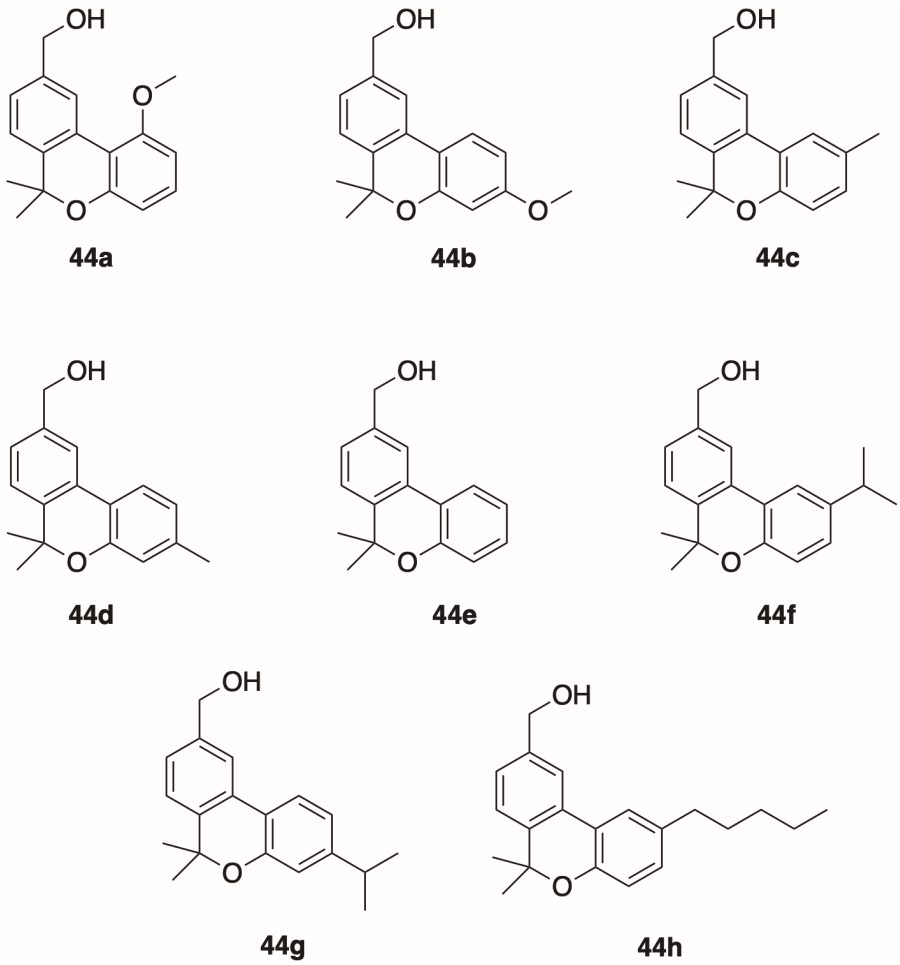

Figure 22
Analogues with modifications in the C-ring

3.3 Antiparasitic Activity

As was indicated in previous chapters, pulchrol has shown to possess activity toward trypanosomatid parasites. The most interesting activity was noted toward *T. cruzi* epimastigotes (IC_{50} 18.5 μM), whereas moderate activity was observed against *L. braziliensis* and *L. amazonensis* promastigotes (59.2 μM and 77.7 μM, respectively).

In Chapter 2, we have discussed the effects that modifications on pulchrol's benzylic alcohol have in the antiparasitic activity. From the results we concluded

that the lipophilic and unsaturated ester analogues of pulchrol significantly increased the potency toward the parasites studied. In Chapter 3, we conducted and evaluation of the effect that modifications in the B- and C-rings have in the biological activity measured toward *T. cruzi* epimastigotes, and *L. braziliensis* and *L. amazonensis* promastigotes. The cytotoxicity was measured on mammalian murine macrophage cell lines (RAW), and the selectivity index was calculated as the ratio between cytotoxicity and the antiparasitic activity (see Table 2).

Table 2
Antileishmanial, antitrypanozomal and cytotoxic activity of the pulchrol analogues, compared to the positive controls Benznidazole and Miltefosine. See Paper 2 for the experimental details.

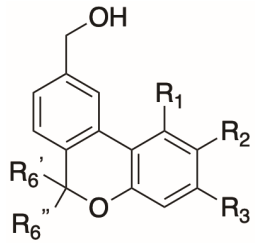

Mol	R_6'	R_6''	R_1	R_2	R_3	*T. cruzi*		*L. braziliensis*		*L. amazonensis*		Cytotoxicity[a]
						IC_{50} (μM)	SI[b]	IC_{50} (μM)	SI[b]	IC_{50} (μM)	SI[b]	IC_{50} (μM)
13	Me	Me	H	OMe	H	18.5 ± 9.6	1.7	59.2 ± 11.8	0.5	77.7 ± 5.5	0.4	30.7 ± 1.1
42a	H	H	H	OMe	H	66.0 ± 18.2	1.3	248.1 ± 54.1	0.3	132.1 ± 29.3	0.6	82.6 ± 9.5
42b	Me	H	H	OMe	H	35.9 ±11.7	1.0	156.1 ± 23.4	0.2	156.1 ± 58.5	0.2	37.1 ± 3.9
42c	H	Me	H	OMe	H	67.1 ± 31.2	0.8	128.8 ± 24.6	0.4	71.8 ± 12.5	0.7	52.7 ± 9.0
42d	Et	H	H	OMe	H	51.8 ± 9.2	0.6	45.9 ± 20.3	0.7	71.4 ± 1.1	0.4	30.0 ± 3.7
42e	H	Et	H	OMe	H	37.0 ± 0.7	1.2	45.1 ± 19.2	1.0	70.3 ± 3.7	0.6	44.4 ± 11.5
42f	Et	Et	H	OMe	H	10.4 ± 0.3	4.2	46.9 ± 5.0	0.9	36.9 ± 3.4	1.2	43.6 ± 15.1
42g	Bu	Bu	H	OMe	H	22.8 ± 8.5	1.5	29.3 ± 1.4	1.2	25.4 ± 1.1	1.4	35.3 ± 17.5
44a	Me	Me	OMe	H	H	92.5 ± 14.8	0.5	48.1 ± 18.5	1.0	179.8	0.3	48.1 ± 18.5
44b	Me	Me	H	H	OMe	88.4	0.7	37.4 ± 1.1	1.6	66.6 ± 7.4	0.9	59.2 ± 25.9
44c	Me	Me	H	Me	H	31.5 ± 7.9	1.3	39.3 ± 2.4	1.0	64.9 ± 12.6	0.6	39.3 ± 1.6
44d	Me	Me	H	H	Me	33.0 ± 3.9	1.1	40.1 ± 8.3	0.9	51.9 ± 13.8	0.7	35.4 ± 7.9
44e	Me	Me	H	H	H	50.8 ± 6.2	1.2	74.9 ± 16.6	0.8	91.6 ± 5.4	0.7	62.4 ± 6.2
44f	Me	Me	H	*i*-Pr	H	12.4 ± 3.5	0.7	18.1 ± 0.7	0.5	15.6 ± 2.8	0.6	8.9 ± 3.5
44g	Me	Me	H	H	*i*-Pr	14.2 ± 4.2	1.6	19.1 ± 1.1	1.1	21.2 ± 7.1	1.0	22.0 ± 7.2
44h	Me	Me	H	*n*-Pen	H	6.4 ± 0.3	2.0	16.4 ± 0.3	0.8	16.8 ± 1.9	0.8	12.9 ± 3.2
Benznidazole						19.2 ± 7.7	3.9					74.7 ± 9.1
Miltefosine								13.0 ± 1.2	5.9	10.8 ± 1.5	7.1	76.6 ± 3.2

[a] Toxicity was measured on RAW cells, see Experimental for details, [b] SI, selectivity index (cytotoxicity/anti-protozoal activity).

3.3.1 Antiparasitic activity toward *T. cruzi*

Initially, the 6.6-didemethyl analogue **42a** was prepared, to see how the lack of alkyl substituents in pulchrol's B-ring would affect its antiparasitic activity. After being assayed against *T. cruzi*, compound **42a** showed to be considerably less active than pulchrol, suggesting that the methyl groups at C-6 are important for the activity, however analogue **42a** was also less cytotoxic compared to pulchrol.

Analogues with just one alkyl substituent were prepared to determine whether the antiparasitic activity would increase or decrease with respect to pulchrol. The results from the biological assays showed the 6-methyl monosubstituted enantiomers **42b** and **42c** to possess less potency than pulchrol toward *T. cruzi*, and similar results were obtained for the 6-ethyl enantiomers **42d** and **42e**. Therefore, the two alkyl substituents in the B-ring appear to be important for the antitrypanosomal activity.

To continue exploring the space availability around C-6, the methyl substituents in the B-ring were replaced with longer alkyl groups. Compound **42f** was substituted with two ethyl groups at position 6, which increased the selectivity and activity (SI 4.2, IC_{50} = 10.4 μM) compared to pulchrol. Analogue **42f** is one of the most potent compounds toward *T. cruzi* in this study. On the other hand, analogue **42g** substituted at C-6 with two butyl groups, was not as active (IC_{50} = 22.8 μM) as **42f**, indicating that around this position may exist a lipophilic pocket with limited size.

To evaluate the effects that transformations in the C-ring may produce, compounds with the methoxy group in different positions in the C-ring were prepared. Compound **44a** with the methoxy substituent at C-1 and compound **44b** with the methoxy substituent at C-3, were found to be less potent and selective than pulchrol toward *T. cruzi*. Similarly, compounds with methyl substituents at C-2 (**44c**) and C-3 (**44d**) were equipotent to each other and less potent than pulchrol (with the methoxy group at C-2), yet more potent than analogues **44a** and **44b**. In contrast, analogue **44e** (with no substituents in the C-ring) showed to be slightly less potent than **44c** and **44d**. We observed that a methyl group in position 3 (**44d**) was preferred over a methoxy group in the same position. However, the opposite was true when the methoxy group was placed in position 2 (as in pulchrol), possibly due to hydrogen bond acceptor interactions with the protein target around this position.

We also prepared analogues with bulkier and longer alkyl substituents to explore the space surrounding positions 2 and 3 in the C-ring. Compounds **44f** and **44g**, substituted with isopropyl groups at positions 2 and 3, respectively, and analogue **44h** substituted with a n-pentyl group at C-3 were prepared and assayed toward *T. cruzi*. The results obtained from the biological assays showed that compounds **44f** and **44g** were more potent than pulchrol and equipotent to analogue **42f** (the most active compound among those with transformations in the B-ring), while compound **44h** (with a n-pentyl substituent at C-2) was found to be the most active compound

in this part of our investigation (IC_{50} = 6.4 μM), showing three times higher potency than pulchrol and the positive control benznidazole. The results observed for compounds **44f**, **44g**, and **44h**, suggest that lipophilic interactions at C-2 are more important than any possible hydrogen bond interactions in which the methoxy group of pulchrol may be involved.

3.3.2 Antiparasitic activity toward *L. braziliensis*

Similar to the results obtained for *T. cruzi*, the analogue with no alkyl substituents in the B-ring (**42a**) was less potent than pulchrol towards *L. braziliensis*, and also the monomethyl enantiomers **42b** and **42c** were less active compared to pulchrol, However, the monoethyl enantiomers (**42d** and **42e**), and the 6,6-diethyl analogue (**42f**) were equipotent with pulchrol. The only compound with modifications in the B-ring that showed to be more potent than pulchrol was analogue **42g** substituted with two *n*-butyl groups at position 6 (IC_{50} = 29.3 μM).

Within the antiparasitic activity results obtained for the analogues with transformations in the C-ring, we observed that changing the position of the methoxy group (placed at position 2 in pulchrol) to C-1 and C-3 (**44a** and **44b**) produced similar results to those observed for analogues **44c** and **44d**, substituted with methyl groups at C-2 and C-3, respectively. All of the previously mentioned analogues (**44a** – **44d**) were slightly more potent than pulchrol. The analogue with no methoxy or alkyl substituents on the C-ring (compound **44e**) showed lower activity toward *L. braziliensis* compared to pulchrol. However, compounds with bulkier and longer alkyl substituents (**44f** to **44h**) were found to possess considerably higher activity than analogues substituted with methoxy groups. Analogues **44f** and **44g** substituted with isopropyl groups at C-2 and C-3, respectively and compound **44h** substituted with a n-pentyl group at C-2 were all more potent than pulchrol. Compounds **44g** and **44h** were the most interesting (IC_{50} values of 19.1 μM and 16.4 μM respectively), showing comparable bioactivity with respect to our positive control Miltefosine, albeit the selectivity indexes calculated for **44g** and **44h** were lower than that of Miltefosine.

3.3.3 Antiparasitic activity toward *L. amazonensis*

The bioactivity results toward *L. amazonensis* showed that analogues substituted with two alkyl groups at position 6 in the B-ring are more potent than compounds substituted either with just one alkyl group or two hydrogen atoms at the same position (**42a**). Analogues with longer alkyl substituents such as the 6,6-diethyl analogue **42f** and the 6,6-dibutyl analogue **42g** were more potent than pulchrol toward *L. amazonensis*.

Different from the results obtained for *T. cruzi*, we observed that the analogue with a methoxy substituent at C-3 in the C-ring (**44a**) was slightly more potent than pulchrol (**13**). In contrast, analogue **44b**, in which the methoxy substituent was placed at C-1, showed to possess considerably less potency. Analogues with methyl substituents at positions 2 and 3 (**44c** and **44d**) showed no significant differences in the antiparasitic activity compared to the analogues with methoxy substitutes in those same positions. Compound **44e**, with neither alkyl nor methoxy substituents in the C-ring was also less active than pulchrol. Similar to the results obtained for *T. cruzi* and *L. braziliensis*, the analogues substituted at positions 2 and 3 with bulkier and longer alkyl groups (**44f**, **44g** and **44h**) were more active than pulchrol.

3.4 Conclusions

In this chapter, analogues with variations in the B- and C-ring were prepared and assayed. In the B-ring there is just one position available for transformations, C-6, which has two methyl substituents in the natural product pulchrol. In this part of the investigation, we intended to evaluate the role that alkyl substituents at position 6 have on the antiparasitic activity. Therefore, we prepared analogues with no alkyl substituents at C-6 (**42a**), with just one alkyl substituent (**42b** to **42e**), and with two alkyl substituents (**42f** and **42g**).

The biological activities measured, show that the unsubstituted analogue **42a** is less potent, and the presence of alkyl substituents in the B-ring is obviously important for the antiparasitic activity. The 6-alkyl monosubstituted analogues affect parasites in different ways, the 6-methyl enantiomers **42b** and **42c** were less potent than pulchrol toward *T. cruzi* and *L. braziliensis*, while the analogue **42c** was found to be equipotent to pulchrol against *L. amazonensis*. Apparently, the methyl substituents in pulchrol's B-ring are not only important for lipophilic interactions, but they may also improve the orientation of the molecule inside the active site. The 6-ethyl enantiomers (**42d** and **42e**) were more potent than pulchrol toward the *Leishmania* parasites but still less potent toward *T. cruzi*. In contrast, the 6,6-disubtituted analogues **42f** and **42g**, with longer alkyl substituents at C-6 were more potent toward all parasites, the increase in the antileishmanial activity seems to be improved with the length of the alkyl substituents. However, for *T. cruzi* it was found that the 6,6-diethyl (**42f**) analogue is more interesting than the 6,6-dibutyl analogue (**42g**). Notably, analogue **42f** was found to be more potent and selective than the positive control Benznidazole.

To study the effect that transformations in the C-ring has on the antiparasitic activity, we have prepared and assayed an analogue with no substitutes in the C-ring with the intention to evaluate the role of the 2-methoxy group in pulchrol's activity. We have also prepared analogues with the methoxy group placed in different

positions in the C-ring, and finally analogues with alkyl substituents instead of methoxy substituents.

The low bioactivity showed by compound **44e** indicate the importance that substituents in the C-ring have for the potency. Particularly, the 2-methoxy group in pulchrol seems to have an important role possibly participating in hydrogen bond acceptor interactions with the binding site. A methoxy substituent at positions 2 or 3 was better for the antiparasitic activity than at position 1. Methyl groups instead of methoxy groups in the C-ring showed no significant differences in the biological results. On the other hand, bulkier and longer alkyl groups at positions 2 and 3 (**44f**, **44g** and **44h**) improved the antiparasitic activity considerably. Compound **44h** substituted with an n-pentyl group in C-2, was the most active compound toward *T. cruzi*. For the *Leishmania* parasites compounds **44h**, **44f** and **44g**, all showed interesting bioactivities.

Most of the changes in this part of the study where related to the lipophilicity of the compounds and their ability to participate in van der Waals interactions with the active site. Our results showed that alkyl groups are beneficial for the antiparasitic activity possibly participating in hydrophobic interactions with the active site, but also perhaps by improving the orientation of the molecules in the target protein. Anyhow, there is still very little knowledge about pulchrol's molecular targets in the trypanosomatid parasites we have studied. Further studies developed systematically would increase our understanding and provide more information about the binding sites.

4 Combined modifications

In previous chapters the antiparasitic activity of analogues of pulchrol (**13**) with variations in the A-ring, concretely transformations of the benzyl alcohol functionality of pulchrol [99]; the activity of analogues with different substituents at positions 1, 2, and 3 in the C-ring; and the activity of analogues substituted with different alkyl groups in the B-ring was discussed [101]. In this chapter, the effects that two functionalities placed in different rings may have on the antiparasitic activity will be investigated (see Figure 23). Additionally, cannabinol (**21**) and its 3-methyl analogue **48c** (see Figure 23), were prepared and assayed. Our main objective in this part is to get more information about the chemical surroundings of any active site to which pulchrol possibly binds.

Compounds with the benzo[*c*]chromene scaffold possess different kinds of biological activities [80, 81, 86, 102, 103, 104], and the effects of the natural tricyclic cannabinoids are probably the most studied. Cannabinoids with the benzochromene scaffold are found together with Δ^9-tetrahydrocannabinol (THC, **6**, see Figure 1) in the leaves of *C. sativa*. THC is the compound responsible for the psychotropic effect experienced by *C. sativa* consumers, this effect is triggered when THC binds to the cannabinoid receptor CB1 which is mainly expressed in the brain cells. In contrast to THC, the natural benzo[*c*]chromene cannabinol (**21**), which possesses the same skeleton as pulchrol, has higher affinity for CB2, another cannabinoid receptor, which has been reported not to produce psychotropic effects [85, 87, 102, 104, 105, 106].

Structure-activity relationship studies have revealed that hydroxyl groups at C1 and C1', with bulky alkyl substituents at C-3 are important for the CB1 affinity [106, 107], whereas bulky substituents at C-2 and a lactone in the B-ring are beneficial for the affinity to CB2 receptors [104, 107].

Cannabinoids with the benzo[*c*]chromene scaffold have also been shown to possess immunomodulatory properties [87, 108, 109] and to inhibit keratinocyte proliferation, which makes them interesting for treating psoriasis [110]. They were also found to possess some antinociceptive properties [108], antineoplastic activity on Lewis lung tumours [103], and antibacterial activity [102].

4.1 Modification on the A-, B- and C- rings

Analogues of pulchrol with a combination of two modifications in the A-, B, and C-rings (See Figure 23) were prepared. In order to do this, the synthetic approach previously reported in this investigation [66, 99] was utilized.

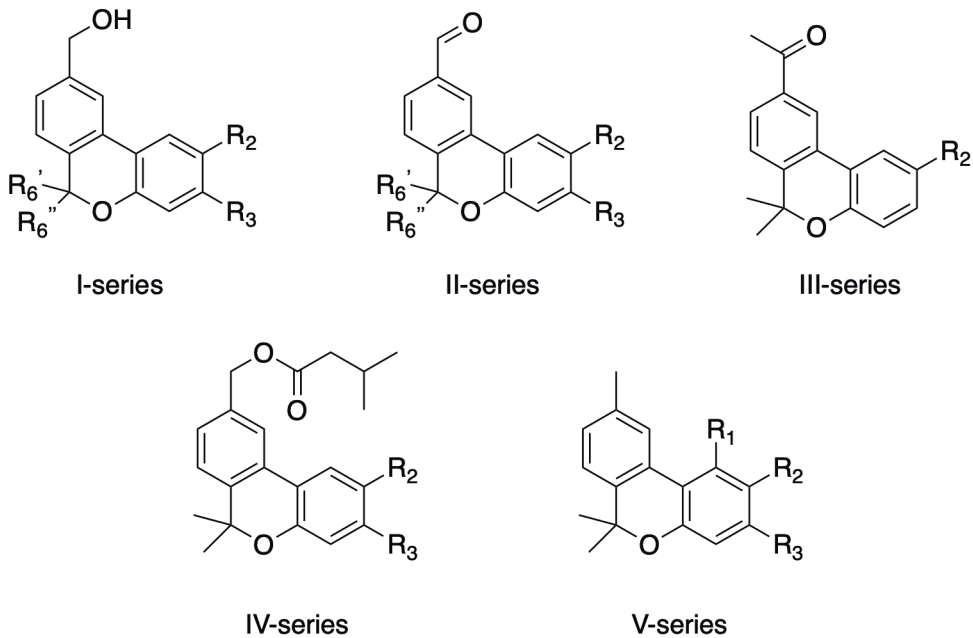

Figure 23

Series of the analogues with modification in the A-, B- and C-rings. *I-series*: **13**, R_2 = OMe, R_3 = H, R_6' = Me, R_6'' = Me; **44f**, R_2 = *i*-Pr , R_3 = H, R_6' = Me, R_6'' = Me; **44g**, R_2 = H, R_3 = *i*-Pr, R_6' = Me, R_6'' = Me; **42c**, R_2 = OMe, R_3 = H, R_6' = Me, R_6'' = H; **42b**, R_2 = OMe, R_3 = H, R_6' = H, R_6'' = Me. *II-series*: **37a**, R_2 = OMe, R_3 = H, R_6' = Me, R_6'' = Me; **45a**, R_2 = *i*-Pr, R_3 = H, R_6' = Me, R_6'' = Me; **45b**, R_2 = H, R_3 = *i*-Pr, R_6' = Me, R_6'' = Me; **45c**, R_2 = OMe, R_3 = H, R_6' = Me, R_6'' = H; **45d**, R_2 = OMe, R_3 = H, R_6' = H, R_6'' = Me. *III-series*: **37b**, R_2 = OMe; **46a**, R_2 = *i*-Pr. *IV-series*: **36e**, R_2 = OMe, R_3 = H; **47a**, R_2 = *i*-Pr, R_3 = H; **47b**, R_2 = H, R_3 = *i*-Pr. *V-series*: **35a**, R_1 = H, R_2 = OMe, R_3 = H; **20**, R_1 = H, R_2 = OH, R_3 = H; **48a**, R_1 = H, R_2 = *i*-Pr, R_3 = H; **48b**, R_1 = H, R_2 = H, R_3 = *i*-Pr; **48c**, R_1 = OH, R_2 = H, R_3 = Me; **21**, R_1 = OH, R_2 = H, R_3 = *n*-Pentyl.

The compounds belonging to the **I**-series were previously discussed, and here were used as precursors to prepare the analogues of the **II**-, **III**-, **IV**- and **V**-series. These series contain analogues with transformations in the B- or C-rings combined with different functionalities in the A-ring, such as 1'-aldehyde (**II**-series), 1'-methyl ketone (**III**-series), 3-methylbutanoic acid ester (**IV**-series) and 9-methyl (**V**-series) (See Figure 23). Additionally, cannabinol (**21**) and its analogue **48c** were obtained through iodine-mediated deconstructive annulation in a one-pot synthesis, using citral and resorcinol analogues as starting material [111]. All the molecules prepared in this part of the study were assayed in vitro toward *T. cruzi* epimastigotes, as well as *L. braziliensis* and *L. amazonensis* promastigotes (See Table 3). The

biological activity data obtained were compared with the bioactivity reported earlier for the compounds used as precursors here (**I**-series). Comparisons with the previously reported compounds **37a** (pulchral), **37b**, **36e**, and **35a** [99], which are related to the analogues prepared for this chapter, are discussed as well. As before, the cytotoxicity of the analogues in murine macrophage cells (RAW) was also determined, and the selectivity index (SI) as the ratio between the cytotoxicity and the antiparasitic activity was calculated.

Table 3
Antileishmanial, antitrypanozomal and cytotoxic activity of the pulchrol analogues, compared to the positive controls Benznidazole and Miltefosine. See Paper 3 for the experimental details.

Serie	Structure	Mol.	R1	R2	R3	R6'	R6''	*T. cruzi*		*L. braziliensis*		*L. amazonensis*		Cytotoxicity
								IC_{50} (μM)	SI[b]	IC_{50} (μM)	SI[b]	IC_{50} (μM)	SI[b]	IC_{50} (μM)
I	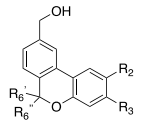	**13**	H	OMe	H	Me	Me	18.5 ± 9.6	1.7	59.2 ± 11.8	0.5	77.7 ± 5.5	0.4	30.7 ± 1.1
		44f	H	*i*-Pr	H	Me	Me	12.4 ± 3.5	0.7	18.1 ± 0.7	0.5	15.6 ± 2.8	0.6	8.9 ± 3.5
		44g	H	H	*i*-Pr	Me	Me	14.2 ± 4.2	1.6	19.1 ± 1.1	1.1	21.2 ± 7.1	1.0	22.0 ± 7.2
		42b	H	OMe	H	Me	H	35.9 ±11.7	1.0	156.1 ± 23.4	0.2	156.1 ± 58.5	0.2	37.1 ± 3.9
		42c	H	OMe	H	H	Me	67.1 ± 31.2	0.8	128.8 ± 24.6	0.4	71.8 ± 12.5	0.7	52.7 ± 9.0
II	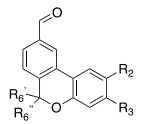	**37a**	H	OMe	H	Me	Me	24.2 ± 4.1	1.6	24.2 ± 7.5	1.6	29.8 ± 11.2	1.3	38.8 ± 3.7
		45a	H	*i*-Pr	H	Me	Me	10.7 ± 4.3	2.0	12.1 ± 4.6	1.8	11.4 ± 3.6	1.9	21.4 ± 5.4
		45b	H	H	*i*-Pr	Me	Me	7.1 ± 1.4	3.5	17.8 ± 1.8	1.4	17.8 ± 0.7	1.4	25.0 ± 7.1
		45c	H	OMe	H	Me	H	125.8 ± 7.9	0.2	70.8 ± 19.7	0.3	44.0 ± 1.6	0.5	20.4 ± 5.5
		45d	H	OMe	H	H	Me	170.3 ± 7.9	0.2	118.0 ± 0.8	0.3	80.6 ± 4.7	0.4	35.4 ± 2.8
II	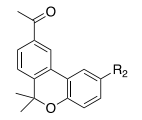	**37b**	H	OMe	H	Me	Me	21.2 ± 9.2	1.5	28.3 ± 7.1	1.1	43.2 ± 8.2	0.7	31.9 ± 7.1
		46	H	*i*-Pr	H	Me	Me	3.4 ± 0.2	2.2	8.8 ± 1.0	0.8	9.5 ± 4.1	0.8	7.5 ± 2.0
IV	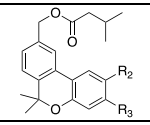	**36e**	H	OMe	H	Me	Me	4.2 ± 1.1	6.7	13.1 ± 0.4	2.2	14.5 ± 0.1	1.9	28.2 ± 9.0
		47a	H	*i*-Pr	H	Me	Me	10.9 ± 3.8	1.6	272.9 ±0.00	0.1	25.9 ± 5.5	0.7	17.2 ± 5.5
		47b	H	H	*i*-Pr	Me	Me	13.6 ± 5.7	3.1	63.3 ± 4.4	0.7	43.7 ± 8.2	1.0	42.0 ± 2.7
V	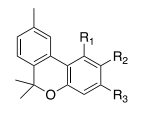	**35a**	H	OMe	H	Me	Me	51.1 ± 17.7	2.0	69.6 ± 5.9	1.4	85.3 ± 5.9	1.2	99.5 ± 22.0
		20	H	OH	H	Me	Me	54.9 ± 0.2	0.5	30.4 ± 2.9	0.8	33.3 ± 5.4	0.8	25.0 ± 8.3
		48a	H	*i*-Pr	H	Me	Me	23.7 ± 8.6	1.8	49.2 ± 15.0	0.9	49.6 ± 4.5	0.9	42.8 ± 18.8
		48b	H	H	*i*-Pr	Me	Me	50.3 ± 11.3	2.1	311.6 ± 50.3	0.3	236.5 ± 48.8	0.4	105.1 ± 26.1
		48c	OH	H	Me	Me	Me	5.9 ± 2.0	4.1	15.7 ± 5.1	1.6	21.2 ± 2.4	1.1	24.4 ± 4.7
		21	OH	H	*n*-Pen	Me	Me	7.4 ± 0.6	2.2	10.3 ± 0.6	1.6	14.2 ± 1.3	1.1	16.1 ± 1.0
		Benznidasole						19.2 ± 7.7	3.9					74.7 ± 9.1
		Miltefosine								13.0 ± 1.2	5.9	10.8 ± 1.5	7.1	76.6 ± 3.2

[a] Toxicity was measured on RAW cells, see Experimental for details, [b] SI, selectivity index (cytotoxicity/anti-protozoal activity).

4.2 Antiparasitic activity and selected functionalities

As mentioned earlier, the natural products pulchrol (**13**) and pulchral (**37a**) have been studied in the past and both were active against *Trypanosoma* and *Leishmania* parasites. In previous chapters we have discussed the effect that individual transformations in the A-, B-, and C-rings have in the antiparasitic activity [99, 101]. We concluded that the benzyl alcohol functionality was important for pulchrol's activity possibly acting as a hydrogen bond acceptor, and that 1'-carbonyl analogues were active toward *Leishmania* species but not so much toward *T. cruzi*. The 9-methyl analogues were considerably less active than pulchrol, while the ester analogues showed higher potency than pulchrol, particularly when substituted with long and branched alkyl groups [99]. The modifications in the B- and C- rings were focused on variations in the lipophilicity and their effect on the antiparasitic activity. A preference for 6,6-dialkyl analogues was established, while longer and branched alkyl substituents in the C-ring increased the antiparasitic activity [101].

The analogues presented in this part of our investigation have in most cases transformations in the A- and C- rings, while a pair have transformations in the A- and B-rings. The functionalities evaluated in the A-ring are the 1'-aldehyde, the 3-methyl butanoic acid ester and the 9-methyl substituent. They were combined with isopropyl substituents at positions 2 and 3 in the C-ring (**45a** and **45b**; **47a** and **47b**; and **48a** and **48b** respectively), to investigate the effect on the antiparasitic activity. The effects of 1'-carbonyl analogues substituted with an isopropyl group at C-2, were further evaluated using the 1'-methyl ketone analogue **46**. The effects of the 9-methyl group with the more polar hydroxy functionality (analogue **20**, also found in nature) were evaluated. We also added to our study the natural compound cannabinol (**21**) and its analogue **48c** substituted with a 9-methyl group in the A-ring, a hydroxyl group at C-1 and an alkyl group at C-3 in the C-ring. Cannabinol (**21**) is substituted with a *n*-pentyl group at C-3 while analogue **48c** has a methyl group in this position. Finally, the effect of combining a 1'-aldehyde functionality with a 6-monomethyl substituent in the B-ring was also analysed by the testing of enantiomers **45c** and **45d** [101].

4.2.1 Antiparasitic activity toward *T. cruzi*

Previously (Paper 1 and 2), we observed that modifying the benzyl alcohol in pulchrol to a 1'-carbonyl functionality resulted only in a small effect on the antitrypanosomal activity (**13**, IC50 = 18.5μM; **37a**, IC50 = 24.2 μM; and **37b**, IC50 = 21.2 μM), and that replacing the methoxy group in pulchrol's C-ring for an isopropyl group either at position 2 or 3 was beneficial for the activity (**44f**, IC50 = 12.4 μM and **44g**, IC50 = 14.2 μM respectively) [99]. For this part of the study, we

prepared analogues with combinations between the 1'-carbonyl functionality in the A-ring and an isopropyl substituent at the C-ring's C-2 or C-3, these analogues were considerably more active and selective (**45a**, IC50 = 10.7 μM, SI = 2.0; and **45b**, IC50 = 7.1 μM, SI = 3.5) compared to their corresponding benzyl alcohols **44f** and **44g**, which biological activities were reported earlier [101] (see also Table 3). A change in the orientation inside the target may produce this improvement in the antitrypanosomal activity, resulting in stronger hydrophobic interactions for the isopropyl analogue. The analogue **46**, also with an isopropyl group at C-2 but with a methyl ketone functionality in the A-ring, was more active than the aldehyde **45a**, and it was the most potent compound toward *T. cruzi* in this investigation (IC50 = 3.4 μM, SI = 2.2), being 6 times more active than the positive control (Benznidazole, IC50 = 19.2 μM).

Contrary to the **II**- and **III**-series, compounds in the **IV**-series, substituted with a 3-methylbutanoic acid ester and an isopropyl group at either position 2 or 3, were less potent against *T. cruzi* (**47a**, IC50 = 10.9 μM, SI = 1.6; **47b**, IC50 = 13.6 μM, SI = 3.1) compared to the ester **36e** substituted with a methoxy group at C-2 (IC50 = 4.2 μM, SI = 6.7) [99].

The compounds belonging to the **V**-series have a 9-methyl substituent in the A-ring and different substituents in the C-ring. In chapter 2 we mentioned that compound **35a** (substituted with a methoxy group at C-2 in the C-ring) was less potent than pulchrol (IC_{50} = 51.1 μM) [99]. Here we replaced the methoxy substituent in **35a** by a hydroxyl group to obtain analogue **20** (also a natural product) which activity was comparable (IC_{50} = 54.9 μM) to that of pulchrol. We understand that possibly both analogues (pulchrol and **20**) interact with the binding site in the same way but in rotated positions. The analogues **48a** and **48b** substituted with isopropyl groups in C-2 and C-3 were less active than pulchrol (IC_{50} = 23.7 μM and IC_{50} = 50.3 μM respectively), while cannabinol (**21**) and its analogue **48c**, substituted with alkyl groups at C-3 and an additional hydroxyl group at C-1 were the most potent and selective of the **V**-series (**21**, IC50 = 7.4 μM, SI = 2.2; **48c**, IC50 = 5.9 μM, SI = 4.1, respectively). Cannabinol's analogue **48c** (with a methyl group at C-3) was slightly more active than cannabinol, suggesting that the size of the C-3 substituent is less important for the activity than the hydroxyl group at C-1, which possibly participates in new hydrogen bond interactions.

Finally, the enantiomer analogues substituted with one alkyl group at C-6 and an aldehyde functionality at C-1'were considerably less active (**45c**, IC_{50} = 125.8 μM; **45d**, IC_{50} = 170.3 μM) compared to pulchrol (**13**, IC_{50} = 18.5 μM) and their synthetic precursors (benzyl alcohols **42b** and **42c**) [101]. The aldehyde may produce a change in orientation, resulting in the weakening of hydrophobic interactions around position 6 in the B-ring.

4.2.2 Antiparasitic activity toward *L. braziliensis*

As mentioned earlier (Chapter 2), in contrast to the results obtained for *T.* cruzi, compounds **37a** and **37b** with a 1'-carbonyl functionality in the A-ring and a 2-methoxy group in the C-ring were considerably more potent (**37a**, IC_{50} = 24.2 μM; and **37b**, IC_{50} = 28.3 μM) than pulchrol (**13**, IC_{50} = 59.2 μM) [99]. In Chapter 3, we observed that analogues substituted with isopropyl groups at C-2 or C-3 increased the potency (**44f**, IC_{50} = 18.1 μM; and **44g**, IC_{50} = 19.1 μM) compared to pulchrol [101]. Here, we evaluated the combination of both functionalities. Analogues **45a** and **45b** with an isopropyl group at C-2 and C-3, respectively, were more potent (**45a**, IC_{50} = 12.1 μM; and **45b**, IC_{50} = 17.8 μM) than pulchrol (**13**) and their precursors **1b** and **1c**. Similar to the results obtained with *T. cruzi*, the 2-isopropyl ketone **46** was the most potent compound toward *L. braziliensis* (IC_{50} = 8.8 μM, SI = 0.8) in this investigation. Analogues **45a** and **46** are more potent than the positive control Miltefosine (IC_{50} = 13.0 μM, SI = 5.9), but their selectivity is lower.

As with *T. cruzi* the 3-methylbutanoic acid esters **47a** and **47b**, substituted with isopropyl groups at C-2 and C-3, were less potent (**47a**, IC_{50} = 272.9 μM; and **47b**, IC_{50} = 63.3 μM) than the ester analogue **36e** (IC_{50} = 13.1 μM) [99].

In chapter 2 we observed that analogue **35a** substituted with a 9-methyl group in the A-ring and a 2-methoxy substituent in the C-ring was less active (IC_{50} = 69.6 μM) than pulchrol (**13**, IC_{50} = 59.2 μM) [99]. Here, we transformed the **35a**'s methoxy substituent at C-2 into a hydroxyl substituent to obtain analogue **20**, in addition we prepared analogues **48a** and **48b** substituted with an isopropyl group at C-2 and C-3, respectively. Opposite to the results obtained with *T. cruzi*, analogues **48a** and **20** were more potent (**48a**, IC_{50} = 49.2 μM; and **20**, IC_{50} = 30.4 μM) than pulchrol (**13**) and **35a**. However, **48b** was inactive (IC_{50} = 311.6 μM) toward *L. braziliensis*, suggesting that a limit in the volume exist around position 3 in the C-ring. Cannabinol (**21**) and its analogue **48c** were more active and selective (IC_{50} = 10.3 μM, SI = 1.6 and IC_{50} = 15.7 μM, SI = 1.6, respectively) than **35a** and pulchrol (**13**). In contrast to the results observed for *T. cruzi* the longer chain in cannabinol (2**1**) was more favourable for the activity toward *L. braziliensis* than the methyl group in **48c**.

Similar to *T. cruzi*, aldehyde enantiomers **45c** and **45d** were less potent and selective (IC_{50} = 70.8 μM, SI = 0.3 and IC_{50} = 118.0 μM, SI = 0.3, respectively) than pulchrol (**13**), but more potent than their benzyl alcohol precursors **42b** and **42c** (IC_{50} = 156.1 μM and IC_{50} = 128.8 μM, respectively) [101].

4.2.3 Antiparasitic activity toward *L. amazonensis*

In Chapter 2 and 3, we observed that pulchral (**37a**) and the aldehydes with isopropyl substituents at C-2 and C-3 in the C-ring (**45a** and **45b)** were more potent

than pulchrol [99, 101]. Here, analogues **45a** and **45b** showed to benefit the activity. Similar to the results obtained for *L. braziliensis*, the aldehyde and methyl ketone analogues with an isopropyl group at C-2 showed the best activities (**45a,** IC_{50} = 11.4 μM; **46**, IC_{50} = 9.5 μM, respectively) of the compounds studied in this part of our investigation. They are both comparable with the positive control Miltefosine (IC_{50} = 10.8 μM). The ester analogues substituted with isopropyl groups at C-2 and C-3 (**47a** and **47b**) were less active and selective than **36e** (with a methoxy substituent on C-2, IC_{50} = 14.5 μM, SI = 1.9) as observed for *T. cruzi* and *L. braziliensis*. Similarly, most of the compounds from the **VI**-series were more potent than pulchrol (**13**, IC50 = 77.7 μM), the only inactive compound from this series was analogue **48b** (with an isopropyl substituent at C-3, IC_{50} = 236.5 μM). On the other hand, cannabinol was the most potent compound from the **V**-series (**21**, IC50 = 14.2 μM, SI = 1.1) followed by its analogue **48c** (IC50 = 21.2 μM, SI = 1.1). Similar to the other parasites, the 6-monomethyl aldehyde enantiomers **45c** (IC50 = 44.0 μM) and **45d** (IC50 = 80.6 μM) were less potent than the corresponding 6,6-dimethyl aldehyde **37a** (pulchral, IC50 = 29.8 μM) [99].

4.3 Conclusions

The combination of isopropyl substituents at positions 2 and 3 in the C-ring and the 1'-carbonyl functionality in the A-ring of the pulchrol scaffold was beneficial for the activity toward the three parasites studied in this investigation. However, the 3-isopropyl aldehyde analogue was more potent toward the *Leishmania* parasites than the 2-isopropyl aldehyde, while the opposite was observed for *T. cruzi*, therefore some differences may exist between the parasites binding sites. Despite that, the 2-isopropyl ketone showed the best activity toward all parasites in this chapter, suggesting that the methyl group in the ketone favours binding in the three species.

Analogues with a methylbutanoic acid ester in the A-ring combined with an isopropyl substituent at C-2 or C-3, were not as active as the ester analogues with a methoxy group at C-2. Moreover, the 2-isopropyl ester was inactive toward *L. braziliensis*, suggesting a limited space around C-2 in the binding site.

The combination of lipophilic substituents in the A- and C-rings (9-methyl and isopropyl substituents in the A- and C-rings, respectively) was unfavourable for the antiparasitic activity. The presence of substituents able to participate in hydrogen bond interactions appears to be an important factor for the activity.

Analogues with the methoxy or hydroxyl functionalities at C-2 combined with a 9-methyl functionality in the A-ring produced different effects for the different parasites. For *T. cruzi*, both analogues were equipotent, but less active than pulchrol. A rotation of the molecules may enable the methoxy and hydroxy groups at C-2 to

bind in the same position as the benzylic alcohol in pulchrol does, however the interaction is weaker. A similar situation may occur for the *Leishmania* species, but instead of weaker interactions stronger ones are produced, increasing the potency of the 2-methoxy and 2-hydroxyl analogues.

A different sort of combination, which includes the 9-methyl functionality in the A-ring, a hydroxy group at C-1 and an alkyl group at C-3 (like in cannabinol, **21**) is favourable for the antiparasitic activity and selectivity. A hydroxyl substituent at position 1 in the C-ring seems to help enhance the antiparasitic activity.

Finally, the combination of a 1'-aldehyde functionality with the 6-monomethyl substituted enantiomers seems to generate an unfavourable change in orientation in the binding site of the *T. cruzi* and *L. braziliensis* parasites. For *L. amazonensis*, the enantiomers showed different results. The bioactivity showed by one of them was comparable with its benzyl alcohol precursor and pulchrol, while the other enantiomer was slightly more potent.

5 Pharmacophore design and qualitative evaluation of predicted ADME-descriptors

Several computational tools used in drug design have contributed to the understanding of the bioactivity of different ligands, and have helped reducing the time and costs spent in the development of new drugs [112]. Among these tools, ligand-based pharmacophore modeling is important for assisting in drug discovery if no macromolecular target structure is available [112-114].

A pharmacophore model is an abstract 3D representation of common steric and electronic features shared by a set of active molecules that presumably interact with a specific biological target [112, 113, 115]. Pharmacophore models are defined by features capable of interaction with biological targets. Hydrogen bond donors, hydrogen bond acceptors, aromatic rings, hydrophobic centers and electrostatic groups are the most common features taken into account in pharmacophore development [112-114, 116]. The relationship of those features in the space is defined by the pharmacophore, which can also make use of exclusion volume constraints to further define the space around the ligands [114, 116].

The common pharmacophore features are identified by aligning low-energy conformers and establishing the better overlay of features [112-114]. Nonetheless, the conformation that the ligand adopts when is bound to the target is in reality unknown. Therefore, it is necessary to assume that the low-energy conformations used will resemble that of the bound ligand [113].

Several software applications can be used for developing pharmacophore models. Here, we used the PHASE module from the Schrödinger suit for the development of pharmacophore hypotheses.

PHASE uses an exhaustive partitioning algorithm to cluster conformers into multiple k-point pharmacophores grouped by feature similarity. The common pharmacophores are identified using a binary decision tree that groups pharmacophores with similar inter-site distances. The pharmacophores are further classified after alignment with each other to reveal poor superpositions. The quality of the alignment is measured by the root-mean-square deviation (RMSD) of the position of each feature and the average cosine of the angles formed by the

corresponding pairs of vector features. After this process, PHASE select one model as the pharmacophore hypothesis [117-119].

The study of structure-activity relationships and the analysis of the spatial distribution of pharmacophoric features are important for understanding possible binding interactions with a protein target. However, it is also important to assess the pharmacokinetic characteristics of the ligands to evaluate their potential as orally administered drugs.

The oral availability of a drug can be evaluated analysing pharmacologically-relevant descriptors predicted *in silico*. Here, we have used QikProp from the Schrödinger suit to predict several descriptors.

The absorption, distribution, metabolism, excretion and toxicity (ADMET) can be evaluated considering the Lipinski's "Rule of 5," The Jorgensen's "Rule of three," and other predicted properties related to the ability of ligands to cross membranes or interact with certain targets.

Lipinski's "Rule of 5" can be used as a guideline to predict which ligands may be orally active, if the ligand complies with at least three of the rules is considered a substance with potential for oral administration. As stated by Lipinski compounds with molecular weight lower than 500 Da, less than five hydrogen bonds donors (HBD < 5), less than 10 hydrogen bond acceptors (HBD < 10), and octanol/water partition coefficient values below 5 (log P < 5) are probably orally absorbed [120].

Jorgensen's "rule of three" is also used to predict the oral availability of drugs, Jorgensen considers the predicted aqueous solubility (QPlogS > -5.7), the predicted apparent Caco-2 cell permeability (QPPCaco > 22 nm/s) and the number of likely metabolic reactions the drug may experience (#metabol < 7) [121 -123].

An overall ADME-compliance descriptor (#star), calculated by QikProp, can also be used to assess the pharmacokinetic profile of drugs. The #star descriptor considers the molecular weight, the dipole moment, the ionization potential, the electron affinity, the total solvent accessible area (and its components), the polar surface area, the total solvent accessible volume, the number of rotatable bonds, the number of hydrogen bond donors and hydrogen bond acceptors, the globularity, the polarizability, the hexadecane/gas partition coefficient, the octanol/gas partition coefficient, the octanol/water partition coefficient, the aqueous solubility, the predicted binding to human serum albumin, the brain/blood partition coefficient, and the number of likely metabolic reactions. The #star parameter is measured on a scale from 0 to 5, where 0 is the value for the most drug-like compound and 5 for the least drug-like compound [122-126].

QikProp also calculates the predicted central nervous activity (CNS), and the predicted IC_{50} value for the blockage of HERG k^+ channels.

In this part the study a pharmacophore hypothesis for *T. cruzi* generated in PHASE (Schrödinger, 2021-1) is presented, as well as the qualitative evaluation of ADMET-predicted values calculated by QikProp (Schrödinger, 2021-1).

5.1 Development of pharmacophore hypotheses

In previous chapters wed discussed the effects that modifications on the pulchrol scaffold have on the antiparasitic activity towards *T. cruzi*, *L. braziliensis* and *L. amazonensis* [99, 101, 127].

In this part of the investigation a pharmacophore hypothesis is presented. The antiparasitic activity data obtained for 54 of the ligands prepared in this study were used for developing several pharmacophore models. The main pharmacophoric features recognized by the PHASE algorithm were two hydrogen bond acceptors and three hydrophobic sites. Features common to all analogues (A, B and C-ring centroids) were excluded from the calculations. The features recognized by PHASE were present in most of the active and some inactive ligands, therefore excluded volumes were generated to identify regions around the ligand where clashing with the binding site could explain low bioactivity.

Different scores were calculated to evaluate the pharmacophore models. The PhaseHypo score, which combines the BEDROC (Boltzmann-Enhanced Discrimination of Receiver Operating Characteristics) score and the survival score, was used to rank the pharmacophore models (see Eq. 2 in Paper 4). In turn, the survival score combines the vector score, site score, volume score, selectivity score, inactive score and the number of matches (see Eq. 3 in Paper 4).

The vector, site and volume scores measure how well the ligands are aligned to the model in terms of directionality, root-mean-deviation of inter-site distances, and volume overlap. The selectivity score estimates the uniqueness of the model toward active ligands, and the inactive score estimates how well inactive ligands match the model. The BEDROC score measures the extent to which the hypothesis extracts active ligands from a diverse set of 1000 drug-like decoys. Finally, the fitness score evaluates how well each ligand align to the model.

The scores were used to evaluate pharmacophore models generated for *T. cruzi*, *L. braziliensis* and *L. amazonensis*. Nine to ten models were obtained for each parasite, the top ranked models were selected for further analysis. The fitness scores showed that pharmacophore hypotheses developed for *L. braziliensis* and *L. amazonensis* did not explain the activity of the ligands accurately. However, the pharmacophore generated for *T. cruzi* showed fitness scores values in accordance with the activity of the ligands. Consequently, the pharmacophore hypothesis developed for *T. cruzi* is the only model showed in this chapter.

5.1.1 Pharmacophore hypothesis for *T. cruzi*

The score values calculated by PHASE for the five top ranked pharmacophore hypotheses developed for *T. cruzi* are shown in Table 4.

Table 4
Scoring results

Hypothesis	SuS[a]	SS[b]	VeS[c]	VS[d]	SeS[e]	NM[f]	IS[g]	BS[h]	PHS[i]
AAHHH_2	5.7257	0.8780	0.9766	0.7985	1.7109	23	2.3271	0.8823	1.226
AAHHH_1	5.7277	0.8832	0.9846	0.7873	1.7109	23	2.3219	0.8817	1.225
AAHHH_3	5.7010	0.8715	0.9643	0.8025	1.7010	23	2.3116	0.8829	1.225
AAHHH_6	5.6795	0.8774	0.9791	0.7657	1.6956	23	2.2873	0.8829	1.224
AAHHH_9	5.3596	0.6134	0.9642	0.7284	1.6919	23	2.2604	0.8772	1.199

[a] Survival score, [b] Site score, [c] Vector score, [d] Volume score, [e] Selectivity score, [f] number of matches, [g] Inactive score, [h] BEDROC score, [i] PhaseHypo score.

The inter-site distances and angles for the highest ranked hypothesis (AAHHH_2) are shown in Paper 4 (See Table 2) and the shape of the pharmacophore is shown in Figure 24.

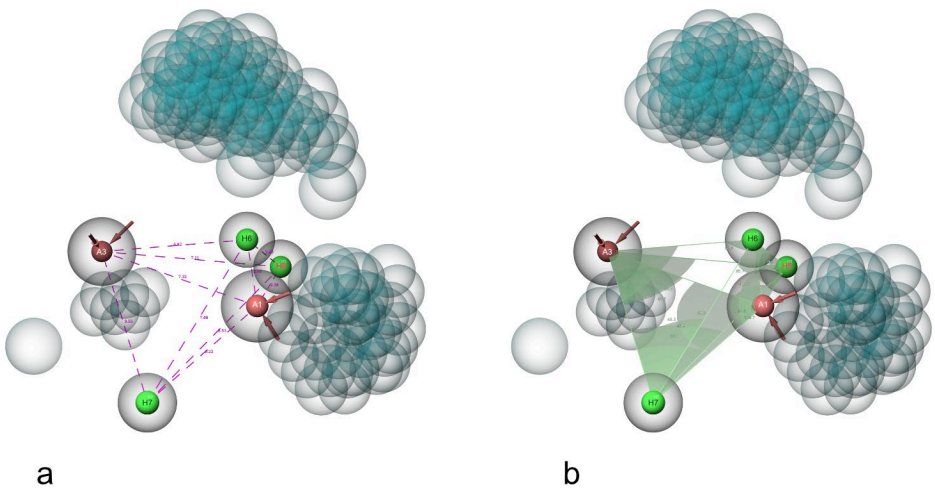

Figure 24
Pharmacophore hypothesis for *T. cruzi* (AAHHH_2). a) inter-site distances, b) inter-site angles

Related to pulchrol's activity, 27 ligands were considered active and 27 inactive, out of them 50 ligands aligned with AAHHH_2.

The excluded volumes were generated near C-6, and also close to the hydrogen bond acceptor sites (see Figure 24). The fitness scores for each ligand are shown in Table 5.

Table 5
Ligand scores for AAHHH_2

Mol	Structure	Activity[a]	Role	FS[b]	Mol	Structure	Activity[a]	Role	FS[b]
A-series					**E-series**				
13	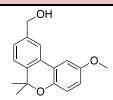	18.50	active	2.6122	**42a**	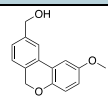	66.04	inactive	2.0377
35a	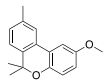	51.11	inactive	2.3511	**42b**	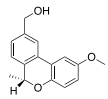	35.90	inactive	2.2431
35b	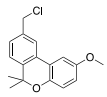	38.09	inactive	2.3783	**42c**	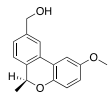	67.11	inactive	2.3732
35c	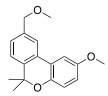	24.62	inactive	2.8315	**42d**	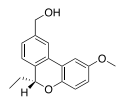	36.99	inactive	2.2572
35d	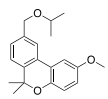	12.80	active	2.9266	**42e**	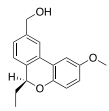	51.79	inactive	2.1936
35e	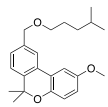	9.08	active	2.8237	**42f**	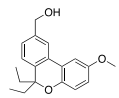	10.39	active	2.4039
35f	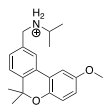	70.64	inactive	2.3624	**42g**	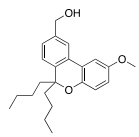	22.85	inactive	2.0281
35g	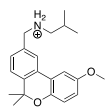	15.36	None	*	**45c**	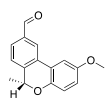	125.84	inactive	2.2288
35h	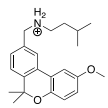	5.89	None	*	**45d**	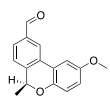	170.28	inactive	2.2326
B-series					**F-series**				
36a	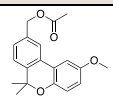	14.41	active	2.9512	**44a**	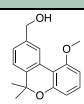	92.48	inactive	2.1944

36b	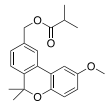	8.81	active	2.9518
36c	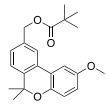	6.49	active	2.9481
36d	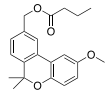	16.16	None	3.0000
36e	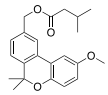	4.23	active	2.7896
36f	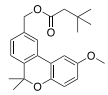	5.70	active	2.8770
36g	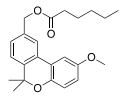	22.80	inactive	2.8537
36h	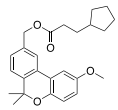	8.36	active	2.5886
36i	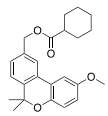	13.14	active	2.6695
36j	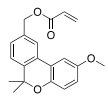	7.40	active	2.9401
36k	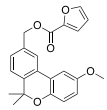	3.84	active	2.9057
36l	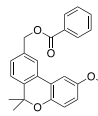	5.88	active	2.8945
C-series				
37a	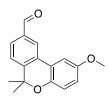	24.23	inactive	2.5657
37b	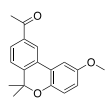	21.25	inactive	2.5572
44b	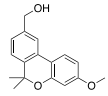	88.41	inactive	2.5229
44c		31.46	inactive	2.3457
44d		33.03	inactive	2.1414
44e		50.77	inactive	2.2084
44h	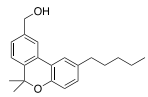	6.44	active	2.1978
G-series				
44f	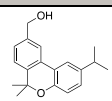	12.39	active	2.5270
45a	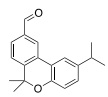	10.70	active	2.5140
46	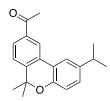	3.40	active	2.5006
47a	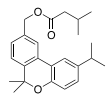	10.91	active	2.6385
48a	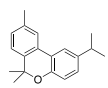	23.65	inactive	2.2265
H-series				
44g	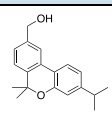	14.17	active	2.3008
45b	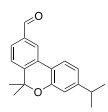	7.13	active	2.0808
47b	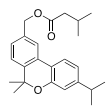	13.64	active	2.3253

37c	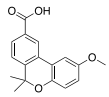	56.28	inactive	2.3696	**48b**	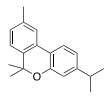	50.30	inactive	2.1138
					I-series				
37d	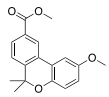	31.84	inactive	2.5538	**20**	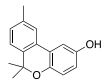	54.93	inactive	1.4595
37e	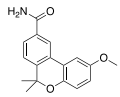	134.47	inactive	2.6114	**48c**		5.90	None	*
D-series									
38	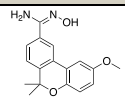	33.42	inactive	2.5912	**21**	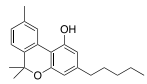	7.41	None	*

[a] Activity measured in μM, [b] Fitness score, and [*] Ligands which did not align to the model

The ester **36d** was the reference ligand and had the highest fitness score (FS = 3). Ligand **48c** and natural product **21** (cannabinol) aligned poorly with the model despite their potency, while natural product **20** (didehydroconicol) with low activity toward *T. cruzi*, showed the lowest fitness score (FS = 1. 4595).

Most of the inactive analogues showed low fitness scores. Analogues from the **E**-series, which had the absence of hydrophobic features H5 or H6 showed low fitness scores. Analogue **42g** with longer alkyl substituents on C-6 aligned with H5 and H6, however, the alkyl substituents appear to clash with the excluded volumes. The only compound from the **E**-series to show good alignment and no clashing was **42f**, substituted with two ethyl groups at C-6. The absence of substituents capable of aligning with feature H7 (C-ring) was also observed in the low scores calculated for **44e** and **44a**. Similarly, analogues without HBA in the A-ring showed low fitness scores. Figure 25 shows the alignment of inactive ligands **35a**, **42a**, **42c**, **45e**, and **44a**.

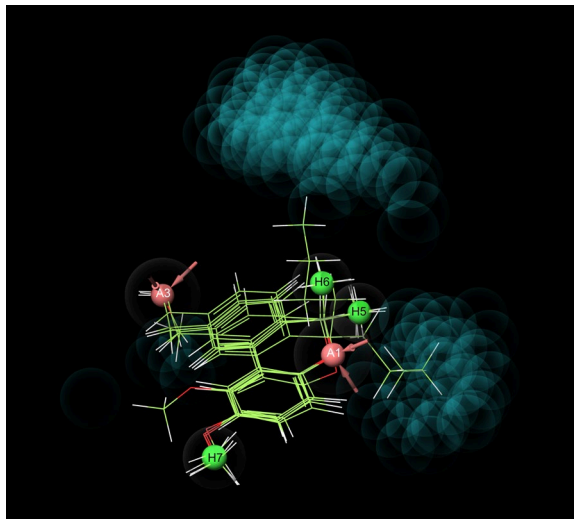

Figure 25
Inactive ligands **35a**, **42a**, **42c**, **45d**, and **44a** aligned to AAHHH_2

The esters from the **B**-series showed the best alignments along with ethers **35c**, **35d**, and **35e**, however, analogue **35c** was not active. Active ligands from the **G**-series had moderately good fitness scores and inactive analogue **48a** fit the model poorly. In contrast, amines **35g** and **35h** did not align well with the model in spite of their activity. Figure 26 shows the alignment of active ligands **13** (pulchrol), **36e**, **42f**, **44h**, and **46**.

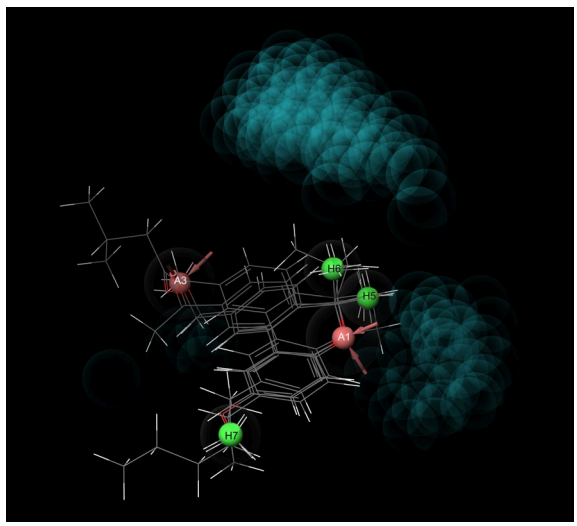

Figure 26
Active ligands **13**, **36e**, **42f**, **44h**, and **46** aligned to AAHHH_2

5.2 Qualitative analysis of ADMET-descriptors

The pharmacokinetic properties of all ligands in this investigation were evaluated using the 51 parameters predicted by QikProp (Schrödinger, 2021-1). The most relevant ADMET-descriptors are discussed below. A description of the parameters and their recommended range of values are presented in Table 6 [121-123].

Table 6
Description of the parameters predicted by QikProp used in this study

Descriptor	Description	Range a
#star [b]	Number of descriptor values that fall outside the 95% range of similar values for known drugs. A large number of stars suggest that a molecule is less drug-like than molecules with few stars.	0 - 5
SASA	Total solvent accessible surface area (Å^2) using a probe with 1.4 Å radius	300 - 1000
PSA	Van der Waals surface area (Å^2)	7 to 200
QPpolarz	Predicted polarizability (Å^3)	13 - 70
Lipinski's rule of 5	Number of violations of Lipinski's rule of five (Lipinski)	Maximum 4
MW	Molecular weight	130 - 725
DonorHB	Estimated number of hydrogen bonds that would be donated by the solute to water molecules in aqueous solutions.	0 - 6
AcceptorHB	Estimated number of hydrogen bonds that would be accepted by the solute to water molecules in aqueous solutions.	2 - 20
QPlogPo/w	Predicted octanol/water partition coefficient	-2 - 6.5
Rule of three	Number of violations of Jorgensen's rule of three.	Maximum 3
QPlogS	Predicted aqueous solubility	-6.5 - 0.5
QPPCaco	Predicted apparent Caco-2 cell permeability (nm/s) for non-active transport.	< 25 poor; > 500 great
#metabol	Number of likely metabolic reactions	1 - 8
#rotor	Number of non-trivial (not CX3), non-hindered (not alkene, amide, small ring) rotatable bonds.	0 - 15
Human Oral Absorption	Predicted qualitative human oral absorption. [c]	1 = low, 2 = medium, 3 = high
QPlogKhsa	Prediction of binding to human serum albumin	-1.5 – 1-5
QPlogBB	for orally delivered drugs.	-3.0 - 1.2
CNS	Predicted central nervous activity on a -2 (inactive) to +2 (active) scale.	-2 - +2
QPlogHERG	Predicted IC_{50} value for blockage of HERG K^+ channels	Concern below -5

[a] Recommended value for 95% of known drugs, [b] Descriptors included in #stars: Molecular weight, dipole moment, ionization potential, electron affinity, total solvent accessible area; hydrophobic, hydrophilic, π and weakly polar components of the SASA, polar surface area , total solvent accessible volume, number or rotatable bonds, hydrogen bond donors, hydrogen bond acceptors, globularity, polarizability, hexadecane/gas partition coefficient, octanol/gas partition coefficient, octanol/water partition coefficient, aqueous solubility, binding to human serum albumin, brain/blood partition coefficient, number of likely metabolic reactions.

The "#star" descriptor considers 29 other descriptors (see Table 6) and can be used to qualify the pharmacokinetic quality of the ligands. A distribution plot of the #star descriptor (see Figure 27a) shows that most of the compounds have #star values equal to 0 or 1. Few compounds may not be able to be orally absorbed according to de #star descriptor, among those, analogues with methyl substituents at position 9 in the A-ring (**35a**, **48a**, **48b**, **20**, and **48c**), chlorinated analogue **35b**, ester analogue **36h**, and the ether **35e**.

Parameters such as the total solvent accessible area (SASA), the total solvent-accessible volume, the globularity, the polar surface (PSA) and the predicted polarizability (QPpolrz) were inside the QikProp's recommended range of values for all ligands.

Most of the ligands complied with all Lipinski's rules [120]. All the molecular weight values were below 500 Da, none of the molecules had more than 5 HBD nor more 10 HBA, but 30% of the ligands had log *P* values above 5 (see Figure 27b). Log *P* values below 5 indicate a favourable hydrophilic/hydrophobic balance necessary in pharmacokinetics. Unfavourable effects such as an inability to cross cell membranes, binding to plasma protein and fast excretion may be observed in very hydrophilic compounds. Similarly, too hydrophobic ligands may be poorly absorbed if they get dissolved in fat globules inside the gut.

Over 60% of the ligands followed the Jorgensen's rule. The values for permeability of the Caco-2 cells and the number of likely metabolic reactions were inside the threshold recommended by Jorgensen for all compounds. The predicted water solubility values (QPlogS), in contrast, were below -5.7 for 37% of the compounds (See Figure 27c) [121, 123].

Molecular flexibility is another factor that may affect oral absorption and reduce the selectivity of the ligand. The presence of no more than 7 rotatable bonds is recommended for good oral absorption [128]. Among the 54 ligands studied here, just four molecules had more than 7 rotatable bonds (see Figure 27d). A parameter defined as "human oral absorption" by QikProp (see Table 6) showed that 72% of the ligands may have good oral absorption.

The predicted serum albumin binding ability (logKhsa) for all ligands was in the recommended range of values, indicating that the compounds are likely to circulate freely within the blood stream and access to the target site in sufficient amounts.

The blood-brain barrier partition coefficient (QPlogBB) values for all ligands were inside QikProp's recommended range of values (see Table 6 and Figure 27e). However, other authors state that compounds with QPlogBB values greater than 0.3 will penetrate the blood-brain barrier; compounds with QPlogBB values between -1 and 0.3 may still pass the blood-brain barrier; and compounds with QPlogBB below -1 will not penetrate the blood-brain barrier [129].

Considering the abovementioned ranges, five ligands would penetrate the brain-blood barrier, while 49 ligands would have less permeability, but maybe, still pass through the blood brain barrier. A "central nervous system" descriptor (CNS) was also predicted, according to the recommended values (see Table 6) most ligands (80%) were not active neither inactive (CNS = 0), 9 compounds were likely to be active (CNS > 0) and 2 compounds were likely to be inactive (CNS < 0).

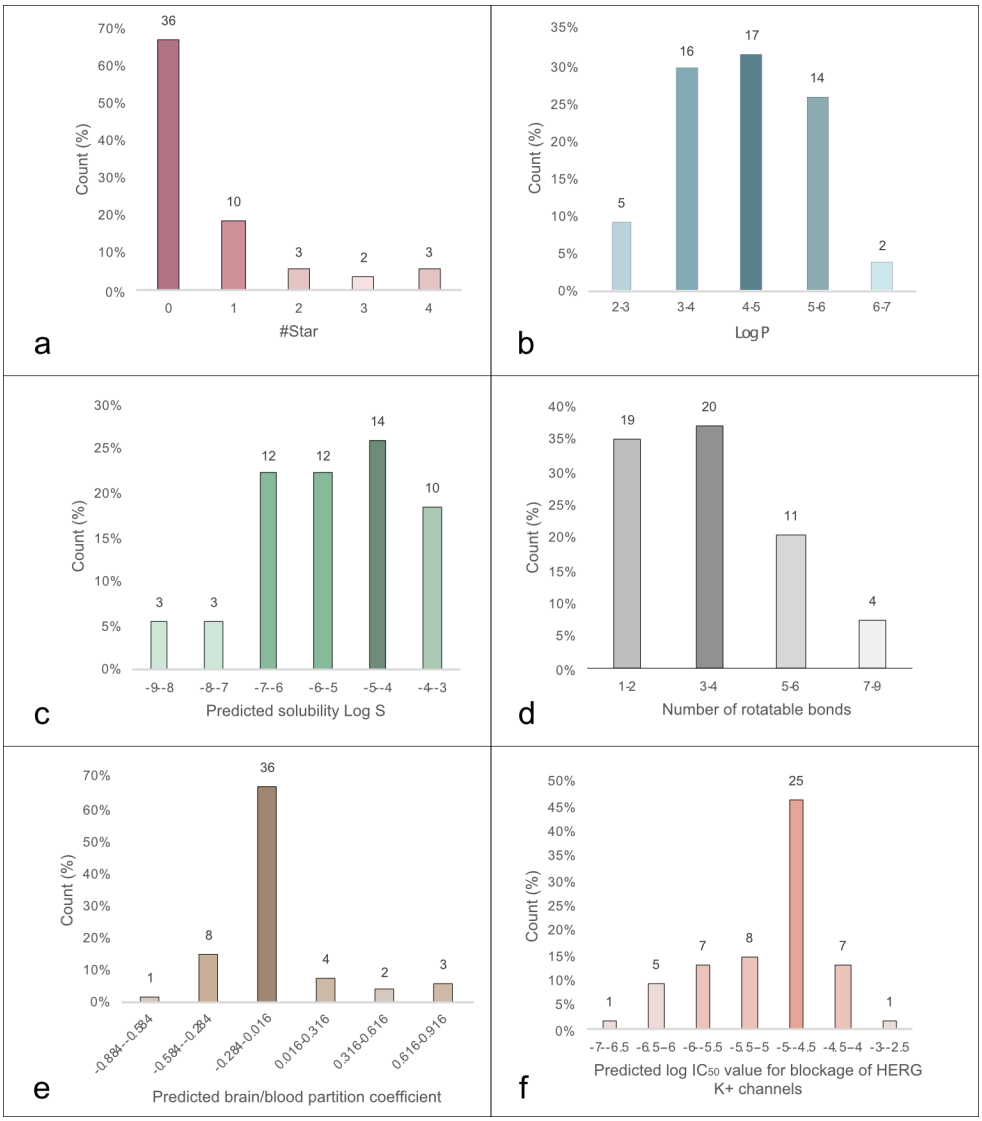

Figure 27
Distribution of predicted descriptors. *a*. #star, *b*. log *P*, *c*. logS, *d*. Number of rotational bonds, *e*. Predicted blood brain partition coeficient, *f*. Predicte log IC_{50} values for blockage of $HERG^+$ channels

The blockage of human ether-a-go-go-related gene potassium (HERG K^+) channel was also predicted to determine possible cardiotoxicity of the ligands. As shown in Figure 27f, 70% of the compounds fall on the recommended range of values for HERG K+ binding.

5.3 Conclusions

We have developed a pharmacophore hypothesis for *T. cruzi*, *L. braziliensis* and *L. amazonensis*), and used several pharmacologically relevant descriptors to qualitatively evaluate the drug-likeness of the 54 pulchrol analogues presented in this study.

Pharmacophore models were generated to visualize the surroundings of the ligands and features involved in binding with the active site. The most important pharmacophoric sites were determined to be two hydrogen bond acceptors (one at the benzylic position in the A-ring and the other on heterocycle oxygen in the B-ring), and three hydrophobic features (one in the C-ring and the other two on the B-ring).

The only pharmacophore model capable of explaining the biological activity was developed for *T. cruzi*, while the models developed for the *Leishmania* species were unable to distinguish between active and inactive ligands. To improve the development of pharmacophore hypotheses for the *Leishmania* species modifying the activity threshold is recommended. The manual addition of excluded volumes to consider possible steric clashes is suggested as well. Validation of the pharmacophore hypothesis developed for *T. cruzi* using an appropriate set of test ligands is strongly advised before going ahead with quantitative structure-activity relationship studies (QSAR).

The pharmacokinetic evaluation showed that most of the molecules in this investigation comply with Lipinski's "Rule of five" and Jorgensen's "Rule of three". The predicted octanol/water partition coefficient and the predicted solubility in water, however, have not optimal values for some of the most hydrophobic compounds.

The rigidity of the pulchrol scaffold may benefit the pharmacokinetics and reduce the probability of interactions with undesired molecular targets.

Most of the compounds may not penetrate the blood brain barrier according to the recommended ranges, however care should be taken in the design of new compounds. Similarly, most of the compounds showed low binding affinity to the $HERGK^{+}$ channels, but those compounds found outside the recommended range of values should be assayed to ascertain that cardiotoxicity is not a risk.

Overall, more than 80% of the compounds have good pharmacokinetic profile for oral administration. However, future studies should focus on the least hydrophobic active ligands may prevent issues concerning blood-brain barrier penetration, undesired central nervous system activity and poor absorption.

6 General Conclusions

Neglected diseases such as leishmaniasis and the Chagas disease are caused by protozoan parasites from the family Trypanosomatidae. The natural product pulchrol, isolated from the roots of the vegetal specie *Bourreria pulchra* showed potential toxicity toward *T. cruzi*, and moderate activity toward *L. braziliensis* and *L. amazonensis*, responsible for the Chagas disease, mucocutaneous leishmaniasis and cutaneous leishmaniasis, respectively.

In this investigation, an improved synthetic protocol to prepare pulchrol and its analogues was developed. Fifty-four compounds bearing the pulchrol scaffold were prepared and assayed toward *T. cruzi* epimastigotes, as well as *L. braziliensis* and *L. amazonensis* promastigotes. Selectivity indexes for each molecule were calculated as the ratio between the cytotoxicity measured in macrophage cells (RAW) and the antiparasitic activity.

The biological results indicate that the benzylic oxygen in the A-ring is important for the activity, probably acting as a hydrogen bond acceptor. A lipophilic pocket of unknown shape and size may exist in the target protein, localized where the hydrophobic substituents are attached to the benzylic oxygen or its ester. However, differences seem to exist between the parasites' hypothetical binding sites. The lipophilic pocket in *L. braziliensis* appears to fit alkyl chains with no more than 4 carbon atoms in the region in which the ester substituent is placed. While for *T. cruzi* and *L. amazonensis*, the same region seems to feature a planar surface in which aromatic and planar substituents may interact with the target. The analogue substituted with a vinyl ester at the benzylic position showed good activity and selectivity for all parasites, if it would act as Michael acceptor in the binding site then it could be used for fishing molecular targets.

Transformations at C-6 in the B-ring showed how important is the presence of two alkyl substituents in this position. Furthermore, the methyl substituents in pulchrol's B-ring not only seemed important for hydrophobic interactions, but they may also improve the orientation of the molecule in the active site. The activity toward the *Leishmania* species seems to improve with the length of the alkyl substituents at C-6, while the same region may have a limited size in *T. cruzi*'s binding site.

The presence of substituents in the C-ring was found to be important for the activity of all parasites. Hydrophobic interactions between bulky or long alkyl

groups at positions 2 and 3 seem to be the most beneficial substituents in the C-ring for the antiparasitic activity.

The combination of an aldehyde in the A-ring and isopropyl groups at C-2 and C-3 in the C-ring was beneficial for the antiparasitic activity. However, *Leishmania* species showed preference for the isopropyl substituent at C-3, whereas for *T. cruzi*, C-2 was the preferred position. The ligand with a ketone substituent in the A-ring and an isopropyl substituent at C-2 was the most potent compound for all parasites, showing that space for hydrophobic interactions with the ketone's methyl group may exist.

Butanoic acid esters in the A-ring combined with isopropyl groups at C-2 and C-3 reduced the activity. Particularly, the compound substituted with an isopropyl group at C-2 was inactive toward *L. braziliensis*, possibly due to steric clashes with the binding site.

The presence of at least one hydrogen bond acceptor (HBA) either in the A-ring or in the C-ring is essential for the antiparasitic activity. The region where the benzylic oxygen is located seems to be where the hydrogen bond interaction occurs. Compounds with the HBA in the C-ring and the hydrophobic group in the A-ring appear to rotate so that the C-ring's HBA is in the right position to interact with the target.

Nevertheless, two alkyl groups, one in the A-ring and the other in the C-ring, may increase the activity if they have a hydroxyl functionality at C-1 in the C-ring. The hydroxyl group at C-1 may participate in hydrogen bond interactions, but further studies are necessary to determine whether it acts as either HBA or HBD. Figure 28 shows a summary of the SARs.

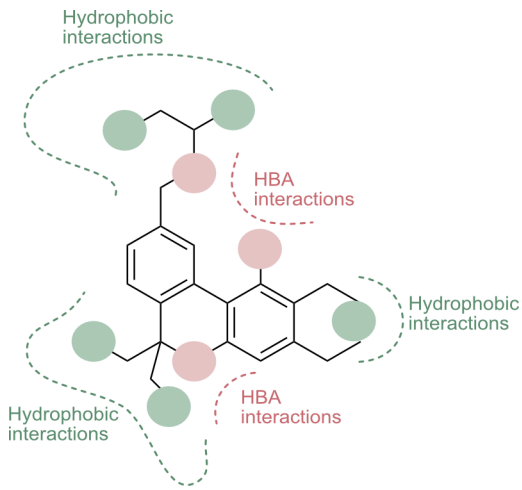

Figure 28
Summary of the structure activity relationship studies

A pharmacophore hypothesis developed for *T. cruzi* seems to agree with the structure activity relationships discussed before. The presence of two HBAs and 3 hydrophobic features shows the importance of the benzylic alcohol in the A-ring, the heterocyclic oxygen in the B-ring, the alkyl groups at C-6 in the B-ring and the alkyl group in the C-ring. However, the development of pharmacophore hypotheses was not successful for all parasites, thus for the *Leishmania* species, we suggest modifying the threshold in the activity values and we also recommend the manual addition of excluded volume. It is advised to validate the pharmacophore hypothesis developed for *T. cruzi*, in order to develop future QSAR studies that will be capable of predicting the antitrypanosomal activity of new molecules.

Most of the molecules showed potential for oral administration. However, the lipophilicity, possible CNS activity and cardiotoxicity, should be considered for the design of new derivatives. It is also recommended to assay the binding affinity of the compounds to the CB1 and CB2 receptors, to evaluate possible unwanted psychotropic activity, or in the contrary, detect possible selectivity to CB2 which may have a modulatory effect in the immune system.

7 Acknowledgments

I would like to sincerely thank…

The *Swedish International Development Cooperation Agency* (SIDA), for funding my doctoral studies.

Universidad Mayor de San Simón, for hosting me when I was in Bolivia.

My supervisor *Olov Sterner*, for your support, guide and consideration in the good times, but most importantly during the difficult times in the course of this investigation.

My supervisor *Marcelo Davila*, for your sympathy and positivity during the development of this work.

My co-supervisor *Sophie Manner*, for always being available when I needed advice.

José Luis Balderrama, agradecerle sinceramente por su apoyo y empatía.

Alberto Gimenez and *Efrain Salamanca*, for the biological assays.

Maria Levin and *Katarina Fredriksson*, for your help with all the administrative work, but also for your good attitude and nice disposition.

Sofia Essén, for the HRMS data presented in this work.

Bodil Eliasson, for your support this last years and for always asking how was I feeling, it was very nice to share the office with you.

Present and past members of the *Olov Sterner group*: Antonio, Leticia, Narda, Rodrigo, Juliao, Zilma, Mariela, Maribel, Eira and Ivan, for the good company.

Annika Beskow, *Lars Kjellberg*, *Mikael Beskow* and *Sofia Beskow*; for allowing me to be part of your family here in Sweden. Thanks for your caring support and all the time we spent together. I love you all.

Katja Beskow, *Maria Bengtsson*, *Kathinka Waldenström*, and *Martin Hjortsjö*, for sharing with me some thoughts and good advice about stress, mental health and life in general.

Eira Ruud Furuseth, for helping me to adjust to the lab work when I arrived for the first time and generously sharing all your experience with me. Also, for the friendship that began in our lab and that I have the luck to still enjoy nowadays.

María Alicia Terrazas, *Laura Terrazas*, *Tania Zubieta*, *Vania Zubieta* y *Doris Poka*, por su apoyo en mi momento mas difícil; por su empatía, comprensión y sabios consejos, siempre las tengo en mi mente.

Ingrid Vargas, *Gabriela Peña* y *Vanesa Castro*, por compartir conmigo la experiencia del doctorado, los momentos de oscuridad y los momentos de luz.

Mi abuela *Hilda Zubieta* y mi padrino *Magín Zubieta*, por su sabiduría, buenos consejos y cariño.

Dr. Walter de Groot (QEPD), por haber sido un modelo de humildad, capacidad y generosidad que me inspira para ser mejor constantemente.

Mi abuela *Alta Gracia Terrazas* (QEPD), por que tu recuerdo me llena de fe en Dios.

A mi papá *Danilo Terrazas*, mi mamá *Gina Villarroel* y mi hermana *Lina Terrazas*, por su increíble apoyo durante este doctorado, por estar siempre en contacto conmigo y cuidando de mi, por decirme constantemente que lo único que esperan de mi es ser feliz. No se como agradecerles por tanto amor y disculparme por haberlos preocupado durante algunos los momentos. Los amo mucho.

To my dear *David*, because you have arrived suddenly to my life and like an angel you have rescued me from the darkness. You have brought an amazingly shining light into my life which is now filled with joy, laughter, love, friendship and a tad of dorkiness. I love you sweetheart, thank you for everything.

8 References

[1] Dewick, P.M. Secondary Metabolism: The Building Blocks and Construction Mechanisms. *Medicinal Natural Products*, 2nd ed.; Wiley: Chichester, U.K., 2009; pp 7-38.

[2] Leicach, S. R.; Chludil, H. D. Plant Secondary Metabolites: Structure–Activity Relationships in Human Health Prevention and Treatment of Common Diseases. In *Studies in Natural Products Chemistry*, Atta ur, R., Ed. Elsevier: 2014; Vol. 42, Chapter 9, pp 267-304.

[3] Hong, J. Natural product synthesis at the interface of chemistry and biology. *Chemistry*. **2014**, 20 (33), 10204-10212.

[4] David, B.; Wolfender, J.L.; Dias, D. A. The pharmaceutical industry and natural products: historical status and new trends. *Phytochem. Rev*. **2015,** *14* (2), 299-315.

[5] Li, G.; Lou, H.-X. Strategies to diversify natural products for drug discovery. *Med. Res. Rev.* **2018,** *38* (4), 1255-1294.

[6] Atanasov, A. G.; Waltenberger, B.; Pferschy-Wenzig, E. M.; Linder, T.; Wawrosch, C.; Uhrin, P.; Temml, V.; Wang, L.; Schwaiger, S.; Heiss, E. H.; Rollinger, J. M.; Schuster, D.; Breuss, J. M.; Bochkov, V.; Mihovilovic, M. D.; Kopp, B.; Bauer, R.; Dirsch, V. M.; Stuppner, H. Discovery and resupply of pharmacologically active plant-derived natural products: A review. *Biotechnol. Adv.* **2015,** *33* (8), 1582-1614.

[7] Drašar, P.; Moravcova, J. Recent advances in analysis of Chinese medical plants and traditional medicines. *J. Chromatogr. B*. **2004,** *812* (1), 3-21.

[8] Benyhe, S. Morphine: New aspects in the study of an ancient compound. *Life Sci*. **1994**, 55 (13), 969-979.

[9] Sertürner, F.W. Säure im opium. *J. Pharmacie*. **1805**,13,234.

[10] Wani, M. C.; Taylor, H. L.; Wall, M. E.; Coggon, P.; McPhail, A. T. Plant antitumor agents. VI. Isolation and structure of taxol, a novel antileukemic and antitumor agent from Taxus brevifolia. *J. Am. Chem. Soc.* **1971,** *93* (9), 2325-2327.

[11] Wall, M. E.; Wani, M. C.; Cook, C. E.; Palmer, K. H.; McPhail, A. T.; Sim, G. A. Plant Antitumor Agents. I. The Isolation and Structure of Camptothecin, a Novel Alkaloidal Leukemia and Tumor Inhibitor from Camptotheca acuminata1,2. J. Am. Chem. Soc. 1966, 88 (16), 3888-3890.

[12] Neuss, N.; Gorman, M.; Hargrove, W.; Cone, N. J.; Biemann, K.; Buchi, G.; Manning, R. E. Vinca Alkaloids. XXI.1 The Structures of the Oncolytic Alkaloids Vinblastine (VLB) and Vincristine (VCR)2. *J. Am. Chem. Soc.* **1964,** *86* (7), 1440-1442.

[13] Nobili, S.; Lippi, D.; Witort, E.; Donnini, M.; Bausi, L.; Mini, E.; Capaccioli, S. Natural compounds for cancer treatment and prevention. *Pharmacol. Res*. **2009**, 59 (6), 365-378.

[14] Oberlies, N. H.; Kroll, D. J. Camptothecin and Taxol: Historic Achievements in Natural Products Research. *J. Nat. Prod*. **2004**, 67 (2), 129-135.

[15] Achan, J.; Talisuna, A. O.; Erhart, A.; Yeka, A.; Tibenderana, J. K.; Baliraine, F. N.; Rosenthal, P. J.; D'Alessandro, U. Quinine, an old anti-malarial drug in a modern world: role in the treatment of malaria. *Malar. J.* **2011,** *10* (1), 144.

[16] White, N. J. Qinghaosu (Artemisinin): The Price of Success. *Science*. **2008**, 320 (5874), 330.

[17] Qinghaosu Antimalarial Coordinating Research Group. *Chin. Med. J. (Engl)*. **1979**, 92 (12), 811-816.

[18] Choudhury, P.R.; Talukdar, A.D.; Saha, P.; Nath, D.; Nath, R. S. R. Traditional Folk Medicine and Drug Discovery: Prospects and Outcome. In *Advances in Pharmaceutical Biotechnology*, Patra, J.K., Shukla, A.C., Das, G., Eds.; Springer: Singapore, 2020; Chapter 1, pp 3-13.

[19] Rodrigues, T.; Reker, D.; Schneider, P.; Schneider, G. Counting on natural products for drug design. *Nat. Chem*. **2016**, 8 (6), 531-541.

[20] Chen, Y.; Garcia de Lomana, M.; Friedrich, N.O.; Kirchmair, J. Characterization of the Chemical Space of Known and Readily Obtainable Natural Products. *J.Chem. Inf. Model.* **2018,** *58* (8), 1518-1532.

[21] Patridge, E.; Gareiss, P.; Kinch, M. S.; Hoyer, D. An analysis of FDA-approved drugs: natural products and their derivatives. *Drug Discovery Today* **2016,** *21* (2), 204-207.

[22] Newman, D. J.; Cragg, G. M. Natural Products as Sources of New Drugs over the Nearly Four Decades from 01/1981 to 09/2019. *J. Nat. Prod*. **2020**, 83 (3), 770-803.

[23] Moffat, J. G.; Vincent, F.; Lee, J. A.; Eder, J.; Prunotto, M. Opportunities and challenges in phenotypic drug discovery: an industry perspective. *Nat. Rev. Drug Discovery*. **2017**, 16 (8), 531-543.

[24] Swinney, D. C.; Anthony, J., How were new medicines discovered? *Nature Reviews Drug Discovery* **2011,** *10* (7), 507-519.

[25] Zheng, W.; Thorne, N.; McKew, J. C. Phenotypic screens as a renewed approach for drug discovery. *Drug Discovery Today.* **2013,** *18* (21), 1067-1073.

[26] Al-Ali, H. The evolution of drug discovery: from phenotypes to targets, and back. *Med. Chem. Commun*. **2016**, 7 (5), 788-798.

[27] Gilbert, I. H. Drug discovery for neglected diseases: molecular target-based and phenotypic approaches. *J. Med. Chem*. **2013**, 56 (20), 7719-7726.

[28] Weng, H.-B.; Chen, H.-X.; Wang, M.W. Innovation in neglected tropical disease drug discovery and development. *Infect. Dis. Poverty.* **2018,** *7* (1), 67.

[29] Reguera, R. M.; Calvo-Álvarez, E.; Álvarez-Velilla, R.; Balaña-Fouce, R. Target-based vs. phenotypic screenings in Leishmania drug discovery: A marriage of convenience or a dialogue of the deaf? *Int. J. Parasitol. Drugs Drug Resist*. **2014**, 4 (3), 355-357.

[30] Haasen, D.; Schopfer, U.; Antczak, C.; Guy, C.; Fuchs, F.; Selzer, P. How Phenotypic Screening Influenced Drug Discovery: Lessons from Five Years of Practice. *Assay Drug Dev. Technol.* **2017,** *15* (6), 239-246.

[31] Eder, J.; Sedrani, R.; Wiesmann, C. The discovery of first-in-class drugs: origins and evolution. *Nat. Rev.s Drug Discovery.* **2014,** *13* (8), 577-587.

[32] World Health Organization Homepage. Available online: https://www.who.int/neglected_diseases/diseases/en/ (accessed on October 2020).

[33] World Health Organization Homepage. A human rights-based approach to neglected tropical diseases. Available online: https://www.who.int/gender-equity-rights/knowledge/ntd-information-sheet-eng.pdf?ua=1 (accessed on 22 October 2020).

[34] Molyneux, D. H.; Savioli, L.; Engels, D. Neglected tropical diseases: progress towards addressing the chronic pandemic. *Lancet*. **2017**, 389 (10066), 312-325.

[35] Jacobson, J.; Bush, S. Neglected Tropical Diseases, Neglected Communities, and Conflict: How Do We Leave No One Behind? *Trends Parasitol*. **2018**, 34 (3), 175-177.

[36] Martins-Melo, F. R.; Ramos, A. N., Jr.; Alencar, C. H.; Heukelbach, J. Mortality from neglected tropical diseases in Brazil, 2000-2011. *Bul.l World. Health. Organ*. **2016**, 94 (2), 103-110.

[37] World Health Organization Homepage. Second WHO report on neglected tropical diseases. Available online: https://www.who.int/neglected_diseases/9789241564540/en/ (accessed on 22 October 2020).

[38] World Health Organization Homepage. Third WHO report on neglected tropical diseases. Available online: https://www.who.int/neglected_diseases/9789241564861/en/ (accessed on 22 October 2020).

[39] Field, M. C.; Horn, D.; Fairlamb, A. H.; Ferguson, M. A. J.; Gray, D. W.; Read, K. D.; De Rycker, M.; Torrie, L. S.; Wyatt, P. G.; Wyllie, S.; Gilbert, I. H. Anti-trypanosomatid drug discovery: an ongoing challenge and a continuing need. *Nat. Rev. Microbiol.* **2017,** *15* (4), 217-231.

[40] Kaufer, A.; Ellis, J.; Stark, D.; Barratt, J. The evolution of trypanosomatid taxonomy. *Parasites Vectors*. **2017**, 10 (1), 287.

[41] World Health Organization Homepage. Chagas disease (also known as American trypanosomiasis). Available online: https://www.who.int/news-room/fact-sheets/detail/chagas-disease-(american-trypanosomiasis) (Accessed on 23 October 2020).

[42] World Health Organization Homepage. World Chagas Disease Day: raising awareness of neglected tropical diseases. Available online: https://www.who.int/neglected_diseases/news/world-Chagas-day-approved/en/ (Accessed on 23 October 2020).

[43] Tarleton, R. L. Chagas Disease: A Solvable Problem, Ignored. *Trends. Mol. Med.* **2016**, 22 (10), 835-838.

[44] World Health Organization Homepage. Chagas disease (also known as American trypanosomiasis), data. Available online: https://www.who.int/docs/default-source/ntds/chagas-disease/chagas-2018-cases.pdf?sfvrsn=f4e94b3b_2 (Accessed on 23 October 2020).

[45] Lewis, M. D.; Kelly, J. M. Putting Infection Dynamics at the Heart of Chagas Disease. *Trends parasitol.* **2016,** *32* (11), 899-911.

[46] Pérez-Molina, J. A.; Molina, I. Chagas disease. Lancet. 2018, 391 (10115), 82-94.

[47] Tanowitz, H. B.; Scherer, P. E.; Mota, M. M.; Figueiredo, L. M. Adipose Tissue: A Safe Haven for Parasites? *Trends parasitol.* **2017,** *33* (4), 276-284.

[48] Chatelain, E., Chagas disease research and development: Is there light at the end of the tunnel? *Comput. Struct. Biotechnol. J.* **2016**, 15, 98-103.

[49] Bermudez, J.; Davies, C.; Simonazzi, A.; Pablo Real, J.; Palma, S. Current drug therapy and pharmaceutical challenges for Chagas disease. *Acta Trop.* **2016,** *156*, 1-16.

[50] World Health Organization Homepage. Leishmaniasis. Available online: https://www.who.int/news-room/fact-sheets/detail/leishmaniasis (Accessed on 23 October 2020).

[51] Shahnawaz, K.; Irfan, K.; Prem, M.S.C. Antileishmanial chemotherapy: present status and future perspectives. *Chem. Biol. Interface*. **2015,** 5(1), 1-28.

[52] Zavitsanou, A.; Koutis, C.; Babatsikou, F. Leishmaniasis: an overlooked public health concern. *Health. Sci. J*. **2008**, 2(4), 196-205.

[53] Veras, P. S. T.; Bezerra de Menezes, J. P. Using Proteomics to Understand How Leishmania Parasites Survive inside the Host and Establish Infection. *Int. J. Mol. Sci*. **2016**, 17 (8), 1270.

[54] Bailey, F.; Eaton, J.; Jidda, M.; van Brakel, W. H.; Addiss, D. G.; Molyneux, D. H. Neglected Tropical Diseases and Mental Health: Progress, Partnerships, and Integration. *Trends Parasitol.* **2019,** *35* (1), 23-31.

[55] World Health Organization Homepage. Leishmaniasis. Available online: https://apps.who.int/gho/data/node.main.NTDLEISH?lang=en (Accessed on 23 October 2020).

[56] Kaye, P.; Scott, P. Leishmaniasis: complexity at the host–pathogen interface. *Nat. Rev. Microbiol*. **2011,** 9 (8), 604-615.

[57] Séguin, O.; Descoteaux, A. Leishmania, the phagosome, and host responses: The journey of a parasite. *Cellular Immunology.* **2016,** *309*, 1-6.

[58] Fernandes, F. R.; Ferreira, W. A.; Campos, M. A.; Ramos, G. S.; Kato, K. C.; Almeida, G. G.; Corrêa, J. D. J.; Melo, M. N.; Demicheli, C.; Frézard, F. Amphiphilic Antimony(V) Complexes for Oral Treatment of Visceral Leishmaniasis. *Antimicrob. Agents. Chemother*. **2013,** 57 (9), 4229-4236.

[59] Croft, S. L.; Sundar, S.; Fairlamb, A. H. Drug Resistance in Leishmaniasis. *Clin. Microbiol. Rev.* **2006,** *19* (1), 111.

[60] Singh, N.; Mishra, B. B.; Bajpai, S.; Singh, R. K.; Tiwari, V. K. Natural product based leads to fight against leishmaniasis. *Bioorg. Med. Chem.* **2014,** *22* (1), 18-45.

[61] Erosa-Rejón, G. J.; Yam-Puc, A.; Chan-Bacab, M. J.; Giménez-Turbax, A.; Salamanca, E.; Peña-Rodríguez, L. M.; Sterner, O. Benzochromenes from the roots of Bourreria pulchra. *Phytochem. Lett.* **2010,** *3* (1), 9-12.

[62] Campos-Ríos, M.G. Revisión del género *Bourreria* P.Browne (Boraginaceae) en México. *Polibotanica* **2005**, 19, 39-103.

[63] Argueta, A.; Cano, L.; Roderte, M.E. *Atlas de las Plantas de la Medicina Tradicional Mexicana*; Instituto Nacional Indigenista: Ciudad de Mexico, Mexico, 1994; pp. 483-485.

[64] Polanco-Hernández, G.; Escalante-Erosa, F.; García-Sosa, K.; Acosta-Viana, K.; Chan-Bacab, M. J.; Sagua-Franco, H.; González, J.; Osorio-Rodríguez, L.; Moo-Puc, R. E.; Peña-Rodríguez, L. M. In vitro and in vivo trypanocidal activity of native plants from the Yucatan Peninsula. *Parasitol. Res*. **2012**, 110 (1), 31-35.

[65] Hayden, W.J. Flora of Kaxil Kiuic. *Bourreria pulchra*. Available online: http://chalk.richmond.edu/flora-kaxil-kiuic/b/bourreria_pulchra.html (Accessed on 23 October 2020)

[66] Killander, D.; Sterner, O. Synthesis of the Bioactive Benzochromenes Pulchrol and Pulchral, Metabolites of Bourreria pulchra. *Eur. J. Org. Chem.* **2014,** *2014* (8), 1594-1596.

[67] Killander, D.; Sterner, O. Reagent-Controlled Cyclization-Deprotection Reaction to Yield either Fluorenes or Benzochromenes. *Eur. J. Org. Chem.* **2014,** 6507-6512.

[68] Emilio, H.; Luis, A.; Guillermo, S.-H.; Jaime, R.; Cristina, T. Metabolites from *Microsphaeropsis olivacea*, an Endophytic Fungus of *Pilgerodendron uviferum*. *Z. Naturforsch*. **2005**, 60 (1-2), 11-21.

[69] Kock, I.; Krohn, K.; Egold, H.; Draeger, S.; Schulz, B.; Rheinheimer, J. New Massarilactones, Massarigenin E, and Coniothyrenol, Isolated from the Endophytic Fungus *Coniothyrium sp*. from *Carpobrotus edulis*. *Eur. J. Org. Chem.* **2007,** *2007* (13), 2186-2190.

[70] Song, Y. C.; Huang, W. Y.; Sun, C.; Wang, F. W.; Tan, R. X. Characterization of graphislactone A as the antioxidant and free radical-scavenging substance from the culture of *Cephalosporium sp*. IFB-E001, an endophytic fungus in *Trachelospermum jasminoides*. *Biol. Pharm. Bull.* **2005**, 28 (3), 506-509.

[71] Zhang, H.-W.; Huang, W.-Y.; Song, Y.-C.; Chen, J.-R.; Tan, R.-X. Four 6H-Dibenzo[b,d]pyran-6-one Derivatives Produced by the Endophyte *Cephalosporium acremonium* IFB-E007. *Helv. Chim. Acta.* **2005,** *88* (11), 2861-2864.

[72] Tanahashi, T.; Takenaka, Y.; Nagakura, N.; Hamada, N. 6H-Dibenzo[b,d]pyran-6-one derivatives from the cultured lichen mycobionts of *Graphis spp.* and their biosynthetic origin. *Phytochemistry*. **2003**, 62 (1), 71-75.

[73] Bukuru, J. F.; Van, T. N.; Van Puyvelde, L.; Mathenge, S. G.; Mudida, F. P.; De Kimpe, N. A Benzochromene from the Roots of *Pentas bussei*. *J. Nat. Prod.* **2002,** *65* (5), 783-785.

[74] Simon-Levert, A.; Arrault, A.; Bontemps-Subielos, N.; Canal, C.; Banaigs, B. Meroterpenes from the Ascidian *Aplidium aff. densum*. *J. Nat. Prod.* **2005,** *68* (9), 1412-1415.

[75] Altemöller, M.; Gehring, T.; Cudaj, J.; Podlech, J.; Goesmann, H.; Feldmann, C.; Rothenberger, A. Total Synthesis of Graphislactones A, C, D, and H, of Ulocladol, and of the Originally Proposed and Revised Structures of Graphislactones E and F. *Eur. J. Org. Chem*. **2009**, 2009 (13), 2130-2140.

[76] Kidwai, M.; Saxena, S.; Rahman Khan, M. K.; Thukral, S. S. Aqua mediated synthesis of substituted 2-amino-4H-chromenes and in vitro study as antibacterial agents. *Bioorg. Med. Chem. Lett*. **2005**, 15 (19), 4295-4298.

[77] Soni, R.; Umar, S.; Shah, N. N.; Balkrishnan, S.; Soman, S. S. Design, Synthesis, and Anticancer Activity of 3H–benzo[f]chromen-3-one Derivatives. *J. Heterocycl. Chem.* **2017**, 54 (4), 2501-2510.

[78] Mirjalili, B. F.; Zamani, L.; Zomorodian, K.; Khabnadideh, S.; Haghighijoo, Z.; Malakotikhah, Z.; Ayatollahi Mousavi, S. A.; Khojasteh, S. Synthesis, antifungal activity and docking study of 2-amino-*4H*-benzochromene-3-carbonitrile derivatives. *J. Mol. Struct*. **2016**, 1116, 102-108.

[79] Halawa, A. H.; Fouda, A. M.; Al-Dies, A. M.; El-Agrody, A. M. Synthesis, Biological Evaluation and Molecular Docking Studies of *4H*-benzo[*h*]chromenes, *7H*-benzo[*h*]chromeno[2,3-d]pyrimidines as Antitumor Agents. *Lett. Drug. Des. Discovery*. **2016**, 13, 77-88.

[80] Gulcan, H. O.; Unlu, S.; Esiringu, İ.; Ercetin, T.; Sahin, Y.; Oz, D.; Sahin, M. F. Design, synthesis and biological evaluation of novel 6H-benzo[*c*]chromen-6-one, and 7,8,9,10-tetrahydro-benzo[*c*]chromen-6-one derivatives as potential cholinesterase inhibitors. *Bioorg. Med. Chem.* **2014,** *22* (19), 5141-5154.

[81] Sun, W.; Cama, L. D.; Birzin, E. T.; Warrier, S.; Locco, L.; Mosley, R.; Hammond, M. L.; Rohrer, S. P. *6H*-Benzo[*c*]chromen-6-one derivatives as selective ERβ agonists. *Bioorg. Med. Chem. Lett.* **2006,** *16* (6), 1468-1472.

[82] Pratap, R.; Ram, V. J. Natural and Synthetic Chromenes, Fused Chromenes, and Versatility of Dihydrobenzo[*h*]chromenes in Organic Synthesis. *Chem. Rev*. **2014**, 114 (20), 10476-10526.

[83] ElSohly, M. A.; Slade, D. Chemical constituents of marijuana: The complex mixture of natural cannabinoids. *Life Sci*. **2005**, 78 (5), 539-548.

[84] Husni, A. S.; McCurdy, C. R.; Radwan, M. M.; Ahmed, S. A.; Slade, D.; Ross, S. A.; ElSohly, M. A.; Cutler, S. J. Evaluation of phytocannabinoids from high-potency Cannabis sativa using in vitro bioassays to determine structure–activity relationships for cannabinoid receptor 1 and cannabinoid receptor 2. *Med. Chem. Res*. **2014**, 23 (9), 4295-4300.

[85] Mahadevan, A.; Siegel, C.; Martin, B. R.; Abood, M. E.; Beletskaya, I.; Razdan, R. K. Novel Cannabinol Probes for CB1 and CB2 Cannabinoid Receptors. *J. Med. Chem*. **2000**, 43 (20), 3778-3785.

[86] Kaplan, B. L. F.; Rockwell, C. E.; Kaminski, N. E. Evidence for Cannabinoid Receptor-Dependent and -Independent Mechanisms of Action in Leukocytes. *J. Pharmacol. Exp. Ther*. **2003**, 306 (3), 1077.

[87] Jan, T.-R.; Rao, G. K.; Kaminski, N. E. Cannabinol Enhancement of Interleukin-2 (IL-2) Expression by T Cells Is Associated with an Increase in IL-2 Distal Nuclear Factor of Activated T Cell Activity. *Mol. Pharmacol.* **2002,** *61* (2), 446.

[88] Zhou, J.; Huang, L.-Z.; Li, Y.-Q.; Du, Z.-T. Synthesis of substituted *6H*-benzo[*c*]chromenes: a palladium promoted ring closure of diazonium tetrafluoroborates. *Tetrahedron Lett.* **2012,** *53* (52), 7036-7039.

[89] Campeau, L.-C.; Parisien, M.; Leblanc, M.; Fagnou, K. Biaryl Synthesis via Direct Arylation: Establishment of an Efficient Catalyst for Intramolecular Processes. *J. Am. Chem. Soc.* **2004,** *126* (30), 9186-9187.

[90] Singha, R.; Ahmed, A.; Nuree, Y.; Ghosh, M.; Ray, J. K. KO^{t}Bu mediated efficient approach for the synthesis of fused heterocycles via intramolecular O-/N-arylations. *RSC Adv.* **2015,** *5* (62), 50174-50177.

[91] Roman, D. S.; Takahashi, Y.; Charette, A. B. Potassium tert-Butoxide Promoted Intramolecular Arylation via a Radical Pathway. *Org. Lett.* **2011,** *13* (12), 3242-3245.

[92] Bajracharya, G. B.; Daugulis, O. Direct Transition-Metal-Free Intramolecular Arylation of Phenols. *Org. Lett.* **2008,** *10* (20), 4625-4628.

[93] Singha, R.; Roy, S.; Nandi, S.; Ray, P.; Ray, J. K. Palladium-catalyzed one-pot Suzuki–Miyaura cross coupling followed by oxidative lactonization: a novel and efficient route for the one-pot synthesis of benzo[*c*]chromene-6-ones. *Tetrahedron Lett.* **2013,** *54* (7), 657-660.

[94] Mahendar, L.; Krishna, J.; Gopi Krishna Reddy, A.; Venkat Ramulu, B.; Satyanarayana, G. A Domino Palladium-Catalyzed C–C and C–O Bonds Formation via Dual O–H Bond Activation: Synthesis of 6,6-Dialkyl-6*H*-benzo[*c*]chromenes. *Org. Lett.* **2012,** *14* (2), 628-631.

[95] Mazimba, O. Synthetic protocols on 6*H*-benzo[*c*]chromen-6-ones: a review. *Turk. J. Chem*. **2016**, 40, 1-27.

[96] Minuti, L.; Temperini, A.; Ballerini, E. High-Pressure-Promoted Diels–Alder Approach to Biaryls: Application to the Synthesis of the Cannabinols Family. *The Journal of Organic Chemistry* **2012,** *77* (18), 7923-7931.

[97] Ballerini, E.; Minuti, L.; Piermatti, O.; Pizzo, F. High Pressure Diels−Alder Approach to Hydroxy-Substituted 6a-Cyano-tetrahydro-6*H*-benzo[*c*]chromen-6-ones: A Route to Δ6-Cis-Cannabidiol. *J. Org. Chem.* **2009,** *74* (11), 4311-4317.

[98] Leadbeater, N.E.; Marco, M. Rapid and amenable Suzuki coupling reaction in water using microwave and conventional heating. *J. Org. Chem*. **2003**, 68, 888–892.

[99] Terrazas, P.; Salamanca, E.; Dávila, M.; Manner, S.; Giménez, A.; Sterner, O. SAR:s for the antiparasitic plant metabolite pulchrol. 1. The benzyl alcohol functionality. *Molecules*. **2020**, 25, 3058.

[100] Norseeda, K.; Tummatorn, J.; Krajangsri, S.; Thongsornkleeb, C.; Ruchirawat, S. Synthesis of 6-Alkyl-6 H-benzo[c]chromene Derivatives by cyclization/selective ether cleavage in one pot: Total synthesis of cannabinol. *Asian J. Org. Chem*. **2016**, 5 (6), 792-800.

[101] Terrazas, P.; Salamanca, E.; Dávila, M.; Manner, S.; Giménez, A.; Sterner, O. SAR:s for the Antiparasitic Plant Metabolite Pulchrol. 2. B- and C-ring substituents. *Molecules*. **2020**, 25, 4510.

[102] Appendino, G.; Gibbons, S.; Giana, A.; Pagani, A.; Grassi, G.; Stavri, M.; Smith, E.; Rahman, M. M. Antibacterial Cannabinoids from Cannabis sativa: A Structure−Activity Study. *J. Nat. Prod*. **2008,** *71* (8), 1427-1430.

[103] Munson, A. E.; Harris, L. S.; Friedman, M. A.; Dewey, W. L.; Carchman, R. A. Antineoplastic Activity of Cannabinoids. *J. Natl. Cancer Inst*. **1975**, 55 (3), 597-602.

[104] Khanolkar, A. D.; Lu, D.; Ibrahim, M.; Duclos, J. R. I.; Thakur, G. A.; Malan, J. T. P.; Porreca, F.; Veerappan, V.; Tian, X.; George, C.; Parrish, D. A.; Papahatjis, D. P.; Makriyannis, A. Cannabilactones: A Novel Class of CB2 Selective Agonists with Peripheral Analgesic Activity. *J. Med. Chem.* **2007,** *50* (26), 6493-6500.

[105] Munro, S.; Thomas, K. L.; Abu-Shaar, M. Molecular characterization of a peripheral receptor for cannabinoids. Nature 1993, 365 (6441), 61-65.

[106] Yamamoto, I.; Watanabe, K.; Kuzuoka, K.; Narimatsu, S.; Yoshimura, H. The pharmacological activity of cannabinol and its major metabolite, 11-Hydroxycanabinol. *Chem. Pharm. Bull*. **1987**, 35 (5), 2144-2147.

[107] Thakur, G. A.; Bajaj, S.; Paronis, C.; Peng, Y.; Bowman, A. L.; Barak, L. S.; Caron, M. G.; Parrish, D.; Deschamps, J. R.; Makriyannis, A. Novel Adamantyl Cannabinoids as CB1 Receptor Probes. *J. Med. Chem*. **2013**, 56 (10), 3904-3921.

[108] Zygmunt, P. M.; Andersson, D. A.; Hogestatt, E. D. Delta 9-tetrahydrocannabinol and cannabinol activate capsaicin-sensitive sensory nerves via a CB1 and CB2 cannabinoid receptor-independent mechanism. *J. Neurosci*. **2002,** 22 (11), 4720-4727.

[109] Rao, G. K.; Kaminski, N. E., Cannabinoid-Mediated Elevation of Intracellular Calcium: A Structure-Activity Relationship. *J. Pharmacol. Exp. Ther.* **2006**, 317 (2), 820.

[110] Wilkinson, J. D.; Williamson, E. M. Cannabinoids inhibit human keratinocyte proliferation through a non-CB1/CB2 mechanism and have a potential therapeutic value in the treatment of psoriasis. *J. Dermatol. Sci*. **2007,** 45 (2), 87-92.

[111] Caprioglio, D.; Mattoteia, D.; Minassi, A.; Pollastro, F.; Lopatriello, A.; Muňoz, E.; Taglialatela-Scafati, O.; Appendino, G. One-Pot Total Synthesis of Cannabinol via Iodine-Mediated Deconstructive Annulation. *Org. Lett*. **2019,** 21 (15), 6122-6125.

[112] Chandrasekaran, B.; Agrawal, N.; Kaushik, S. Pharmacophore Development. In Encyclopedia of Bioinformatics and Computational Biology. **2019**; pp 677-687.

[113] Roy, K.; Kar, S.; Das, R. N. Chapter 10 - Other Related Techniques. In Understanding the Basics of QSAR for Applications in Pharmaceutical Sciences and Risk Assessment. Roy, K.; Kar, S.; Das, R. N. Eds. Academic Press: Boston, **2015**; pp 357-425.

[114] Wolber, G.; Seidel, T.; Bendix, F.; Langer, T. Molecule-pharmacophore superpositioning and pattern matching in computational drug design. *Drug Discovery Today.* **2008,** *13* (1), 23-29.

[115] Yang, S.-Y. Pharmacophore modelling and applications in drug discovery: challenges and recent advances. *Drug Discovery Today.* **2010,** *15* (11), 444-450.

[116] Leach, A. R.; Gillet, V. J.; Lewis, R. A.; Taylor, R. Three-Dimensional Pharmacophore Methods in Drug Discovery. *J. Med. Chem.* **2010,** *53* (2), 539-558.

[117] Dixon, S. L.; Smondyrev, A. M.; Knoll, E. H.; Rao, S. N.; Shaw, D. E.; Friesner, R. A. PHASE: a new engine for pharmacophore perception, 3D QSAR model development, and 3D database screening: 1. Methodology and preliminary results. *J. Comput.-Aided Mol. Des.* **2006,** *20* (10), 647-671.

[118] Dixon, S. L.; Smondyrev, A. M.; Rao, S. N. PHASE: A Novel Approach to Pharmacophore Modeling and 3D Database Searching. *Chem. Biol. Drug Des.* **2006,** *67* (5), 370-372.

[119] Sanders, M. P. A.; Barbosa, A. J. M.; Zarzycka, B.; Nicolaes, G. A. F.; Klomp, J. P. G.; de Vlieg, J.; Del Rio, A. Comparative Analysis of Pharmacophore Screening Tools. *J. Chem. Inf. Model.* **2012,** *52* (6), 1607-1620.

[120] Lipinski, C. A. Lead- and drug-like compounds: the rule-of-five revolution. *Drug Discov. Today*: Technologies. **2004**, 1 (4), 337-341.

[121] Jorgensen, W. L.; Duffy, E. M. Prediction of Drug Solubility from Monte Carlo Simulations. Bioorg. *Med. Chem. Lett*. **2000**, 10, 1155-1158.

[122] Duffy, E. M.; Jorgensen, W. L. Prediction of Properties from Simulations: Free Energies of Solvation in Hexadecane, Octanol, and Water. *J. Am. Chem. Soc*. **2000**, 122, 2878-2888.

[123] Jorgensen, W. L.; Duffy, E. M. Prediction of Drug Solubility from Structure. *Adv. Drug Delivery Rev*. **2002**, 54, 355-366.

[124] Colmenarejo, G.; Alvarez-Pedraglio, A.; Lavandera, J.-L. Cheminformatic Models To Predict Binding Affinities to Human Serum Albumin. *J. Med. Chem*. **2001**, 44, 4370-4378.

[125] Luco, J. M. Prediction of the Brain-Blood Distribution of a Large Set of Drugs from Structurally Derived Descriptors Using Partial Least-Squares (PLS) Modeling. *J. Chem. Inf. Comput. Sci*. **1999**, 39, 396-404.

[126] Potts, R. O.; Guy, R. H. Predicting skin permeability. *Pharm. Res*. **1992**, 9, 663–669. Kelder J.; Grootenhuis, P. D.;Bayada, D.M.; Delbressine, L.P., Ploemen, J.P. Polar molecular surface as a dominating determinant for oral absorption and brain penetration of drugs. *Pharm. Res*. **1999**, 16, 1514–1519.

[127] Terrazas, P.; Salamanca, E.; Dávila, M.; Manner, S.; Giménez, A.; Sterner, O. SAR:s for the Antiparasitic Plant Metabolite Pulchrol. 3. New substituents in A/B-rings and A/C-rings. *In manuscript*.

[128] Patrick, G. L. An Introduction to Medicinal Chemistry, 5th ed.; Oxford University Press: Oxford, U.K., **2013**; pp 227-265.

[129] Kunwittaya, S.; Nantasenamat, C.; Treeratanapiboon, L.; Srisarin, A.; Isarankura-Na-Ayudhya, C.; Prachayasittikul, V. Influence of logBB cut-off on the prediction of blood-brain barrier permeability. *Biomedical and Applied Technology Journal*. **2013**, 16-34.

Paper I

molecules

MDPI

Article

SAR:s for the Antiparasitic Plant Metabolite Pulchrol. 1. The Benzyl Alcohol Functionality

Paola Terrazas [1,2], Efrain Salamanca [3], Marcelo Dávila [2], Sophie Manner [1], Alberto Giménez [3] and Olov Sterner [1,*]

1 Department of Chemistry, Centre for Analysis and Synthesis, Lund University, 22100 Lund, Sweden; paola.terrazas_villarroel@chem.lu.se (P.T.); sophie.manner@chem.lu.se (S.M.)
2 Centre of Agroindustrial Technology, San Simón University, 3299 Cochabamba, Bolivia; marcelodavila@fcyt.umss.edu.bo
3 Institute for Pharmacological and Biochemical Sciences, San Andrés University, 3299 La Paz, Bolivia; efrain_salamanca@hotmail.com (E.S.); agimenez@megalink.com (A.G.)
* Correspondence: Olov.Sterner@chem.lu.se; Tel.: +46-70-5306649

Received: 15 June 2020; Accepted: 1 July 2020; Published: 4 July 2020

Abstract: Pulchrol (**1**) is a natural benzochromene isolated from the roots of *Bourreria pulchra*, shown to possess potent antiparasitic activity towards both *Leishmania* and *Trypanozoma* species. As it is not understood which molecular features of **1** are important for the antiparasitic activity, several analogues were synthesized and assayed. The ultimate goal is to understand the structure–activity relationships (SAR:s) and create a QSAR model that can be used for the development of clinically useful antiparasitic agents. In this study, we have synthesized 25 2-methoxy-6,6-dimethyl-6*H*-benzo[*c*]chromen analogues of **1** and its co-metabolite pulchral (**5a**), by semi-synthetic procedures starting from the natural product pulchrol (**1**) itself. All 27 compounds, including the two natural products **1** and **5a**, were subsequently assayed in vitro for antiparasitic activity against *Trypanozoma cruzi*, *Leishmania brasiliensis* and *Leishmania amazoniensis*. In addition, the cytotoxicity in RAW cells was assayed, and a selectivity index (SI) for each compound and each parasite was calculated. Several compounds are more potent or equi-potent compared with the positive controls Benznidazole (*Trypanozoma*) and Miltefosine (*Leishmania*). The compounds with the highest potencies as well as SI-values are esters of **1** with various carboxylic acids.

Keywords: *Trypanozoma cruzi*; *Leishmania amazoniensis*; *Leishmania brasiliensis*; pulchrol; benzo[*c*]chromenes; SAR

1. Introduction

Parasites belonging to the *Trypanozoma* and *Leishmania* genera affect a large proportion of the world's inhabitants, approximately 12 and 8 million people, respectively, especially in the tropic regions. Surprisingly little is known about these organisms, and there are few efficient drugs against them on the market. This is partly due to the fact that the affected regions in general are poor and cannot pay for advanced medications, and these parasitic diseases are consequently labelled as neglected [1,2]. Benzochromenes are polycyclic aromatic compounds formed by the fusion of a benzene ring with a chromene moiety [3]. The benzochromene structure is found in many natural products isolated from plants [4–8], lichens and fungi [9], and a wide range of biological activities such as antibacterial [5,10], antioxidant and anticancer activities have been reported for natural benzochromenes [9,11]. They have been reported to be able to intercalate with DNA [11,12], and to bind selectively to the estrogen receptor ERβ [13]. Several cannabinoids are benzochromenes and bind to the cannabinoid receptors CB1 and CB2 [5,14].

This work focuses on the natural benzo[*c*]chromene pulchrol (**1**), isolated from the heptane fraction of the roots of *Bourreria pulchra* together with the corresponding aldehyde pulchral (**5a**) [4]. *B. pulchra*, also known locally as "bakalche" and "azar del monte", is part of the traditional medicine of the Yucatan peninsula (Mexico) and has been used to treat cutaneous diseases, injuries, viral infections and fevers [15,16]. We have reported antiparasitic activity against *Leishmania* (*L. brasiliensis*, *L. amazoniensis*, *L. Mexicana*) and *Trypanozoma* (*T. cruzi*) species of **1** and **5a** (see Figure 1 for structures) in vitro [4], and more recently an ethanol extract of *B. pulchra* was reported to possess potent activity against *T. cruzi* [17]. As only limited amounts of the compounds **1** and **5a** are available from natural sources, which is insufficient for a complete biological characterization, a synthetic route to both compounds was developed. To facilitate the semi-synthesis of new analogues starting from pulchrol (**1**), the synthetic procedure of **1** was further developed in order to improve the yields and increase the throughput. In this study, we present the synthesis of 25 pulchrol analogues systematically varied in the benzyl alcohol region while keeping the 2-methoxy-6,6-dimethyl-6*H*-benzo[*c*]chromen structure intact, and report their in vitro antiparasitic activity against *T. cruzi* epimastigotes and *L. amazoniensis*, as well as *L. brasiliensis* promastigotes. In addition, their cytotoxicity in a murine macrophage RAW cell line was investigated, in order to get a general overview of the selectivity of the assayed compounds. The SAR:s that this and future studies suggest will be used for the development of a QSAR model to enable the design of more potent and selective antiparasitic drug candidates. In addition, improved understanding of the molecular targets of the parasites could be obtained, facilitating the developing novel antiparasitic agents.

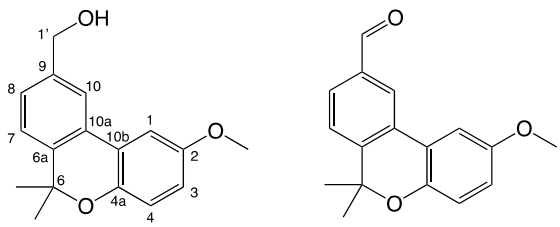

Figure 1. The structures of pulchrol (**1**) and its co-metabolite pulchral (**5a**).

2. Results and Discussion

2.1. Improvements of the Synthetic Route to Pulchrol (**1**)

Several synthetic strategies to prepare benzo[*c*]chromenes have been reported in the literature [18,19]. However, as the focus in this study is on the benzyl alcohol functionality of **1**, we essentially relied on the synthetic manipulation of pulchrol (**1**) itself. An important intermediate in the synthesis of **1** is the biaryl intermediate **2** (see Scheme 1), which can be transformed into **1** by intramolecular cyclization. **2** can be obtained by a metal catalyzed Suzuki-Miyaura cross coupling reaction, using phenyl boronic acid and a *o*-halo-benzoic acid [3,13,14,20,21]. Other synthetic routes to **2** are by a dicarbonyl cycloaddition to chromenes [20], or by the direct intramolecular biaryl formation from phenylbenzyl ethers, as the subsequent cyclization can be performed by metal catalysis [20,22,23] or by a radical reaction promoted by K*t*BuO [20,24]. A synthetic route to pulchrol was reported in 2014, in which the biaryl formation was achieved with a Suzuki-Miyaura coupling and the final cyclization was acid catalyzed [18]. The procedure for preparing **1** in this study was based on this strategy, although we introduced conditions that are milder, increased the yields, and shortened the reaction times.

As in the reported synthesis [18], commercially available 3-iodo-4-(methoxycarbonyl)benzoic acid (also known as 1-methyl-2-iodoterephthalate) was used as the starting material. This was reduced to the corresponding benzyl alcohol (methyl 4-(hydroxymethyl)-2-iodobenzoate) using a borane-tetrahydrofuran complex in THF as solvent, at 0 °C (step a). The benzylic hydroxyl group

was protected with *tert*-butyldiphenylchlorosilane (TBDPSCl) using pyridine as solvent (step b), and this intermediate was then coupled with 2,5-dimethoxyphenyl boronic acid using palladium-tetrakis(triphenylphosphine) ($Pd(PPh_3)_4$) as catalyst and K_2CO_3 as base, in dimethoxyethane (DME)/H_2O 4:1, to yield the biaryl precursor of **2** (step c). This coupling was reported to work successfully at 120 °C for a period of 14 h in 83% yield [18]. However, microwave-assisted Suzuki couplings have been shown to reduce the reaction time and increase the yields [25], and we obtained 85–90% yield at 100 °C in 30 min using a microwave reactor. Instead of MeMgBr in tetrahydrofuran (THF) at 40 °C for 18 h, the methyl ester group was transformed to the tertiary alcohol **2** by two equivalents of methyllithium (MeLi) in THF at 0 °C for 8 h in similar yields, and the milder conditions produced a cleaner product that was considerably easier to purify (step d). By using a larger excess of hydroiodic acid (HI) (10 equiv) for the cyclization of **2** to **1** (step e) we completely avoided the formation of cannabidiol-type biaryl by-products and obtained the deprotected product directly.

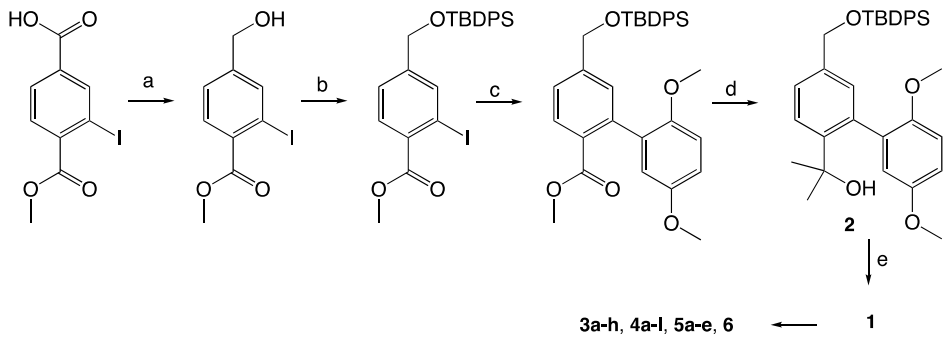

Scheme 1. An overview of the synthetic route used for preparing **1**. See text and Experimental for details.

2.2. Transformations of the Benzylic Alcohol Functionality

Figure 2 summarizes the structure types of the analogues prepared from **1**. See the experimental part for details about how each individual analogue was prepared. The biological activities are given in Table 1.

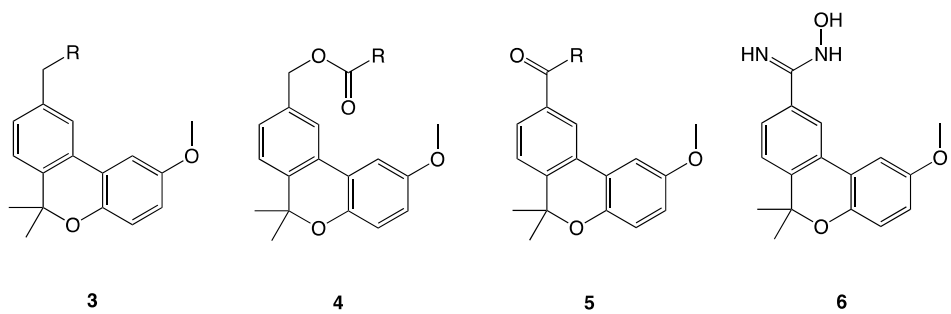

Figure 2. Analogues prepared from **1**. **3a** R = H; **3b** R = Cl; **3c** R = methoxy; **3d** R = isopropyloxy; **3e** R = 4-methylpentyloxy; **3f** R = isopropylamino; **3g** R = isobutylamino; **3h** R = isopentylamino; **4a** R = Me; **4b** R = isopropyl; **4c** R = *tert*-butyl; **4d** R = propyl; **4e** R = isobutyl; **4f** R = neopentyl; **4g** R = pentyl; **4h** R = 2-cyclopentylethyl; **4i** R = cyclohexyl; **4j** R = vinyl; **4k** R = 2-furanyl; **4l** R = phenyl; **5a** R = H; **5b** R = Me; **5c** R = OH; **5d** R = methoxy; **5e** R = NH_2. See Experimental for synthetic details.

Table 1. Antileishmanial, antitrypanozomal and cytotoxic activity of the semisynthetic pulchrol (**1**) derivatives, compared to the positive controls Benznidazole and Miltefosine. See Experimental for details about the assays.

Mol.	R	*T. cruzi*		*L. brasiliensis*		*L. amazoniensis*		Cytotoxicity [a]
		IC_{50} (μM)	SI [b]	IC_{50} (μM)	SI [b]	IC_{50} (μM)	SI [b]	IC_{50} (μM)
1		18.5 ± 9.6	1.7	59.2 ± 11.8	0.5	77.7 ± 5.6	0.4	30.7 ± 1.1
3a		51.1 ± 17.7	2.0	69.6 ± 5.9	1.4	85.3 ± 5.9	1.2	99.5 ± 22.0
3b		38.1 ± 0.4	1.6	17.1 ± 0.1	3.5	35.0 ± 2.8	1.7	59.2 ± 14.5
3c		24.6 ± 3.5	1.3	49.2 ± 15.8	0.7	56.3 ± 12.0	0.6	33.1 ± 2.1
3d		12.9 ± 0.3	2.5	35.2 ± 3.2	0.9	35.2 ± 3.8	0.9	32.0 ± 0.3
3e		9.0 ± 0.6	3.5	127.2 ± 11.3	0.3	28.2 ± 8.5	1.1	31.6 ± 5.6
3f		70.6 ± 9.6	0.4	83.5 ± 32.1	0.4	67.8 ± 13.8	0.4	29.5 ± 9.6
3g		15.4 ± 4.0	0.8	25.8 ± 6.2	0.5	15.4 ± 3.1	0.8	12.3 ± 1.2
3h		5.9 ± 1.2	1.3	15.9 ± 0.9	0.5	17.7 ± 7.4	0.4	7.4 ± 2.4
4a		14.4 ± 1.6	2.3	28.8 ± 0.3	1.1	26.9 ± 0.6	1.2	32.7 ± 22.4
4b		8.8 ± 0.9	3.0	17.6 ± 0.9	1.5	26.7 ± 2.4	1.0	26.4 ± 5.9
4c		6.4 ± 0.1	3.0	17.4 ± 1.7	1.1	20.5 ± 0.6	1.0	19.8 ± 0.9
4d		16.2 ± 3.2	6.4	57.8 ± 2.4	1.8	79.3 ± 9.4	1.3	102.8 ± 35.3
4e		4.2 ± 1.1	6.7	13.1 ± 0.4	2.2	14.5 ± 0.1	1.9	28.2 ± 9.0
4f		5.7 ± 0.3	3.3	20.0 ± 4.2	1.0	19.5 ± 0.8	1.0	19.0 ± 3.0
4g		22.8 ± 5.7	2.3	27.7 ± 0.3	1.9	42.3 ± 8.7	1.2	52.1 ± 8.1
4h		8.4 ± 3.3	6.1	122.4 ± 27.9	0.4	30.9 ± 3.0	1.6	50.7 ± 17.7
4i		13.1 ± 0.5	3.9	24.3 ± 0.8	2.1	40.5 ± 8.7	1.3	51.3 ± 8.2
4j		7.4 ± 0.9	5.4	5.7 ± 0.5	7.0	6.9 ± 1.7	5.8	40.1 ± 12.6
4k		3.8 ± 0.3	7.9	12.8 ± 0.1	2.4	12.8 ± 1.8	2.4	30.5 ± 3.6
4l		5.9 ± 0.5	4.7	21.0 ± 4.3	1.3	21.9 ± 7.7	1.3	27.8 ± 10.7
5a		24.2 ± 4.1	1.6	24.2 ± 7.5	1.6	29.8 ± 11.2	1.3	38.8 ± 3.7
5b		21.2 ± 9.2	1.5	28.3 ± 7.1	1.1	43.2 ± 8.2	0.7	31.9 ± 7.1
5c		56.3	4.4	65.1 ±16.5	3.8	198.7	1.2	246.2 ± 24.6
5d		31.8 ± 2.4	1.2	18.4 ± 5.7	2.1	59.0 ± 1.3	0.7	38.2 ± 2.7
5e		134.5 ± 38.8	0.4	144.7 ± 43.1	0.3	120.7 ± 21.2	0.4	49.8 ± 17.7
6		33.4 ± 14.9	0.8	52.0 ± 18.6	0.5	52.0 ± 16.7	0.5	26.4 ± 1.5
	Benznidazole	19.2 ± 7.7	3.9					74.7 ± 9.1
	Miltefosine			13.0 ± 1.2	5.9	10.8 ± 1.5	7.1	76.6 ± 3.2

[a] Toxicity was measured on RAW cells, see Experimental for details, [b] SI, selectivity index (cytotoxicity/anti-protozoal activity).

Tables 2 and 3 give the 1D ^{1}H and ^{13}C-NMR shifts of the assayed compounds. In general, 1-H is a doublet (d) with coupling constant (*J*) close to 2 Hz, 3-H is a doublet of doublet (dd) with *J* = 9 and 2 Hz, while 4-H is a d with *J* close to 9 Hz. 10-H is a d with *J* close to 2 Hz, 8-H is a dd with *J* = 8 and 2 Hz, while 7-H is a d with *J* close to 8 Hz.

Table 2. Proton chemical shifts (in ppm) for the compounds prepared in this study, measured in $CDCl_3$ at 400 MHz. The assignments were made with 2D NMR spectroscopy, COSY, HMQC and HMBC experiments.

Compd	1-H	3-H	4-H	7-H	8-H	10-H	1′-H/H_2	2-OCH_3	6,6-CH_3
1	7.26	6.81	6.89	7.23	7.30	7.68	4.74	3.85	1.61
3a	7.25	6.79	6.88	7.14	7.12	7.49	2.40	3.85	1.60
3b	7.25	6.82	6.89	7.23	7.32	7.68	4.64	3.86	1.61
3c [a]	7.28	6.80	6.88	7.26	7.22	7.65	4.50	3.85	1.61
3d [b]	7.27	6.80	6.88	7.20	7.29	7.65	4.55	3.85	1.60
3e [c]	7.27	6.81	6.89	7.22	7.29	7.66	4.55	3.85	1.61
3f [d]	7.31	6.79	6.86	7.19	7.28	7.72	3.84	3.86	1.58
3g [e]	7.28	6.80	6.88	7.20	7.26	7.66	3.83	3.85	1.61
3h [f]	7.28	6.81	6.87	7.19	7.25	7.65	3.84	3.85	1.60
4a [g]	7.26	6.82	6.89	7.24	7.30	7.66	5.15	3.85	1.61
4b [h]	7.27	6.83	6.90	7.25	7.30	7.65	5.17	3.86	1.62
4c [i]	7.24	6.81	6.89	7.22	7.27	7.63	5.15	3.85	1.61
4d [j]	7.24	6.81	6.89	7.24	7.29	7.65	5.16	3.85	1.61
4e [k]	7.24	6.81	6.89	7.23	7.29	7.65	5.16	3.85	1.61
4f [l]	7.24	6.81	6.89	7.23	7.29	7.66	5.14	3.85	1.61
4g [m]	7.25	6.81	6.89	7.23	7.29	7.65	5.15	3.85	1.61
4h [n]	7.27	6.83	6.90	7.24	7.31	7.66	5.16	3.85	1.62
4i [o]	7.24	6.81	6.88	7.24	7.28	7.63	5.14	3.85	1.61
4j [p]	7.26	6.82	6.89	7.24	7.32	7.67	5.24	3.85	1.61
4k [q]	7.25	6.81	6.89	7.27	7.38	7.73	5.38	3.85	1.61
4l [r]	7.26	6.82	6.89	7.27	7.40	7.74	5.40	3.85	1.62
5a	7.31	6.86	6.91	7.42	7.80	8.18	10.12	3.87	1.64
5b [s]	7.32	6.84	6.90	7.33	7.87	8.26	-	3.86	1.62
5c	7.32	6.83	6.89	7.32	7.98	8.37	-	3.85	1.62
5d [t]	7.31	6.84	6.90	7.32	7.96	8.35	-	3.87	1.63
5e	7.23	6.82	6.90	7.26	7.33	7.72	-	3.83	1.61
6	7.29	6.82	6.89	7.27	7.54	7.94	-	3.84	1.61

[a] Methoxy signal at 3.43 ppm. [b] Isopropyloxy signals at 3.72 and 1.26 ppm. [c] 4-Methylpentyloxy signals at 3.50, 1.65, 1.27, 1.56 and 0.90 ppm. [d] Isopropylamino signals at 2.95 and 1.18 ppm. [e] Isobutylamino signals at 2.48, 1.81 and 0.94 ppm. [f] Isopentylamino signals at 2.69, 1.44, 1.66 and 0.90 ppm. [g] Methyl signal at 2.13 ppm. [h] Isopropyl signals at 2.64 and 1.23 ppm. [i] *t*-Butyl signal at 1.25 ppm. [j] Propyl signals at 2.36, 1.70 and 0.97 ppm. [k] *i*-Butyl signals at 2.27, 2.14 and 0.97 ppm. [l] *neo*-Pentyl signals at 2.28 and 1.05 ppm. [m] Pentyl signals appear at 2.37, 1.67, 1.31, 1.33 and 0.89 ppm. [n] (2-Cyclopentyl)ethyl signals at 2.41, 1.69, 1.79, 1.76, 1.10, 0.89 and 1.54 ppm. [o] Cyclohexyl signals at 2.38, 1.95, 1.49, 1.76, 1.30 and 1.26 ppm. [p] Vinyl signals appear at 6.19, 6.47 and 5.87 ppm. [q] 2-Furyl signals at 6.51, 7.23 and 7.59 ppm. [r] Phenyl signals at 8.09, 7.45 and 7.57 ppm. [s] Methyl signal appear at 2.61 ppm. [t] Methoxy signal appear at 3.96 ppm.

Table 3. ^{13}C-NMR chemical shifts (in ppm) for the assayed compounds **1**, **3a**–**h**, **4a**–**l**, **5a**–**e** and **6** determined at 100 MHz in $CDCl_3$. The assignments were made with 2D NMR spectroscopy, COSY, HMQC and HMBC experiments.

Compd	C-1	C-2	C-3	C-4	C-4a	C-6	C-6a	C-7	C-8	C-9	C-10	C-10a	C-10b	C-1′	2-OCH_3	6,6-CH_3
1	108.0	154.6	115.5	118.8	146.9	77.4	139.5	123.7	126.8	140.4	121.0	129.1	123.0	65.3	56.0	27.5
3a	108.0	154.5	115.0	118.7	147.0	77.3	137.3	123.3	129.0	137.3	123.0	128.6	123.3	21.5	56.0	27.6
3b	108.1	154.6	115.7	118.9	147.0	77.3	140.2	123.9	128.4	137.0	122.7	129.4	122.7	46.2	56.0	27.4
3c [a]	108.1	154.6	115.5	118.8	147.0	77.4	139.5	123.5	127.6	137.8	121.8	129.0	123.1	74.7	56.0	27.6
3d [b]	108.1	154.4	115.0	118.6	146.8	77.2	139.1	123.3	127.4	138.5	121.5	128.7	122.8	69.9	55.8	27.4
3e [c]	108.1	154.5	115.3	118.8	146.9	77.4	139.3	123.5	127.6	138.2	121.7	128.9	123.1	72.8	55.9	27.5
3f [d]	108.2	154.6	115.4	118.7	146.9	77.3	139.0	123.6	128.5	137.0	122.7	129.1	123.0	50.8	56.1	27.5
3g [e]	108.1	154.5	115.2	118.7	146.9	77.4	140.0	123.4	128.0	138.8	122.1	128.8	123.2	54.0	56.0	27.6
3h [f]	108.1	154.6	115.3	118.8	146.9	77.4	139.6	123.5	128.2	138.9	122.3	128.9	123.2	54.1	56.0	27.5
4a [g]	108.2	154.6	115.4	118.8	147.0	77.3	140.1	123.7	128.2	135.5	122.5	129.2	122.8	66.3	56.0	27.5
4b [h]	108.1	154.6	115.4	118.9	147.0	77.5	139.9	123.7	127.8	135.8	122.1	129.1	122.9	66.0	56.0	27.5

Table 3. *Cont.*

Compd	C-1	C-2	C-3	C-4	C-4a	C-6	C-6a	C-7	C-8	C-9	C-10	C-10a	C-10b	C-1′	2-OCH_3	6,6-CH_3
4c [i]	108.0	154.6	115.5	118.9	147.0	77.5	139.8	123.7	127.5	136.1	121.7	129.1	122.9	65.9	55.9	27.5
4d [j]	108.1	154.6	115.4	118.9	147.0	77.4	140.0	123.7	128.1	135.7	122.3	129.2	122.9	66.0	56.0	27.5
4e [k]	108.0	154.4	115.3	118.7	147.0	77.2	140.0	123.5	127.9	135.6	122.1	129.0	122.7	65.8	55.8	27.3
4f [l]	107.9	154.4	115.3	118.7	146.8	77.2	139.8	123.5	127.9	135.6	122.1	129.0	122.7	65.7	55.8	27.3
4g [m]	108.0	154.4	115.3	118.7	146.8	77.3	139.8	123.6	127.9	135.5	122.2	129.0	122.7	65.9	55.8	27.3
4h [n]	108.2	154.6	115.4	118.8	146.9	77.3	140.0	123.7	128.1	135.7	122.4	129.2	122.8	66.0	56.0	27.5
4i [o]	108.1	154.6	115.5	118.9	147.0	77.3	139.9	123.7	127.9	135.9	122.1	129.1	122.9	65.8	56.0	27.5
4j [p]	108.2	154.6	115.5	118.8	147.0	77.5	140.1	123.8	128.2	135.4	122.5	129.2	122.8	66.3	56.0	27.5
4k [q]	108.1	154.6	115.5	118.9	147.0	77.4	140.3	123.8	128.4	135.1	122.7	129.3	122.8	66.6	56.0	27.5
4l [r]	108.1	154.6	115.5	118.9	147.0	77.4	140.1	123.8	128.2	135.6	122.5	130.7	122.8	66.7	56.0	27.5
5a	107.9	154.8	116.6	119.1	146.8	77.4	146.2	124.3	129.8	136.0	123.4	130.1	122.0	192.1	56.0	27.3
5b [s]	108.3	154.8	116.1	119.0	146.8	77.4	144.8	123.7	128.2	136.7	122.2	129.5	122.4	197.8	56.0	27.3
5c	108.0	154.7	116.2	118.9	146.8	77.4	144.8	123.6	129.7	129.5	124.1	129.3	122.3	168.9	56.0	27.3
5d [t]	108.1	154.7	116.1	119.0	146.8	77.4	144.6	123.6	129.3	129.7	123.7	129.7	122.4	167.0	56.1	27.3
5e	107.8	154.7	116.2	119.0	146.9	77.4	141.2	123.5	126.6	135.9	121.2	129.3	122.5	171.5	56.0	27.4
6	108.1	154.7	115.9	118.9	146.9	77.3	141.7	123.8	125.6	132.2	120.0	129.4	122.6	152.7	56.0	27.4

[a] Methoxy signal at 58.4 ppm. [b] Isopropyloxy signals at 71.1 and 22.1 ppm. [c] 4-Methylpentyloxy signals at 71.1, 28.1, 35.5, 27.8 and 22.7 ppm. [d] Isopropylamino signals at 48.5 and 22.3 ppm. [e] Isobutylamino signals at 57.6, 28.5 and 20.9 ppm. [f] Isopentylamino signals at 47.8, 39.1, 26.3 and 22.8 ppm. [g] Acetyl signals at 171.0 and 21.2 ppm. [h] Isobutyrate signals at 177.1, 34.2 and 19.2 ppm. [i] Pivalate signals at 178.5, 39.0 and 27.4 ppm. [j] Propyl signals at 173.7, 36.4, 18.6 and 13.9 ppm. [k] 3-Methylbutanoate signals at 173.0, 43.4, 25.7 and 22.4 ppm. [l] 3,3-Dimethylbutanoate signals at 172.2, 47.9, 30.9 and 29.7 ppm. [m] Hexanoate signals appear at 173.7, 34.3, 24.7, 31.3, 22.3 and 13.9 ppm. [n] 3-Cyclopentylpropanoate signals at 174.0, 33.8, 31.3, 39.8, 32.5 and 25.2 ppm. [o] Cyclohexanecarboxylate signals appear at 176.1, 43.4, 29.2, 25.6 and 25.9 ppm. [p] Acrylate signals appear at 166.2, 128.4 and 131.5 ppm. [q] Furan-2-carboxylate signals at 158.7, 144.7, 112.1, 118.5 and 146.7 ppm. [r] Benzoate signals at 166.6, 129.0, 129.9, 128.6 and 133.3 ppm. [s] Methyl signal appear at 26.8 ppm. [t] Methoxy signal appear at 52.4 ppm.[u] Methyl signal appear at 25.3 ppm.

2.3. Antiparasitic Activity of Pulchrol (**1**), the Starting Point

Pulchrol (**1**) and pulchral (**5a**) have previously been shown to possess antiparasitic activity, **1** towards *T.cruzi* epimastigotes and three strains of *Leishmania* promastigotes (*L. mexicana*, *L. brasiliensis* and *L. amazoniensis*), and **5a** towards *L. brasiliensis* and *L. amazoniensis* [4]. The IC_{50} value of **1** against *T.cruzi* in this investigation was 18.5 μM (see Table 3), and it is thereby equipotent with the positive control benznidazole (19.2 μM). Benznidazole is currently on the market for the treatment of Chagas disease, caused by *T. cruzi*, under the trade names Rochagan and Radanil. The potency of pulchrol against the *Leishmania* parasites, with the IC_{50} values 59.2 μM for *L. brasiliensis* and 77.7 μM for *L. amazoniensis*, is more moderate, although promastigotes of *L. mexicana* (not part of this investigation) are more sensitive with an IC_{50} value of 17 μM [4]. As the chemical structure of pulchrol (**1**) does not raise any red flags, it contains no functionalities that are associated with reactivity or unspecific biological activity, we were motivated to synthesize and assay analogues of **1**. This study focuses on the importance of the benzyl alcohol functionality for the biological activity, and the natural products (**1** and **5a**) together with 25 analogues were prepared as discussed above, and assayed. The assays against *T. cruzi* epimastigotes and *L. amazoniensis* as well as *L. brasiliensis* promastigotes essentially follows the protocol used in previous investigations, but the cytotoxicity in a mammalian murine macrophage RAW cell line was also assayed in order to get an impression of the compounds selectivity for the parasites over a mammalian cell line. The biological results are presented in Table 1.

2.4. Antiparasitic Activities towards Trypanozoma cruzi Epimastigotes

To determine the importance of the hydroxyl group for pulchrol's activity, the 9-methyl analogue (**3a**) was prepared and found to be considerably less active (IC_{50} = 51.1 μM) compared to **1**. With the intention of mimicking the Van der Waals interactions around the benzylic carbon, the hydroxyl group was replaced by a chlorine (**3b**), but this analogue was also less potent than **1** (IC_{50} = 38.1 μM). It would appear to be beneficial to have an oxygen in the benzylic position, although **3a** and **3b** are by no means inactive. To evaluate if the hydroxyl group acts as a hydrogen bond donor, the methyl ether **3c** was prepared and assayed. It is slightly less potent compared to **1** (IC_{50} = 24.6 μM), indicating that the hydroxyl group is more a hydrogen bond acceptor than donor. However, the two bulkier ethers **3d** and **3e** were actually more potent than **1** (IC_{50} = 12.9 and 9.0 μM, respectively), suggesting that there also

is a lipophilic pocket close to the binding site of the benzylic moiety in a target protein. In addition, **3d** and **3e** show an improved SI compared to **1** and **3c**. Somewhat surprisingly, the isopropylamino analogue **3f** is considerably less potent and selective compared to the isopropyl ether **3d**, while the isobutyl and isopentyl analogues **3g** and **3h** (IC_{50} = 15.4 and 5.9 μM, respectively) are as potent as the bulkier ethers but less selective.

Moving to the pulchrol esters **4a**–**4l**, it is clear that this group of analogues is interesting as most of them are more potent and selective compared to **1**. For the saturated esters **4a**–**4i** it is especially those with branched alkyl groups that are good, with the 3-methylbutanoic acid ester **4e** standing out with IC_{50} = 4.2 μM and SI = 6.7. All the unsaturated esters **4j**–**4l** prepared and assayed are potent and selective, indicating that a π-π interaction with the binding pocket is favourable. The furan-2-carboxylic acid ester **4k** is actually the most potent (IC_{50} = 3.8 μM) and the most selective (SI = 7.9) towards *T. cruzi* of all analogues prepared in this investigation, and has considerably better antiparasitic activity towards *T. cruzi* epimastigotes compared to the positive control Benznidazol (see Table 1). Also the selectivity is noteworthy, as it is twice that of the positive control.

Among the 1′-carbonyl analogues (**5a**–**5e**) included in this study, the aldehyde **5a** and the methyl ketone **5b** can be compared to **1**, both with respect to potency and selectivity. However, the carboxylic acid **5c**, the methyl ester **5d** and especially the amide **5e** are less potent, although the carboxylic acid **5c** is considerably less cytotoxic than the others. The *N*-hydroxy-9-carboximidamide **6** was obtained as a by-product and assayed; it did not show any interesting activities, although it was more potent than the 9-carboxamide **5e**. If anything, analogue **6** underlines the importance of a lipophilic component at the benzylic moiety.

2.5. Antiparasitic Activities towards Leishmania brasiliensis Promastigotes

As for *T.cruzi*, transforming the benzylic alcohol moiety to a methyl group is not beneficial, and **3a** was found to be slightly less potent than **1**. On the contrary, the benzyl chloride (**3b**) showed both an interesting potency (IC_{50} = 17.1 μM) and selectivity (SI = 3.5), suggesting that the presence of an oxygen in the benzylic position is less important. The differences in antiparasitic effects of **3b** in *T. cruzi* epimastigotes and *L. brasiliensis* promastigotes indicate that the molecular targets in the two species are different. Although the two ethers **3c** and **3d** are slightly more potent than **1**, the 4-methylpentyl ether **3e** is considerably less potent and the positive effect of bulky ethers observed for *T. cruzi* is not seen with *L. brasiliensis*. However, for the secondary amines **3f**–**3h** the trend is identical, and the isopentylamino analogue **3h** (IC_{50} = 15.9 μM) is one of the most potent against *L. brasiliensis*. Most of the esters **4a**–**4l**, except for **4h**, are more potent compared to **1**, and among the saturated esters there is again a tendency that branched alkyl groups are better than straight. The aromatic esters **4k** and **4l** are potent towards *L. brasiliensis* as well, **4k** (IC_{50} = 12.8 μM) is as potent as the positive control, although the selectivity observed towards *T. cruzi* is less prominent. The vinyl ester **4j** is the most potent and selective towards *L. brasiliensis*, with IC_{50} = 5.7 μM and SI = 7.0, overshadowing the positive control. For the 1′-carbonyl analogues, the aldehyde **5a**, the methyl ketone **5b** and especially the methyl ester **5d** are more potent, while the carboxylic acid **5c** and the *N*-hydroxy-9-carboximidamide (**6**) are comparable to **1**. The carboxamide **5e** is considerably less potent than **1**.

2.6. Antiparasitic activities towards Leishmania amazoniensis promastigotes

For *L. amazoniensis*, too, the replacement of the benzylic alcohol moiety for a methyl group (**3a**) does not improve the antiparasitic activity, and as for *L. brasiliensis*, a chlorine substituent in this position (**3b**) increases the potency more than two-fold. Ethers of pulchrol (**1**) are more potent; the methyl and isopropyl ethers (**3c** and **3d**) only slightly, but the 4-methylpentyl ether **3e** more clearly. This is in contrast to the poor potency of **3e** towards *L. brasiliensis*. For the secondary amines the sensitivity of *L. amazoniensis* follows that observed already for T. cruzi and *L. brasiliensis*, lower potency for the isopropylamino analogue **3f** and higher for the isobutyl- and isopentylamino analogues **3g** and **3h**. For the esters **4a**–**4l**, the results follow those obtained with *L. brasiliensis* (*vide supra*) closely.

There is only one exception, the 3-cyclopentylpropanic acid ester **4h**, which displays a more expected potency towards *L. amazoniensis* than towards *L. brasiliensis* (*vide supra*). Again, the vinyl ester **4j** is the most potent towards *L. amazoniensis* among the esters, and actually among all compounds assayed here, and as the SI value is 5.8 it is also by far the most selective compound. Among the 9-carbonyl analogues, the aldehyde **5a** and the methyl ketone **5b** are more potent, while the methyl ester **5d** and the *N*-hydroxy-9-carboximidamide (**6**) are only slightly more potent. The carboxylic acid **5c** and the carboxamide **5e** are both considerably less potent compared to **1**.

3. Materials and Methods

3.1. General

^{1}H-NMR spectra (400 MHz) and ^{13}C-NMR spectra (100 MHz) were recorded with a Bruker Avance II (Bruker Biospin AG, Industriestrasse 26, 8117 Fällanden, Switzerland) in $CDCl_3$. The individual 1D signals were assigned using 2D NMR experiments (COSY, HSQC, HMBC). The chemical shifts are given in ppm with the solvent signal as reference (7.27 ppm for ^{1}H and 77.0 for ^{13}C). Infrared spectra were recorded with a Bruker Alpha-P FT/IR instrument (Bruker Biospin AG, Industriestrasse 26, 8117 Fällanden, Switzerland) with a Diamond ATR sensor as films, and the intensities are given as vw (very weak), w (weak), m (medium), s (strong) and vs (very strong). High-resolution mass spectra (HRMS) were recorded with a Waters XEVO-G2 QTOF equipment (Waters Corp, Milford, Worcester County, Massachusetts, United States), with electrospray ionization (ESI). Synthetic reactions were monitored by TLC using alumina plates coated with silica gel and visualized using either UV light and/or spraying/heating with vanillin/H_2SO_4. Flash chromatography was performed with silica gel (35–70 μm, 60 Å). THF was distilled from sodium, acetonitrile was distilled from CaH_2 and other reaction solvents were dried with Al_2O_3. Commercially available compounds were obtained from Aldrich.

3.2. Synthetic Procedures

Methyl 4-(hydroxymethyl)-2-iodobenzoate (intermediate in the synthesis of **1**) BH_3-THF (1 M, 65 mL, 65.0 mmol) was slowly added to a stirred solution of 3-iodo-4-(methoxycarbonyl)benzoic acid (5 g, 16.3 mmol) in dry THF (200 mL) at 0 °C. After 30 h, saturated aqueous $NaHCO_3/H_2O$ was added, the aqueous phase was extracted with ethyl acetate (3 × 200 mL) before drying (Na_2SO_4) and removal of solvent under reduced pressure. Purification by column chromatography (SiO_2, 4:6 heptane/ethyl acetate) gave (3.74 g, 78%) of the pure product as yellow crystals, identical to that previously reported [18].

Methyl 4-(((tert-butyldiphenylsilyl)oxy)methyl)-2-iodobenzoate (intermediate in the synthesis of **1**), TBDPSCl (4.0 mL, 15.3 mmol) was added to a stirred solution of methyl 4-(hydroxymethyl)-2-iodobenzoate (prepared as described above, 3.74 g, 12.8 mmol) in pyridine (60 mL) at rt. After 24 h, saturated aqueous NH_4Cl/H_2O was added and the aqueous phase was extracted with diethyl ether (3 × 200 mL), the organic phase was washed with brine (2 × 500 mL) before drying (Na_2SO_4) and removal of solvent under reduced pressure. Purification by column chromatography (SiO_2, 20:2 heptane/ethyl acetate) gave (6.1 g, 89%) of the product as white crystals, identical to that previously reported [18].

Methyl 5-(((tert-butyldiphenylsilyl)oxy)methyl)-2′,5′-dimethoxy-[1,1′-biphenyl]-2-carboxylate (intermediate in the synthesis of **1**), 2,5-dimethoxyphenylboronic acid (155 mg, 0.85 mmol), K_2CO_3 (394 mg, 2.85 mmol) and tetrakis(triphenylphosphine)palladium(0) (115 mg, 0.1 mmol), were added to a stirred solution of methyl 4-(((tert-butyldiphenylsilyl)oxy)methyl)-2-iodobenzoate (prepared as described above, 300 mg, 0.57 mmol) dissolved in 4:1 DME/water (15 mL). The mixture (contained in a microtube) was degasified under vacuum/N_2 at −78 °C five times. The microwave reaction conditions were 100 °C, high pressure, and 10 s of pre-stirring. After 30 min in the microwave reactor, the mixture was filtered through a plug of celite and washed with ethyl acetate (250 mL) before drying (Na_2SO_4) and removal of solvent under

reduced pressure. Purification by column chromatography (SiO_2, 20:3 heptane/ethyl acetate) gave the pure product as a yellowish wax (263 mg, 86%), identical to that previously reported [18].

2-(5-(((tert-butyldiphenylsilyl)oxy)methyl)-2′,5′-dimethoxy-[1,1′-biphenyl]-2-yl)propan-2-ol (**2**), Methyl lithium (3 M, 3 mL, 8.8 mmol) was added to a stirred solution of methyl 5-(((*tert*-butyldiphenylsilyl)oxy)methyl)-2′,5′-dimethoxy-[1,1′-biphenyl]-2-carboxylate (prepared as described above, 1.2 g, 2.2 mmol) in dry THF (70 mL) at 0 °C. After 8 h, saturated aqueous NH_4Cl/H_2O was added, and the aqueous phase was extracted with ethyl acetate (3 × 100 mL). The organic phase was dried (Na_2SO_4) and after the removal of the solvent under reduced pressure, column chromatography (SiO_2, 20:4 heptane/ethyl acetate 20:4) gave the pure product as yellowish wax (0.88 g, 74%), identical to that previously reported [18].

Pulchrol, or (2-methoxy-6,6-dimethyl-6H-benzo[c]chromen-9-yl)methanol (**1**), HI (55% wt, 0.75 mL, 5.5 mmol) was added to a stirred solution of **2** (50 mg, 0.09 mmol) in MeCN (12.5 mL) at rt. After 70 min, saturated aqueous $Na_2S_2O_3/H_2O$ was added, and the aqueous phase was extracted with ethyl acetate (3 × 12.5 mL), the organic phase was dried (Na_2SO_4) and after the removal of the solvent under reduced pressure the crude product was purified by column chromatography (SiO_2, 20:4 heptane/ethyl acetate) to give pure **1** as a yellowish wax (16.3 mg, 65%). NMR data are shown in Tables 2 and 3. HRMS-ESI+ (*m/z*): $[M + H]^+$ calcd for $C_{17}H_{19}O_3$, 271.1334; found, 271.1339. IR (cm^{-1}): 3402 (br, OH), 2933 (w, CH), 1503 (s), 1463 (m), 1281 (w), 1217 (vs), 1156 (w), 1040 (m), 820 (w).

2-Methoxy-6,6,9-trimethyl-6H-benzo[c]chromene (**3a**)**,** Et3SiH (0.16 mL, 1.0 mmol) and PdCl2 (73.5 mg, 0.4 mmol) were added to a stirred solution of 1 (56 mg, 0.2 mmol) in EtOH (25 mL) at rt. After 150 min, ethyl acetate was added and the mixture was filtered through a plug of celite and washed with ethyl acetate (500 mL). After drying of the organic phase (Na_2SO_4) and the removal of solvent under reduced pressure, purification by column chromatography (SiO_2, 20:1 heptane/ethyl acetate) gave pure 3a as a colorless oil (48 mg, 92%). 1H and 13C-NMR data are shown in Tables 2 and 3. HRMS-ESI+ (*m/z*): $[M + H]^+$ calcd for $C_{17}H_{19}O_2$, 255.1385; found, 255.1392. IR (cm^{-1}): 2931 (m, CH), 1723 (vw), 1504 (m), 1217 (s), 1129 (m), 755 (vs).

9-(chloromethyl)-2-methoxy-6,6-dimethyl-6H-benzo[c]chromene (**3b**), *p*-Toluensulfonylchloride (20.9 mg, 0.11 mmol), DMAP (10.7 mg, 0.09 mmol) and pyridine (8.9 uL, 0.11 mmol) were added to a stirred solution of **1** (19.8 mg, 0.07 mmol) in CH_2Cl_2 (10 mL) at 0 °C. After 24 h, diethyl ether was added, the mixture was stirred for 30 min, and filtered. The filtrate was washed once with saturated aqueous $NaHCO_3/H_2O$ and once with brine, before drying (Na_2SO_4) and removal of the solvent under reduced pressure. The purification of the crude product by column chromatography (SiO_2, 20:2 heptane/ethyl acetate) gave **3b** as a colorless oil (5 mg, 23%). ^1H and ^{13}C-NMR data are shown in Tables 2 and 3. HRMS-ESI+ (*m/z*): $[M + NH_4]^+$ calcd for $C_{17}H_{18}O_2Cl$, 289.0995; found, 289.0992. IR (cm^{-1}): 2938 (w, CH), 1723 (w), 1504 (s), 1424 (m), 1281 (m), 1218 (vs), 1157 (m), 1114 (w), 1040 (m), 814 (w).

General procedure to prepare compounds **3c**–**3e**, $CuBr_2$ (0.1 equiv) was added to 1 (1 equiv) in the corresponding alcohol as solvent (1 mL), at *re*flux. After 12 h, the mixture was cooled to rt, whereafter 10% Na_2CO_3/H_2O was added and the aqueous phase was extracted with $CHCl_3$ (3 × 1 mL). The mixture was filtered through a pad of silica gel and washed with heptane before the solvent was removed from the organic phase under reduced pressure. Purification of the crude products by column chromatography (SiO_2, 40:1 heptane/ethyl acetate) gave the desired products **3c**–**3e**.

2-Methoxy-9-(methoxymethyl)-6,6-dimethyl-6H-benzo[c]chromene (**3c**), Yield 33%. ^1H and ^{13}C shifts are shown in Tables 2 and 3. HRMS-ESI+ (*m/z*): $[M + H]^+$ calcd for $C_{18}H_{21}O_3$, 285.1491; found, 285.1494. IR (cm^{-1}): 2941 (w, CH), 1502 (s), 1424 (m), 1262 (vs), 1105 (w), 1040 (m), 817 (m).

9-(Isopropoxymethyl)-2-methoxy-6,6- dimethyl-6H-benzo[c]chromene (**3d**), Yield 26%. ^1H and ^{13}C shifts are shown in Tables 2 and 3. HRMS-ESI+ (*m/z*): $[M + H]^+$ calcd for $C_{20}H_{24}O_3Na$, 335.1623; found, 335.1627. IR (cm^{-1}): 2931 (w, CH), 1726 (w), 1503 (m), 1463 (w), 1428 (w), 1280 (m), 1218 (s), 1111 (s), 1040 (w), 822 (vw), 756 (vs), 704 (w).

2-Methoxy-6,6-dimethyl-9-(((4-methoxypentyl)oxy)methyl)-6H-benzo[c]chromene (**3e**), Yield 41%. ^{1}H and ^{13}C shifts are shown in Tables 2 and 3. HRMS-ESI+ (*m/z*): $[M + H]^+$ calcd for $C_{23}H_{30}O_3Na$, 377.2093; found, 377.2100. IR (cm^{-1}): 2953 (m, CH), 1503 (s), 1465 (w), 1424 (w), 1281 (w), 1218 (vs), 1156 (w), 1098 (m), 1042 (m), 818 (w).

General procedure to prepare **3f**–**3h**, $[Cp^*IrCl_2]_2$ (0.005 eq), $NaHCO_3$ (0.005 eq), and the corresponding amine (2 eq) were added to a stirred solution of **1** (1 eq) in dry toluene (2 mL), at 100 °C. After 36 h, the solvent was removed under reduced pressure, and purification of the crude product by column chromatography (SiO2, 20:3:0.1 heptane/ethyl acetate/triethylamine) gave the desired products **3f**–**3h**.

N-((2-Methoxy-6,6-dimethyl-6H-benzo[c]chromen-9-yl)methyl)propan-2-amine (**3f**), Yield 25%. ^{1}H and ^{13}C shifts are shown in Tables 2 and 3. HRMS-ESI+ (*m/z*): $[M + H]^+$ calcd for $C_{20}H_{26}NO_2$, 312.1963; found, 312.1964. IR (cm^{-1}): 2929 (w, CH), 1504 (w), 1218 (m), 1155 (w), 1041 (w), 755 (vs).

N-((2-Methoxy-6,6-dimethyl-6H-benzo[c]chromen-9-yl)methyl)-2-methylpropan-1-amine (**3g**), Yield 27%. ^{1}H and ^{13}C shifts are shown in Tables 2 and 3. HRMS-ESI+ (*m/z*): $[M + H]^+$ calcd for $C_{21}H_{28}NO_2$, 326.2120; found, 326.2120. IR (cm^{-1}): 2954 (w, CH), 1503 (w), 1217 (m), 1156 (w), 1041 (w), 755 (vs).

N-((2-Methoxy-6,6-dimethyl-6H-benzo[c]chromen-9-yl)methyl)-3-methylbutan-1-amine (**3h**), Yield 33%. ^{1}H and ^{13}C shifts are shown in Tables 2 and 3. HRMS-ESI+ (*m/z*): $[M + H]^+$ calcd for $C_{22}H_{30}NO_2$, 340.2277; found, 340.2275. IR (cm^{-1}): 2957 (m, CH), 1503 (s), 1422 (m), 1218 (vs), 1158 (w), 1041 (w), 754 (m).

General procedure to obtain compounds **4a-4l**, The corresponding acid anhydride or acid chloride (1.5 equiv), DMAP (1.2 equiv), and Et_3N (1.5 equiv) were added to a stirred solution of **1** (1 equiv) in CH_2Cl_2 (25 ml) at rt. After three hours, saturated aqueous NH_4Cl/H_2O was added, and the aqueous phase was extracted with CH_2Cl_2 (3 × 25 mL) before drying (Na_2SO_4) and removal of the solvent under reduced pressure. Purification by column chromatography (SiO2, 20:4 heptane/ethyl acetate) gave the desired products.

(2-Methoxy-6,6-dimethyl-6H-benzo[c]chromen-9-yl)methyl acetate (**4a**), Yield 92%. ^{1}H and ^{13}C shifts are shown in Tables 2 and 3. HRMS-ESI+ (*m/z*): $[M + H]^+$ calcd for $C_{19}H_{21}O_4$, 313.1440; found, 313.1432. IR (cm^{-1}): 2935 (vw, CH), 1739 (m, C=O), 1504 (m), 1425 (w), 1221 (vs), 1039 (w), 819 (vw).

(2-Methoxy-6,6-dimethyl-6H-benzo[c]chromen-9-yl)methyl isobutyrate (**4b**), Yield 67%. ^{1}H and ^{13}C shifts are shown in Tables 2 and 3. HRMS-ESI+ (*m/z*): $[M + H]^+$ calcd for $C_{21}H_{25}O_4$, 341.1753; found, 341.1749. IR (cm^{-1}): 2974 (w, CH), 1733 (s, C=O), 1504 (m), 1425 (w), 1218 (s), 1156 (s), 1041 (w), 821 (w), 737 (w).

(2-Methoxy-6,6-dimethyl-6H-benzo[c]chromen-9-yl)methyl pivalate (**4c**), Yield 62% ^{1}H and ^{13}C shifts are shown in Tables 2 and 3. HRMS-ESI+ (*m/z*): $[M + NH_4]^+$ calcd for $C_{22}H_{30}O_4N$, 372.2175; found, 372.2170. IR (cm^{-1}): 2975 (m, CH), 1730 (s, C=O), 1505 (m), 1425 (w), 1282 (m), 1219 (m), 1155 (s), 1040 (w), 819 (vw).

(2-Methoxy-6,6-dimethyl-6H-benzo[c]chromen-9-yl)methyl butyrate (**4d**), Yield 58%. ^{1}H and ^{13}C shifts are shown in Tables 2 and 3. HRMS-ESI+ (*m/z*): $[M + NH_4]^+$ calcd for $C_{21}H_{28}O_4N$, 358.2018; found, 358.2014. IR (cm^{-1}): 2966 (w, CH), 1735 (s, C=O), 1505 (m), 1425 (w), 1219 (s), 1173 (s), 1041 (w), 819 (vw), 738 (vw).

(2-Methoxy-6,6-dimethyl-6H-benzo[c]chromen-9-yl)methyl 3-methylbutanoate (**4e**), Yield 79%. ^{1}H and ^{13}C shifts are shown in Tables 2 and 3. HRMS-ESI+ (*m/z*): $[M + NH_4]^+$ calcd for $C_{22}H_{30}O_4N$, 372.2175; found, 372.2180. IR (cm^{-1}): 2961 (m, CH), 1735 (vs, C=O), 1505 (m), 1425 (w), 1283 (w), 1218 (s), 1159 (m), 1094 (w), 1041 (w), 819 (w), 738 m).

(2-Methoxy-6,6-dimethyl-6H-benzo[c]chromen-9-yl)methyl 3,3-dimethylbutanoate (**4f**), Yield 92%. ^{1}H and ^{13}C shifts are shown in Tables 2 and 3. HRMS-ESI+ (*m/z*): $[M + NH_4]^+$ calcd for $C_{23}H_{32}O_4N$, 386.2331; found, 386.2326. IR (cm^{-1}): 2958 (m, CH), 1733 (s, C=O), 1505 (m), 1425 (w), 1221 (vs), 1130 (s), 1042 (w), 819 (vw).

(2-Methoxy-6,6-dimethyl-6H-benzo[c]chromen-9-yl)methyl hexanoate (**4g**), Yield 78%. ^{1}H and ^{13}C shifts are shown in Tables 2 and 3. HRMS-ESI+ (*m/z*): $[M + NH_4]^+$ calcd for $C_{23}H_{32}O_4N$, 386.2331; found, 386.2325. IR (cm^{-1}): 2957 (m, CH), 1736 (vs, C=O), 1505 (s), 1425 (m), 1219 (vs), 1159 (s), 1041 (w), 819 (vw).

(2-Methoxy-6,6-dimethyl-6H-benzo[c]chromen-9-yl)methyl 3-cyclopentylpropanoate (**4h**), Yield 67%. ^{1}H and ^{13}C shifts are shown in Tables 2 and 3. HRMS-ESI+ (*m/z*): $[M + NH_4]^+$ calcd for $C_{25}H_{34}O_4N$, 412.2488; found, 412.2487. IR (cm^{-1}): 2948 (m, CH), 1735 (vs, C=O), 1504 (m), 1425 (m), 1219 (vs), 1158 (s), 1042 (w), 818 (vw).

(2-Methoxy-6,6-dimethyl-6H-benzo[c]chromen-9-yl)methyl cyclohexanecarboxylate (**4i**), Yield 57%. ^{1}H and ^{13}C shifts are shown in Tables 2 and 3. HRMS-ESI+ (*m/z*): $[M + NH_4]^+$ calcd for $C_{24}H_{32}O_4N$, 398.2331; found, 398.2330. IR (cm^{-1}): 2934 (s, CH), 1732 (s, C=O), 1504 (m), 1425 (m), 1219 (vs), 1164 (s), 1131 (m), 1040 (m), 819 (w).

(2-Methoxy-6,6-dimethyl-6H-benzo[c]chromen-9-yl)methyl acrylate (**4j**), Yield 25%. ^{1}H and ^{13}C shifts are shown in Tables 2 and 3. HRMS-ESI+ (*m/z*): $[M + NH_4]^+$ calcd for $C_{20}H_{24}O_4N$, 342.1705; found, 342.1703. IR (cm^{-1}): 2939 (w, CH), 1724 (vs, C=O), 1505 (s), 1425 (m), 1269 (s), 1218 (vs), 1177 (vs), 1114 (w), 1041 (m), 822 (vw).

(2-Methoxy-6,6-dimethyl-6H-benzo[c]chromen-9-yl)methyl furan-2-carboxylate (**4k**), Yield 96%. ^{1}H and ^{13}C shifts are shown in Tables 2 and 3. HRMS-ESI+ (*m/z*): $[M + NH_4]^+$ calcd for $C_{22}H_{24}O_5N$, 382.1654; found, 382.1653. IR (cm^{-1}): 2979 (vw, CH), 1720 (s, C=O), 1572 (vw), 1504 (s), 1425 (m), 1294 (vs), 1218 (s), 1177 (s), 1113 (vs), 1041 (w), 947 (vw), 821 (w), 763 (m), 737 (m).

(2-Methoxy-6,6-dimethyl-6H-benzo[c]chromen-9-yl)methyl benzoate (**4l**), Yield 80%. ^{1}H and ^{13}C shifts are shown in Tables 2 and 3. HRMS-ESI+ (*m/z*): $[M + NH_4]^+$ calcd for $C_{24}H_{26}O_4N$, 392.1862; found, 392.1855. IR (cm^{-1}): 2979 (vw, CH), 1718 (s, C=O), 1504 (m), 1425 (m), 1269 (vs), 1218 (m), 1109 (m), 1040 (w), 821 (vw), 712 (s).

2-Methoxy-6,6-dimethyl-6H-benzo[c]chromene-9-carbaldehyde (**5a**), Dess Martin periodinane 15% (1.4 mL, 0.7 mmol) was added to a stirred solution of **1** (60 mg, 0.2 mmol) in CH_2Cl_2 (50 mL) at rt. After five hours, saturated aqueous $Na_2S_2O_3/H_2O$ was added, and the aqueous phase was extracted with CH_2Cl_2 (3 × 50 mL) before drying (Na_2SO_4) and removal of solvent under reduced pressure. Purification by column chromatography (SiO_2, 20:1 CH_2Cl_2/methanol) gave (55 mg, 93%) as a yellowish wax. ^{1}H and ^{13}C shifts are shown in Tables 2 and 3. HRMS-ESI+ (*m/z*): $[M + H]^+$ calcd for $C_{17}H_{17}O_3$, 269.1178; found, 269.1176. IR (cm^{-1}): 2961 (vw, CH), 1699 (vs, C=O), 1500 (vs), 1426 (m), 1279 (w), 1219 (vs), 1154 (m), 1092 (w), 1039 (m), 946 (vw), 821 (m), 703 (vw).

1-(2-Methoxy-6,6-dimethyl-6H-benzo[c]chromen-9-yl)ethan-1-ol (intermediate in the synthesis of **5b**), MeMgI (3 M, 0.42 mL, 1.2 mmol) was added to **5a** (100 mg, 0.42 mg) in dry ethyl ether (5 mL), at 0 °C. After 20 h, saturated aqueous NH_4Cl/H_2O was added, and the aqueous phase was extracted with diethyl ether (3 × 5 mL). The organic product was washed with brine once before drying (Na_2SO_4) and removal of solvent under reduced pressure. Purification by column chromatography (SiO_2, 20:5 hept/ethyl acetate) gave 61 mg, 51% as a yellowish wax. ^{1}H-NMR (400 MHz, $CDCl_3$) δ 7.64 (d, *J* = 2.0 Hz, 1H), 7.25 (d, *J* = 8.1 Hz, 1H), 7.24 (d, *J* = 1.1 Hz, 1H), 7.17 (d, *J* = 8.1 Hz, 1H), 6.86 (d, *J* = 8.8 Hz, 1H), 6.78 (dd, *J* = 8.7, 2.9 Hz, 1H), 4.90 (q, *J* = 6.4 Hz, 1H), 3.81 (s, 3H), 2.27 (s, 1H), 1.58 (d, *J* = 1.8 Hz, 6H), 1.50 (d, *J* = 6.5 Hz, 3H). ^{13}C-NMR (100 MHz, $CDCl_3$) δ 154.51, 146.85, 145.38, 139.16, 128.85, 125.28, 123.50, 123.10, 119.41, 118.75, 115.30, 108.05, 77.32, 70.31, 55.93, 27.45, 25.29. HRMS-ESI+ (*m/z*): $[M + Na]^+$ calcd for $C_{18}H_{20}O_3$, 307.1310; found, 307.1306. IR (cm^{-1}): 3392 (br, OH), 2969 (m, CH), 1503 (s), 1381 (m), 1282 (m), 1216 (vs), 1157 (m), 1039 (m), 868 (w).

1-(2-Methoxy-6,6-dimethyl-6H-benzo[c]chromen-9-yl)ethan-1-one (**5b**), Celite (250 mg) and PCC (69 mg, 0.31 mmol) were added to a stirred solution of 1-(2-methoxy-6,6-dimethyl-6H-benzo[c]chromen-9-yl)ethan-1-ol (prepared as described above, 61 mg, 0.21 mmol) in dry CH_2Cl_2 (5 mL) under nitrogen, at rt. After 12 h diethyl ether (10 mL) was added and the mixture was filtered over a plug of silica gel and washed

with ethyl acetate (50 mL) before removal of solvent under reduce pressure. Purification by column chromatography (SiO_2, 20:4 hept/ethyl acetate) gave 51.5 mg, 87% as a yellowish wax. ^1H and ^{13}C shifts are shown in Tables 2 and 3. HRMS-ESI+ (*m/z*): $[M + H]^+$ calcd for $C_{18}H_{19}O_3$, 283.1334; found, 283.1334. IR (cm^{-1}): 2980 (vw, CH), 1684 (s, C=O), 1500 (vs), 1421 (m), 1244(s), 1212 (s), 1040 (m), 756 (vs).

2-Methoxy-6,6-dimethyl-6H-benzo[c]chromene-9-carboxylic acid (**5c**), Jones reagent (1 M, 0.5 mL) was added to **1** (60 mg, 0.22 mmol) in acetone (25 mL), at rt. After three hours, isopropanol (25 mL) was added, the organic phase was extracted with saturated aqueous $NaHCO_3$ (3 × 25 mL). HCl (5% v/v) was added to the collected aqueous phase until acid pH (2), then mixture was extracted with EtOAc (2 × 100 mL) before drying (Na_2SO_4) and removal of solvent under reduced pressure, the procedure gave (25.5 mg, 41%) as yellowish wax. ^1H and ^{13}C shifts can be found in Tables 2 and 3. HRMS-ESI+ (*m/z*): $[M + H]^+$ calcd for $C_{17}H_{17}O_4$, 285.1127; found, 285.1132. IR (cm^{-1}): 2928 (vw, CH), 1691 (vs, C=O), 1502 (s), 1429 (w), 1302 (m), 1255 (s), 1041 (w), 948 (w), 758 (m).

Methyl 2-Methoxy-6,6-dimethyl-6H-benzo[c]chromene-9-carboxylate (**5d**), TMSCl (6.7 uL, 0.01 mmol) was added to **5c** (15 mg, 0.052 mmol) in methanol (2 mL) at rt. After 12 h, methanol was removed under reduced pressure and diethyl ether was added to the dry product; the resulting mixture was washed with saturated aqueous $NaHCO_3/H_2O$ before drying (Na_2SO_4) and removal of solvent under reduced pressure. Purification by column chromatography (SiO_2, 20:5 heptane/ethyl) gave (15 mg, 96%) as a colorless wax. ^1H and ^{13}C shifts are shown in Tables 2 and 3. HRMS-ESI+ (*m/z*): $[M + H]^+$ calcd for $C_{18}H_{19}O_4$, 299.1283; found, 299.1290. IR (cm^{-1}): 2950 (vw, CH), 1722 (vs, C=O), 1501 (s), 1412 (w), 1299 (m), 1282 (m), 1251 (vs), 1213 (m), 1156 (m), 1089 (w), 947 (vw), 871 (vw), 771 (vw).

2-Methoxy-6,6-dimethyl-6H-benzo[c]chromene-9-carboxamide (**5e**), Hydroxylamine (74.3 mg, 1.07 mmol) and copper acetate (20 mg, 0.11 mmol) were added to a stirred solution of **5a** (257 mg, 1.07 mmol) in dioxane (5 mL) at 104 °C. After 48 h, saturated aqueous NH_4Cl/H_2O was added, and the aqueous phase was extracted with ethyl acetate (3 × 5 mL) before drying (Na_2SO_4) and removal of solvent under reduced pressure. Purification by column chromatography on silica gel (SiO_2, 99:1 ethyl acetate/methanol) and later on cross-linked dextran polymer beads (Sephadex LH50, 1:1 $CHCl_3$/methanol) gave 22 mg, 7% as a yellowish wax. ^1H and ^{13}C shifts are shown in Tables 2 and 3. HRMS-ESI+ (*m/z*): $[M + H]^+$ calcd for $C_{17}H_{18}NO_3$, 284.1287; found, 284.1286. IR (cm^{-1}): 2964 (vw, CH), 1699 (vs, C=O), 1502 (s), 1434 (m), 1283 (m), 1262 (m), 1215 (s), 1040 (w), 749 (w).

N-hydroxy-2-methoxy-6,6-dimethyl-6H-benzo[c]chromene-9-carboximidamide (**6**), Hydroxylamonium chloride (120 mg, 1.7 mmol) was added to **5a** (83.4 mg, 0.35 mmol) in EtOH (25 mL), at 80 °C. After 12 h, concentrated HCl (0.12 mL, 1.4 mmol) and zinc dust (57.2 mg, 0.90 mmol) were added slowly, at room temperature. After 30 min ammonia (0.5 mL) and 6 M NaOH (7 mL) where added until basic pH (10), the aqueous phase was extracted with CH_2Cl_2 (3 × 25 mL) before drying (Na_2SO_4) and solvent removal under reduced pressure. Purification by column chromatography (SiO_2, 20:1 heptane/ethyl acetate) gave 5.5 mg, 6% as a yellowish wax. ^1H and ^{13}C shifts are shown in Tables 2 and 3. HRMS-ESI+ (*m/z*): $[M + H]^+$ calcd for $C_{17}H_{19}N_2O_3$, 299.1396; found, 299.1399. IR (cm^{-1}): 2967 (m CH), 1682 (m, C=N), 1500 (s), 1214 (s), 1040 (m), 756 (vs).

3.3. Biological Assays

Evaluations against *Leishmania* parasites: Promastigotes of Leishmania-Leishmania: *L. amazonensis*, Clone 1, NHOM-BR-76-LTB-012 (Lma, donated by the Paul Sabatier Université, France) and Leishmania-Viannia: *L. braziliensis* M2904 C192 RJA (M2904, donated by Dr. Jorge Arévalo from Universidad Peruana Cayetano Heredia, Peru) [26]. All strains were cultured in Schneider's insect medium, (pH 6.2) supplemented with 10% FBS and incubated at 26 °C. Medium changes were made every 72 h to maintain a viable parasitic population. Leishmanicidal activity was determined according to Williams with some modifications [27]. Samples were dissolved in DMSO (maximum final concentration 1%) at 10 mg/mL. Promastigotes in logarithmic phase of growth, at the concentration

3×106 parasites/mL, were distributed (100 µL/well) in 96-well flat bottom microtiter plates. Samples with different concentrations (3.1–100 µg/mL) were added (100 µL). Miltefosine (3.1–100 µg/mL), was used as control drug [28]. Assays were performed in triplicates. The microwell plates were incubated for 72 h at 26 °C. After incubation, a solution of XTT (1 mg/mL) in PBS (pH 7.0 at 37 °C) with PMS (0.06 mg/mL) was added (50 µL/well), and incubated for 3 h at 26 °C. The optical density of each well was measured and the IC_{50} values calculated.

Evaluations against *Trypanosoma cruzi*: Cultures of *Trypanosoma cruzi* (epimastigotes, donated by the Parasitology Department of INLASA, Tc-INLASA), were maintained in medium LIT (pH 7.2), supplemented with 10% FBS and incubated at 26 °C. Medium changes were made every 72 h to maintain a viable parasitic population. Trypanocidal activity was determined according to Muelas-Serrano with some modifications [29]. Samples were dissolved in DMSO (maximum final concentration 1%) at 10 mg/mL. Epimastigotes in logarithmic phase of growth, at a concentration of 3×10^6 parasites/mL, were distributed (100 µL/well) in 96-well flat bottom microtiter plates. Samples at different concentrations (3.1–100 µg/mL) were added (100 µL). Benznidazol (3.1–100 µg/mL) was used as the control drug. Assays were performed in triplicates. The microwell plates were incubated for 72 h at 26 °C. After incubation, a solution of XTT (1 mg/mL) in PBS (pH 7.0 at 37 °C) with PMS (0.06 mg/mL) was added (50 µL/well) and incubated for 4 h at 26 °C. The optical density of each well was measured and the IC_{50} values were calculated.

Evaluations against RAW cells: The Raw 264.7 murine macrophage cell line was purchased from the American Type Culture Collection (ATCC-TIB71). The cells were maintained in DMEM-HG medium supplemented with 10% fetal bovine serum, 100 U/mL of penicillin and 100 µg/mL of streptomycin, and sodium bicarbonate (2.2 g/L) in humidified atmosphere at 37 °C with 5% CO_2. Samples were prepared as described above and added (in 100 µL DMSO) at different concentrations (6.2–200 µg/mL). Medium blank, control drugs and cell growth controls were included to evaluate cell viability. The plates were incubated for 72 h at 37 °C with 5% CO_2. After incubation for the indicated time, the cells were washed, after which 10 µL of Resazurin reagent (2.0 mM) was added. They were further incubated at 37 °C for 3 h in a humidified incubator. The IC_{50} values were assessed using a fluorometric reader (540 nm excitation, 590 nm emission) and the Gen5 software. All assays were performed in triplicate.

4. Conclusions

A more efficient synthetic protocol for preparing the antiparasitic plant metabolites pulchrol (**1**) and pulchral (**5a**) was developed. 25 analogues of **1** and **5a** with chemical variations of the benzylic alcohol functionality were prepared starting from **1**, and their antiparasitic activity against *T. cruzi*, *L. brasiliensis* and *L. amazoniensis* was tested. Although it was not possible to establish structure–activity relationships for such complex biological activities with the limited number of analogues available here, focusing on only one part of the core structure investigated, only some general suggestions can be made. In addition, nothing is known about the molecular targets that pulchrol (**1**) and its analogues interact with, it could be several and they may differ in the different organisms. In addition, changes in a chemical structure will give a new analogue somewhat different chemical properties. Changes in for example the solubility will affect the ability of a compound to penetrate cell membranes and thereby its capability to reach critical molecular targets in the required concentrations, and it is difficult to separate changes in the chemical properties with ability to target proteins. Hence, the better activity of the esters may be due to their higher lipophilicity, resulting in higher bioavailability, acting as 'prodrugs'. In addition, we have no knowledge about the metabolic capacities of these organisms, which may affect the fate of the assayed compounds strongly. With that said, indications suggest that the benzylic oxygen in pulchrol is important for the anti-parasitic activity against *T. cruzi*, *L. amazoniensis* and *L. brasiliensis*, in some kind of hydrogen bond accepting capacity. The hydrogen bond donor role for pulchrol has been discarded for all cases, but hydrogen bond acceptor capability appears to be important from comparisons with the corresponding ethers, amines and esters analogues. In general, the more branched ethers and esters are more potent, suggesting a lipophilic pocket at the binding site.

This presumed active site on which pulchrol and its analogues may be acting, is probably somewhat different in the different organisms. In *L. brasiliensis* there appear to be limited for branched chains of around five carbons, while *T. cruzi* and *L. amazoniensis* seem to have some flat hydrophobic regions that enhance the activity of aromatic and planar substituents. The selectivity as the SI is below or around 1 for most of the compounds, but is considerably higher in some examples. This is an important property to learn to understand, if compounds developed from this model ever should move forward into clinic trials. The best compound developed in this investigation is the vinyl ester **4j**. It shows potencies well below those of the positive controls and selectivity indexes of more than 5 for all three organisms. Another name for **4j** is an acrylic acid ester, and it is known that the acrylic acid derivatives may be weakly reactive as Michael acceptors. However, this is only relevant when an acrylic acid ester is bound to a pocket of a protein and presented to a highly reactive nucleophile (e.g., a thiol group of a cysteine, acting as an irreversible 'covalent inhibitor'). If this is the explanation for the potency and selectivity of **4j** in this investigation, this type of analogues can eventually be used for the fishing out of the molecular targets of the parasites, and enable studies of such.

Author Contributions: P.T. is a PhD student that has planned and carried out the syntheses of the assayed compounds and written the manuscript, E.S. has carried out the biological assays, M.D. has supervised PT:s research in Cochabamba, S.M. has supervised PT:s work in Lund, A.G. has supervised ES:s work in La Paz, while O.S. has supervised PT:s work in Lund and compiled the manuscript. All authors have read and agreed to the published version of the manuscript.

Funding: This research was funded by the Swedish International Development Cooperation Agency (SIDA), including a Ph.D. scholarship for PT is gratefully acknowledged.

Conflicts of Interest: The authors declare no conflict of interest. The sponsors had no role in the design, execution, interpretation, or writing of the study.

References

1. World Health Organization Home Page. Available online: https://www.who.int/chagas/disease/en/ (accessed on 19 December 2019).
2. World Health Organization Home Page. WHO Report on Global Surveillance of Epidemic-prone Infectious Diseases – Leishmaniasis. Available online: https://www.who.int/csr/resources/publications/CSR_ISR_2000_1leish/en/ (accessed on 19 December 2019).
3. Pratap, R.; Ram, V.J. Natural and synthetic chromenes, fused chromenes, and versatility of dihydrobenzo[h]chromenes in organic synthesis. *Chem. Rev.* **2014**, *114*, 10476–10526. [CrossRef] [PubMed]
4. Erosa-Rejón, G.J.; Yam-Puc, A.; Chan-Bacab, M.J.; Giménez-Turbax, A.; Salamanca, E.; Peña-Rodríguez, L.M.; Sterner, O. Benzochromenes from the roots of *Bourreria pulchra*. *Phytochem. Lett.* **2010**, *3*, 9–12. [CrossRef]
5. Appendino, G.; Gibbons, S.; Giana, A.; Pagani, A.; Grassi, G.; Stavri, M.; Smith, E.; Rahman, M.M. Antibacterial cannabinoids from *Cannabis sativa*: A structure−activity study. *J. Nat. Prod.* **2008**, *71*, 1427–1430. [CrossRef] [PubMed]
6. Carroll, A.R.; Bowden, B.F.; Coll, J.C. Studies of australian ascidians. III. A new tetrahydrocannabinol derivative from the ascidian *Synoicum castellatum*. *Aust. J. Chem.* **1993**, *46*, 1079–1083. [CrossRef]
7. Simon-Levert, A.; Arrault, A.; Bontemps-Subielos, N.; Canal, C.; Banaigs, B. Meroterpenes from the ascidian *Aplidium aff. densum*. *J. Nat. Prod.* **2005**, *68*, 1412–1415. [CrossRef] [PubMed]
8. Bukuru, J.F.; Van, T.N.; Van Puyvelde, L.; Mathenge, S.G.; Mudida, F.P.; De Kimpe, N. A benzochromene from the roots of *Pentas bussei*. *J. Nat. Prod.* **2002**, *65*, 783–785. [CrossRef]
9. Altemöller, M.; Gehring, T.; Cudaj, J.; Podlech, J.; Goesmann, H.; Feldmann, C.; Rothenberger, A. Total synthesis of graphislactones A, C, D, and H, of ulocladol, and of the originally proposed and revised structures of graphislactones E and F. *Eur. J. Org. Chem.* **2009**, *2009*, 2130–2140. [CrossRef]
10. Kidwai, M.; Saxena, S.; Rahman Khan, M.K.; Thukral, S.S. Aqua mediated synthesis of substituted 2-amino-4H-chromenes and in vitro study as antibacterial agents. *Bioorg Med. Chem. Lett.* **2005**, *15*, 4295–4298. [CrossRef]
11. Soni, R.; Umar, S.; Shah, N.N.; Balkrishnan, S.; Soman, S.S. Design, synthesis, and anticancer activity of 3H–benzo[f]chromen-3-one derivatives. *J. Heterocycl. Chem.* **2017**, *54*, 2501–2510. [CrossRef]

12. Bhattacharya, P.; Senapati, K.; Chattopadhyay, K.; Mandal, S.M.; Basak, A. Synthesis of benzochromenes and dihydrophenanthridines with helical motifs using Garratt–Braverman and Buchwald–Hartwig reactions. *RSC Adv.* **2015**, *5*, 61562–61574. [CrossRef]
13. Sun, W.; Cama, L.D.; Birzin, E.T.; Warrier, S.; Locco, L.; Mosley, R.; Hammond, M.L.; Rohrer, S.P. 6H-Benzo[c]chromen-6-one derivatives as selective ERβ agonists. *Bioorg, Med. Chem. Lett.* **2006**, *16*, 1468–1472. [CrossRef]
14. Khanolkar, A.D.; Lu, D.; Ibrahim, M.; Duclos, J.R.I.; Thakur, G.A.; Malan, J.T.P.; Porreca, F.; Veerappan, V.; Tian, X.; George, C.; et al. A novel class of CB2 selective agonists with peripheral analgesic activity. *J. Med. Chem.* **2007**, *50*, 6493–6500. [CrossRef] [PubMed]
15. Campos-Ríos, M.G. Revisión del género Bourreria P. Browne (Boraginaceae) en México. *Polibotánica* **2005**, *19*, 39–103.
16. Argueta, A.; Cano, L.; Roderte, M.E. *Atlas de las plantas de la medicina tradicional Mexicana*; Instituto Nacional Indigenista: Mexico, 1994; pp. 483–485.
17. Polanco-Hernández, G.; Escalante-Erosa, F.; García-Sosa, K.; Acosta-Viana, K.; Chan-Bacab, M.J.; Sagua-Franco, H.; González, J.; Osorio-Rodríguez, L.; Moo-Puc, R.E.; Peña-Rodríguez, L.M. In vitro and in vivo trypanocidal activity of native plants from the Yucatan peninsula. *Parasitol. Res.* **2012**, *110*, 31–35. [CrossRef]
18. Killander, D.; Sterner, O. Synthesis of the Bioactive Benzochromenes pulchrol and pulchral, metabolites of *Bourreria pulchra*. *Eur. J. Org. Chem.* **2014**, *2014*, 1594–1596. [CrossRef]
19. Killander, D.; Sterner, O. Reagent-controlled cyclization–deprotection reaction to yield either fluorenes or benzochromenes. *Eur. J. Org. Chem.* **2014**, *2014*, 6507–6512. [CrossRef]
20. Mazimba, O. Synthetic protocols on 6H-benzo[c]chromen-6-ones: A review. *Turk. J. Chem.* **2016**, *40*, 1–27. [CrossRef]
21. Singha, R.; Roy, S.; Nandi, S.; Ray, P.; Ray, J.K. Palladium-catalyzed one-pot Suzuki–Miyaura cross coupling followed by oxidative lactonization: A novel and efficient route for the one-pot synthesis of benzo[c]chromene-6-ones. *Tetrahedron Lett.* **2013**, *54*, 657–660. [CrossRef]
22. Zhou, J.; Huang, L.-Z.; Li, Y.-Q.; Du, Z.-T. Synthesis of substituted 6H-benzo[c]chromenes: A palladium promoted ring closure of diazonium tetrafluoroborates. *Tetrahedron Lett.* **2012**, *53*, 7036–7039. [CrossRef]
23. Campeau, L.-C.; Parisien, M.; Leblanc, M.; Fagnou, K. Biaryl Synthesis via direct arylation: Establishment of an efficient catalyst for intramolecular processes. *J. Am. Chem. Soc.* **2004**, *126*, 9186–9187. [CrossRef]
24. Roman, D.S.; Takahashi, Y.; Charette, A.B. Potassium *tert*-butoxide promoted intramolecular arylation via a radical pathway. *Org. Lett.* **2011**, *13*, 3242–3245. [CrossRef] [PubMed]
25. Leadbeater, N.E.; Marco, M. Rapid and amenable Suzuki coupling reaction in water using microwave and conventional heating. *J. Org. Chem.* **2003**, *68*, 888–892. [CrossRef]
26. Bilbao-Ramos, P.; Dea-Ayuela, M.A.; Cardenas-Alegría, O. Leishmaniasis in the major endemic region of Plurinational state of Bolivia: Species identification, phylogeography and drug susceptibility implications. *Acta Trop.* **2017**, *176*, 150–161. [CrossRef] [PubMed]
27. Williams, C.; Espinosa, O.A.; Montenegro, H. Hydrosoluble formazan XTT: Its application to natural products drug discovery for *Leishmania*. *J. Microbiol. Methods* **2003**, *55*, 813–816. [CrossRef] [PubMed]
28. Campos-Buzzi, F.; Fracasso, M.; Clase, B.K.; Ticona, J.C.; Gimenez, A.; Cechinel-Filho, V. Evaluation of antinociceptive effects of *Galipea longiflora* alkaloid extract and major alkaloid 2-fenilquinoline. *Methods Find. Exp. Clin. Pharmacol.* **2010**, *32*, 707–711. [CrossRef] [PubMed]
29. Muelas-Serrano, S.; Nogal-Ruiz, J.; Gomez-Barrio, A. Setting of a colorimetric method to determine the viability of *Trypanosoma cruzi* epimastigotes. *Parasitol Res.* **2000**, *86*, 999–1002. [CrossRef]

Sample Availability: No samples of the compounds assayed here are available from the authors, but their synthesis in good yields is described in detail.

Paper II

molecules

MDPI

Article

SARs for the Antiparasitic Plant Metabolite Pulchrol. Part 2: B- and C-Ring Substituents

Paola Terrazas [1,2], Sophie Manner [1], Olov Sterner [1,*], Marcelo Dávila [2], Alberto Giménez [3] and Efrain Salamanca [3]

[1] Department of Chemistry, Centre for Analysis and Synthesis, Lund University, 22100 Lund, Sweden; paola.terrazas_villarroel@chem.lu.se (P.T.); sophie.manner@chem.lu.se (S.M.)
[2] Centre of Agroindustrial Technology, San Simón University, Cochabamba 3299, Bolivia; marcelodavila@fcyt.umss.edu.bo
[3] Institute for Pharmacological and Biochemical Sciences, San Andrés University, La Paz 3299, Bolivia; agimenez@megalink.com (A.G.); efrain_salamanca@hotmail.com (E.S.)
* Correspondence: Olov.Sterner@chem.lu.se; Tel.: +46-70-5306649

Received: 31 August 2020; Accepted: 29 September 2020; Published: 1 October 2020

Abstract: Neglected tropical diseases affect most of the underprivileged populations in tropical countries. Among these are chagas and leishmaniasis, present mainly in South and Central America, Africa and East Asia. Current treatments are long and have severe adverse effects, therefore there is a strong need to develop alternatives. In this study, we base our research on the plant metabolite pulchrol, a natural benzochromene which has been shown to possess antiparasitic activity against *Trypanosoma* and *Leishmania* species. In a recent study, we investigated how changes in the benzyl alcohol functionality affected the antiparasitic activity, but the importance of B- and C-ring substituents is not understood. Fifteen derivatives of pulchrol with different substituents in positions 1, 2, 3, and 6 while leaving the A-ring intact, were therefore prepared by total synthesis, assayed, and compared with pulchrol and positive controls. The generated series and parental molecule were tested in vitro for antiparasitic activity against *Trypanosoma cruzi*, *Leishmania braziliensis*, and *L. amazonensis*, and cytotoxicity using RAW cells. Substantial differences in the activity of the compounds synthesized were observed, of which some were more potent towards *Trypanosoma cruzi* than the positive control benznidazole. A general tendency is that alkyl substituents improve the potency, especially when positioned on C-2.

Keywords: *Trypanosoma cruzi*; *Leishmania amazonensis*; *Leishmania braziliensis*; pulchrol; benzo[*c*]chromenes; Structure-Activity Relationships (SARs)

1. Introduction

Neglected Tropical Diseases (NTDs) native to tropical regions, affect around 1 billion people in 149 countries [1], most of them part of underprivileged populations [2–4]. Some NTDs are associated to parasites from the family Trypanosomatidae, among them *Trypanosoma cruzi* which causes the chagas disease, while several *Leishmania* species are responsible for leishmaniasis. Chagas disease (transmitted by a Triatominae bug) affects around 8 million people, mainly in South and Central America [5]. It may remain asymptomatic for decades until the heart tissue is eventually damaged sufficiently to cause death [6,7]. The antiparasitic drugs benznidazole and nifurtimox are used to treat chagas, and are efficient when given immediately after infection. However, they lose efficiency with time, and present serious adverse effects [8,9]. Leishmaniasis (transmitted by Phlebotomine sand flies) is found mainly in Africa, Latin America and East Asia. It exists in three forms: cutaneous, mucocutaneous, and visceral, and some 700,000 to 1 million new cases occur annually [10]. The treatment, mainly pentavalent

antimonials, amphotericin B or miltefosine, can be associated to serious adverse effects, and in some cases require hospitalization [11].

An important source for the development of new drug candidates is Nature itself, and natural products may provide new bioactive and selective chemical leads [12]. However, the isolation of novel drug candidates from natural sources is often hampered by the minute amounts available, which prevent them from being assayed in pharmacological tests [12–14]. The development of synthetic routes to obtain these natural materials solve the problem, and also allows derivatives and analogues to be prepared in order to understand SARs [12,15].

A scaffold for biologically active natural products is benzo[*c*]chromene, and benzo[*c*]chromenes have been shown to possess a wide range of biological activities, and this study is based on pulchrol (**1**). They have been isolated from lichens belonging to the *Graphis* genus, the fungus *Acremonium* (which also produces cephalosporin antibiotics), and many plants [16]. Benzo[*c*]chromenes may for example inhibit cholinesterase enzymes [17], and have an affinity for the cannabinoid receptors CB1 and CB2 [18]. Cannabinol (**2,** see Figure 1), isolated from the plant *Cannabis sativa*, has 10 times stronger affinity for the CB2 receptor compared to the main constituent of *Cannabis*, THC (**3**), which is responsible for its psychotropic activity [19]. Cannabinol (**2**) was also found to possess immunomodulatory [20], and antineoplastic activity in Lewis lung tumor cells [21].

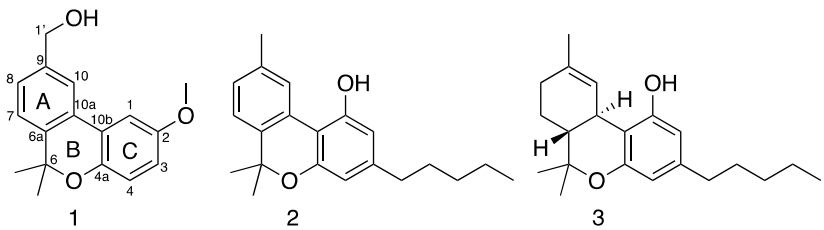

Figure 1. Structures of pulchrol (**1**), cannabinol (**2**) and tetrahydrocannabinol (THC) (**3**).

The benzo[*c*]chromene pulchrol (**1**), found in the roots of *Bourreria pulchra*, [22] is known as "Bakalche" in Yucatan (Mexico) and used to treat cutaneous diseases, injuries, viral infections and fevers [23,24]. Pulchrol (**1**) was found to possess antiparasitic activity against *Leishmania braziliensis*, *L. amazonensis*, *L. mexicana* and *Trypanosoma cruzi* [22,25]. A synthetic route was developed in 2014 [26,27], and recently we reported the effects that transformations of its A-ring benzyl alcohol functionality have against *T. cruzi* epimastigotes, *L. amazonensis* promastigotes and *L. braziliensis* promastigotes, as well as their cytotoxicity towards mammalian cells (assayed in RAW cells) [28]. We are now interested to expand the previous study [28] with compounds having various substituents in the B- and C-rings. Our aim is to use the synthetic routes and some of the intermediates used for the synthesis of pulchrol (**1**), to obtain new derivatives. The only position available for exchange in the B-ring is C-6, and we were especially interested in examining the role of the alkyl substituents. Ring C has theoretically four positions open for substitution, but in practice only three. Here we focused on the presence and position of a methoxy group, as well as various alkyl substituents. As a result, we have prepared 15 new analogues (**8a–10g**, **10a–10h**) and we have tested them for antiparasitic activity towards *T. cruzi*, *L. amazonensis* and *L. braziliensis* together with **1** and the positive controls benznidazole and miltefosine. The cytotoxicity towards mammalian cells of all the compounds was determined with murine macrophage cells (RAW). This and additional studies of the antiparasitic activities of pulchrol analogues will eventually provide us with a model that can be used for the design of more potent antiparasitic structures with lower cytotoxicity.

2. Results and Discussion

2.1. Modifications in the B-Ring

The synthetic routes used to prepare derivatives with variations in ring B were partly based on an already published synthetic route to yield pulchrol [26]. The common intermediate **4** was used as the starting material for the synthesis of all ring B derivatives (see Scheme 1).

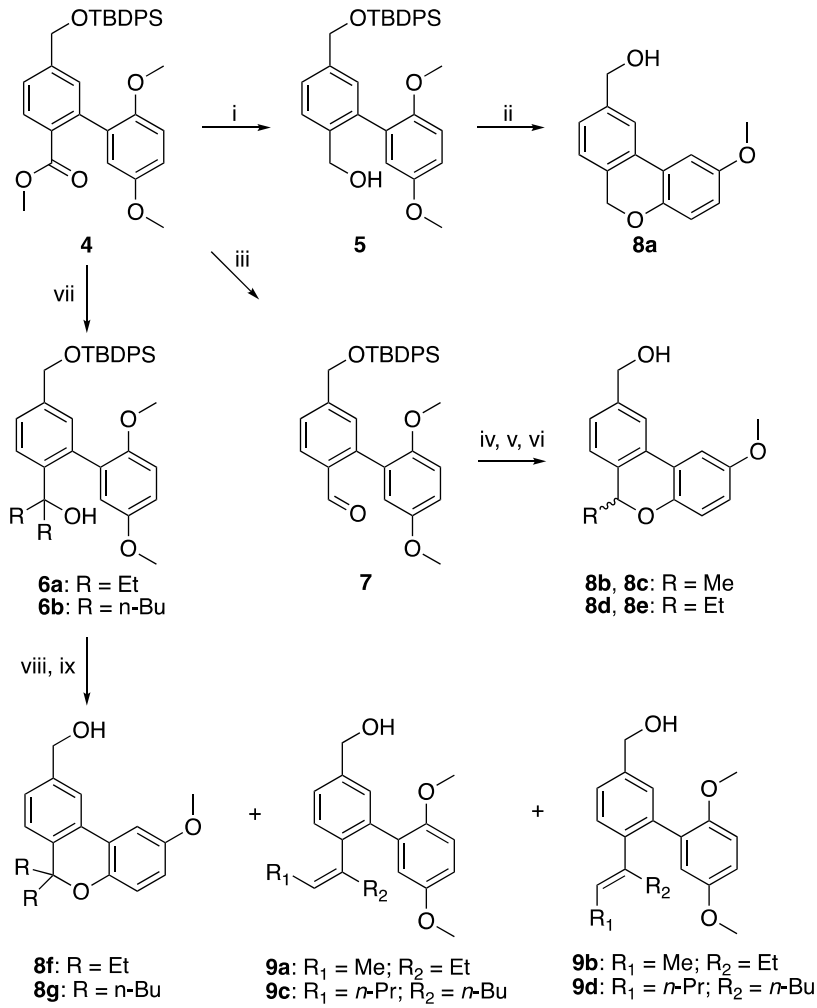

Scheme 1. *Reagents and conditions*: (i) **4** (1 equiv), DIBALH (2.4 equiv), dry toluene, −78 °C; (ii) **5** (1 equiv), NaSEt (4 equiv), dry DMF, 110 °C; (iii) **4** (1 equiv), morpholine (2 equiv), DIBALH (1 equiv), dry THF, 0 °C; (iv) **7** (1 equiv), corresponding organolithium reagent (2 equiv), dry THF, 0 °C or −78 °C depending on the organolithium reagent; (v) PBr_3 (0.34 equiv), LiI (3 equiv), dry CH_2Cl_2, rt; (vi) TBAF (2 equiv), THF, rt; (vii) **4** (1 equiv), organolithium reagent (4 equiv), dry THF, 0 °C or −78 °C depending on the organolithium reagent; (viii) **6** (1 equiv), HI (10 equiv), MeCN, rt; (ix) TBAF (1.1 equiv), THF, rt.

Derivative **8a** was prepared by reducing the ester group in **4** to the alcohol **5**, which was treated with NaSEt in dry DMF at 110 °C to obtain an *ortho* demethylated phenol, which was not isolated as an intermediate as it spontaneously cyclized and was deprotected to the desired product **8a**,

the 6-demethylated analogue of **1**, albeit in low yields (7%). The monosubstituted analogues **8b**–**8e** were prepared by reducing the ester functionality of **4** to the aldehyde **7**, which by alkyl addition was transformed to the corresponding secondary alcohol. Cyclization using PBr_3 in the presence of LiI gave the desired compounds [29]. The products **8b**–**8e** were obtained as racemic pairs, and the enantiomers were separated by HPLC with a normal phase semipreparative chiral column. The pure enantiomers were obtained in low yields (less than 10%). The determination of the absolute configuration of **8b**–**8e**, which could have been done with the secondary alcohols by the Mosher's method, was not attempted as the enantiomers were approximately equipotent (*vide infra*). The absolute configuration of C-6 does not appear to influence the potency.

The 6.6-diethyl and 6.6-dibutyl analogues **8f** and **8g** were prepared from **6**a and **6b**, based on the pulchrol synthetic route [26]. The new alkyl groups were introduced by a double addition step to the ester group in **4** using the corresponding organolithium reagents. For the cyclization of **6a** and **6b** to **8f** and **8g**, an excess in hydroiodic acid was used, to avoid the formation of cannabidiol type byproducts as a result of elimination [28]. Nevertheless, the byproducts **9a** and **9b** appeared together with **8f**, and **9c** and **9d** with **8g**. The desired products were obtained by HPLC purification, with moderate yields (**8f** 30% and **8g** 56%).

2.2. *Modifications in the C-Ring*

Analogues modified in the C-ring (see Figure 2 for the structures of compounds **10a** to **10h**) were prepared based on the procedure used to synthesize pulchrol (**1**) [26], but with different methoxylated phenyls forming the biaryl (corresponding to **4**) through a Suzuki coupling reaction. The major difference in the biaryl formation was that the reaction time in the microwave reactor had to be increased from 30 min to 60 min. The yields were generally good, varying from 75% to 92%. During the cyclization most of the alkyl substituted analogues were obtained in better yields (72% to 85%) than the derivatives **10a** and **10b** substituted with methoxy groups.

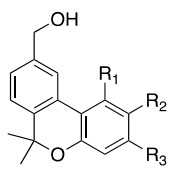

10

Figure 2. Modifications on ring C: **10a** R_1 = H, R_2 = H, R_3 = OMe; **10b** R_1 = OMe, R_2 = H, R_3 = H; **10c** R_1 = H, R_2 = Me, R_3 = H; **10d** R_1 = H, R_2 = H, R_3 = Me; **10e** R_1 = H, R_2 = H, R_3 = H; **10f** R_1 = H, R_2 = *i*-Pr, R_3 = H; **10g** R_1 = H, R_2 = H, R_3 = *i*-Pr; **10h** R_1 = H, R_2 = *n*-Pen, R_3 = H. See the Section 3 for synthetic details.

The biological activities of all the synthesized derivatives are given in Table 1, while the ^{1}H- and ^{13}C-NMR chemical shifts of the assayed compounds are given in Tables 2 and 3.

Table 1. Antileishmanial, antitrypanozomal and cytotoxic activity of the synthesised derivatives, compared to the positive controls Benznidazole and Miltefosine. The IC_{50} values are given in mM as average data, with the standard deviations from at least three independent experiments. See Experimental for details about the assays.

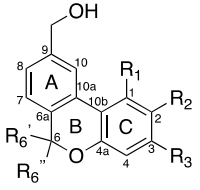

Mol.	$R_{6'}$	$R_{6'}{}'$	R_1	R_2	R_3	*T. cruzi*		*L. brasiliensis*		*L. amazoniensis*		Cytotoxicity [a]
						IC_{50} (μM)	SI [b]	IC_{50} (μM)	SI [b]	IC_{50} (μM)	SI [b]	IC_{50} (μM)
1	Me	Me	H	OMe	H	18.5 ± 9.6	1.7	59.2 ± 11.8	0.5	77.7 ± 5.5	0.4	30.7 ± 1.1
8a	H	H	H	OMe	H	66.0 ± 18.2	1.3	248.1 ± 54.1	0.3	132.1 ± 29.3	0.6	82.6 ± 9.5
8b	Me	H	H	OMe	H	35.9 ± 11.7	1.0	156.1 ± 23.4	0.2	156.1 ± 58.5	0.2	37.1 ± 3.9
8c	H	Me	H	OMe	H	67.1 ± 31.2	0.8	128.8 ± 24.6	0.4	71.8 ± 12.5	0.7	52.7 ± 9.0
8d	Et	H	H	OMe	H	51.8 ± 9.2	0.6	45.9 ± 20.3	0.7	71.4 ± 1.1	0.4	30.0 ± 3.7
8e	H	Et	H	OMe	H	37.0 ± 0.7	1.2	45.1 ± 19.2	1.0	70.3 ± 3.7	0.6	44.4 ± 11.5
8f	Et	Et	H	OMe	H	10.4 ± 0.3	4.2	46.9 ± 5.0	0.9	36.9 ± 3.4	1.2	43.6 ± 15.1
8g	Bu	Bu	H	OMe	H	22.8 ± 8.5	1.5	29.3 ± 1.4	1.2	25.4 ± 1.1	1.4	35.3 ± 17.5
10a	Me	Me	H	H	OMe	88.4 ± 12.2	0.7	37.4 ± 1.1	1.6	66.6 ± 7.4	0.9	59.2 ± 25.9
10b	Me	Me	OMe	H	H	92.5 ± 14.8	0.5	48.1 ± 18.5	1.0	179.8 ± 21.9	0.3	48.1 ± 18.5
10c	Me	Me	H	Me	H	31.5 ± 7.9	1.3	39.3 ± 2.4	1.0	64.9 ± 12.6	0.6	39.3 ± 1.6
10d	Me	Me	H	H	Me	33.0 ± 3.9	1.1	40.1 ± 8.3	0.9	51.9 ± 13.8	0.7	35.4 ± 7.9
10e	Me	Me	H	H	H	50.8 ± 6.2	1.2	74.9 ± 16.6	0.8	91.6 ± 5.4	0.7	62.4 ± 6.2
10f	Me	Me	H	*i*-Pr	H	12.4 ± 3.5	0.7	18.1 ± 0.7	0.5	15.6 ± 2.8	0.6	8.9 ± 3.5
10g	Me	Me	H	H	*i*-Pr	14.2 ± 4.2	1.6	19.1 ± 1.1	1.1	21.2 ± 7.1	1.0	22.0 ± 7.1
10h	Me	Me	H	*n*-Pen	H	6.4 ± 0.3	2.0	16.4 ± 0.3	0.8	16.8 ± 1.9	0.8	12.9 ± 3.2
		Benznidazole				19.2 ± 7.7	3.9	-	-	-	-	74.7 ± 9.1
		Miltefosine				-	-	13.0 ± 1.2	5.9	10.8 ± 1.5	7.1	76.6 ± 3.2

[a] Toxicity was measured on RAW cells, see Experimental for details, [b] SI, selectivity index (cytotoxicity/anti-protozoal activity).

Table 2. Proton chemical shifts (in ppm) for the compounds prepared in this study, measured in $CDCl_3$ at 400 MHz. The assignments were made with 2D NMR spectroscopy, COSY, HMQC and HMBC experiments.

Compd.	1-H	2-H	3-H	4-H	7-H	8-H	10-H	1′-H/H_2	2-OCH_3	6-H/H_2	6,6-CH_3
1	7.26	-	6.81	6.89	7.23	7.30	7.68	4.74	3.85	-	1.61
8a	7.27	-	6.82	6.93	7.15	7.29	7.68	4.76	3.85	5.06	-
8b	7.26	-	6.81	6.92	7.15	7.29	7.67	4.75	3.84	5.20	1.60
8c	7.26	-	6.82	6.92	7.16	7.29	7.68	4.75	3.85	5.20	1.60
8d [a]	7.25	-	6.81	6.92	7.12	7.28	7.68	4.75	3.85	4.98	-
8e [b]	7.26	-	6.81	6.92	7.12	7.28	7.68	4.75	3.85	4.99	-
8f [c]	7.25	-	6.80	6.87	7.11	7.28	7.71	4.75	3.84	-	-
8g [d]	7.24	-	6.79	6.85	7.11	7.28	7.70	4.75	3.84	-	-
10a [e]	7.65	6.60	-	6.51	7.21	7.24	7.65	4.73	-	-	1.63
10b [f]	-	6.63	7.17	6.64	7.25	7.30	8.43	4.72	-	-	1.61
10c [g]	7.56	-	7.04	6.85	7.23	7.28	7.73	4.74	-	-	1.62
10d [h]	7.62	6.84	-	6.78	7.21	7.24	7.68	4.71	-	-	1.62
10e	7.74	7.03	7.24	6.96	7.22	7.27	7.72	4.72	-	-	1.64
10f [i]	7.59	-	7.10	6.87	7.23	7.28	7.75	4.76	-	-	1.62
10g [j]	7.66	6.89	-	6.83	7.22	7.26	7.70	4.73	-	-	1.63
10h [k]	7.55	-	7.05	6.86	7.22	7.27	7.74	4.74	-	-	1.62

[a] Ethyl signals at 1.89, 1.69 and 1.03 ppm. [b] Ethyl signals at 1.89, 1.69 and 1.03 ppm. [c] Ethyl signals at 1.91 and 0.88 ppm. [d] *n*-butyl signals at 1.86, 1.28, 1.24, 0.83 ppm. [e] Methoxy signal at 3.82 ppm. [f] Methoxy signal at 3.95 ppm. [g] Methyl signal at 2.36 ppm. [h] Methyl signal at 2.34 ppm. [i] Isopropyl signals at 2.93 and 1.29 ppm. [j] Isopropyl signals at 2.88 and 1.26 ppm. [k] *n*-Pentyl signals at 2.61, 1.66, 1.36, 0.93 ppm.

Table 3. ^{13}C-NMR chemical shifts (in ppm) for the assayed compounds **1**, **3a–h**, **4a–l**, **5a–e** and **6** determined at 100 MHz in $CDCl_3$. The assignments were made with 2D NMR spectroscopy, COSY, HMQC and HMBC experiments.

Compd	C-1	C-2	C-3	C-4	C-4a	C-6	C-6a	C-7	C-8	C-9	C-10	C-10a	C-10b	C-1′	2-OCH_3	6,6-CH_3/6-CH_3
1	108.0	154.6	115.5	118.8	146.9	77.4	139.5	123.7	126.8	140.4	121.0	129.1	123.0	65.3	56.0	27.5
8a	108.3	155.0	115.6	118.2	149.0	68.6	131.4	125.1	126.5	141.2	120.8	130.7	123.5	65.4	56.0	-
8b	108.1	154.8	115.6	118.6	147.7	73.6	135.8	124.5	126.7	140.8	121.0	129.9	123.2	65.4	56.0	20.1
8c	108.1	154.8	115.6	118.6	147.7	73.6	135.8	124.5	126.7	140.8	121.0	129.9	123.2	65.4	56.0	20.1
8d[a]	108.1	154.7	115.5	118.7	146.9	78.9	134.9	125.3	126.5	140.8	121.0	129.6	123.1	65.4	56.0	-
8e[b]	108.1	154.7	115.5	118.7	146.9	78.9	134.9	125.4	126.5	140.8	121.0	129.6	123.1	65.5	56.0	-
8f[c]	107.8	154.2	115.4	118.4	147.1	82.4	136.3	125.2	126.2	139.9	120.8	130.0	122.2	65.3	55.9	-
8g[d]	107.9	154.3	115.6	118.5	147.2	82.2	137.1	125.3	126.4	140.0	120.9	129.9	122.2	65.4	56.0	-
10a[e]	124.0	108.5	161.2	102.9	154.2	78.1	137.9	123.6	125.7	140.4	120.2	129.2	115.4	65.4	-	27.7
10b[f]	157.7	104.7	129.2	111.4	154.7	77.3	139.5	122.9	126.2	139.8	125.8	128.0	112.3	65.8	-	27.1
10c[g]	123.5	130.8	130.4	117.9	150.7	77.5	139.2	123.6	126.5	140.3	120.9	129.2	122.0	65.4	-	27.6
10d[h]	122.8	122.6	140.0	118.6	152.8	77.5	138.6	123.6	126.2	140.3	120.6	129.1	119.6	65.3	-	27.7
10e	123.0	121.7	129.7	118.2	152.9	77.6	139.0	123.6	126.6	140.4	120.9	129.0	122.4	65.2	-	27.7
10f[i]	120.8	142.1	127.7	117.9	150.9	77.4	139.3	123.7	126.5	140.3	120.9	129.4	121.9	65.5	-	27.7
10g[j]	122.8	120.1	151.3	115.8	152.9	77.6	138.7	123.6	126.2	140.3	120.7	129.2	119.8	65.4	-	27.8
10h[k]	122.8	136.1	129.7	117.9	150.8	77.5	139.2	123.6	126.5	140.3	120.9	129.3	121.9	65.4	-	27.7

[a] Ethyl signals at 27.6 and 10.2 ppm. [b] Ethyl signals at 27.6 and 10.2 ppm. [c] Ethyl signals at 30.6 and 8.2 ppm. [d] *n*-Butyl signals at 38.4, 26.1, 23.2 and 14.2 ppm. [e] Methoxy signal at 55.5 ppm. [f] Methoxy signal at 55.8 ppm. [g] Methyl signal at 21.1 ppm. [h] Methyl signal at 21.5 ppm. [I] Isopropyl signals at 33.9 and 24.4 ppm. [j] Isopropyl signals at 34.1 and 23.9 ppm. [k] *n*-Pentyl signals at 35.7, 31.7, 31.6, 22.7 and 14.2 pp.

2.3. Antiparasitic Activity of Pulchrol (**1**)

The natural product pulchrol has previously been investigated and shown to be toxic towards *Trypanosoma* and *Leishmania* parasites in vitro. The highest activity was reported towards *T. cruzi* epimastigotes (IC_{50} 18.5 μM) which is comparable to the potency shown by the drug benznidazole (19.2 μM) that currently is used to treat the chagas disease. Pulchrol also showed moderate leishmanicidal activity against *L. braziliensis* and *L. amazonesis* promastigotes, with IC_{50} values of 59.2 μM and 77.7 μM, respectively. The effects that modifications of the benzylic alcohol functionality of **1** have on the antiparasitic activity were studied previously [28], and especially esters of the alcohol increased the potency significantly. In this study, we evaluate how modifications on ring B and C affect the antiparasitic activity against *T. cruzi*, *L. braziliensis* and *L. amazonensis*. As a comparison, the cytotoxicity to mammalian murine macrophage cell lines (RAW) was determined, and the quotas IC_{50} RAW cells/ IC_{50} parasite is given as the selectivity index (SI) in Table 1.

2.3.1. Antiparasitic Activity Against *Trypanosoma cruzi* Epimastigotes

Compared to pulchrol (**1**), the 6,6-didemethyl analogue **8a** is considerably less active (66.6 μM), indicating the importance of alkyl substituents on C-6 for the activity against *T. cruzi*. However, the toxicity to mammalian cells (SI) is also less. The 6-methyl enantiomers **8b** and **8c** were less potent than **1**, as are the 6-ethyl enantiomers **8d** and **8e**, suggesting the importance of a dialkylated C-6. In **8f** the two methyls of **1** have been exchanged for ethyls and compared to **1** as well as benznidazole the antiparasitic activity (10.4 μM) is higher. In addition, **8f** showed the highest selectivity (SI 4.2) among all molecules assayed towards *T. cruzi* in this study. Unlike **8f**, analogue **8g** with two *n*-butyl substituents was slightly less potent (22.8 μM) than **1**, and less selective than **8f**. A possibility is that the compounds for their effect on *T. cruzi* interact with a lipophilic pocket in a target protein around C-6, although its volume is limited.

Changing the position of the methoxy substituent in the C-ring to positions C-1 (compound **10a**) and C-3 (compound **10b**) was not beneficial, and the SI-value was lower. A methoxy group in the C-ring is only efficient in position 2, as in pulchrol (**1**), and the replacement of the methoxy groups in positions 2 and 3 with methyls (compounds **10c** and **10d**) resulted in equipotent compounds that were more active than **10a** and **10b** but less active than **1**. The analogue with no substituent in the C-ring, **10e**, was slightly less potent than **10c** and **10d**. It is possible that a methoxy group in position 2 enables a hydrogen bond at the target, while a methyl group in position 3 is better than a methoxy or no substituent at all. To further explore the effects of alkyl substituents in the positions 2 and 3, the isopropyl analogues **10f** and **10g** were prepared and assayed. Both were more potent than **1**, and comparable with the 6,6-diethyl analogue **8f**. Finally, **10h**, with a *n*-pentyl group in position 2, was found to possess the highest activity towards *T. cruzi* of all compounds assayed in this investigation (6.4 μM), being approximately three times as potent as pulchrol (**1**) and the positive control benznidazole. This contradicts the suggestion that the methoxy substituent at C-2 enables a hydrogen bond, and instead propose that the lipophilicity of the pulchrol analogues is correlated with the antiparasitic activity towards *T. cruzi*.

2.3.2. Antiparasitic Activity Against *Leishmania braziliensis* Promastigotes

Similar to the results obtained for *T. cruzi*, the 6,6-didemethyl analogue **8a** was considerably less potent than **1**, and this is also true for the monomethyl enantiomers **8b** and **8c**. However, the monoethyl enantiomers **8d** and **8e** as well as the 6,6-diethyl analogue **8f** were more potent towards *L. braziliensis* and actually slightly more so compared to **1**. For the 6,6-dibutyl analogue **8g** with the IC_{50}-value 29.3 μM this trend is even stronger. Towards *L. braziliensis* the positioning of the methoxy group in the C-ring at C-3 (**10a**) or C-1 (**10b**) instead of C-2 (**1**), as well as replacing the methoxy substituent at C-2 and C-3 for a methyl (analogues **10c** and **10d**) results in almost equipotent compounds that are slightly more potent than **1**. The analogue without substituents in the C-ring (**10e**) is less impressive,

while the compounds with bigger alkyl substituents at C-2 and C-3 are the most potent towards *L. braziliensis*. The C-2 isopropyl analogue **10f**, as well as **10g** (C-3 isopropyl) and **10h** (C-2 *n*-pentyl) were all considerably more potent than **1** towards *L. braziliensis*, with IC_{50}-values between 15 and 20 μM, close to that of the positive control miltefosine. However, their selectivity for the parasite over the mammalian cells was less impressing.

2.3.3. Antiparasitic Activity Against *Leishmania amazonensis* Promastigotes

As can be seen in Table 1, the antiparasitic activity towards *L. amazonensis* is not improved compared to **1** by replacing the 6,6-dimethyl substituents in **1** for hydrogens (**8a**), one methyl and one hydrogen (**8b** and **8c**), or one ethyl and one hydrogen (**8d** and **8f**). More potent analogues are the 6,6-diethyl and 6,6-dibutyl analogues with IC_{50}-values of 36.9 and 25.4 μM, respectively. This is similar to what was observed with *T. cruzi* and *L. braziliensis* (*vide supra*). For the C-ring analogues, there is a strong variation in the potency depending on the position of the methoxy group, and while the C-3 methoxy analogue **10a** is slightly more potent than **1**, the C-1 methoxy analogue (**10b**) is considerably less potent. Methyl groups in positions 2 and 3 (**10c** and **10d**) do not really change things, neither does the nonsubstituted **10e**. Again, the most potent analogues are those with larger alkyl groups in positions 2 and 3 (**10f**, **10g** and **10h**).

3. Materials and Methods

3.1. General

^{1}H-NMR spectra (400 MHz) and ^{13}C-NMR spectra (100 MHz) were recorded in $CDCl_3$ with a Bruker Avance II instrument (Bruker Biospin AG, Fällanden, Switzerland). The individual 1D signals were assigned using 2D NMR experiments (COSY, HSQC, HMBC). The chemical shifts are given in ppm with the solvent signal as reference (7.27 ppm for ^{1}H and 77.0 for ^{13}C). Infrared spectra were recorded with a Bruker Alpha-P FT/IR instrument (Bruker Biospin AG) with a Diamond ATR sensor as films, and the intensities are given as vw (very weak), w (weak), m (medium), s (strong) and vs (very strong). High resolution mass spectra (HRMS) were recorded with a Waters XEVO-G2 QTOF instrument (Waters Corp, Milford, MA, USA) equipped with electrospray ionization (ESI). A weak solution (10 mg/mL) was leaked into the ionizing unit, and the mass spectrum was recorded. Synthetic reactions were monitored by TLC using alumina plates coated with silica gel and visualized using either UV light and/or spraying/heating with vanillin/H_2SO_4. Flash chromatography was performed with silica gel (35–70 μm, 60 Å). Chiral separations were performed by semipreparative HPLC (mod. 1260 Infinity system, column CHIRALPAK® IB, 4 mL/min, 96:4 hexane/isopropyl, UV detector 254 nm, Agilent (Santa Clara, CA, USA). THF was distilled from sodium, acetonitrile was distilled from CaH_2 and other reaction solvents were dried with Al_2O_3. Commercially available compounds were obtained from Aldrich (St. Louis, MO, USA). More detailed data are available in the supplementary materials.

3.2. Synthetic Procedures

Methyl 4-(hydroxymethyl)-2-iodobenzoate (intermediate in the synthesis of **4**), BH_3-THF (1 M, 68 mL, 68.2 mmol) was slowly added to a stirred solution of 3-iodo-4-(methoxycarbonyl)benzoic acid (5.2 g, 17.1 mmol) in dry THF (250 mL) at 0 °C. After 30 h, saturated aqueous $NaHCO_3/H_2O$ was added, and the aqueous phase was extracted with ethyl acetate (3 × 250 mL) before drying (Na_2SO_4) and removal of solvent under reduced pressure. Purification by column chromatography (SiO_2, 4:6 heptane/ethyl acetate) gave (3.65 g, 73%) of the pure product as yellow crystals, identical to that previously reported [26].

Methyl 4-(((tert-butyldiphenylsilyl)oxy)methyl)-2-iodobenzoate (used in the synthesis of **4**), TBDPSCl (4.2 mL, 16.0 mmol) was added to a stirred solution of methyl 4-(hydroxymethyl)-2-iodobenzoate (prepared as described above, 3.90 g, 13.3 mmol) in pyridine (50 mL) at rt. After 24 h, saturated aqueous NH_4Cl/H_2O was added and the aqueous phase was extracted with diethyl ether (3 × 200 mL), the organic phase

was washed with brine (2 × 500 mL) before drying (Na_2SO_4) and removal of solvent under reduced pressure. Purification by column chromatography (SiO_2, 20:2 heptane/ethyl acetate) gave (4.3 g, 61%) of the pure product as white crystals, identical to that previously reported [26].

General procedure for Suzuki coupling (compound **4** and intermediates in the synthesis of **10a**–**10h**). The corresponding boronic acid (1.5 equiv), K_2CO_3 (5 equiv) and tetrakis(triphenyl phosphine)-palladium(0) (0.17 equiv), were added to a stirred solution of methyl 4-(((*tert*-butyl-diphenylsilyl)oxy)methyl)-2- iodobenzoate (prepared as described above, 1 equiv) dissolved in 4:1 DME/water (15 mL), the mixture (contained in a microtube) was degasified under vaccum/N_2 at −78 °C five times. The microwave reaction conditions were 100 °C, high pressure, and 10 s of pre-stirring. After 30 to 60 min in the microwave reactor, the mixture was filtered through a plug of celite and washed with ethyl acetate (250 mL) before drying (Na_2SO_4) and removal of solvent under reduced pressure. Purification by column chromatography (SiO_2, 20:3 heptane/ethyl acetate) gave the pure products.

Methyl 5-(((tert-butyldiphenylsilyl)oxy)methyl)-2′,5′-dimethoxy-[1,1′-biphenyl]-2-carboxylate (**4**) The pure product was obtained as an orange wax (yield 91 %) identical to that previously reported [26].

Methyl 5-(((tert-butyldiphenylsilyl)oxy)methyl)-2′,4′-dimethoxy-[1,1′-biphenyl]-2-carboxylate (used in the synthesis of **10a**), the pure product was obtained as an orange wax (yield 75%). ^{1}H-NMR δ 7.83 (d, *J* = 8.0 Hz, 1H), 7.72–7.67 (m, 4H), 7.46–7.41 (m, 2H), 7.41–7.37 (m, 4H), 7.36 (t, *J* = 1.5 Hz, 1H), 7.27 (d, *J* = 2.3 Hz, 1H), 7.15 (d, *J* = 8.4 Hz, 1H), 6.56 (dd, *J* = 8.3, 2.4 Hz, 1H), 6.48 (d, J = 2.4 Hz, 1H), 4.82 (s, 2H), 3.85 (s, 3H), 3.70 (s, 3H), 3.68 (s, 3H), 1.10 (s, 9H). ^{13}C-NMR δ 168.94, 160.57, 157.19, 144.87, 138.54, 135.69, 133.41, 130.43, 130.30, 129.91, 129.66, 128.97, 127.90, 124.32, 123.56, 104.40, 98.34, 65.23, 55.48, 55.33, 51.80, 26.96, 19.45. HRMS-ESI+ (*m*/*z*): $[M + Na]^+$ calcd for $C_{33}H_{36}O_5NaSi$, 563.2230; found, 563.2225. IR (cm^{-1}): 2952 (w, CH aliphatic), 2933 (w, CH aliphatic), 2857 (w, C-H aliphatic), 1727 (s, C=O), 1610 (m, C C aromatic), 1462 (m, C-C aromatic), 1286 (s, C-O), 1208 (m, C-O), 1110 (s, C-O), 824 (m), 704 (s), 505 (m).

Methyl 5-(((tert-butyldiphenylsilyl)oxy)methyl)-2′,6′-dimethoxy-[1,1′-biphenyl]-2-carboxylate (used in the synthesis of **10b**), the pure product was obtained as an orange wax (yield 90%). ^{1}H-NMR δ 7.94 (d, *J* = 8.0 Hz, 1H), 7.72–7.68 (m, 4H), 7.45–7.41 (m, 2H), 7.40–7.37 (m, 4H), 7.36 (t, *J* = 1.6 Hz, 1H), 7.34 (d, *J* = 1.1 Hz, 1H), 7.29 (d, *J* = 8.4 Hz, 1H), 6.63 (d, *J* = 8.4 Hz, 2H), 4.83 (s, 2H), 3.70 (s, 6H), 3.64 (s, 3H), 1.09 (s, 9H). ^{13}C-NMR δ 168.21, 157.19, 144.49, 135.70, 135.02, 133.48, 130.24, 130.06, 129.91, 129.86, 128.78, 127.87, 124.47, 119.17, 104.10, 65.25, 55.94, 51.69, 26.92, 19.45. HRMS-ESI+ (*m*/*z*): $[M + Na]^+$ calcd for $C_{33}H_{36}O_5NaSi$, 563.2229; found, 563.2230. IR (cm^{-1}): 2932 (w, C-H aliphatic), 2856 (w, C-H aliphatic), 1729 (m, C=O), 1610 (w, C=C aromatic), 1470 (m, C-C aromatic), 1285 (m, C-O), 1244 (m, C-O), 1110 (s, C-O), 823 (w), 704 (m), 505 (w).

Methyl 5-(((tert-butyldiphenylsilyl)oxy)methyl)-2′-methoxy-5′-methyl-[1,1′-biphenyl]-2-carboxylate (used in the synthesis of **10c**), the pure product was obtained as a yellowish wax (yield 92%). ^{1}H-NMR δ 7.86 (d, *J* = 8.0 Hz, 1H), 7.73–7.69 (m, 4H), 7.45 (td, *J* = 5.6, 2.2 Hz, 2H), 7.40 (dd, *J* = 7.8, 2.0 Hz, 4H), 7.37 (d, *J* = 1.7 Hz, 1H), 7.29 (d, *J* = 1.8 Hz, 1H), 7.12 (dd, *J* = 8.3, 2.4 Hz, 1H), 7.06 (d, *J* = 2.5 Hz, 1H), 6.80 (d, *J* = 8.4 Hz, 1H), 4.84 (s, 2H), 3.70 (s, 3H), 3.68 (s, 3H), 2.34 (s, 3H), 1.12 (s, 9H). ^{13}C-NMR δ 168.77, 154.14, 144.91, 138.87, 135.69, 133.43, 130.79, 130.44, 130.31, 129.99, 129.91, 129.61, 129.17, 128.96, 127.90, 124.58, 110.16, 65.26, 55.45, 51.76, 26.96, 20.68, 19.47. HRMS-ESI+ (*m*/*z*): $[M + H]^+$ calcd for $C_{33}H_{37}O_4Si$, 525.2461; found, 525.2452. IR (cm^{-1}): 2950 (m, C-H aliphatic), 1727 (s, C=O), 1503 (m, C-C aromatic), 1429 (m, C-C aromatic), 1289 (s, C-O), 1108 (vs, C-O), 807 (w), 703 (vs), 505 (m).

Methyl 5-(((tert-butyldiphenylsilyl)oxy)methyl)-2′-methoxy-4′-methyl-[1,1′-biphenyl]-2-carboxylate (used in the synthesis of **10d**), the pure product was obtained as a yellowish wax (yield 80%). ^{1}H-NMR δ 7.83 (d, *J* = 7.9 Hz, 1H), 7.71–7.67 (m, 4H), 7.46–7.41 (m, 2H), 7.40–7.37 (m, 4H), 7.36 (t, *J* = 1.6 Hz, 1H), 7.28 (d, *J* = 2.2 Hz, 1H), 7.11 (d, *J* = 7.6 Hz, 1H), 6.84 (ddd, *J* = 7.6, 1.6, 0.7 Hz, 1H), 6.71 (d, *J* = 2.1 Hz, 1H), 4.81 (s, 2H), 3.71 (s, 3H), 3.68 (s, 3H), 2.40 (s, 3H), 1.09 (s, 9H). ^{13}C-NMR (101 MHz, $CDCl_3$) δ 168.81, 156.02, 144.88, 138.95, 138.89, 135.70, 133.43, 130.29, 129.91, 129.82, 129.62, 128.98, 127.91, 124.46,

121.55, 111.26, 65.27, 55.29, 51.78, 26.97, 21.85, 19.46. HRMS-ESI+ (*m*/*z*): $[M + H]^+$ calcd for $C_{33}H_{37}O_4Si$, 525.2461; found, 525.2472. IR (cm^{-1}): 2931 (w, C-H aliphatic), 2857 (w, C-H aliphatic), 1721 (m, C=O), 1610 (w, C=C aromatic), 1462 (vw, C-C aromatic), 1428 (w, C-C aromatic), 1282 (s, C-O), 1092 (vs, C-O), 818 (m), 702 (vs), 505 (m).

Methyl 5-(((tert-butyldiphenylsilyl)oxy)methyl)-2′-methoxy-[1,1′-biphenyl]-2-carboxylate (intermediate in the synthesis of **10e**), the pure product was obtained as a yellowish wax (yield 91%). ^{1}H-NMR δ 7.95 (d, *J* = 8.0 Hz, 1H), 7.82–7.74 (m, 4H), 7.51 (dq, *J* = 2.1, 1.3 Hz, 1H), 7.49–7.47 (m, 2H), 7.44 (tt, *J* = 7.8, 1.5 Hz, 4H), 7.41–7.36 (m, 2H), 7.30 (dd, *J* = 7.5, 1.8 Hz, 1H), 7.10 (td, *J* = 7.5, 1.1 Hz, 1H), 6.96 (dd, *J* = 8.3, 1.1 Hz, 1H), 4.91 (d, *J* = 0.9 Hz, 2H), 3.78 (s, 3H), 3.72 (s, 3H), 1.18 (s, 9H). ^{13}C-NMR δ 168.61, 156.17, 144.89, 138.83, 135.63, 133.34, 130.74, 130.22, 129.98, 129.88, 129.65, 128.88 (d, *J* = 3.7 Hz), 127.87, 124.61, 120.83, 110.16, 65.21, 55.28, 51.68, 26.93, 19.40. HRMS-ESI+ (*m*/*z*): $[M + H]^+$ calcd for $C_{32}H_{35}O_4Si$, 511.2305; found, 511.2302. IR (cm^{-1}): 2931 (w, C-H aliphatic), 1726 (m, C=O), 1429 (w, C-C aromatic), 1249 (m, C-O), 1106 (vs, C-O), 823 (w), 703 (vs), 505 (m).

Methyl 5-(((tert-butyldiphenylsilyl)oxy)methyl)-5′-isopropyl-2′-methoxy-[1,1′-biphenyl]-2-carboxylate (used in the synthesis of **10f**), the pure product was obtained as a colorless wax (yield 90%). ^{1}H-NMR δ 7.84 (d, *J* = 7.9 Hz, 1H), 7.72–7.69 (m, 4H), 7.47–7.42 (m, 2H), 7.41–7.38 (m, 4H), 7.38–7.37 (m, 1H), 7.37 (d, *J* = 1.0 Hz, 1H), 7.18 (ddd, *J* = 8.4, 2.4, 0.7 Hz, 1H), 7.13 (d, *J* = 2.4 Hz, 1H), 6.83 (d, *J* = 8.4 Hz, 1H), 4.85 (s, 2H), 3.71 (s, 3H), 3.67 (s, 3H), 2.91 (hept, *J* = 6.9 Hz, 1H), 1.27 (d, *J* = 6.9 Hz, 6H), 1.11 (s, 9H). ^{13}C-NMR δ 168.92, 154.25, 144.86, 141.15, 139.05, 135.68, 133.40, 130.39, 130.32, 129.92, 129.52, 128.94, 128.30, 127.91, 126.50, 124.43, 110.04, 65.16, 55.43, 51.78, 33.43, 26.95, 24.35, 19.46. HRMS-ESI+ (*m*/*z*): $[M + H]^+$ calcd for $C_{35}H_{41}O_4Si$, 553.2774; found, 553.2773. IR (cm^{-1}): 2956 (m, C-H aliphatic), 1727 (s, C=O), 1609 (w, C=C aromatic), 1500 (m, C-C aromatic), 1429 (m, C-C aromatic), 1288 (s, C-O), 1106 (vs, C-O), 821 (m), 703 (vs), 505 (m).

Methyl 5-(((tert-butyldiphenylsilyl)oxy)methyl)-2′-methoxy-4′-isopropyl-[1,1′-biphenyl]-2-carboxylate (used in the synthesis of **10g**), the pure product was obtained as a yellowish wax (yield 38%). ^{1}H-NMR δ 7.83 (d, *J* = 8.1 Hz, 1H), 7.71–7.66 (m, 4H), 7.45–7.41 (m, 2H), 7.40–7.37 (m, 4H), 7.35 (d, *J* = 1.7 Hz, 1H), 7.27 (d, *J* = 1.8 Hz, 1H), 7.14 (d, *J* = 7.7 Hz, 1H), 6.89 (dd, *J* = 7.7,1.7Hz,1H), 6.75 (d, *J* = 1.7Hz, 1H), 4.81 (s, 2H), 3.72 (s, 3H), 3.66 (s, 3H), 2.94 (hept, *J* = 7.0 Hz, 1H), 1.30 (d, *J* = 7.0 Hz, 6H), 1.09 (s, 9H). ^{13}C-NMR δ 168.90, 156.16, 150.03, 144.81, 138.92, 135.72, 133.50, 130.40, 129.91, 129.65, 129.09, 128.17, 127.91, 124.49, 118.73, 108.77, 65.35, 55.31, 51.71, 34.39, 27.00, 24.13, 19.47. HRMS-ESI+ (*m*/*z*): $[M + H]^+$ calcd for $C_{35}H_{41}O_4Si$, 553.2724; found, 553.2770. IR (cm^{-1}): 2957 (w, C-H aliphatic), 1722 (m, C=O), 1609 (w, C=C aromatic), 1461 (m, C-C aromatic), 1428 (m, C-C aromatic), 1254 (s, C-O), 1104 (vs, C-O), 822 (s), 700 (vs), 504 (vs).

Methyl 5-(((tert-butyldiphenylsilyl)oxy)methyl)-2′-methoxy-5′-pentyl-[1,1′-biphenyl]-2-carboxylate (used in the synthesis of **10h**), the pure product was obtained as a yellowish wax (yield 91%) ^{1}H-NMR δ 7.83 (d, *J* = 8.0 Hz, 1H), 7.72–7.67 (m, 4H), 7.45–7.41 (m, 2H), 7.40–7.37 (m, 4H), 7.36 (t, *J* = 1.6 Hz, 1H), 7.31 (d, *J* = 1.7 Hz, 1H), 7.12 (dd, *J* = 8.3, 2.3 Hz, 1H), 7.05 (d, *J* = 2.3 Hz, 1H), 6.80 (d, *J* = 8.3 Hz, 1H), 4.83 (s, 2H), 3.69 (s, 3H), 3.66 (s, 3H), 2.62–2.55 (m, 2H), 1.67–1.58 (m, 2H), 1.33 (ddd, *J* = 7.1, 4.0, 2.9 Hz, 4H), 1.10 (s, 9H), 0.93–0.85 (m, 3H). ^{13}C-NMR δ 168.85, 154.31, 144.86, 139.05, 135.72, 135.23, 133.48, 130.47, 130.41, 130.18, 129.91, 129.60, 128.99, 128.49, 127.91, 124.53, 110.16, 65.28, 55.48, 51.73, 35.26, 31.70, 31.50, 26.99, 22.69, 19.48, 14.20. HRMS-ESI+ (*m*/*z*): $[M + H]^+$ calcd for $C_{37}H_{45}O_4Si$, 581.3087; found, 581.3097. IR (cm^{-1}): 2929 (m, C-H aliphatic), 2857 (w, C-H aliphatic), 1725 (s, C=O), 1609 (w, C=C aromatic), 1500 (m, C-C aromatic), 1429 (m, C-C aromatic), 1285 (s, C-O), 1107 (vs, C-O), 823 (m), 703 (s), 505 (m).

General procedure for organolithium addition (compound **6** and intermediates in the synthesis of **8f**, **8g**, and **10a**–**10h**), corresponding organolithium reagent (4 equiv) was added to a stirred solution of the Suzuki coupling product (1 equiv) in dry THF (70 mL), at 0 or −78 °C, depending on the organo-lithic reagent. After 12 h, saturated aqueous NH_4Cl/H_2O was added, and the aqueous phase was extracted

with ethyl acetate (3 × 100 mL) before drying (Na_2SO_4) and removal of solvent under reduced pressure. Purification by column chromatography (SiO_2, 20:4 heptane/ethyl acetate 20:4) gave the pure product.

2-(5-(((tert-Butyldiphenylsilyl)oxy)methyl)-2′,4′-dimethoxy-[1,1′-biphenyl]-2-yl)propan-2-ol (used in the synthesis of **10a**), the pure product was obtained as a light yellow wax (yield 45%). ^{1}H-NMR δ 7.70–7.68 (m, 4H), 7.58 (d, *J* = 8.3 Hz, 1H), 7.43 (td, *J* = 3.0, 1.8 Hz, 1H), 7.40 (q, *J* = 1.6 Hz, 2H), 7.38 – 7.36 (m, 4H), 7.05–7.02 (m, 1H), 6.92 (d, *J* = 1.9 Hz, 1H), 6.54–6.51 (m, 2H), 4.75 (d, *J* = 4.3 Hz, 2H), 3.85 (s, 3H), 3.72 (s, 3H), 1.52 (s, 3H), 1.39 (s, 3H), 1.07 (s, 9H). ^{13}C-NMR δ 160.45, 157.33, 145.68, 139.21, 135.76, 133.65, 131.60, 130.84, 129.78, 127.91, 127.81 (d, *J* = 2.2 Hz), 126.00, 125.27, 104.10, 98.76, 77.36, 65.25, 55.51 (d, *J* = 4.8 Hz), 32.10, 31.44, 26.98, 19.46. HRMS-ESI+ (*m*/*z*): $[M + Na]^+$ calcd for $C_{34}H_{40}O_4NaSi$, 563.2594; found, 563.2591. IR (cm^{-1}): 3500 (vw, br, O-H), 2957 (m, C-H aliphatic), 2931 (m, C-H aliphatic), 2857 (m, C-H aliphatic), 1610 (m, C=C aromatic), 1463 (m, C-C aromatic), 1208 (s, C-O), 1111 (vs, C-O), 824 (m), 704 (s), 505 (m).

2-(5-(((tert-Butyldiphenylsilyl)oxy)methyl)-2′,6′-dimethoxy-[1,1′-biphenyl]-2-yl)propan-2-ol (used in the synthesis of **10b**), the pure product was obtained as a light yellow wax (yield 50%). ^{1}H-NMR δ 7.70–7.67 (m, 4H), 7.61 (d, *J* = 8.1 Hz, 1H), 7.41 (d, *J* = 2.8 Hz, 2H), 7.39 (t, *J* = 1.5 Hz, 1H), 7.38–7.34 (m, 4H), 7.31 (t, *J* = 8.4 Hz, 1H), 6.90 (d, *J* = 2.0 Hz, 1H), 6.63 (d, *J* = 8.5 Hz, 2H), 4.76 (s, 2H), 3.71 (s, 6H), 1.44 (s, 6H), 1.07 (s, 9H). ^{13}C-NMR δ 157.39, 145.52, 139.54, 135.78, 133.72, 132.07, 130.71, 129.74, 129.01, 127.77, 126.01, 125.24, 121.52, 104.11, 73.18, 65.32, 55.75, 30.87, 26.97, 19.46. HRMS-ESI+ (*m*/*z*): $[M + Na]^+$ calcd for $C_{34}H_{40}O_4NaSi$, 563.2594; found, 563.2592. IR (cm^{-1}): 3500 (vw, br, O-H), 2958 (w, C-H aliphatic), 2931 (w, C-H aliphatic), 2857 (vw, C-H aliphatic), 1589 (w, C=C aromatic), 1470 (m, C-C aromatic), 1248 (m, C-O), 1110 (vs, C-O), 824 (w), 703 (m), 505 (w).

2-(5-(((tert-Butyldiphenylsilyl)oxy)methyl)-2′-methoxy-5′-methyl-[1,1′-biphenyl]-2-yl)propan-2-ol (used in the synthesis of **10c**), the pure product was obtained as a transparent wax (yield 49%). ^{1}H-NMR δ 7.75–7.71 (m, 4H), 7.61 (d, *J* = 8.1 Hz, 1H), 7.48–7.44 (m, 2H), 7.43 (d, *J* = 1.5 Hz, 1H), 7.42–7.38 (m, 4H), 7.15 (dd, *J* = 8.4, 3.1 Hz, 1H), 6.97 (dd, *J* = 11.6, 2.3 Hz, 2H), 6.86 (d, *J* = 8.4 Hz, 1H), 4.80 (d, *J* = 5.1 Hz, 2H), 3.74 (s, 3H), 2.34 (s, 3H), 1.58 (s, 3H), 1.43 (s, 3H), 1.12 (s, 9H). ^{13}C-NMR δ 154.15, 145.26, 139.14, 136.17, 135.73, 133.65, 132.75, 132.02, 130.36, 129.76 (d, *J* = 1.8 Hz), 129.09, 127.79 (d, *J* = 2.9 Hz), 126.02, 125.30, 110.81, 73.64, 65.30, 55.56, 32.07, 31.48, 26.98, 20.59, 19.44. HRMS-ESI+ (*m*/*z*): $[M + NH_4]^+$ calcd for $C_{34}H_{44}NO_3Si$, 542.3090; found, 542.3094. IR (cm^{-1}): 3500 (vw, br, O-H), 2930 (m, C-H aliphatic), 1502 (m, C-C aromatic), 1428 (m, C-C aromatic), 1236 (m, C-O), 1110 (vs, C-O), 824 (m), 703 (vs), 505 (m).

2-(5-(((tert-Butyldiphenylsilyl)oxy)methyl)-2′-methoxy-4′-methyl-[1,1′-biphenyl]-2-yl)propan-2-ol (used in the synthesis of **10d**), the pure product was obtained as a transparent wax (yield 71%). ^{1}H-NMR δ 7.68 (ddd, *J* = 7.9, 5.3, 1.5 Hz, 4H), 7.57 (d, *J* = 8.3 Hz, 1H), 7.45–7.40 (m, 2H), 7.39 (d, *J* = 1.6 Hz, 1H), 7.39–7.35 (m, 4H), 7.01 (d, *J* = 7.6 Hz, 1H), 6.92 (d, *J* = 1.7 Hz, 1H), 6.80 (ddd, *J* = 7.6, 1.6, 0.8 Hz, 1H), 6.75 (s, 1H), 4.74 (d, *J* = 4.0 Hz, 2H), 3.73 (s, 3H), 2.40 (s, 3H), 1.53 (s, 3H), 1.37 (s, 3H), 1.07 (s, 9H).^{13}C-NMR δ 156.12, 146.42, 138.87, 136.18, 135.76, 133.67, 131.09, 130.55, 129.78, 127.80, 125.99, 125.27, 121.08, 111.83, 73.65, 65.30, 55.42, 32.08, 31.48, 26.99, 21.79, 19.46. HRMS-ESI+ (*m*/*z*): $[M + Na]^+$ calcd for $C_{34}H_{40}O_3NaSi$, 547.2644; found, 547.2642. IR (cm^{-1}): 3421 (vw, br, O-H), 2930 (w, C-H aliphatic), 2857 (w, C-H aliphatic), 1606 (vw, C=C aromatic), 1502 (w, C-C aromatic), 1427 (w, C-C aromatic), 1236 (w, C-O), 1110 (m, C-O), 823 (w), 703 (m), 505 (w).

2-(5-(((tert-Butyldiphenylsilyl)oxy)methyl)-2′-methoxy-[1,1′-biphenyl]-2-yl)propan-2-ol (used in the synthesis of **10e**), The pure product was obtained as a transparent wax (yield 93%). ^{1}H-NMR δ 7.85 (ddd, *J* = 7.7, 5.5, 1.8 Hz, 4H), 7.77 (d, *J* = 8.3 Hz, 1H), 7.53 (d, *J* = 1.7 Hz, 1H), 7.51 (dd, *J* = 3.6, 1.8 Hz, 2H), 7.50–7.45 (m, 4H), 7.28 (dd, *J* = 7.4, 1.9 Hz, 1H), 7.11 (s, 2H), 7.05 (d, *J* = 8.4 Hz, 1H), 5.28 (s, 1H), 4.93 (d, *J* = 3.7 Hz, 2H), 3.83 (s, 3H), 1.67 (s, 3H), 1.52 (s, 3H), 1.25 (s, 9H). ^{13}C-NMR δ 156.24, 145.34, 139.04, 136.01, 135.62, 133.52, 132.96, 131.23, 130.22, 129.71, 128.72, 127.74, 125.99, 125.26, 120.25, 110.73, 73.47, 65.22, 55.27, 32.04, 31.34, 26.91, 19.35. HRMS-ESI+ (*m*/*z*): $[M + NH_4]^+$ calcd for $C_{33}H_{42}NO_4Si$, 528.2934; found,

528.2920. IR (cm^{-1}): 3500 (vw, br, O-H), 2931 (m, C-H aliphatic), 1461 (m, C-C aromatic), 1428 (m, C-C aromatic), 1238 (m, C-O), 1111 (vs, C-O), 823 (m), 703 (vs), 505 (s).

2-(5-(((tert-Butyldiphenylsilyl)oxy)methyl)-5′-isopropyl-2′-methoxy-[1,1′-biphenyl]-2-yl)propan-2-ol (used in the synthesis of **10f**), the pure product was obtained as a transparent wax (yield 55%). ^{1}H-NMR δ 7.71–7.66 (m, 4H), 7.59 (d, *J* = 8.3 Hz, 1H), 7.46–7.40 (m, 2H), 7.40 (d, *J* = 1.9 Hz, 1H), 7.39–7.35 (m, 4H), 7.17 (ddd, *J* = 8.4, 2.4, 0.6 Hz, 1H), 7.00 (d, *J* = 2.5 Hz, 1H), 6.95 (d, *J* = 2.0 Hz, 1H), 6.86 (d, *J* = 8.5 Hz, 1H), 4.76 (d, *J* = 2.9 Hz, 2H), 3.72 (s, 3H), 2.87 (hept, *J* = 6.8 Hz, 1H), 1.53 (s, 3H), 1.37 (s, 3H), 1.23 (dd, *J* = 6.9, 0.9 Hz, 6H), 1.08 (s, 9H). ^{13}C-NMR δ 154.35, 145.25, 140.76, 139.24, 136.50, 135.76, 133.64, 132.55, 130.35, 129.78 (d), 129.55, 127.80 (d), 126.51, 125.99, 125.28, 110.68, 73.57, 65.27, 55.56, 33.36, 32.03, 31.37, 26.98, 24.39, 24.26, 19.46. HRMS-ESI+ (*m*/*z*): $[M + Na]^+$ calcd for $C_{36}H_{44}O_3NaSi$, 575.2957; found, 575.2957. IR (cm^{-1}): 3500 (vw, br, O-H), 2960 (s, C-H aliphatic), 2932 (m, C-H aliphatic), 2858 (m, C-H aliphatic), 1501 (m, C-C aromatic), 1463 (m, C-C aromatic), 1428 (m, C-C aromatic), 1237 (m, C-O), 1111 (vs, C-O), 823 (m), 703 (vs), 505 (m).

2-(5-(((tert-Butyldiphenylsilyl)oxy)methyl)-2′-methoxy-4′-isopropyl-[1,1′-biphenyl]-2-yl)propan-2-ol (used in the synthesis of **10g**), the pure product was obtained as a transparent wax (yield 64%). ^{1}H-NMR δ 7.68 (ddd, *J* = 8.1, 5.4, 1.5 Hz, 4H), 7.57 (d, *J* = 8.2 Hz, 1H), 7.45–7.40 (m, 2H), 7.39 (d, *J* = 1.6 Hz, 1H), 7.39–7.34 (m, 4H), 7.04 (d, *J* = 7.7 Hz, 1H), 6.92 (d, *J* = 2.1 Hz, 1H), 6.85 (dd, *J* = 7.7, 1.7 Hz, 1H), 6.78 (d, *J* = 1.8 Hz, 1H), 4.74 (d, *J* = 4.2 Hz, 2H), 3.74 (s, 3H), 2.94 (hept, *J* = 7.0 Hz, 1H), 1.53 (s, 3H), 1.38 (s, 3H), 1.30 (d, *J* = 6.8 Hz, 6H), 1.08 (s, 9H). ^{13}C-NMR δ 156.17, 150.05, 145.45, 139.16, 136.20, 135.77, 133.74, 131.14, 130.65, 130.24, 129.77, 127.82, 126.03, 125.31, 118.32, 109.37, 73.72, 65.37, 55.44, 34.38, 32.08, 31.61, 27.02, 24.17, 19.47. HRMS-ESI+ (*m*/*z*): $[M + Na]^+$ calcd for $C_{36}H_{44}O_3NaSi$, 575.2957; found, 575.2955. IR (cm^{-1}): 3500 (vw, br, O-H), 2959 (m, C-H aliphatic), 2931 (m, C-H aliphatic), 2857 (m, C-H aliphatic), 1461 (m, C-C aromatic), 1427 (m, C-C aromatic), 1106 (s, C-O), 822 (s), 701 (vs), 504 (s).

2-(5-(((tert-Butyldiphenylsilyl)oxy)methyl)-2′-methoxy-5′-pentyl-[1,1′-biphenyl]-2-yl)propan-2-ol (used in the synthesis of **10h**) The product was obtained as a mixture and was used directly in the next step (yield 33%).

3-(5-(((tert-Butyldiphenylsilyl)oxy)methyl)-2′,5′-dimethoxy-[1,1′-biphenyl]-2-yl)pentan-3-ol (used in the synthesis of **8f**), the pure product was obtained as a light yellow wax (yield 64%). ^{1}H-NMR δ 7.70–7.66 (m, 4H), 7.42–7.39 (m, 2H), 7.38 (d, *J* = 0.9 Hz, 2H), 7.37–7.33 (m, 4H), 6.90 (dd, *J* = 1.6, 0.8 Hz, 1H), 6.83–6.82 (m, 2H), 6.67 (dd, *J* = 2.3, 1.2 Hz, 1H), 4.76 (d, *J* = 6.1 Hz, 2H), 3.76 (s, 3H), 3.67 (s, 3H), 1.93 (dd, *J* = 14.0, 7.5 Hz, 1H), 1.73–1.66 (m, 2H), 1.61 (dd, *J* = 13.9, 7.4 Hz, 1H), 1.07 (s, 9H), 0.82 (t, *J* = 7.4 Hz, 3H), 0.71 (t, *J* = 7.4 Hz, 3H). ^{13}C-NMR δ 153.07, 150.72, 142.14, 138.68, 136.49, 135.78, 134.42, 133.69, 130.25, 129.77, 127.78 (d), 127.46, 125.07, 116.96, 112.86, 111.45, 65.33, 55.87 (d), 35.15, 34.63, 27.00, 19.46, 8.47, 8.16. HRMS-ESI+ (*m*/*z*): $[M + Na]^+$ calcd for $C_{36}H_{44}O_4NaSi$, 591.2907; found, 591.2903. IR (cm^{-1}): 3500 (vw, br, O-H), 2960 (s, C-H aliphatic), 2932 (s, C-H aliphatic), 2832 (s, C-H aliphatic), 1503 (m, C-C aromatic), 1463 (m, C-C aromatic), 1427 (m, C-C aromatic), 1218 (s, C-O), 1111 (vs, C-O), 823 (m), 703 (vs), 505 (m).

5-(5-(((tert-Butyldiphenylsilyl)oxy)methyl)-2′,5′-dimethoxy-[1,1′-biphenyl]-2-yl)nonan-5-ol (used in the synthesis of **8g**), the pure product was obtained as a light yellow wax (yield 39%). ^{1}H-NMR δ 7.70–7.66 (m, 4H), 7.41–7.39 (m, 2H), 7.38 (d, *J* = 3.1 Hz, 2H), 7.37–7.34 (m, 4H), 6.89 (d, *J* = 2.4 Hz, 1H), 6.83–6.81 (m, 2H), 6.65 (dd, *J* = 2.6, 0.9 Hz, 1H), 4.76 (d, *J* = 6.4 Hz, 2H), 3.75 (s, 3H), 3.67 (s, 3H), 1.72–1.56 (m, 4H), 1.37–1.23 (m, 4H), 1.23–1.14 (m, 4H), 1.07 (s, 9H), 0.87 (t, *J* = 7.1 Hz, 3H), 0.82 (t, *J* = 7.1 Hz, 3H). ^{13}C-NMR δ 153.06, 150.63, 142.94, 138.59, 136.21, 135.79, 134.27, 133.69, 130.25, 129.77, 127.78 (d), 127.27, 125.08, 116.79, 113.16, 111.39, 78.66, 65.33, 55.84, 55.80, 42.89, 42.57, 27.01, 26.22, 26.00, 23.39, 23.32, 19.46, 14.36, 14.28. HRMS-ESI+ (*m*/*z*): $[M + Na - H_2O]^+$ calcd for $C_{40}H_{50}O_3NaSi$, 629.3427; found, 629.3421. IR (cm^{-1}): 3500 (vw, br, O-H), 2955 (vs, C-H aliphatic), 2931 (vs, C-H aliphatic), 2833 (s, C-H aliphatic), 1504 (s, C-C aromatic), 1463 (s, C-C aromatic), 1428 (m, C-C aromatic), 1252 (s, C-O), 1111 (vs, C-O), 824 (m), 702 (vs), 505 (m).

(5-(((tert-Butyldiphenylsilyl)oxy)methyl)-2′,5′-dimethoxy-[1,1′-biphenyl]-2-yl)methanol (**5**), DIBALH (1 M, 1.3 mL, 1.3 mmol) was slowly added to a stirred solution of **4** (291 mg, 0.5 mmol) in dry toluene (30 mL) at −78 °C. After 35 min, aqueous HCL (1 N, 10 mL) was added, followed by water (10 mL), and the aqueous phase was extracted with ethyl acetate (3 × 50 mL) before drying (Na_2SO_4) and removal of solvent under reduced pressure. Purification by column chromatography (SiO_2, 2:1 heptane/ethyl acetate) gave the pure product as light yellow wax (230.5 mg, 84%). ^{1}H-NMR δ 7.73–7.66 (m, 4H), 7.52 (d, *J* = 7.9 Hz, 1H), 7.47–7.43 (m, 1H), 7.43–7.40 (m, 2H), 7.40–7.33 (m, 4H), 7.17 (d, *J* = 1.5 Hz, 1H), 6.93 (d, *J* = 8.4 Hz, 1H), 6.88 (dd, *J* = 8.9, 2.9 Hz, 1H), 6.73 (d, *J* = 2.3 Hz, 1H), 4.80 (s, 2H), 4.41 (d, *J* = 12.5 Hz, 2H), 3.78 (s, 3H), 3.69 (s, 3H), 1.09 (s, 9H). ^{13}C-NMR δ 154.09, 150.71, 140.80, 138.12, 137.42, 135.75, 133.63, 131.32, 129.85, 129.10, 128.01, 127.86, 125.99, 117.05, 113.89, 113.02, 65.46, 63.83, 56.87, 55.87, 27.00, 19.48. HRMS-ESI+ (*m*/*z*): $[M + H]^+$ calcd for $C_{32}H_{37}O_4Si$, 495.2355; found, 495.2362. IR (cm^{-1}): 3411 (vw, br, O-H), 2931 (w, C-H aliphatic), 2856 (w, C-H aliphatic), 1492 (m, C-C aromatic), 1462 (m, C-C aromatic), 1426 (m, C-C aromatic), 1215 (s, C-O), 1109 (s, C-O), 822 (s), 700 (vs), 503 (s).

5-(((tert-Butyldiphenylsilyl)oxy)methyl)-2′,5′-dimethoxy-[1,1′-biphenyl]-2-carbaldehyde (**7**), Morpholine (0.2 mL, 2.2 mmol) was added to a solution of DIBALH (1 M, 1.1 mL, 1.1 mmol) in dry THF (30 mL) at 0 °C. After 3 h, **4** (600 mg, 1.1 mmol) in dry THF (20 mL) was added, 10 min later, DIBALH (1 M, 1.1 mL, 1.1 mmol) was added again at 0 °C. After 4 h, aqueous HCL (1 N, 20 mL) was added, and the aqueous phase was extracted with diethyl ether (3 × 50 mL) before drying (Na_2SO_4) and removal of solvent under reduced pressure. Purification by column chromatography (SiO_2, 20:4 heptane/ethyl acetate) gave the pure product as a light yellow wax (89.1 mg, 16%). ^{1}H-NMR δ 9.77 (d, *J* = 0.9 Hz, 1H), 7.98 (d, *J* = 7.9 Hz, 1H), 7.71–7.67 (m, 4H), 7.48 (ddd, *J* = 8.1, 1.7, 0.9 Hz, 1H), 7.46–7.41 (m, 2H), 7.40–7.36 (m, 4H), 7.33 (d, *J* = 1.1 Hz, 1H), 6.94 (dd, *J* = 8.9, 3.1 Hz, 1H), 6.89 (d, *J* = 8.7 Hz, 1H), 6.84 (d, *J* = 2.6 Hz, 1H), 4.85 (s, 2H), 3.80 (s, 3H), 3.68 (s, 3H), 1.11 (s, 9H). ^{13}C-NMR δ 192.51, 153.92, 150.90, 147.38, 141.74, 135.71, 133.29, 133.01, 129.99, 128.45, 127.95, 126.95, 125.40, 117.23, 114.74, 111.91, 65.31, 56.06, 55.95, 26.98, 19.48. HRMS-ESI+ (*m*/*z*): $[M + H]^+$ calcd for $C_{32}H_{35}O_4Si$, 511.2305; found, 511.2304. IR (cm^{-1}): 2931 (m, C-H aliphatic), 2856 (m, C-H aliphatic), 1694 (s, C=O), 1500 (m, C-C aromatic), 1462 (m, C-C aromatic), 1427 (m, C-C aromatic), 1218 (s, C-O), 1111 (s, C-O), 824 (m), 703 (s), 505 (m).

(2-Methoxy-6H-benzo[c]chromen-9-yl)methanol (**8a**), NaSEt (100.9 mg, 1.2 mmol) was added to a stirred solution of **5** (150 mg, 0.3 mmol) in dry DMF (2 mL), the mixture was heated to 110 °C. After 6 h, the mixture was cooled to rt, saturated aqueous NH_4Cl (2 mL) was added, the aqueous phase was extracted with ethyl acetate (3 × 10 mL), and the organic layer was washed with brine (3 × 30 mL), before drying (Na_2SO_4) and removal of solvent under reduced pressure. Purification by column chromatography (SiO_2, 1:1 heptane/ethyl acetate, Sephadex LH20 1:1 chloroform/methanol) gave the pure product as a light yellow wax (4.8 mg, 7%). ^{1}H- and ^{13}C-NMR data are shown in Tables 2 and 3. HRMS-ESI+ (*m*/z): $[M - H]^-$ calcd for $C_{15}H_{13}O_3$, 241.0865; found, 241.0875. IR (cm^{-1}): 3435 (vw, br, O-H), 2956 (m, C-H aliphatic), 2919 (m, C-H aliphatic), 2850 (w, C-H aliphatic), 1505 (m, C-C aromatic), 1463 (w, C-C aromatic), 1427 (m, C-C aromatic), 1221 (m, C-O), 1195 (m, C-O), 1040 (m, C-O), 821 (w), 705 (vw), 507 (vw).

General procedure to prepare compounds **8b**–**8e**. The corresponding organolithium reagent (2 equiv) was added to **7** (1 equiv) in dry THF (5 mL) at 0 °C or −78 °C depending on the organolithium reagent. After 6 h, saturated aqueous NH_4Cl/H_2O was added, and the aqueous phase was extracted with ethyl acetate (3 × 20 mL) before drying (Na_2SO_4) and removal of solvent under reduced pressure. PBr_3 (0.34 equiv) was added to the crude product (1 equiv) in dichloromethane (10 mL) at rt. After 2 h, LiI (3 equiv) was added at rt. After 12 h, saturated aqueous $Na_2S_2O_3/H_2O$ was added, and the aqueous phase was extracted with ethyl acetate (3 × 20 mL) before drying (Na_2SO_4) and removal of solvent under reduced pressure. TBAF (2 equiv) was added to the crude product in THF (25 mL) at rt, after 5 h, saturated aqueous $NaHCO_3/H_2O$ was added, and the aqueous phase was extracted with ethyl acetate (3 × 25 mL) before drying (Na_2SO_4) and removal of solvent under reduced pressure. Purification by

column chromatography (SiO_2, 1:1 heptane/ethyl acetate) and the enantiomers were separated using a semipreparative HPLC (Chiralpack B column, 96:4 hexane/isopropanol).

(2-Methoxy-6-methyl-6H-benzo[c]chromen-9-yl)methanol (**8b**), the pure product was obtained as a light yellow wax (yield 3%), $[\alpha]^{D}_{20} = -20.8°$. ^{1}H- and ^{13}C-NMR data are shown in Tables 2 and 3. HRMS-ESI+ (*m*/*z*): $[M - H]^-$ calcd for $C_{16}H_{15}O_3$, 255.1021; found, 255.1018. IR (cm^{-1}): 3401 (w, br, O-H), 2960 (m, C-H aliphatic), 2930 (m, C-H aliphatic), 2867 (w, C-H aliphatic), 1503 (s, C-C aromatic), 1463 (w, C-C aromatic), 1426 (s, C-C aromatic), 1216 (vs, C-O), 1194 (s, C-O), 1039 (s, C-O), 821 (m), 705 (w).

(2-Methoxy-6-methyl-6H-benzo[c]chromen-9-yl)methanol (**8c**), the pure product was obtained as a light yellow wax (yield 3%), $[\alpha]^{D}_{20} = +21.8°$. ^{1}H- and ^{13}C-NMR data are shown in Tables 2 and 3. HRMS-ESI+ (*m*/*z*): $[M - H]^-$ calcd for $C_{16}H_{15}O_3$, 255.1021; found, 255.1028. IR (cm^{-1}): 3434 (w, br, O-H), 2931 (m, C-H aliphatic), 2859 (w, C-H aliphatic), 1504 (s, C-C aromatic), 1464 (m, C-C aromatic), 1425 (s, C-C aromatic), 1216 (vs, C-O), 1195 (s, C-O), 1038 (s, C-O), 822 (m), 705 (w).

(6-Ethyl-2-methoxy-6H-benzo[c]chromen-9-yl)methanol (**8d**), the pure product was obtained as a light yellow wax (yield 6%), $[\alpha]^{D}_{20} = -63.2°$. ^{1}H- and ^{13}C-NMR data are shown in Tables 2 and 3. HRMS-ESI+ (*m*/*z*): $[M - H]^-$ calcd for $C_{17}H_{17}O_3$, 269.1178; found, 269.1187. IR (cm^{-1}): 3432 (vw, br, O-H), 2930 (w, C-H aliphatic), 2856 (vw, C-H aliphatic), 1502 (m, C-C aromatic), 1463 (m, C-C aromatic), 1426 (m, C-C aromatic), 1217 (m, C-O), 1040 (m, C-O), 822 (w), 704 (w).

(6-Ethyl-2-methoxy-6H-benzo[c]chromen-9-yl)methanol (**8e**), the pure product was obtained as a light yellow wax (yield 7%), $[\alpha]^{D}_{20} = +62.3°$. ^{1}H- and ^{13}C-NMR data are shown in Tables 2 and 3. HRMS-ESI+ (*m*/*z*): $[M - H]^-$ calcd for $C_{17}H_{17}O_3$, 269.1178; found, 269.1178. IR (cm^{-1}): 3427 (vw, br, O-H), 2929 (w, C-H aliphatic), 2856 (vw, C-H aliphatic), 1503 (m, C-C aromatic), 1462 (m, C-C aromatic), 1426 (m, C-C aromatic), 1217 (m, C-O), 1041 (m, C-O), 823 (w), 704 (w).

General procedure to prepare compounds **8f**, **8g**, *and* **10a**–**10h**. HI (55%, 10 equiv) was added to a stirred solution of the appropriate starting material in acetonitrile (25 mL), at rt. After 30 min, saturated aqueous $Na_2S_2O_3$ (25 mL) was added, and the aqueous layer was extracted with ethyl acetate (3 × 50 mL), before drying (Na_2SO_4) and removal of solvent under reduced pressure. TBAF (1 M, 1.1 equiv) was added to the crude product in THF (150 mL). After 3 h, aqueous saturated $NaHCO_3$ (50 mL) was added, and the aqueous layer was extracted with ethyl acetate (3 × 50 mL), before drying (Na_2SO_4) and removal of solvent under reduced pressure. Purification by column chromatography (SiO_2, 1:1 heptane/ethyl acetate) gave the pure product.

(6,6-Diethyl-2-methoxy-6H-benzo[c]chromen-9-yl)methanol (**8f**), the pure product was obtained as a light yellow wax (yield 56%). ^{1}H- and ^{13}C-NMR data are shown in Tables 2 and 3. HRMS-ESI+ (*m*/*z*): $[M + H]^+$ calcd for $C_{19}H_{23}O_3$, 299.1647; found, 299.1646. IR (cm^{-1}): 3400 (vw, br, O-H), 2962 (s, C-H aliphatic), 2928 (vs, C-H aliphatic), 2868 (m, C-H aliphatic), 1595 (m, C=C aromatic), 1505 (m, C-C aromatic), 1463 (s, C-C aromatic), 1256 (s, C-O).

(6,6-Dibutyl-2-methoxy-6H-benzo[c]chromen-9-yl)methanol (**8g**), the pure product was obtained as a light yellow wax (yield 13%). ^{1}H- and ^{13}C-NMR data are shown in Tables 2 and 3. HRMS-ESI+ (*m*/*z*): $[M + H]^+$ calcd for $C_{23}H_{31}O_3$, 355.2273; found, 355.2272. IR (cm^{-1}): 3400 (vw, br, O-H), 2957 (vs, C-H aliphatic), 2928 (vs, C-H aliphatic), 2869 (m, C-H aliphatic), 1504 (s, C-C aromatic), 1214 (s, C-O) 1027 (m, C-O).

(3-Methoxy-6,6-dimethyl-6H-benzo[c]chromen-9-yl)methanol (**10a**), the pure product was obtained as a light yellow wax (yield 38%). ^{1}H- and ^{13}C-NMR data are shown in Tables 2 and 3. HRMS-ESI+ (*m*/*z*): $[M + H]^+$ calcd for $C_{17}H_{19}O_3$, 271.1334; found, 271.1338. IR (cm^{-1}): 3379 (m, br, O-H), 2966 (m, C-H aliphatic), 2932 (m, C-H aliphatic), 2857 (w, C-H aliphatic), 1615 (vs, C=C aromatic), 1589 (m, C=C aromatic), 1510 (m, C-C aromatic), 1496 (m, C-C aromatic), 1417 (m, C-C aromatic), 1290 (s, C-O), 1273 (s, C-O), 1201 (s, C-O), 1055 (vs, C-O), 1110 (s, C-O), 981(m).

(1-Methoxy-6,6-dimethyl-6H-benzo[c]chromen-9-yl)methanol (**10b**), the pure product was obtained as a light yellow wax (yield 48%). ^{1}H- and ^{13}C-NMR data are shown in Tables 2 and 3. HRMS-ESI+ (*m*/*z*): $[M + H]^+$ calcd for $C_{17}H_{19}O_3$, 271.1334; found, 271.1338. IR (cm^{-1}): 3395 (w, br, O-H), 2970 (w, C-H aliphatic), 2930 (w, C-H aliphatic), 2863 (vw, C-H aliphatic), 1600 (m, C=C aromatic), 1586 (m, C=C aromatic), 1503 (m, C-C aromatic), 1462 (s, C-C aromatic), 1436 (m, C-C aromatic), 1413 (m, C-C aromatic), 1234 (vs, C-O), 1088 (vs, C-O), 1080 (vs, C-O).

(2,6,6-Trimethyl-6H-benzo[c]chromen-9-yl)methanol (**10c**), the pure product was obtained as a transparent wax (yield 73%). ^{1}H- and ^{13}C-NMR data are shown in Tables 2 and 3. HRMS-ESI+ (*m*/*z*): $[M + H]^+$ calcd for $C_{17}H_{19}O_2$, 255.1385; found, 255.1383. IR (cm^{-1}): 3400 (w, br, O-H), 2978 (m, C-H aliphatic), 1505 (s, C-C aromatic), 1425 (s, C-C aromatic), 1256 (vs, C-O), 1114 (m), 818 (s).

(3,6,6-Trimethyl-6H-benzo[c]chromen-9-yl)methanol (**10d**), the pure product was obtained as a transparent wax (yield 85%). ^{1}H- and ^{13}C-NMR data are shown in Tables 2 and 3. HRMS-ESI+ (*m*/*z*): $[M - OH]^-$ calcd for $C_{17}H_{17}O$, 237.1285; found, 237.1281. IR (cm^{-1}): 3405 (w, br, O-H), 2928 (w, C-H aliphatic), 1589 (w, C=C aromatic), 1502 (m, C-C aromatic), 1270 (w, C-O), 1115 (w).

(6,6-Dimethyl-6H-benzo[c]chromen-9-yl)methanol (**10e**) the pure product was obtained as a transparent wax (yield 68%). ^{1}H- and ^{13}C-NMR data are shown in Tables 2 and 3. HRMS-ESI+ (*m*/*z*): $[M + H]^+$ calcd for $C_{16}H_{17}O_2$, 241.1229; found, 241.1227. IR (cm^{-1}): 3300 (w, br, O-H), 2979 (w, C-H aliphatic), 1589 (w, C=C aromatic), 1492 (m, C-C aromatic), 1419 (m, C-C aromatic), 1253 (vs, C-O), 1105 (m), 752 (s).

(2-Isopropyl-6,6-dimethyl-6H-benzo[c]chromen-9-yl)methanol (**10f**), the pure product was obtained as a transparent wax (yield 31%). ^{1}H- and ^{13}C-NMR data are shown in Tables 2 and 3. HRMS-ESI+ (*m*/*z*): $[M + H]^+$ calcd for $C_{19}H_{23}O_2$, 283.1698; found, 283.1701. IR (cm^{-1}): 3361 (m, br, O-H), 2961 (w, C-H aliphatic), 2927 (m, C-H aliphatic), 2870 (m, C-H aliphatic), 1613 (w, C=C aromatic), 1588 (w, C=C aromatic), 1504 (s, C-C aromatic), 1462 (s, C-C aromatic), 1416 (m, C-C aromatic), 1255 (vs, C-O), 1156 (m), 1114 (m), 818 (m).

(3-Isopropyl-6,6-dimethyl-6H-benzo[c]chromen-9-yl)methanol (**10g**), the pure product was obtained as a transparent wax (yield 85%). ^{1}H- and ^{13}C-NMR data are shown in Tables 2 and 3. HRMS-ESI+ (*m*/*z*): $[M - OH]^-$ calcd for $C_{19}H_{21}O_2$, 265.1592; found, 265.1597. IR (cm^{-1}): 3439 (vw, br, O-H), 2960 (m, C-H aliphatic), 2931 (m, C-H aliphatic), 2858 (w, C-H aliphatic), 1610 (vw, C=C aromatic), 1567 (vw, C=C aromatic), 1462 (m, C-C aromatic), 1414 (m, C-C aromatic), 1110 (s), 822 (m), 703 (s).

(6,6-Dimethyl-2-pentyl-6H-benzo[c]chromen-9-yl)methanol (**10h**), the pure product was obtained as a transparent wax (yield 72%). ^{1}H- and ^{13}C-NMR data are shown in Tables 2 and 3. HRMS-ESI+ (*m*/*z*): $[M - OH]^-$ calcd for $C_{21}H_{25}O_2$, 293.1905; found, 293.1902. IR (cm^{-1}): 3397 (w, br, O-H), 1588 (w, C=C), 1116 (w).

3.3. Biological Assays

3.3.1. Evaluations Against *Leishmania parasites*

Promastigotes of Leishmania-Leishmania: *L. amazonensis*, Clone 1, NHOM-BR-76-LTB-012 (Lma, donated by the Paul Sabatier Université, Toulouse, France) and Leishmania-Viannia: *L. braziliensis* M2904 C192 RJA (M2904, donated by Dr. Jorge Arévalo from Universidad Peruana Cayetano Heredia, San Martin des Porres, Peru), [30]. All strains were cultured in Schneider's insect medium, (pH 6.2) supplemented with 10% FBS and incubated at 26 °C. Medium changes were made every 72 h to maintain a viable parasitic population. Leishmanicidal activity was determined according to Williams with some modifications [31]. Samples were dissolved in DMSO (maximum final concentration 1%) at 10 mg/mL. Promastigotes in logarithmic phase of growth, at the concentration 3 × 106 parasites/mL, were distributed (100 µL/well) in 96-well flat bottom microtiter plates. Samples with different concentrations (3.1–100 µg/mL) were added (100 µL). Miltefosine (3.1–100 µg/mL), was used as control

drug [32]. Assays were performed in triplicates. The microwell plates were incubated for 72 h at 26 °C. After incubation, a solution of XTT (1 mg/mL) in PBS (pH 7.0 at 37 °C) with PMS (0.06 mg/mL) was added (50 μL/well), and incubated for 3 h at 26 °C. The optical density of each well was measured and the IC_{50} values calculated. A negative control experiments with only 1% DMSO was carried out, showing that the solvent by itself has no antiparasitic activity.

3.3.2. Evaluations Against *Trypanosoma cruzi*

Cultures of *Trypanosoma cruzi* (epimastigotes, donated by the Parasitology Department of INLASA, Tc-INLASA, city, country), were maintained in medium LIT (pH 7.2), supplemented with 10% FBS and incubated at 26 °C. Medium changes were made every 72 h to maintain a viable parasitic population. Trypanocidal activity was determined according to Muelas-Serrano with some modifications [33]. Samples were dissolved in DMSO (maximum final concentration 1%) at 10 mg/mL. Epimastigotes in logarithmic phase of growth, at a concentration of 3 × 106 parasites/mL, were distributed (100 μL/well) in 96-well flat bottom microtiter plates. Samples at different concentrations (3.1–100 μg/mL) were added (100 μL). Benznidazole (3.1–100 μg/mL) was used as the control drug. Assays were performed in triplicates. The microwell plates were incubated for 72 h at 26 °C. After incubation, a solution of XTT (1 mg/mL) in PBS (pH 7.0 at 37 °C) with PMS (0.06 mg/mL) was added (50 μL/well) and incubated for 4 h at 26 °C. The optical density of each well was measured and the IC_{50} values were calculated. A negative control experiments with only 1% DMSO was carried out, showing that the solvent by itself has no antiparasitic activity.

3.3.3. Evaluations Against RAW Cells

The Raw 264.7 murine macrophage cell line was purchased from the American Type Culture Collection (ATCC-TIB71, ARCC (Manassas, VA, USA). The cells were maintained in DMEM-HG medium supplemented with 10% fetal bovine serum, 100 U/mL of penicillin and 100 μg/mL of streptomycin, and sodium bicarbonate (2.2 g/L) in humidified atmosphere at 37 °C with 5% CO_2. Samples were dissolved in DMSO and diluted (maximum final concentration of DMSO: 1%) at different concentrations (6.2–200 μg/mL). Medium blank, control drugs and cell growth controls were included to evaluate cell viability. The plates were incubated for 72 h at 37 °C with 5% CO_2 and 3×10^4 cells/well. After incubation for the indicated time, the cells were washed, after which 10 μL of resazurin reagent (2.0 mM) was added. They were further incubated at 37 °C for 3 h in a humidified incubator. The IC_{50} values were assessed using a fluorometric reader (BioTek (Winooski, VT, USA), 540 nm excitation, 590 nm emission) and the Gen5 software (v. 2017, BioTek). All assays were performed in triplicate.

4. Conclusions

Fifteen derivatives of pulchrol with modifications on ring B and ring C were prepared and tested towards *T. cruzi*, *L. braziliensis* and *L. amazonensis*, together with **1**. The importance of the presence of methyl substituents on ring B was investigated, and the unsubstituted derivative **8a** was shown to be less active compared to **1** towards all the three parasites. The effect on bioactivity that just one substituent has on C-6 was different between the parasites. The 6-methyl monosubstituted enantiomers were not more active than **1**, suggesting that two methyl substituents instead of one may improve orientation and lipophilic interactions in the binding site. 6-Ethyl monosubstituted derivatives are slightly more potent towards the two *Leishmania* species, but with *T. cruzi* they are less potent. The longer the alkyl substituents on C-6 are, the more interesting is the activity. A preference for disubstituted rather than monosubstituted analogues appears to be at hand, but with *T. cruzi* the 6,6-diethyl analogue is better that the 6,6-dibutyl analogue, and **8f** was found to be more potent and selective than the positive control benznidazole. This suggests that additional derivatives with larger and branched alkyl groups at C-6 should be prepared and assayed.

The methoxy group in the C-ring was also shown to play a role for pulchrol's bioactivity, as a derivative without substituents (**10e**) was considerably less active compared to **1**. A methoxy substituent in either C-3 or C-2 appears beneficial compared to C-1, although the differences are not massive. A methyl at C-2 or C-3 instead of a methoxy group has a small impact, although for *T. cruzi* **1** is still the most potent. Longer and more bulky alkyl substituents in positions C-2 and C-3 (**10f**, **10g** and **10h**) are clearly more potent, with all three parasites. The C-2 *n*-pentyl analogue **10h** showed the best activities towards *T. cruzi*, while **10h** together with the C-2 isopropyl analogues **10f** and **10g** showed the best results with *L. braziliensis* and *L. amazonensis*.

Most of the differences in the antiparasitic activity observed in this study can be tentatively suggested to be linked to the lipophilicity of the compounds. However, nothing is known about the molecular targets in these parasites, and to increase our understanding it is necessary to expand our studies in a systematic way. Compared to the QSARs suggested in the previous study of the benzyl alcohol function, we have now a new wish list of compounds to prepare and assay.

The 1D ^{1}H and ^{13}C-NMR shifts of the assayed compounds are given in Tables 2 and 3, and as the shifts reflects the electronic conditions in the vicinity of each nucleus they may indicate SARs. However, with the data available in this study, no SARs are obvious from the NMR shifts.

Supplementary Materials: The following are available online: ^{1}H and ^{13}C NMR spectra of all intermediates and all pulchrol analogues prepared and assayed in this investigation.

Author Contributions: Conceptualization, P.T. and O.S.; methodology, P.T., O.S. and A.G.; software, P.T. and A.G.; validation, P.T., A.G. and O.S.; formal analysis, P.T., A.G. and O.S.; investigation, all aothors; resources, A.G. and O.S.; data curation, P.T., A.G. and O.S.; writing—original draft preparation, P.T.; writing—review and editing, all authors; visualization, P.T., A.G. and O.S.; supervision, S.M., A.G. and O.S.; project administration, O.S.; funding acquisition, O.S. All authors have read and agreed to the published version of the manuscript.

Funding: This research was funded by the Swedish International Development Cooperation Agency (SIDA), including a Ph.D. scholarship for PT is gratefully acknowledge grant number 621.2015.04730.

Conflicts of Interest: The authors declare no conflict of interest. The sponsors had no role in the design, execution, interpretation, or writing of the study.

References

1. World Health Organization Homepage. Available online: https://www.who.int/neglected_diseases/diseases/en/ (accessed on 14 July 2020).
2. Jacobson, J.; Bush, S. Neglected tropical diseases, beglected communities, and conflict: How do we leave no one behind? *Trends Parasitol.* **2018**, *34*, 175–177. [CrossRef] [PubMed]
3. World Health Organisation. Second WHO Report on Neglected Tropical Diseases. Available online: https://www.who.int/neglected_diseases/9789241564540/en/ (accessed on 14 July 2020).
4. Molyneux, D.H.; Savioli, L.; Engels, D. Neglected tropical diseases: Progress towards addressing the chronic pandemic. *Lancet* **2017**, *389*, 312–325. [CrossRef]
5. Field, M.C.; Horn, D.; Fairlamb, A.H.; Ferguson, M.A.J.; Gray, D.W.; Read, K.D.; De Rycker, M.; Torrie, L.S.; Wyatt, P.G.; Wyllie, S.; et al. Anti-trypanosomatid drug discovery: An ongoing challenge and a continuing need. *Nat. Rev. Microbiol.* **2017**, *15*, 217–231. [CrossRef] [PubMed]
6. Pérez-Molina, J.A.; Molina, I. Chagas disease. *Lancet* **2018**, *391*, 82–94. [CrossRef]
7. World Health Organization Home Page. Available online: https://www.who.int/chagas/disease/en/ (accessed on 14 July 2020).
8. Chatelain, E. Chagas disease research and development: Is there light at the end of the tunnel? *Comput. Struct. Biotechnol. J.* **2016**, *15*, 98–103. [CrossRef]
9. Tarleton, R.L. Chagas disease: A solvable problem, ignored. *Trends. Mol. Med.* **2016**, *22*, 835–838. [CrossRef]
10. World Health Organization Home Page. Available online: https://www.who.int/news-room/fact-sheets/detail/leishmaniasis (accessed on 14 July 2020).

11. Croft, S.L.; Sundar, S.; Fairlamb, A.H. Drug resistance in leishmaniasis. *Clin. Microbiol. Rev.* **2006**, *19*, 111–126. [CrossRef]
12. Li, G.; Lou, H.-X. Strategies to diversify natural products for drug discovery. *Med. Res. Rev.* **2018**, *38*, 1255–1294. [CrossRef]
13. David, B.; Wolfender, J.-L.; Dias, D.A. The pharmaceutical industry and natural products: Historical status and new trends. *Phytochem. Rev.* **2015**, *14*, 299–315. [CrossRef]
14. Atanasov, A.G.; Waltenberger, B.; Pferschy-Wenzig, E.-M.; Linder, T.; Wawrosch, C.; Uhrin, P.; Temml, V.; Wang, L.; Schwaiger, S.; Heiss, E.H.; et al. Discovery and resupply of pharmacologically active plant-derived natural products: A review. *Biotechnol. Adv.* **2015**, *33*, 1582–1614. [CrossRef]
15. Rodrigues, T.; Reker, D.; Schneider, P.; Schneider, G. Counting on natural products for drug design. *Nat. Chem.* **2016**, *8*, 531–541. [CrossRef] [PubMed]
16. Bukuru, J.F.; Van, T.N.; Van Puyvelde, L.; Mathenge, S.G.; Mudida, F.P.; De Kimpe, N. A Benzochromene from the roots of *Pentas bussei*. *J. Nat. Prod.* **2002**, *65*, 783–785. [CrossRef] [PubMed]
17. Gulcan, H.O.; Unlu, S.; Esiringu, İ.; Ercetin, T.; Sahin, Y.; Oz, D.; Sahin, M.F. Design, synthesis and biological evaluation of novel 6H-benzo[c]chromen-6-one, and 7,8,9,10-tetrahydro-benzo[c]chromen-6-one derivatives as potential cholinesterase inhibitors. *Bioorg. Med. Chem.* **2014**, *22*, 5141–5154. [CrossRef] [PubMed]
18. Husni, A.S.; McCurdy, C.R.; Radwan, M.M.; Ahmed, S.A.; Slade, D.; Ross, S.A.; El Sohly, M.A.; Cutler, S.J. Evaluation of phytocannabinoids from high potency *Cannabis sativa* using in vitro bioassays to determine structure-activity relationships for Cannabinoid receptor 1 and Cannabinoid receptor 2. *Med. Chem. Res.* **2014**, *23*, 4295–4300. [CrossRef] [PubMed]
19. Kaplan, B.L.F.; Rockwell, C.E.; Kaminski, N.E. Evidence for cannabinoid receptor-dependent and -independent mechanisms of action in leukocytes. *J. Pharmacol. Exp. Ther.* **2003**, *306*, 1077. [CrossRef]
20. Jan, T.-R.; Rao, G.K.; Kaminski, N.E. Cannabinol enhancement of interleukin-2 (IL-2) expression by T cells is associated with an increase in IL-2 distal nuclear factor of activated T cell activity. *Mol. Pharmacol.* **2002**, *61*, 446. [CrossRef]
21. Munson, A.E.; Harris, L.S.; Friedman, M.A.; Dewey, W.L.; Carchman, R.A. Antineoplastic activity of cannabinoids2. *JNCI J. Natl. Cancer Inst.* **1975**, *55*, 597–602. [CrossRef]
22. Erosa-Rejón, G.J.; Yam-Puc, A.; Chan-Bacab, M.J.; Giménez-Turbax, A.; Salamanca, E.; Peña-Rodríguez, L.M.; Sterner, O. Benzochromenes from the roots of *Bourreria pulchra*. *Phytochem. Lett.* **2010**, *3*, 9–12. [CrossRef]
23. Campos-Ríos, M.G. Revisión del género *Bourreria P*. Browne (Boraginaceae) en México. *Polibotánica* **2005**, *19*, 39–103.
24. Argueta, A.; Cano, L.; Roderte, M.E. *Atlas de las Plantas de la Medicina Tradicional Mexicana*; Instituto Nacional Indigenista: Ciudad de Mexico, Mexico, 1994; pp. 483–485.
25. Polanco-Hernández, G.; Escalante-Erosa, F.; García-Sosa, K.; Acosta-Viana, K.; Chan-Bacab, M.J.; Sagua-Franco, H.; González, J.; Osorio-Rodríguez, L.; Moo-Puc, R.E.; Peña-Rodríguez, L.M. In vitro and in vivo trypanocidal activity of native plants from the Yucatan peninsula. *Parasitol. Res.* **2012**, *110*, 31–35. [CrossRef]
26. Killander, D.; Sterner, O. Synthesis of the bioactive benzochromenes pulchrol and pulchral, metabolites of *Bourreria pulchra*. *Eur. J. Org. Chem.* **2014**, *2014*, 1594–1596. [CrossRef]
27. Killander, D.; Sterner, O. Reagent-controlled cyclization–deprotection reaction to yield either fluorenes or benzochromenes. *Eur. J. Org. Chem.* **2014**, *2014*, 6507–6512. [CrossRef]
28. Terrazas, P.; Salamanca, E.; Dávila, M.; Manner, S.; Giménez, A.; Sterner, O. SARs for the antiparasitic plant metabolite pulchrol. 1. The benzyl alcohol functionality. *Molecules* **2020**, *25*, 3058. [CrossRef]
29. Norseeda, K.; Tummatorn, J.; Krajangsri, S.; Thongsornkleeb, C.; Ruchirawat, S. Synthesis of 6-Alkyl-6 H-benzo[c]chromene Derivatives by cyclization/selective ether cleavage in one pot: Total synthesis of cannabinol. *Asian J. Org. Chem.* **2016**, *5*, 792–800. [CrossRef]
30. Bilbao-Ramos, P.; Dea-Ayuela, M.A.; Cardenas-Alegría, O. Leishmaniasis in the major endemic region of Plurinational State of Bolivia: Species identification, phylogeography and drug susceptibility implications. *Acta Trop.* **2017**, *176*, 150–161. [CrossRef]
31. Williams, C.; Espinosa, O.A.; Montenegro, H. Hydrosoluble formazan XTT: Its application to natural products drug discovery for *Leishmania*. *J. Microbiol. Methods* **2003**, *55*, 813–816. [CrossRef]

32. Campos-Buzzi, F.; Fracasso, M.; Clase, B.K.; Ticona, J.C.; Gimenez, A.; Cechinel-Filho, V. Evaluation of antinociceptive effects of *Galipea longiflora* alkaloid extract and major alkaloid 2-fenilquinoline. *Methods Find. Exp. Clin. Pharmacol.* **2010**, *32*, 707–711. [CrossRef]
33. Muelas-Serrano, S.; Nogal-Ruiz, J.; Gomez-Barrio, A. Setting of a colorimetric method to determine the viability of *Trypanosoma cruzi* epimastigotes. *Parasitol. Res.* **2000**, *86*, 999–1002. [CrossRef]

Sample Availability: Samples of the compounds are not available from the authors, but can be synthesized following the information given in the manuscript and supplementary materials.

Paper III

molecules

MDPI

Article

SARs for the antiparasitic plant metabolite pulchrol. 3. Combinations of new substituents in A/B-rings and A/C-rings

Paola Terrazas[1,2], Efrain Salamanca[3], Marcelo Dávila[2], Sophie Manner[1], Alberto Gimenez[3] and Olov Sterner[1,*]

[1] Department of Chemistry, Centre for Analysis and Synthesis, Lund University, 22100 Lund, Sweden; paola.terrazas_villarroel@chem.lu.se (P.T.); sophie.manner@chem.lu.se (S.M.)
[2] Centre of Agroindustrial Technology, San Simón University, 3299 Cochabamba, Bolivia; marcelodavila@fcyt.umss.edu.bo (M.D.)
[3] Institute for Pharmacological and Biochemical Sciences, San Andrés University, 3299 La Paz, Bolivia;
* Correspondence: Olov.Sterner@chem.lu.se; Tel.: +46-70-5306649

Abstract. The natural products pulchrol and pulchral, isolated from the roots of the Mexican plant *Bourreria pulchra*, have previously been shown to possess an antiparasitic activity toward *Trypanosoma cruzi*, *Leishmania braziliensis* and *L. amazonensis*, protozoa responsible for the Chagas disease and leishmaniasis. These infections have been classified as neglected diseases, and still require the development of safer and more efficient alternatives to their current treatments. Recent SAR studies, based on the pulchrol scaffold, showed which effect the exchanges of its substituents have on the antileishmanial and antitrypanosomal activity. Many of the analogues prepared were shown to be more potent *in vitro* than pulchrol and the current drugs used to treat Leishmaniasis and the Chagas disease (Miltefosine and Benznidazole respectively). Moreover, indications of some of the possible interactions that may take place in the binding sites were also identified. In this study, 12 analogues with modifications at two or three different positions in two of the three rings were prepared by synthetic and semi-synthetic procedures. The molecules were assayed *in vitro* toward *T. cruzi* epimastigotes, *L. braziliensis* promastigotes and *L. amazonensis* promastigotes. Some compounds had higher antiparasitic activity than the parent compound pulchrol, and in some cases even Benznidazole and Miltefosine. The best combinations in this subset are with carbonyl functionalities in the A-ring and isopropyl groups in the C-ring, as well as with alkyl substituents in both the A- and C-rings combined with a hydroxyl group in position 1 (C-ring). The latter corresponds to cannabinol, which was shown to be potent toward all parasites.

Keywords: *Trypanosoma cruzi*, *Leishmania braziliensis*, *Leishmania amazonensis*, pulchrol, pulchral, cannabinol, SARs

Citation: Terrazas, P.; Salamanca, E.; Davila, M.; Manner, S.; Gimenez, A.; Sterner, O. SARs for the antiparasitic plant metabolite pulchrol. 3. Combinationsß of new substituents in A/B-rings and A/C-rings. *Molecules* **2021**, *26*, x. https://doi.org/10.3390/xxxxx

Academic Editor:

Received:
Accepted:
Published: date

Publisher's Note: MDPI stays neutral with regard to jurisdictional claims in published maps and institutional affiliations.

1. Introduction

Natural products have been one of the main sources for bioactive compounds used to treat a wide range of diseases [1]. The chemical diversity, potential selectivity, and the availability of traditional knowledge about the use of natural materials, played an important role in the development of modern drugs. Examples are morphine isolated from opium [2]; taxol isolated from *Taxus brevifolia* [3]; important antiparasitic drugs such as quinine isolated from *Cinchona officinalis* [4]; and artemisinin extracted from *Artemisia annua* [5].

Natural products are often isolated in limited quantities and can be assayed in just a few biological systems. In order to extend the bioactivity scope, synthetic routes can be designed to obtain sufficient quantities of the product, and can also be used to prepare new derivatives and analogues which may possess superior biological properties [1, 6]. For diseases in which the mechanism of action and the drug target is not fully understood,

as is the case for leishmaniasis and the Chagas disease [7–9], derivatives can be prepared and assayed towards cells or whole organisms to measure their activity [10–13], leading to the development of structure activity relationships studies (SARs). These can be used to design more potent and less toxic analogues, assuming that just one biological target is involved [11, 14].

The vegetal specie, *Bourreria pulchra*, which is native from the Yucatan province in Mexico, is traditionally used to treat cutaneous diseases, fevers and infections [15]. The isolation of the main chemical compounds from its roots yielded pulchrol (**1a**, see Figure 1), which was shown to possess antiparasitic activity against *Leishmania braziliensis*, *L. amazonensis* and *L. mexicana* promastigotes, as well as against *Trypanosoma cruzi* epimastigotes [16].

Leishmania and *Trypanosoma* parasites are part of the family Trypanosomatidae, and are responsible for leishmaniasis and the Chagas disease, respectively. Both are considered neglected diseases but still affect millions of people in developing countries mainly placed in the tropical and subtropical regions of the world [7, 17–21]. Leishmaniasis can appear as cutaneous, mucocutaneous or visceral leishmaniasis, and around 700 000 to 1 million new cases are diagnosed every year. The treatments for Leishmaniasis (mainly Amphotericin, Miltefosine and pentavalent antimonials) may give several toxic side effects and may require hospitalization [22–23]. Likewise, Chagas disease is able to produce damage in the hearth tissue and eventually cause death. Twelve million people are affected by this disease and the existing treatments are far from ideal (Nifurtimox or Benznidazole) [24–28]. Currently, there are few validated drug targets for leishmaniasis and the Chagas disease, and too little is understood of the complex life cycle of these pathogens [9].

Pulchrol (**1a**) is an example of the many natural products that are based on a benzo[*c*]chromene scaffold. This type of compound has been shown to possess different kinds of biological activities [29–34]. The most studied benzo[*c*]chromenes are probably the cannabinoids, isolated mainly from the plant *Cannabis sativa* and known for their affinity to the cannabinoid receptors CB1 and CB2. The natural product cannabinol (**5f**, see Figure 1), which possess the same skeleton as pulchrol, has been shown to be selective for CB2, a receptor expressed on immune cells, macrophages and in other peripheral organs, while Δ^9-tetrahydrocannabinol (THC, **6**, see Figure 1) also isolated from *C. sativa*, showed greater affinity for CB1, the receptor associated with *C. sativa* psychotropic activity [35]. SARs including cannabinol (**5f**) have been studied previously, and indicated that hydroxyl groups at positions 1 and 1′ together with bulky alkyl substituents at position 3 are important for the affinity to CB1 [36]. In addition, shorter and bulkier alkyl substituents at C-3 improved the affinity for the CB2-receptor [37, 38]. Cannabinoids have also shown immunomodulatory properties in the treatment of psoriasis [39], antinociceptive properties related to their capacity to induce vasorelaxation and release of neuropeptides [40–41], and antineoplastic activity on Lewis lung tumors [33].

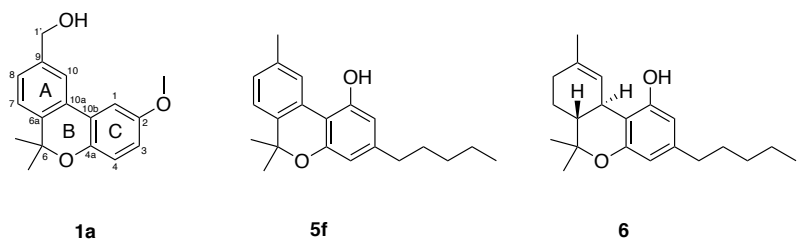

1a **5f** **6**

Figure 1. Structures of pulchrol (**1a**), cannabinol (**5f**) and Δ^9-tetrahydrocannabinol (**6**).

The potential shown by pulchrol (**1a**) as an antiparasitic agent against *T. cruzi* and the *Leishmania* species, led to the development of a synthetic route [42, 43] that yields sufficient amounts of pulchrol to perform additional biological assays. This were also adapted for the preparation of a series of analogues with individual transformations of the benzyl alcohol moiety in the A-ring [44], variations at positions 1, 2 and 3 in the C-ring, and modifications at the only available position in the B-ring (C-6) [45]. In this investigation, we prepared analogues with combinations of different functionalities in the A-, B-, and C-rings (See Figure 2), inspired by some of the SARs observed in the previous studies [44, 45]. Cannabinol (**5f**) and its 3-methyl analogue **5e** (see Figure 2), were also prepared and assayed. Our main objective was to study the effect that several substituents coexisting at different positions in the benzo[*c*]chromene skeleton may have in the activity toward the parasites under study, and get more information about the chemical surroundings of the active site in which pulchrol and its analogues may be interacting.

2. Results

2.1. Preparation

In this study, analogues of pulchrol were prepared containing combinations of two or three modifications in the A-, B, and C-rings (See Figure 2). The synthetic routes used to prepare the analogues were partially based on the previously reported procedure used to synthesize pulchrol from biaryl intermediates [42, 43]. The molecules in the **1**-series (See Figure 2) were previously reported [44, 45], and were used as starting material to prepare the compounds from the **2**-, **3**-, **4**- and **5**- series, containing a 1'-aldehyde, 1'-methyl ketone, 3-methylbutanoic acid ester and 9-methyl functionalities, respectively (See Figure 2). Compounds **5f** (cannabinol) and its analogue **5e** were obtained through iodine-mediated deconstructive annulation in a one-pot synthesis, using citral and resorcinol analogues as starting material [46]. In total 12 molecules were prepared and assayed *in vitro* against *T. cruzi* epimastigotes as well as *L. braziliensis* and *L. amazonensis* promastigotes (See Table 1). Their antiparasitic activities were compared with those previously reported for the analogues in the **1**- series in addition to compounds **2a** (pulchral), **3a**, **4a**, and **5a** [44]. Figure 2 summarizes the structure types of the analogues prepared, while the biological activities are given in Table 1.

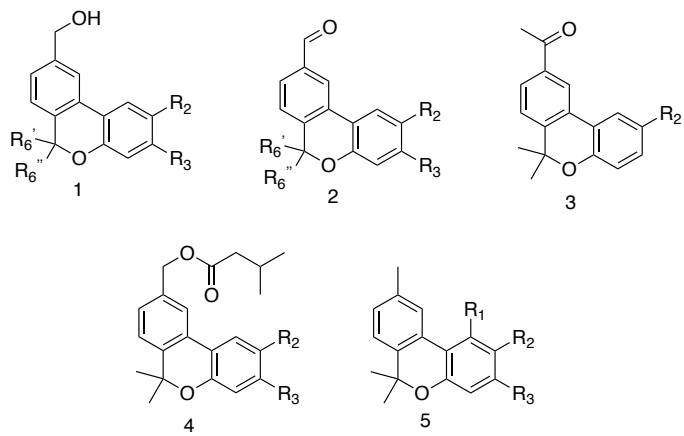

Figure 2. Prepared derivatives. **1a** R_2 = OMe, R_3 = H, $R_{6'}$ = Me, $R_{6''}$ = Me; **1b** R_2 = isopropyl, R_3 = H, $R_{6'}$ = Me, $R_{6''}$ = Me; **1c** R_2 = H, R_3 = isopropyl, $R_{6'}$ = Me, $R_{6''}$ = Me; **1d** R_2 = OMe, R_3 = H, $R_{6'}$ = Me, $R_{6''}$ =

H; **1e** R_2 = OMe, R_3 = H, $R_{6'}$ = H, $R_{6''}$ = Me; **2a** R_2 = OMe, R_3 = H, $R_{6'}$ = Me, $R_{6''}$ = Me; **2b** R_2 = isopropyl, R_3 = H, $R_{6'}$ = Me, $R_{6''}$ = Me; **2c** R_2 = H, R_3 = isopropyl, $R_{6'}$ = Me, $R_{6''}$ = Me**;** **2d** R_2 = OMe, R_3 = H, $R_{6'}$ = Me, $R_{6''}$ = H; **2e** R_2 = OMe, R_3 = H, $R_{6'}$ = H, $R_{6''}$ = Me; 3**a** R_2 = OMe; **3b** R_2 = isopropyl; **4a** R_2 = OMe, R_3 = H; **4b** R_2 = isopropyl, R_3 = H; **4c** R_2 = H, R_3 = isopropyl; **5a** R_1 = H, R_2 = OMe, R_3 = H; **5b** R_1 = H, R_2 = isopropyl, R_3 = H; **5c** R_1 = H, R_2 = H, R_3 = isopropyl; **5d** R_1 = H, R_2 = OH, R_3 = H; **5e** R_1 = OH, R_2 = H, R_3 = Me; **5f** R_1 = OH, R_2 = H, R_3 = *n*-pentyl. See Experimental part for synthetic details.

Table 1. Antileishmanial and antitrypanozomal activity of pulchrol derivatives, compared to the positive controls Benznidazole and Miltefosine. See experimental for details about the assays.

Serie	Structure	Mol.	R1	R2	R3	R6′	R6′′	*T. cruzi*	*L. braziliensis*	*L. amazonensis*
								IC_{50} (μM)	IC_{50} (μM)	IC_{50} (μM)
1		**1a**[a]	H	OMe	H	Me	Me	18.5 ± 9.6	59.2 ± 11.8	77.7 ± 5.5
		1b[b]	H	*i*-Pr	H	Me	Me	12.4 ± 3.5	18.1 ± 0.7	15.6 ± 2.8
		1c[b]	H	H	*i*-Pr	Me	Me	14.2 ± 4.2	19.1 ± 1.1	21.2 ± 7.1
		1d[b]	H	OMe	H	Me	H	35.9 ±11.7	156.1 ± 23.4	156.1 ± 58.5
		1e[b]	H	OMe	H	H	Me	67.1 ± 31.2	128.8 ± 24.6	71.8 ± 12.5
2		**2a**[a]	H	OMe	H	Me	Me	24.2 ± 4.1	24.2 ± 7.5	29.8 ± 11.2
		2b	H	*i*-Pr	H	Me	Me	10.7 ± 4.3	12.1 ± 4.6	11.4 ± 3.6
		2c	H	H	*i*-Pr	Me	Me	7.1 ± 1.4	17.8 ± 1.8	17.8 ± 0.7
		2d	H	OMe	H	Me	H	125.8 ± 7.9	70.8 ± 19.7	44.0 ± 1.6
		2e	H	OMe	H	H	Me	170.3 ± 7.9	118.0 ± 0.8	80.6 ± 4.7
3	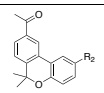	**3a**[a]	H	OMe	H	Me	Me	21.2 ± 9.2	28.3 ± 7.1	43.2 ± 8.2
		3b	H	*i*-Pr	H	Me	Me	3.4 ± 0.2	8.8 ± 1.0	9.5 ± 4.1
4	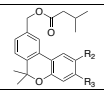	**4a**[a]	H	OMe	H	Me	Me	4.2 ± 1.1	13.1 ± 0.4	14.5 ± 0.1
		4b	H	*i*-Pr	H	Me	Me	10.9 ± 3.8	272.9 ±0.00	25.9 ± 5.5
		4c	H	H	*i*-Pr	Me	Me	13.6 ± 5.7	63.3 ± 4.4	43.7 ± 8.2
5		**5a**[a]	H	OMe	H	Me	Me	51.1 ± 17.7	69.6 ± 5.9	85.3 ± 5.9
		5b	H	*i*-Pr	H	Me	Me	23.7 ± 8.6	49.2 ± 15.0	49.6 ± 4.5
		5c	H	H	*i*-Pr	Me	Me	50.3 ± 11.3	311.6 ± 50.3	236.5 ± 48.8
		5d	H	OH	H	Me	Me	54.9 ± 0.2	30.4 ± 2.9	33.3 ± 5.4
		5e	OH	H	Me	Me	Me	5.9 ± 2.0	15.7 ± 5.1	21.2 ± 2.4
		5f	OH	H	*n*-Pen	Me	Me	7.4 ± 0.6	10.3 ± 0.6	14.2 ± 1.3
		Benznidasole						19.2 ± 7.7		
		Miltefosine							13.0 ± 1.2	10.8 ± 1.5

[a] Previously reported derivatives by Terrazas et al, 2020 [44]; [b] Previously reported derivatives by Terrazas et al, 2020 [45]

Tables 2 and 3 give the 1D ^{1}H and ^{13}C NMR shifts of the assayed compounds.

Table 2. Proton chemical shifts (in ppm) for the compounds prepared in this study, measured at 400 MHz. The assignments were made with 2D NMR spectroscopy, COSY, HMQC and HMBC experiments.

Compd	1-H	2-H	3-H	4-H	7-H	8-H	10-H	1′-H/H_2/H_3	2-OCH_3	6-H/H_2	6,6-CH_3
1a	7.26	-	6.81	6.89	7.23	7.30	7.68	4.74	3.85	-	1.61
2b [a]	7.65	-	7.15	6.90	7.41	7.79	8.24	10.07	-	-	1.65
2c [b]	7.73	6.94	-	6.85	7.40	7.77	8.19	10.05	-	-	1.66
2d	7.31	-	6.87	6.94	7.34	7.81	8.17	10.07	3.87	5.25	1.63
2e	7.32	-	6.87	6.94	7.34	7.81	8.17	10.07	3.87	5.27	1.63
3b [c]	7.65	-	7.13	6.89	7.32	7.85	8.32	-	-	-	1.64
4b [d]	7.57	-	7.11	6.88	7.23	7.28	7.71	5.17	-	-	1.62
4c [e]	7.64	6.90	-	6.82	7.22	7.24	7.66	5.14	-	-	1.63
5b [f]	7.59	-	7.10	6.89	7.15	7.12	7.58	2.43	-	-	1.63
5c [g]	7.63	6.88	-	6.82	7.12	7.08	7.51	2.39	-	-	1.62
5d	7.20	-	6.70	6.83	7.12	7.12	7.45	2.39	-	-	1.60
5e [h]	-	6.28	-	6.43	7.15	7.07	8.17	2.39	-	-	1.60
5f [i]	-	6.29	-	6.43	7.14	7.07	8.16	2.38	-	-	1.59

[a] Isopropyl signals at 2.95 and 1.30 ppm. [b] Isopropyl signals at 2.90 and 1.27 ppm. [c] Methyl signal at 2.66 ppm and isopropyl signals at 2.95 and 1.30 ppm. [d] i-Butyl signals at 2.28, 2.16 and 0.99 ppm; and isopropyl signals at 2.94 and 1.30 ppm. [e] i-Butyl signals at 2.26, 2.15 and 0.97 ppm; and isopropyl signals at 2.88 and 1.26 ppm. [f] Isopropyl signals at 2.95 and 1.31 ppm. [g] Isopropyl signals at 2.88 and 1.26 ppm. [h] Methyl signal at 2.26 ppm.in-Pentyl signals at 2.50, 1.61, 1.33, 1.31, 0.88 ppm.

Table 3. ^{13}C-NMR chemical shifts (in ppm) for compounds of series **1** to **5** determined at 100 MHz in $CDCl_3$. The assignments were made with 2D NMR spectroscopy, COSY, HMQC and HMBC experiments.

Compd	C-1	C-2	C-3	C-4	C-4a	C-6	C-6a	C-7	C-8	C-9	C-10	C-10a	C-10b	C-1′	2-OCH_3	6,6-CH_3/6-CH_3
1a	108.0	154.6	115.5	118.8	146.9	77.4	139.5	123.7	126.8	140.4	121.0	129.1	123.0	65.3	56.0	27.5
2b [a]	121.1	142.5	128.6	118.1	150.9	77.4	146.0	124.2	129.5	135.9	123.2	130.3	121.0	192.2	-	27.5
2c [b]	123.1	120.5	152.2	115.9	152.8	77.7	145.4	124.2	129.0	136.0	123.2	130.2	118.9	192.1	-	27.6
2d	108.0	155.0	116.7	118.8	147.5	73.6	142.5	125.1	129.8	136.4	123.1	130.8	122.1	192.1	56.0	19.9
2e	108.0	155.1	116.7	118.9	147.5	73.6	142.6	125.1	129.8	136.4	123.1	130.8	122.1	192.1	56.0	19.9
3b [c]	121.1	142.4	128.2	118.0	150.9	77.4	144.6	123.7	128.0	136.6	122.0	129.7	121.3	198.0	-	27.5
4b [d]	120.8	142.0	127.8	117.9	150.9	77.4	139.7	123.7	127.7	135.6	122.1	129.4	121.7	66.0	-	27.7
4c [e]	122.8	120.1	151.4	115.8	152.9	77.6	139.2	123.6	127.4	135.6	121.9	129.3	119.7	66.0	-	27.8
5b [f]	120.7	141.9	127.4	117.8	151.0	77.4	137.1	123.3	128.6	137.2	122.8	127.7	122.1	21.5	-	27.8
5c [g]	122.7	119.9	150.9	115.8	152.9	77.6	136.5	123.2	128.3	137.2	122.6	128.7	120.1	64.8	-	27.9
5d	109.5	150.1	116.3	118.9	146.9	77.4	137.4	123.3	129.1	137.3	123.1	128.4	123.5	21.4	-	27.6
5e [h]	153.2	110.7	139.5	111.6	154.8	77.4	137.0	122.8	127.7	137.0	126.6	127.6	108.7	21.7	-	27.2
5f [i]	153.2	110.0	144.7	110.9	154.8	77.4	137.0	122.8	127.7	127.7	126.5	137.0	108.8	21.7	-	27.2

[a] Isopropyl signals at 33.9 and 24.4 ppm. [b] Isopropyl signals at 34.2 and 23.9 ppm. [c] Methyl signal at 26.9 ppm and isopropyl signals at 33.9 and 24.4 ppm. [d] 3-Methylbutanoate signals at 173.1, 43.6, 25.9 and 22.6 ppm and isopropyl signals at 33.8 and 24.4 ppm. [e] 3-Methylbutanoate signals at 173.1, 43.6, 25.9 and 22.6 ppm and isopropyl signals at 34.1 and 23.9 ppm. [f] Isopropyl signals at 33.9 and 24.4 ppm. [g] Isopropyl signals at 34.1 and 24.0 ppm. [h] Methyl signal at 21.4 ppm. [i] n-Pentyl signals at 35.8, 31.6, 30.6, 22.7 and 14.2 ppm.

2.2. Selected functionalities

The natural products pulchrol (**1a**) and pulchral (**2a**) have been studied in the past and both of them were active against *Trypanosoma* and *Leishmania* parasites [44]. Pulchrol (**1a**) was moderately active against *L. braziliensis* and *L. amazonensis* promastigotes (IC_{50} 59.2 μM and IC_{50} 77.7 μM respectively), while was shown to possess a potent toxicity toward *T. cruzi* epimastigotes (IC_{50} 18.5 μM), comparable to that of the drug Benznidazole (19.2 μM). Meanwhile, pulchral (**2a**), had activity toward all the three parasites (*T. cruzi*, IC_{50} 24.2 μM; *L. braziliensis*, IC_{50} 24.2 μM; *L. amazonensis*, IC_{50} 29.8 μM) [44, 45].

In previous investigations, we studied the effect that individual transformations in the A-, B-, and C-rings have on the activity toward *T. cruzi*, *L. braziliensis* and *L. amazonensis* [44, 45]. Initially, we reported the effect of modifications at position 1′ in the A-ring, and preliminarily concluded that the benzyl alcohol functionality was important for pulchrol's antiparasitic activity, possibly acting as a hydrogen bond acceptor. It was also observed that 1′-carbonyl analogues were equipotent toward *T. cruzi* compared to pulchrol, while they were more potent toward *L. braziliensis* and *L. amazonensis*. In contrast, the 9-methyl analogue was reported to possess a considerably less activity than pulchrol against all parasites. Finally, the ester analogues showed to be, in general, more potent than pulchrol, with longer and branched alkyl substituents showing considerable improvements [44]. The effects that modifications in the B- and C- rings have on the antiparasitic activity were

also investigated, and were mainly focused on the effects that variations in the lipophilicity may have in the antiparasitic activity. The 6-monoalkyl (methyl and ethyl) derivatives, as pure enantiomers, were less potent compared to pulchrol, and a preference for 6,6-dialkyl analogues was established. Alkyl substituents in the C-ring were shown to be beneficial for the antiparasitic activity, most notably longer and branched alkyl substituents at positions 2 and 3 increased the potency considerably [45].

In this study, we analyse the effect that two or three transformations in the different rings of the pulchrol scaffold may have on the antiparasitic activity. Most of the analogues have transformations in the A- and C- rings, whereas just a pair have the A- and B-rings modified. The 1′-aldehyde, 3-methyl butanoic acid ester and 9-methyl functionalities in the A-ring were combined with isopropyl substituents at C-2 and C-3 in the C-ring (**2b** and **2c**; **4b** and **4c**; and **5b** and **5c** respectively), to evaluate the effect of an increase in the lipophilicity. An analogue with the 1′-methyl ketone functionality in the A-ring and an isopropyl substituent at position 2 was also prepared (**3b**) to determine if any differences would arise with respect to the corresponding 1′-aldehyde analogue (**2b**). The 9-methyl functionality was also combined with an hydroxyl substituent at C-2 in the C-ring (**5d**), and the natural compound cannabinol (**5f**) and its analogue **5e** were prepared, both of them containing a 9-methyl substituent in the A-ring, an hydroxyl group at C-1 and an alkyl group at C-3 in the C-ring; cannabinol (**5f**) with a *n*-pentyl substituent and **5e** with a methyl substituent at C-3. Finally, the 1′-aldehyde functionality was combined with the 6-monomethyl substituent in the B-ring, as a pair of enantiomers (**2d** and **2e**), to evaluate whether the carbonyl group helps improving their activity or hamper it compared with the already reported benzyl alcohol enantiomers **1d** and **1e** [45].

2.3. Antiparasitic activities towards Trypanosoma cruzi epimastigotes.

It has previously been reported that the transformation of the benzyl alcohol functionality in pulchrol to a 1′-carbonyl group was not beneficial for the antiparasitic activity toward *T. cruzi* [44], while the replacement of the methoxy functionality (in **1a**) for an isopropyl group in positions 2 and 3 in the C-ring was shown to improve the IC_{50} values for this parasite (**1b**, IC_{50} = 12.4 μM and **1c**, IC_{50} = 14.2 μM respectively) [45]. Analogues combining the aldehyde functionality in the A-ring with an isopropyl substituent at positions 2 or 3 in the C-ring were prepared and found to be considerably active (**2b,** IC_{50} = 10.7 μM; **2c,** IC_{50} = 7.1 μM). The methyl ketone **3b**, substituted also with an isopropyl group at C-2, was actually the most potent compound toward *T. cruzi* (IC_{50} = 3.4 μM) in this study.

Analogues **4b** and **4c** substituted with isopropyl groups at C-2 and C-3, respectively, and combined with a 3-methylbutanoic acid ester in the A-ring, were less potent against *T. cruzi* (**4b**, IC_{50} = 10.9 μM; **4c**, IC_{50} = 13.6 μM) than the 2-methoxy ester (**4a**, IC_{50} = 4.2 μM). Among the analogues from the **5**-series (which contain a 9-methyl substituent in the A-ring), analogue **5d** with a hydroxyl functionality at C-2 showed comparable activity (IC_{50} = 54.8 μM) to **5a** (with a methoxy group at C-2). While analogues **5b** and **5c**, with isopropyl substituents at positions 2 and 3 (IC_{50} = 23.7 μM and IC_{50} = 50.3 μM, respectively) were less toxic than pulchrol (**1a**, IC_{50} = 18.5 μM)**.** However**,** cannabinol (**5f**) and its analogue **5e**, with also alkyl substituent in the C-ring (position 3), but an additional hydroxyl functionality at C-1, were the most potent compounds from the **5**-series (**5f**, IC_{50} = 7.4 μM; **5e**, IC_{50} = 5.9 μM) .

Finally, the aldehyde enantiomers **2d** and **2e** (IC_{50} = 125.8 μM and IC_{50} = 170.3 μM respectively), substituted with a single methyl group at position 6 in the B-ring, possess considerably lower antiparasitic activity compared to pulchrol (**1a**, IC_{50} = 18.5 μM**)** and their corresponding benzyl enantiomers (**1d**, IC_{50} = 35.9 μM and **1e**, IC_{50} = 67.1 μM).

2.4. Antiparasitic activities towards Leishmania braziliensis promastigotes

The transformation of pulchrol's benzyl alcohol to a 1'-carbonyl functionality showed to considerably increase the activity toward *L. braziliensis* (**2a**, IC_{50} = 24.2 μM; and **3a**, IC_{50} = 28.3 μM) [44]. Likewise, isopropyl substituents in the C-ring (**1b** and **1c**) also increased the potency (**1b**, IC_{50} = 18.1 μM; and **1c**, IC_{50} = 19.1 μM) compared to pulchrol (**1a**) [45]. Here, aldehydes **2b** and **2c** (with isopropyl substituents at C-2 and C-3 respectively**)** were more toxic toward *L. braziliensis* (**2b**, IC_{50} = 12.1 μM; and **2c**, IC_{50} = 17.8 μM) than their benzyl alcohol precursors (**1b** and **1c**). While the 2-isopropyl ketone **3b** was the most potent compound (IC_{50} = 8.8 μM).

The 2- and 3-isopropyl esters **4b** and **4c** were less active toward *L. braziliensis* (**4b**, IC_{50} = 272.9 μM; and **4c**, IC_{50} = 63.3 μM). A 9-methyl substituent in the A-ring has previously been shown to be unfavourable for the activity (**5a**, IC_{50} = 69.6 μM) [44]. Here, the 9-methyl/2-isopropyl analogue **5b** and the 9-methyl/2-hydroxy analogue **5d** were more potent toward *L. braziliensis* (**5b**, IC_{50} = 49.2 μM; and **5d**, IC_{50} = 30.4 μM). While, the 9-methyl/3-isopropyl analogue **5c** was essentially inactive (IC_{50} = 312 μM). Analogue **5e** and cannabinol (**5f**) were found to possess higher activity (IC_{50} = 15.7 μM and IC_{50} = 10.3 μM, respectively) than **5a** and pulchrol (**1a**). The aldehyde enantiomers **2d** and **2e** were less potent (IC_{50} = 70.8 μM and IC_{50} = 118 μM, respectively) than pulchrol (**1a**), but more potent than their corresponding benzyl alcohol enantiomers **1d** and **1e** (IC_{50} = 156.1 μM and IC_{50} = 128.8 μM, respectively) [45].

2.5. Antiparasitic activities towards Leishmania amazonensis promastigotes

The combination of the 9-aldehyde functionality with isopropyl substituents at positions 2 and 3 (**2b** and **2c**, respectively) was beneficial for the antiparasitic activity, and the highest activities were shown by the aldehyde **2b** (IC_{50} = 11.4 μM), and the methyl ketone **3b** (IC_{50} = 9.5 μM). All ester analogues (**4a** to **4b**) were more toxic than pulchrol toward *L. amazonensis*, but **4b** and **4c** were less potent than the 2-methoxy ester **4a**.

Most of the 9-methyl analogues (**5b**, **5d**, **5e**, and **5f**) were more potent than pulchrol (**1a**, IC_{50} = 77.7 μM), while the 9-methyl/3-isopropyl analogue **5c** was inactive (IC_{50} = 236.5 μM). The most potent compounds in the **5**-series were cannabinol (**5f**, IC_{50} = 14.2 μM) and its analogue **5e** (IC_{50} = 21.2 μM). The enantiomers **2d** (IC_{50} = 44.0 μM) and **2e** (IC_{50} = 80.6 μM) were less potent than the corresponding 6,6-dimethyl aldehyde **2a** (pulchral, IC_{50} = 29.8 μM) [44].

3. Discussion

For *T. cruzi* and *L. braziliensis*, the aldehyde **2b** and **2c** (with isopropyl groups at positions 2 and 3, respectively) were more active than the corresponding benzyl alcohols **1b** and **1c** [45], probably due to a change in orientation generated by the combination of those substituents, which may enhance hydrophobic interactions. Moreover, an analogue with a methyl ketone in the A-ring and an isopropyl group at C-2 (**3b**) was the most potent compound for all parasites. Analogue **3b** was 6 times more potent than the positive control for *T. cruzi* (Benznidazole) and comparable to the positive control for the *Leishmania* species (Miltefosine), indicating that interactions involving the methyl substituent in the ketone may contribute to the activity.

In contrast, 2- and 3-isopropyl analogues of the **4**-series (combined with a 3-methylbutanoic acid ester) were less potent than the corresponding 2-methoxy ester **4a** for all parasites. Particularly, analogue **4b** showed to be inactive toward *L. braziliensis*, indicating a possible limitation in the volume of the lipophilic pocket where the 3-alkyl substituents interact.

Analogues substituted with isopropyl groups at C-2 and C-3 as well as with a 9-methyl substituent in the A-ring (**5b** and **5c**, respectively) were less potent than pulchrol toward *T. cruzi***.** Whereas the 9-methyl/2-isopropyl analogue **5b** was, in contrast, more potent toward the *Leishmania* species. The 9-methyl/3-isopropyl analogue **5c**, not only

showed a decrease in activity compared to pulchrol, as observed with *T. cruzi*, but was essentially inactive toward the *Leishmania* species, suggesting again that there is a limit in the volume around positions 2 and 3 in the binding site for the *Leishmania* parasites.

The combination of a 9-methyl substituent in the A-ring with a methoxy or hydroxy group at C-2 (**5a** and **5d**, respectively) decreased the activity toward *T. cruzi* compared to pulchrol (**1a**). Possibly those analogues (**5a** and **5d**), interact with the binding site in a rotated position in which the methoxy group in **5a** and the hydroxy group in **5d** act as hydrogen bond acceptors, where usually pulchrol's benzyl alcohol interacts. However, this interaction is weaker than that of the benzyl alcohol in pulchrol for *T. cruzi*, while for the *Leishmania* parasites it seems to be stronger.

Despite the unfavourable outcome observed when a 9-methyl substituent is combined with alkyl groups at positions 2 or 3 in the C-ring, analogues **5e** and **5f** (with a methyl or n-pentyl substituent at C-3) were more potent than pulchrol for all parasites. However, they possessed an additional hydroxy group at C-1 in the C-ring, which may have important interactions with the binding site. The effect the length of the alkyl substituent has on the antiparasitic activity seems to differ between parasites. The longer chain in cannabinol (**5f**) seems to benefit the activity toward the *Leishmania* species, while the methyl group at C-3 is better for the activity toward *T. cruzi*.

The aldehyde enantiomers combined with a methyl substituent at C-6 in the B-ring (as in analogues **2d** and **2e**) showed less potency than their corresponding benzyl alcohol enantiomers (**1d** and **1e**) toward *T. cruzi*. In contrast, analogues **2d** and **2e** were more potent toward *L. braziliensis* than **1d** and **1e**. The results obtained for *L. amazonensis*, showed enantiomer **2d** to be more potent than corresponding enantiomer **1d**, while enantiomer **2e** was less potent than **1e**. Possible changes in orientation generated by the presence of just one alkyl substituent in the B-ring may be responsible for the differences in activity between the aldehyde enantiomers and the benzyl alcohol enantiomers.

4. Materials and Methods

4.1. General

^{1}H NMR spectra (400 MHz) and ^{13}C NMR spectra (100 MHz) were recorded with a Bruker Avance II (Bruker Biospin AG, Industriestrasse 26, 8117 Fällanden, Switzerland) in $CDCl_3$. The individual 1D signals were assigned using 2D NMR experiments (COSY, HSQC, HMBC). The chemical shifts are given in ppm with the solvent signal as reference (7.27 ppm for ^{1}H and 77.0 for ^{13}C). Infrared spectra were recorded with a Bruker Alpha-P FT/IR instrument (Bruker Biospin AG, Industriestrasse 26, 8117 Fällanden, Switzerland) with a Diamond ATR sensor as films, and the intensities are given as vw (very weak), w (weak), m (medium), s (strong) and vs (very strong). High resolution mass spectra (HRMS) were recorded with a Waters XEVO-G2 QTOF equipment (Waters Corp, Milford, Worcester County, Massachusetts, United States), with electrospray ionization (ESI). Synthetic reactions were monitored by TLC using alumina plates coated with silica gel and visualized using either UV light and/or spraying/heating with vanillin/H_2SO_4. Flash chromatography was performed with silica gel (35-70 μm, 60 Å). THF was distilled from sodium, acetonitrile was distilled from CaH_2 and other reaction solvents were dried with Al_2O_3. Commercially available compounds were obtained from Aldrich.

4.2. Synthetic Procedures

Methyl 4-(hydroxymethyl)-2-iodobenzoate (intermediate in the synthesis of **1a** – **1e**), BH_3-THF (1 M, 47.1 mL, 47.1 mmol) was slowly added to a stirred solution of 1-methyl-2-iodoterephthalate (4.8 g, 15.7 mmol) in dry THF (250 mL) at 0 °C. After 30 h, saturated aqueous $NaHCO_3/H_2O$ was added, and the aqueous phase was extracted with ethyl acetate

(3×250 mL) before drying (Na_2SO_4) and removal of solvent under reduced pressure. Purification by column chromatography (SiO_2, 4:6 heptane/ethyl acetate) gave (4.06 g, 89%) of the pure product as yellow crystals, identical to that previously reported [42].

Methyl 4-(((tert-butyldiphenylsilyl)oxy)methyl)-2-iodobenzoate (intermediate in the synthesis of **1a** – **1e**), TBDPSCl (4.3 mL, 16.7 mmol) was added to a stirred solution of methyl 4-(hydroxymethyl)-2-iodobenzoate (4.06 g, 13.9 mmol) in pyridine (80 mL) at rt. After 24 h, saturated aqueous NH_4Cl/H_2O was added and the aqueous phase was extracted with diethyl ether (3×200 mL), then the organic phase was washed with brine (2×500 mL) before drying (Na_2SO_4) and removal of solvent under reduced pressure. Purification by column chromatography (SiO_2, 20:2 heptane/ethyl acetate) gave (4.2 g, 57%) of the pure product as white crystals, identical to that previously reported [42].

General procedure for Suzuki coupling (intermediates in the synthesis of **1a** – **1e**), corresponding boronic acid (1.5 equiv), K_2CO_3 (5 equiv) and Tetrakis(triphenylphosphine)palladium(0) (0.17 equiv), were added to a stirred solution of methyl 4-(((tert-butyldiphenylsilyl)oxy)methyl)-2-iodobenzoate (1 equiv) dissolved in 4:1 DME/water (15 mL), the mixture (contained in a microtube) was degasified under vaccum/N_2 at -78 °C five times. The microwave reaction conditions were 100 °C, high pressure, and 10 s of pre-stirring. After 30 to 60 min in the microwave reactor, the mixture was filtered through a plug of celite and washed with ethyl acetate (250 mL) before drying (Na_2SO_4) and removal of solvent under reduced pressure. Purification by column chromatography (SiO_2, 20:3 heptane/ethyl acetate) gave the pure products.

Methyl 5-(((tert-butyldiphenylsilyl)oxy)methyl)-2′,5′-dimethoxy-[1,1′-biphenyl]-2-carboxylate (intermediate in the synthesis of **1a**), the pure product was obtained as an orange wax (yield 94%) identical to that previously reported [42].

Methyl 5-(((tert-butyldiphenylsilyl)oxy)methyl)-5′-isopropyl-2′-methoxy-[1,1′-biphenyl]-2-carboxylate (intermediate in the synthesis of **1b**), the pure product was obtained as colorless wax (yield 97%) identical to that previously reported [45].

Methyl 5-(((tert-butyldiphenylsilyl)oxy)methyl)-2′-methoxy-4′-isopropyl-[1,1′-biphenyl]-2-carboxylate (intermediate in the synthesis of **1c**), the pure product was obtained as a yellowish wax (yield 38%) identical to that previously reported [45].

General procedure for organolithic addition (intermediate in the synthesis of **1a** – **1e**), corresponding organo-lithic reagent (4 equiv) was added to a stirred solution of the suzuki coupling product (1 equiv) in dry THF (70 mL), at 0 or -78 °C, depending on the organolithic reagent. After 12 h, saturated aqueous NH_4Cl/H_2O was added, and the aqueous phase was extracted with ethyl acetate (3×100 mL) before drying (Na_2SO_4) and removal of solvent under reduced pressure. Purification by column chromatography (SiO_2, 20:4 heptane/ethyl acetate 20: 4) gave the pure product.

2-(5-(((tert-butyldiphenylsilyl)oxy)methyl)-2′,5′-dimethoxy-[1,1′-biphenyl]-2-yl)propan-2-ol (Intermediate in the synthesis of **1a**), the pure product was obtained as a yellowish wax (yield 65.2%) identical to that previously reported [42].

2-(5-(((tert-butyldiphenylsilyl)oxy)methyl)-5′-isopropyl-2′-methoxy-[1,1′-biphenyl]-2-yl)propan-2-ol (Intermediate in the synthesis of **1b**), the pure product was obtained as a transparent wax (yield 78.5%) identical to that previously reported [45].

2-(5-(((tert-butyldiphenylsilyl)oxy)methyl)-2′-methoxy-4′-isopropyl-[1,1′-biphenyl]-2-yl)propan-2-ol (Intermediate in the synthesis of **1c**), the pure product was obtained as a transparent wax (yield 64%) identical to that previously reported [45].

General procedure to prepare compounds **1a** – **1c**, HI (55%, 10 equiv) was added to a stirred solution of the corresponding starting material in acetonitrile (25 ml), at rt. After 30 min, saturated aqueous $Na_2S_2O_3$ (25 mL) was added, and the aqueous layer was extracted with ethyl acetate (3 × 50 mL), before drying (Na_2SO_4) and removal of solvent under reduced pressure. TBAF (1 M, 1.1 equiv) was added to the crude product in THF (150 mL). After 3 h, aqueous saturated $NaHCO_3$ (50 mL) was added, and the aqueous layer

was extracted with ethyl acetate (3 × 50 mL), before drying (Na_2SO_4) and removal of solvent under reduced pressure. Purification by column chromatography (SiO_2, 1:1 heptane/ethyl acetate) gave the pure product.

(2-methoxy-6,6-dimethyl-6H-benzo[c]chromen-9-yl)methanol (**1a**), the pure product was obtained as a yellowish wax (yield 77%) identical to that previously reported [42].

(2-isopropyl-6,6-dimethyl-6H-benzo[c]chromen-9-yl)methanol (**1b**), the pure product was obtained as a transparent wax (yield 88%) identical to that previously reported [45].

(3-isopropyl-6,6-dimethyl-6H-benzo[c]chromen-9-yl)methanol (**1c**), the pure product was obtained as a transparent wax (yield 85%) identical to that previously reported [45].

5-(((tert-butyldiphenylsilyl)oxy)methyl)-2',5'-dimethoxy-[1,1'-biphenyl]-2-carbaldehyde (Intermediate in the synthesis of **1d** and **1e**), Morpholine (0.2 mL, 2.2 mmol) was added to a solution of DIBALH (1 M, 1.1 mL, 1.1 mmol) in dry THF (30 mL) at 0 °C. After 3 h, methyl 5-(((*tert*-butyldiphenylsilyl)oxy)methyl)-2',5'-dimethoxy-[1,1'-biphenyl]-2-carboxylate (600 mg, 1.1 mmol) in dry THF (20 mL) was added, 10 min later, DIBALH (1 M, 1.1 mL, 1.1 mmol) was added again at 0 °C. After 4 h, aqueous HCL (1 N, 20 mL) was added, and the aqueous phase was extracted with diethyl ether (3 × 50 mL) before drying (Na_2SO_4) and removal of solvent under reduced pressure. Purification by column chromatography (SiO_2, 20:4 heptane/ethyl acetate) gave the pure product as a yellowish wax (89.1 mg, 16%) identical to that previously reported [45].

General procedure to prepare compounds **1d** *and* **1e**, MeLi (3 M, 2 equiv) was added to 5-(((tert-butyldiphenylsilyl)oxy)methyl)-2',5'-dimethoxy-[1,1'-biphenyl]-2-carbaldehyde (1 equiv) in dry THF (5 mL) at 0 °C. After 6 h, saturated aqueous NH_4Cl/H_2O was added, and the aqueous phase was extracted with ethyl acetate (3 × 20 mL) before drying (Na_2SO_4) and removal of solvent under reduced pressure. PBr_3 (0.34 equiv) was added to the crude product (1 equiv) in dichloromethane (10 mL) at rt. After 2 h, LiI (3 equiv) was added at rt. After 12 h, saturated aqueous $Na_2S_2O_3/H_2O$ was added, and the aqueous phase was extracted with ethyl acetate (3 × 20 mL) before drying (Na_2SO_4) and removal of solvent under reduced pressure. TBAF (2 equiv) was added to the crude product in THF (25 mL) at rt, after 5 h, saturated aqueous $NaHCO_3/H_2O$ was added, and the aqueous phase was extracted with ethyl acetate (3×25 mL) before drying (Na_2SO_4) and removal of solvent under reduced pressure. Purification by column chromatography (SiO_2, 1:1 heptane/ethyl acetate) and the enantiomers were separated using a semipreparative HPLC (Chiralpack B column, 96:4 hexane/isopropanol).

(2-methoxy-6-methyl-6H-benzo[c]chromen-9-yl)methanol (**1d**), the pure product was obtained as a yellowish wax (yield 3%), αD20 -17.8 identical to that previously reported [45].

(2-methoxy-6-methyl-6H-benzo[c]chromen-9-yl)methanol (**1e**), the pure product was obtained as a yellowish wax (yield 3%), αD20 +23.8 ° identical to that previously reported [45].

General procedure to obtain compounds **2b** -**2e**, Dess Martin periodinane 15% (2 equiv) was added to a stirred solution of corresponding starting material (1 equiv) in CH_2Cl_2 at rt. After five hours, saturated aqueous $Na_2S_2O_3/H_2O$ was added and the aqueous phase was extracted three times with CH_2Cl_2 before drying (Na_2SO_4) and removal of solvent under reduced pressure. Purification by column chromatography (SiO_2, 20:1 CH_2Cl_2/methanol).

2-isopropyl-6,6-dimethyl-6H-benzo[c]chromene-9-carbaldehyde (**2b**), the pure product was obtained as a transparent wax (85.7 mg, yield 88%). ^{1}H NMR and ^{13}C NMR data in Table 2 and Table 3, respectively. HRMS-ESI+ (*m*/*z*): $[M + Na]^+$ calcd for $C_{19}H_{20}O_2$, 303.1361; found, 303.1355.

3-isopropyl-6,6-dimethyl-6H-benzo[c]chromene-9-carbaldehyde (**2c**), the pure product was obtained as a transparent wax (15.3 mg, yield 77%). %). ^{1}H NMR and ^{13}C NMR data in Table 2 and Table 3, respectively. HRMS-ESI+ (*m*/*z*): $[M + Na]^+$ calcd for $C_{19}H_{20}O_2$, 303.1361; found, 303.1357.

2-methoxy-6-methyl-6H-benzo[c]chromene-9-carbaldehyde (**2d**), the pure product was obtained as a yellowish wax (5.4 mg, yield 96%). %). ^{1}H NMR and ^{13}C NMR data in Table 2

and Table 3, respectively. HRMS-ESI+ (*m*/z): $[M + Na]^+$ calcd for $C_{16}H_{14}O_5$, 309.0738; found, 309.0739 (+2O due to oxidation).

2-methoxy-6-methyl-6H-benzo[c]chromene-9-carbaldehyde (**2e**), the pure product was obtained as a yellowish wax (6.7 mg, yield 95%). %). ^{1}H NMR and ^{13}C NMR data in Table 2 and Table 3, respectively. HRMS-ESI+ (*m*/z): $[M + Na]^+$ calcd for $C_{16}H_{14}O_5$, 309.0739; found, 309.0739 (+2O due to oxidation).

1-(2-isopropyl-6,6-dimethyl-6H-benzo[c]chromen-9-yl)ethan-1-one (**3b**), MeMgI (3 M, 0.24 mL, 0.7 mmol) was added to **2b** (65 mg, 0.23 mol) in dry ethyl ether (5 mL), at 0 °C. After 20 h, saturated aqueous NH_4Cl/H_2O was added, and the aqueous phase was extracted with diethyl ether (3×5 mL). The organic product was washed with brine once before drying (Na_2SO_4) and removal of solvent under reduced pressure. Celite (250 mg) and PCC (63 mg, 0.25 mmol) were added to the crude product in dry CH_2Cl_2 (5 mL) under nitrogen, at rt. After 12 h diethyl ether (10 mL) was added and the mixture was filtered over a plug of silica gel and washed with ethyl acetate (50 mL) before removal of solvent under reduce pressure. Purification by column chromatography (SiO_2, 20:4 hept/ethyl acetate) gave 30.0 mg, 44% as a transparent wax. %). ^{1}H NMR and ^{13}C NMR data in Table 2 and Table 3, respectively. HRMS-ESI+ (*m*/z): $[M + Na]^+$ calcd for $C_{20}H_{22}O_2$, 317.1514; found, 317.1517.

General procedure to obtain compounds **4b** – **4c**, isovaleric anhydride (1.5 equiv), DMAP (1.2 equiv), and Et_3N (1.5 equiv) were added to a stirred solution of appropriate starting material (1 equiv) in CH_2Cl_2 (25 ml) at rt. After three hours, saturated aqueous NH_4Cl/H_2O was added and the aqueous phase was extracted with CH_2Cl_2 (3×25 mL) before drying (Na_2SO_4) and removal of solvent under reduced pressure. Purification by column chromatography (SiO2, 20:4 heptane/ethyl acetate) gave the desired products.

(2-isopropyl-6,6-dimethyl-6H-benzo[c]chromen-9-yl)methyl 3-methylbutanoate (**4b**), the pure product was obtained as a transparent wax (64.9, yield 53%). %). ^{1}H NMR and ^{13}C NMR data in Table 2 and Table 3, respectively. HRMS-ESI+ (*m*/z): $[M + Na]^+$ calcd for $C_{24}H_{30}O_3$, 389.2093; found, 389.2099.

(3-isopropyl-6,6-dimethyl-6H-benzo[c]chromen-9-yl)methyl 3-methylbutanoate (**4c**), the pure product was obtained as a transparent wax (15.2, yield 59%). %). ^{1}H NMR and ^{13}C NMR data in Table 2 and Table 3, respectively. HRMS-ESI+ (*m*/z): $[M + Na]^+$ calcd for $C_{24}H_{30}O_3$, 389.2093; found, 389.2091.

General procedure to obtain compounds **5a** – **5c**, Et_3SiH (5 equiv) and $PdCl_2$ (2 equiv) were added to a stirred solution of corresponding starting material (1 equiv) in EtOH. After 3h, ethyl acetate was added and the mixture was filtered through a plug of celite and washed with ethyl acetate before, drying (Na_2SO_4) and removal of solvent under reduced pressure. Purification by column chromatography (SiO_2, 20:1 heptane/ethyl acetate).

2-Methoxy-6,6,9-trimethyl-6H-benzo[c]chromene (**5a**), the pure product was obtained as a yellowish wax (yield 92%) identical to that previously reported [44].

2-isopropyl-6,6,9-trimethyl-6H-benzo[c]chromene (**5b**), the pure product was obtained as a transparent wax (105 mg, yield 89%). %). ^{1}H NMR and ^{13}C NMR data in Table 2 and Table 3, respectively HRMS-ESI+ (*m*/z): $[M + Na]^+$ calcd for $C_{19}H_{22}O$, 289.1568; found, 289.1563.

3-isopropyl-6,6,9-trimethyl-6H-benzo[c]chromene (**5c**), the pure product was obtained as a transparent wax (16 mg, yield 85%). %). ^{1}H NMR and ^{13}C NMR data in Table 2 and Table 3, respectively. HRMS-ESI+ (*m*/z): $[M + Na]^+$ calcd for $C_{19}H_{22}O$, 289.1568; found, 289.1565.

6,6,9-trimethyl-6H-benzo[c]chromen-2-ol (**5d**), sodium ethanethiolate (132 mg, 1.57 mmol2) was added to a stirred solution of **5a** (0.157 mmol) in DMF (4 mL), and reacted in a microwave reactor at 160 °C. After one hour, saturated aqueous NH_4Cl/H_2O was added and the aqueous phase was extracted with ethyl acetate (3 × 100 mL) before drying (Na_2SO_4) and removal of solvent under reduced pressure. Purification by column chromatography (SiO_2, 20:4 heptane/ethyl acetate) gave (27 mg, 72%) of the pure product as an orange wax. %). ^{1}H NMR and ^{13}C NMR data in Table 2 and Table 3, respectively. HRMS-ESI+ (*m*/z): $[M + H]^+$ calcd for $C_{16}H_{17}O_2$, 241.1229; found, 241.1231.

General procedure to obtain compounds **5e** *and* **5f**, citral (1 equiv) and *n*-butylamine (1 equiv) were added to the corresponding resorcinol analogue (1 equiv) in toluene at 110 °C. After 12 hours, DOWEX 50WX8 (200 mg) was added to the stirred mixture at rt. After 10 min the mixture was filtered over a plug of celite. Iodine (2 equiv) was added to the filtrate at 110 °C. After 3 h, saturated aqueous $Na_2S_2O_3/H_2O$ was added and the aqueous phase was extracted three times with EtOAc before drying (Na_2SO_4) and removal of solvent under reduced pressure. Purification by column chromatography (SiO_2, 100:5 heptane/ethyl acetate).

3,6,6,9-tetramethyl-6H-benzo[c]chromen-1-ol (**5e**), the pure product was obtained as a orange wax (26 mg, yield 18%). %). ^{1}H NMR and ^{13}C NMR data in Table 2 and Table 3, respectively. HRMS-ESI+ (*m*/*z*): $[M + Na]^+$ calcd for $C_{17}H_{18}O_2$, 277.1204; found, 277.1201.

6,6,9-trimethyl-3-pentyl-6H-benzo[c]chromen-1-ol (**5f**), the pure product was obtained as a brownish wax (6.7 mg, yield 4%). %). ^{1}H NMR and ^{13}C NMR data in Table 2 and Table 3, respectively. HRMS-ESI+ (*m*/*z*): $[M + Na]^+$ calcd for $C_{21}H_{26}O_2$, 333.1830; found, 333.1825.

4.3. Biological Assays

4.3.1. Evaluations against *Leishmania* parasites

Promastigotes of Leishmania-Leishmania: *L. amazonensis*, Clone 1, NHOM-BR-76-LTB-012 (Lma, donated by the Paul Sabatier Université, France) and Leishmania-Viannia: *L. braziliensis* M2904 C192 RJA (M2904, donated by Dr. Jorge Arévalo from Universidad Peruana Cayetano Heredia, Peru) [47]. All strains were cultured in Schneider's insect medium, (pH 6.2) supplemented with 10 % FBS and incubated at 26 °C. Medium changes were made every 72 h to maintain a viable parasitic population. Leishmanicidal activity was determined by correlation of parasite growth curves and the optical density (OD) values, according to Williams with some modifications [48]. Samples were dissolved in DMSO (maximum final concentration 1 %) at 10 mg/mL. Promastigotes in logarithmic phase of growth, at the concentration $3x10^6$ parasites/mL, were distributed (100 µL/well) in 96-well flat bottom microtiter plates. Samples with different concentrations (3.1-100 µg/mL) were added (100 µL). Miltefosine (3.1-100 µg/mL), was used as control drug [49]. Assays were performed in triplicates. The microwell plates were incubated for 72 h at 26 °C. After incubation, a solution of the tetrazolium salt, sodium-2,3-bis-[2-methoxy-4-nitro-5sulfophenyl]-2*H*-tetrazolium-5carboxanilide (XTT, 1 mg/mL) in Phosphate buffered saline (PBS, pH 7.0 at 37 °C) with the electron coupling agent phenazine methosulfate (PMS, 0.06 mg/mL) was added (50 µL/well), and incubated for 3 h at 26 °C. The optical density of each well was measured and the IC_{50} values calculated.

4.3.2. Evaluations against *Trypanosoma cruzi*

Cultures of *Trypanosoma cruzi* (epimastigotes, donated by the Parasitology Department of INLASA, Tc-INLASA), were maintained in medium LIT (pH 7.2), supplemented with 10 % FBS and incubated at 26 °C. Medium changes were made every 72 h to maintain a viable parasitic population. Trypanocidal activity was determined according to Muelas-Serrano with some modifications [50]. Samples were dissolved in DMSO (maximum final concentration 1 %) at 10 mg/mL. Epimastigotes in logarithmic phase of growth, at a concentration of $3x10^6$ parasites/mL, were distributed (100 µL/well) in 96-well flat bottom microtiter plates. Samples at different concentrations (3.1-100 µg/mL) were added (100 µL). Benznidazol (3.1-100 µg/ml) was used as the control drug. Assays were performed in triplicates. The microwell plates were incubated for 72 h at 26 °C. After incubation, a solution of XTT (1 mg/mL) in PBS (pH 7.0 at 37 °C) with PMS (0.06 mg/mL) was added (50 µL/well) and incubated for 4 h at 26 °C. The optical density of each well was measured and the IC_{50} values were calculated.

5. Conclusions

Twelve compounds with chemical transformations on the benzyl alcohol functionality in the A-ring, and either the C-ring or the B-ring were prepared and assayed toward *T. cruzi*, *L. braziliensis* and *L. amazonensis*. Pulchrol's binding sites for each parasite seemed to have similarities, but also differences in spite of belonging to the same family (Trypanosomatidae). The carbonyl/isopropyl combination was beneficial for the activity toward all parasites in most cases. However, 2-isopropyl analogues are better for *T. cruzi*, while 3-isopropyl analogues are better for the *Leishmania* parasites. A 1′-methyl ketone functionality along with a 2-isopropyl substituent was the most beneficial for all parasites. It appears this combination may improve the orientation enhancing hydrophobic interactions. A 3-methyl butanoic acid with 2- or 3-isopropyl substituents was not as beneficial as the corresponding 2-methoxy ester toward all parasites, moreover the 2-isopropyl derivative was inactive toward *L. braziliensis*, indicating that less space exists around C-2 in its binding site. The presence of at least one substituent with hydrogen bond capabilities is important for the activity. The most important positions where hydrogen bond interactions may occur are C-1′ and C-1. The 6-monomethyl enantiomers combined with a 1′-aldehyde may generate changes in the orientation, that either weakened or strengthen the interactions depending on the parasites.

Supplementary Materials: The following are available online at www.mdpi.com/xxx/s1, Figure S1: title, Table S1: title, Video S1: title. They contain 1D and 2D NMR spectra of all isolated compounds.

Author Contributions: P.T is a PhD student and has planned and carried out the synthesis of the reported compounds, and written the manuscript, E.S. has carried out the biological assays, supervised by A.G., M.D. has supervised the work of P.T.. at UMSS, S.M. has supervised the work of P.T.. in Lund, while O.S. has supervised the work of P.T. in Lund and compiled the manuscript. All authors have read and agreed to the published version of the manuscript.

Funding: This research was funded by the Swedish International Development Agency (SIDA), and a Ph.D. scholarships for P.T. from SIDA is gratefully acknowledge.

Institutional Review Board Statement: Not applicable, as the study did not involve humans or animals.

Informed Consent Statement: Not applicable, as the study did not involve humans or animals.

Data Availability Statement: All data are available in this publication and in the Supplementary Materials.

Conflicts of Interest: The authors declare no conflict of interest. The sponsors had no role in the design, execution, interpretation, or writing of the study.

References

1. Li, G.; Lou, H.-X. Strategies to diversify natural products for drug discovery. *Med. Res. Rev.* **2018,** *38* (4), 1255-1294.
2. Sertürner, F.W. Säure im opium. *J. Pharmacie.* **1805**, 13, 234.
3. Wani, M. C.; Taylor, H. L.; Wall, M. E.; Coggon, P.; McPhail, A. T. Plant antitumor agents. VI. Isolation and structure of taxol, a novel antileukemic and antitumor agent from *Taxus brevifolia*. *J. Am. Chem. Soc.* **1971,** *93* (9), 2325-2327.
4. Achan, J.; Talisuna, A. O.; Erhart, A.; Yeka, A.; Tibenderana, J. K.; Baliraine, F. N.; Rosenthal, P. J.; D'Alessandro, U. Quinine, an old anti-malarial drug in a modern world: role in the treatment of malaria. *Malar. J.* **2011,** *10* (1), 144.
5. Qinghaosu Antimalarial Coordinating Research Group. *Chin Med J. (Engl.).* **1979,** 92 (12), 811-816.
6. Rodrigues, T.; Reker, D.; Schneider, P.; Schneider, G. Counting on natural products for drug design. *Nat. Chem.* **2016,** *8* (6), 531-541.

7. Molyneux, D. H.; Savioli, L.; Engels, D. Neglected tropical diseases: progress towards addressing the chronic pandemic. *The Lancet* **2017,** *389* (10066), 312-325.
8. Gilbert, I. H. Drug discovery for neglected diseases: molecular target-based and phenotypic approaches. *J Med Chem.* **2013,** *56* (20), 7719-7726.
9. Weng, H.-B.; Chen, H.-X.; Wang, M.-W. Innovation in neglected tropical disease drug discovery and development. *Infect Dis Poverty*. **2018,** *7* (1), *67*.
10. Atanasov, A. G.; Waltenberger, B.; Pferschy-Wenzig, E.-M.; Linder, T.; Wawrosch, C.; Uhrin, P.; Temml, V.; Wang, L.; Schwaiger, S.; Heiss, E. H.; Rollinger, J. M.; Schuster, D.; Breuss, J. M.; Bochkov, V.; Mihovilovic, M. D.; Kopp, B.; Bauer, R.; Dirsch, V. M.; Stuppner, H. Discovery and resupply of pharmacologically active plant-derived natural products: A review. *Biotechnol. Adv.* **2015,** *33* (8), 1582-1614.
11. Moffat, J. G.; Vincent, F.; Lee, J. A.; Eder, J.; Prunotto, M. Opportunities and challenges in phenotypic drug discovery: an industry perspective. *Nat. Rev. Drug Discovery*. **2017,** 16 (8), 531-543.
12. Zheng, W.; Thorne, N.; McKew, J. C. Phenotypic screens as a renewed approach for drug discovery. *Drug Discovery Today*. **2013,** 18 (21), 1067-1073.
13. Al-Ali, H. The evolution of drug discovery: from phenotypes to targets, and back. *Med. Chem. Commun*. **2016,** 7 (5), 788-798.
14. Haasen, D.; Schopfer, U.; Antczak, C.; Guy, C.; Fuchs, F.; Selzer, P. How Phenotypic Screening Influenced Drug Discovery: Lessons from Five Years of Practice. *Assay Drug Dev. Technol*. **2017,** 15 (6), 239-246.
15. Campos-Ríos, M. G. REVISIÓN DEL GÉNERO Bourreria P. Browne (Boraginaceae) EN MÉXICO. *Polibotánica* **2005**, No.19, 39-103.
16. Erosa-Rejón, G. J.; Yam-Puc, A.; Chan-Bacab, M. J.; Giménez-Turbax, A.; Salamanca, E.; Peña-Rodríguez, L. M.; Sterner, O. Benzochromenes from the roots of *Bourreria pulchra*. *Phytochem. Lett.* **2010**, *3* (1), 9-12.
17. World Health Organization Home Page. Chagas disease (American tripanosomiasis). Retrieved from https://www.who.int/chagas/disease/en/ (accessed Dec 19, 2019).
18. World Health Organization Home Page. WHO Report on Global Surveillance of Epidemic-prone Infectious Diseases – Leishmaniasis. Retrieved from https://www.who.int/csr/resources/publications/CSR_ISR_2000_1leish/en/ (accessed Dec 19, 2019).
19. World Health Organization Homepage. Available online: https://www.who.int/neglected_diseases/diseases/en/ (accessed on 14 July 2020).
20. Jacobson, J.; Bush, S. Neglected Tropical Diseases, Neglected Communities, and Conflict: How Do We Leave No One Behind? *Trends in Parasitol*. **2018,** 34 (3), 175-177.
21. World Health Organisation Home Page. Second WHO report on neglected tropical diseases. Available online: https://www.who.int/neglected_diseases/9789241564540/en/ (accessed on 14 July 2020).
22. World Health Organization Home Page. Available online: https://www.who.int/news-room/fact-sheets/detail/leishmaniasis (accessed on 14 July 2020).
23. Croft, S. L.; Sundar, S.; Fairlamb, A. H. Drug resistance in leishmaniasis. *Clin. Microbiol. Rev.* **2006,** *19* (1), 111-126.
24. Field, M. C.; Horn, D.; Fairlamb, A. H.; Ferguson, M. A. J.; Gray, D. W.; Read, K. D.; De Rycker, M.; Torrie, L. S.; Wyatt, P. G.; Wyllie, S.; Gilbert, I. H. Anti-trypanosomatid drug discovery: an ongoing challenge and a continuing need. *Nat. Rev. Microbiol*. **2017,** *15* (4), 217-231.
25. Pérez-Molina, J. A.; Molina, I. Chagas disease. *The Lancet* **2018,** *391* (10115), 82-94.
26. World Health Organization Home Page. Available online: https://www.who.int/chagas/disease/en/ (accessed on 14 July 2020).
27. Chatelain, E. Chagas disease research and development: Is there light at the end of the tunnel? *Comput. Struct. Biotechnol. J.* **2016,** *15*, 98-103.
28. Tarleton, R. L. Chagas Disease: A Solvable Problem, Ignored. *Trends. Mol. Med.* **2016,** *22* (10), 835-838.
29. Gulcan, H. O.; Unlu, S.; Esiringu, İ.; Ercetin, T.; Sahin, Y.; Oz, D.; Sahin, M. F. Design, synthesis and biological evaluation of novel 6H-benzo[c]chromen-6-one, and 7,8,9,10-tetrahydro-benzo[c]chromen-6-one derivatives as potential cholinesterase inhibitors. *Bioorg. Med. Chem.* **2014,** *22* (19), 5141-5154.
30. Sun, W.; Cama, L. D.; Birzin, E. T.; Warrier, S.; Locco, L.; Mosley, R.; Hammond, M. L.; Rohrer, S. P. 6H-Benzo[c]chromen-6-one derivatives as selective ERβ agonists. *Bioorg, Med. Chem. Lett*. **2006,** *16* (6), 1468-1472.
31. Appendino, G.; Gibbons, S.; Giana, A.; Pagani, A.; Grassi, G.; Stavri, M.; Smith, E.; Rahman, M. M. Antibacterial Cannabinoids from Cannabis sativa: A Structure−Activity Study. *J. Nat. Prod*. **2008,** *71* (8), 1427-1430.
32. Kaplan, B. L. F.; Rockwell, C. E.; Kaminski, N. E. Evidence for Cannabinoid Receptor-Dependent and -Independent Mechanisms of Action in Leukocytes. *J. Pharmacol. Exp. Ther*. **2003,** *306* (3), 1077.
33. Munson, A. E.; Harris, L. S.; Friedman, M. A.; Dewey, W. L.; Carchman, R. A. Antineoplastic Activity of Cannabinoids2. *JNCI: J. Natl. Cancer Inst.* **1975,** *55* (3), 597-602.
34. Khanolkar, A. D.; Lu, D.; Ibrahim, M.; Duclos, J. R. I.; Thakur, G. A.; Malan, J. T. P.; Porreca, F.; Veerappan, V.; Tian, X.; George, C.; Parrish, D. A.; Papahatjis, D. P.; Makriyannis, A. Cannabilactones: A Novel Class of CB2 Selective Agonists with Peripheral Analgesic Activity. *J. Med. Chem.* **2007,** *50* (26), 6493-6500.

35. Munro, S.; Thomas, K. L.; Abu-Shaar, M. Molecular characterization of a peripheral receptor for cannabinoids. *Nature* **1993,** *365* (6441), 61-65.
36. Thakur, G. A.; Bajaj, S.; Paronis, C.; Peng, Y.; Bowman, A. L.; Barak, L. S.; Caron, M. G.; Parrish, D.; Deschamps, J. R.; Makriyannis, A. Novel Adamantyl Cannabinoids as CB1 Receptor Probes. *J Med Chem.* **2013,** *56* (10), 3904-3921.
37. Husni, A. S.; McCurdy, C. R.; Radwan, M. M.; Ahmed, S. A.; Slade, D.; Ross, S. A.; ElSohly, M. A.; Cutler, S. J. Evaluation of Phytocannabinoids from High Potency Cannabis sativa using In Vitro Bioassays to Determine Structure-Activity Relationships for Cannabinoid Receptor 1 and Cannabinoid Receptor 2. *Med. Chem. Res.* **2014,** *23* (9), 4295-4300.
38. Mahadevan, A.; Siegel, C.; Martin, B. R.; Abood, M. E.; Beletskaya, I.; Razdan, R. K. Novel Cannabinol Probes for CB1 and CB2 Cannabinoid Receptors. *J Med Chem.* **2000,** *43* (20), 3778-3785.
39. Wilkinson, J. D.; Williamson, E. M. Cannabinoids inhibit human keratinocyte proliferation through a non-CB1/CB2 mechanism and have a potential therapeutic value in the treatment of psoriasis. *J. Dermatol. Sci.* **2007,** 45 (2), 87-92.
40. Zygmunt, P. M.; Andersson, D. A.; Hogestatt, E. D. Delta 9-tetrahydrocannabinol and cannabinol activate capsaicin-sensitive sensory nerves via a CB1 and CB2 cannabinoid receptor-independent mechanism. *J Neurosci.* **2002,** 22 (11), 4720-4727.
41. Pertwee, R. G. Novel Pharmacological Targets for Cannabinoids. *Curr. Neuropharmacol.* **2004,** 2 (1), 9-29.
42. Killander, D.; Sterner, O. Synthesis of the Bioactive Benzochromenes Pulchrol and Pulchral, Metabolites of *Bourreria pulchra*. *Eur. J. Org. Chem.* **2014**, *2014* (8), 1594-1596.
43. Killander, D.; Sterner, O. Reagent-Controlled Cyclization–Deprotection Reaction to Yield either Fluorenes or Benzochromenes. *Eur. J. Org. Chem.* **2014**, *2014* (29), 6507-6512.
44. Terrazas, P.; Salamanca, E.; Dávila, M.; Manner, S.; Giménez, A.; Sterner, O. SAR:s for the Antiparasitic Plant Metabolite Pulchrol. 1. The Benzyl Alcohol Functionality. *Molecules*. **2020**, 25, 3058.
45. Terrazas, P.; Salamanca, E.; Dávila, M.; Manner, S.; Giménez, A.; Sterner, O. SAR:s for the Antiparasitic Plant Metabolite Pulchrol. 2. B- and C-ring substituents. *In press, Molecules*.
46. Caprioglio, D.; Mattoteia, D.; Minassi, A.; Pollastro, F.; Lopatriello, A.; Muňoz, E.; Taglialatela-Scafati, O.; Appendino, G. One-Pot Total Synthesis of Cannabinol via Iodine-Mediated Deconstructive Annulation. *Org. Lett.* **2019,** 21 (15), 6122-6125.
47. Bilbao-Ramos, P.; Dea-Ayuela, M. A.; Cardenas-Alegría, O. Leishmaniasis in the major endemic region of Plurinational State of Bolivia: Species identification, phylogeography and drug susceptibility implications. *Acta Trop.* **2017**, *176*, 150-161
48. Williams, C.; Espinosa, O.A.; Montenegro, H. Hydrosoluble formazan XTT: Its application to natural products drug discovery for *Leishmania*. *J. Microbiol. Methods*. **2003**, *55*, 813-816.
49. Campos-Buzzi, F.; Fracasso, M.; Clase, B. K.; Ticona, J.C.; Gimenez, A.; Cechinel-Filho, V. Evaluation of antinociceptive effects of *Galipea longiflora* alkaloid extract and major alkaloid 2-fenilquinoline. *Methods Find. Exp. Clin. Pharmacol.* **2010**. *32*, 707-711
50. Muelas-Serrano, S.; Nogal-Ruiz, J.; Gomez-Barrio, A. Setting of a colorimetric method to determine the viability of *Trypanosoma cruzi* epimastigotes. *Parasitol Res*, **2000**, *86*, 999-1002.

Paper IV

SARs for the antiparasitic plant metabolite pulchrol. 4. Pharmacophore design hypothesis and qualitative assessment of predicted pharmacokinetic properties

Paola Terrazas [1,2], Marcelo Dávila [2], Sophie Manner [1], and Olov Sterner[1,*]

1 Department of Chemistry, Center for Analysis and Synthesis, Lund University, 22100 Lund, Sweden; paola.terrazas_villarroel@chem.lu.se (P.T.); sophie.manner@chem.lu.se (S.M.)

2 Centre of Agroindustrial Technology, San Simón University, 3299 Cochabamba, Bolivia; marcelodavila@fcyt.umss.edu.bo (M.D.)

* Correspondence: Olov.Sterner@chem.lu.se; Tel : +46-70-5306649

Abstract.

The natural product pulchrol and its synthetic analogues have been shown to possess antiparasitic activity toward *Trypanosoma cruzi*, *Leishmania braziliensis* and *L. amazonensis*. Those species are responsible for the Chagas disease and Leishmaniasis, respectively. The previously reported SARs based on pulchrol and its analogues lead to the identification of functional groups relevant for their antiparasitic activity. In this study, recently reported antiparasitic data regarding pulchrol and 53 of its analogues, was used in the development of pharmacophore hypotheses for *T. cruzi*, *L. braziliensis* and *L. amazonensis* performed in the Phase module of the Schrödinger software (Schrödinger 2021-1). Pharmacologically relevant descriptors were also predicted by QikProp (Schrödinger 2021-1) and they were qualitatively analyzed. A pharmacophore hypothesis able to predict most of the antiparasitic activity toward *T. cruzi* was developed, although a future validation of the hypotheses will be required. In contrast, the pharmacophore hypotheses developed for the *Leishmania* species could not explain the bioactivity data. The qualitative analysis of the descriptors generated by QikProp showed that most of the ligands in this study may be important for the absorption of orally administered drugs.

Keywords: *Trypanosoma cruzi*, *Leishmania braziliensis*, *Leishmania amazonensis*, pulchrol, SARs, pharmacophore development, pharmacokinetic assessment.

1. Introduction

Natural product pulchrol (**1a**, see Table 3) isolated from the roots of the vegetal specie *Bourreria pulchra*, has shown potential as an antiparasitic agent toward species belonging to the Trypanosomatidae family [1, 2]. Parasites from the genus *Leishmania* and *Trypanosoma* are responsible for leishmaniasis and the Chagas disease, respectively. Leishmaniasis can be contracted as visceral, cutaneous or mucocutaneous leishmaniasis depending on the species responsible for the infection, while Chagas disease is produced only by *Trypanosoma cruzi* [3-6].

Pulchrol and their synthetic derivatives have shown potential activity toward *T. cruzi*, *L. braziliensis* (responsible for cutaneous leishmaniasis) and *L. amazonensis* (responsible for mucocutaneous leishmaniasis) [7-9]. The bioactivity results along with structure activity relationship studies (SARs) contributed to the identification of relevant functional groups for the activity [7-9], however, the molecular target or molecular targets involved remain unknown [10-12].

When the binding site of an active ligand is unknown, a pharmacophore model can be developed to get more information about the functional groups relevant for the activity and their relative positions in the space. Pharmacophores provide a way to visualize a three-dimensional representation of the functional groups, and the excluded volumes around them where stearic clashes may occur [13-15]. Nevertheless, before any binding or clashing, the ligand must reach target.

The current treatment of diseases such as Leishmaniasis and Chagas (mostly found in underdeveloped areas) is unideal, may require parenteral administration, and in some cases hospitalization [16-18]. The development of orally administered drugs may facilitate the access to treatment and prevent the affected from traveling to bigger cities to get the medical care needed.

The evaluation of properties related to the pharmacokinetics of a drug may help predict its capacity to be absorbed, distributed, metabolized and excreted (ADME). Pharmacologically relevant parameters can be predicted using *in silico* methods by several software applications. The drug-likeness of the ligands can be evaluated considering the compliance to guidelines such as the Lipinski's "Rule of 5", which considers the molecular weight, the number of

hydrogen bond acceptors and donors, and the octanol/water partition coefficient [19]; or Jorgensen's "Rule of three", which considers water solubility, the number of likely metabolic reactions, and the apparent Caco-2 permeability [20, 21].

The flexibility of the molecule, the predicted binding to human serum albumin, the blood/brain barrier partition coefficient, among others can also contribute to the analysis of the ADME characteristics of a ligand [22-27].

In this study, pharmacophore hypotheses for *T. cruzi*, *L. braziliensis* and *L. amazonensis* were developed and were evaluated using the Phase module included in the Schrödinger suit software. Pharmacologically relevant descriptors were generated using QikProp (Schrödinger 2021-1) and their oral availability was assessed by the qualitative analysis of the predicted parameters.

2. Materials and methods

2.1. Computational details

All the calculations reported in this study were performed using the Schrödinger suite software (Schrödinger 2021-1). Three-dimensional structures were built in the builder panel found in the Maestro module, and were optimized using the LigPrep application. The development of the pharmacophore hypotheses was performed using the Phase module. Pharmaceutically relevant descriptors were calculated using the QikProp module.

2.2. Data set preparation

A set of 54 compounds were used for the calculations in this investigation. The set included pulchrol (**1a**), and 53 of their analogues (**1a** to **9c**, see Table 3). All the compounds were assayed toward *T. cruzi*, *L. braziliensis* and *L. amazonensis*, and their antiparasitic activity data were reported previously as the half maximal inhibitory concentration (IC_{50}) [7 - 9]. For developing the pharmacophore hypothesis, the IC_{50} values were transformed into molar units and then into pIC_{50} values using the equation below.

$$pIC_{50} = -\log10[IC_{50}] \quad \text{Eq. 1}$$

2.3.Structure preparation

The structures were built using the 3D builder menu in Maestro, and were prepared in the LigPrep application. The OPLS3e force field was used to optimize the structures, and possible ionization and tautomerization states were generated with Epic at a target pH = 7 ± 2. Last of all, the chiralities of the ligands were determined from their 3D structures.

2.4. Pharmacophore hypothesis development

The Phase module was used for developing the pharmacophore hypotheses. The optimized structures were imported from the project table to the "Develop pharmacophore model" panel. The pharmacophore model was created using multiple ligands, which were considered active if their IC_{50} values were inferior to that of pulchrol (**1a**, see Table 3) and inactive if they were superior.

The pharmacophore method was set to find the best alignment and common pharmacophoric features among the ligands after the generation of their conformers. The common pharmacophore was developed using a tree-based partitioning algorithm, which required at least 50% of the actives to match the hypotheses. Between 5 to 7 pharmacophore features (but preferably 5) were included: a minimum of 2 hydrogen bond acceptor (HBA) features with a tolerance of 1.3 Å, and a minimum of 3 hydrophobic features with a tolerance of 1.0 Å. Common features for all ligands (active and inactive) were excluded from the hypotheses. The hypothesis difference criterion was set at 0.5, and 10 hypotheses were calculated for each feature were. The pharmacophore models generated were ranked according to the PhaseHypo score. Excluded volume shells were created from active and inactive ligands, and at least one inactive were required to experience a clash, the minimum distance between the active surface and the shell was set at 1.0 Å, and the excluded volume sphere radii were also set at 1.0 Å. Finally, several descriptors for each ligand were calculated using QikProp in the normal mode.

3. Results and discussion

3.1. Development of pharmacophore hypotheses

The natural benzo[*c*]chromene pulchrol has been found to be active toward parasites from the Trypanosomatidae family, particularly toward *T. cruzi* (IC_{50} = 18.5 μM), and moderately toward *L. braziliensis* (IC_{50} = 59.19 μM) and *L. amazonensis* (IC_{50} = 77.68 μM) [2]. Earlier, a

series of congeneric pulchrol analogues were synthesized and their biological activities were measured toward *T. cruzi* epimastigotes, and *L. braziliensis* and *L. amazonensis* promastigotes. Structure activity relationship studies (SARs) were conducted, and the results showed the effect that modifications in the A-, B- and C-rings produce in the antiparasitic activity [7 - 9].

Bioactivity data from 53 pulchrol analogues (**1b** to **9c**) and the natural product pulchrol (**1a**) were used for generating several ligand-based pharmacophore hypotheses [7 - 9]. The optimized ligands were used to generate 9 to 10 pharmacophore hypotheses for each parasite. All the pharmacophore models had five features, two hydrogen bond acceptors (A) and three hydrophobic (H) sites. The hydrophobic site centered on the B-ring and the aromatic features (A- and C-ring) were excluded from the pharmacophore hypotheses development. Excluded volumes were generated for most of the pharmacophore models showing the regions where steric clashes can occur.

The five best hypotheses were ranked based on their PhaseHypo score (See Table 1). The PhaseHypo score is a combination of two other scores calculated by Phase, the survival score and the BEDROC (Boltzmann-Enhanced Discrimination of Receiver Operating Characteristic) score. The PhaseHypo score is calculated as shown in Equation 2.

$$\text{PhaseHypoScore} = W_{BEDROC} \cdot \text{Score}_{BEDROC} + W_{survival} \cdot \text{Score}_{survival} \qquad \text{Eq. 2}$$

Where $W_{BEDROC} = 0.06$ and $W_{survival} = 1$. In turn, the survival score is calculated by combining the vector score, site score, volume score, selectivity score, inactive score and the number of matches (Eq. 3).

$$\text{Score}_{Survival} = W_{Vector} \cdot \text{Score}_{Vector} + W_{Site} \cdot \text{Score}_{Site} + W_{Volume} \cdot \text{Score}_{Volume} + W_{Selectivity} \cdot \text{Score}_{Selectivity} - W_{Inactive} \cdot \text{Score}_{Inactive} + W_{Matches} \cdot \text{Log}_{10}(\text{Number of matches}) \qquad \text{Eq. 3}$$

All the weights in Eq. 3 have a value of 1. The survival score is calculated to rank the models prioritizing those that are not generic, those with good superpositions and those that have most active matches.

The vector, site and volume scores are a measure of how well the ligands are aligned to the hypothesis in terms of directionality, root-mean-deviation of inter-site distances, and volume overlap. The selectivity score estimates if the hypothesis is more likely to be unique to the active ligands and the inactive score estimates how well inactive ligands match the hypothesis. The

BEDROC score measures the extent to which the hypothesis extracts active ligands from a diverse set of 1000 drug-like decoys.

The values calculated for the survival, site, vector, volume, selectivity, inactive, BEDROC and PhaseHypo score along with the number of active ligands that match the 5 best ranked models are shown in Table 1. The models are sorted from highest to lowest PhaseHypo score, and the highest rated hypothesis was selected for further analysis (AAHHH_2 for *T. cruzi*, AAHHH_6 for *L. braziliensis* and AAHHH_ 3 for *L. amazonensis*).

The inter-site distances and angles for AAHHH_2, AAHHH_6, and AAHHH_3 are presented in Table 2. The pharmacophore hypotheses for all parasites share the same pharmacophoric sites. The hydrogen bond acceptor sites are at the benzylic position in the A-ring and at the heterocycle's oxygen (Ring B). The three hydrophobic sites are placed at both C-6 substituent positions and at the C-2 substituent position. Although all models possess the same pharmacophoric features, differences in the spatial distribution of the site points can be observed for the different parasites (See Table 2).

Table 1. Scoring results calculated by Phase

Parasite	Hypothesis	Survival Score	Site Score	Vector Score	Volume Score	Selectivity Score	Num Matched	Inactive Score	BEDROC Score	PhaseHypo Score
T. cruzi	AAHHH_2	5.7257	0.8780	0.9766	0.7985	1.7109	23	2.3271	0.8823	1.226
	AAHHH_1	5.7277	0.8832	0.9846	0.7873	1.7109	23	2.3219	0.8817	1.225
	AAHHH_3	5.7010	0.8715	0.9643	0.8025	1.7010	23	2.3116	0.8829	1.225
	AAHHH_6	5.6795	0.8774	0.9791	0.7657	1.6956	23	2.2873	0.8829	1.224
	AAHHH_9	5.3596	0.6134	0.9642	0.7284	1.6919	23	2.2604	0.8772	1.199
L. Braziliensis	AAHHH_6	5.3686	0.5255	0.9401	0.6824	1.7021	33	2.1358	0.9151	1.237
	AAHHH_2	5.6737	0.7375	0.9436	0.7917	1.6956	32	2.4136	0.8736	1.214
	AAHHH_1	5.7057	0.7693	0.9529	0.7955	1.7109	30	2.2837	0.8695	1.212
	AAHHH_5	5.3773	0.5657	0.8620	0.7251	1.7193	32	2.0598	0.8788	1.201
	AAHHH_4	5.4110	0.5753	0.9270	0.7249	1.6786	32	2.0899	0.8678	1.197
L. Amazonensis	AAHHH_3	5.8139	0.8461	0.9762	0.8136	1.7010	30	2.4369	0.7959	1.145
	AAHHH_1	5.8392	0.8593	0.9822	0.8096	1.7109	30	2.4655	0.7786	1.129
	AAHHH_2	5.8381	0.8533	0.9853	0.8115	1.7109	30	2.4816	0.7782	1.128
	AAHHH_4	5.8035	0.8479	0.9718	0.8057	1.7010	30	2.4186	0.7790	1.127
	AAHHH_8	5.4976	0.5790	0.9771	0.7581	1.7062	30	2.2333	0.7973	1.127

Table 2. Inter-site distances and angles between pharmacophoric sites

Hypothesis for *T. cruzi* AAHHH_2				Hypothesis for *L. Braziliensis* AAHHH_6				Hypothesis for *L. amazonensis* AAHHH_3			
Site 1	**Site 2**		**Distance[a]**	**Site 1**	**Site 2**		**Distance[a]**	**Site 1**	**Site 2**		**Distance[a]**
A1	H5		2.38	A1	H4		2.38	A1	H4		2.39
A1	H6		2.39	A1	H5		2.39	A1	H5		2.38
A1	H7		6.22	A1	H7		5.38	A1	H6		6.22
A1	A3		7.32	A1	A2		6.87	A1	A2		6.91
A3	H5		7.11	A2	H4		7.21	A2	H4		7.28
A3	H6		6.82	A2	H5		7.20	A2	H5		7.08
A3	H7		9.55	A2	H7		8.97	A2	H6		8.62
H7	H5		8.53	H7	H4		7.76	H6	H4		7.48
H7	H6		7.48	H7	H5		6.84	H6	H5		8.53
H5	H6		2.40	H5	H4		2.40	H5	H4		2.40
Site 1	**Site 2**	**Site 3**	**Angle[b]**	**Site 1**	**Site 2**	**Site 3**	**Angle[b]**	**Site 1**	**Site 2**	**Site 3**	**Angle[b]**
H7	A1	A3	89.3	H7	A1	A2	93.4	H6	A1	A2	81.9
H7	A1	H5	164.7	H7	A1	H4	177.6	H6	A1	H4	112.8
H7	A1	H6	112.8	H7	A1	H5	118.2	H6	A1	H5	164.7
H7	A3	A1	40.6	H7	A2	A1	36.8	H6	A2	A1	45.6
H7	A3	H5	59.5	H7	A2	H4	56.0	H6	A2	H4	55.3
H7	A3	H6	51.1	H7	A2	H5	48.6	H6	A2	H5	65.0
A3	H7	A1	50.0	A1	H7	H5	17.9	A2	H6	A1	52.5
A3	H7	H5	45.9	H5	H7	A2	52.1	A2	H6	H4	53.2
A3	H7	H6	45.2	H5	H7	H4	17.5	A2	H6	H5	48.7
A1	H6	H5	59.2	A1	H5	H7	43.9	A2	H5	A1	76.2
H5	H6	A3	86.9	H7	H5	A2	79.4	A2	H5	H4	85.3
H5	H6	H7	108.2	H7	H5	H4	103.3	A2	H5	H6	66.3
A1	H5	A3	85.7	A1	H4	H5	60.1	H5	H4	A1	59.5
A1	H5	H6	60.1	H5	H4	A2	80.2	H5	H4	A2	75.6
A1	H5	H7	11.1	H5	H4	H7	59.1	H5	H4	H6	108.2

[a] Distance is measure in Å, [b] Angles are measure in degrees

The antiparasitic activity for the ligands, and their role and fitness score in models AAHHH_2, AAHHH_6 and AAHHH_3 are presented in Table 3. The antiparasitic activity is measured as IC_{50} values, which varied between 3.4 μM to 170.3 μM for *T. cruzi*, 5.7 μM and 311.6 μM for *L. braziliensis*, and 6.9 μM and 236.5 μM for *L. amazonensis*. The role of each ligand was determined in relation to the antiparasitic activity of pulchrol, they were considered active if more potent than pulchrol and inactive if less potent than pulchrol. The fitness score was calculated by Phase to measure how well the ligands align to the pharmacophore hypothesis.

Table3. Antiparasitic activity, role and fitness score

Molecule	Structure	TC			LB			LA		
		Activity[a]	Role	Fitness	Activity[a]	Role	Fitness	Activity[a]	Role	Fitness
1a		18.50	active	2.6122	59.19	active	2.3921	77.68	active	2.8274
1b		51.11	inactive	2.3511	69.59	inactive	1.4356	85.32	inactive	2.4932
1c		38.09	inactive	2.3783	17.07	active	1.3484	34.98	None	*
1d		24.62	inactive	2.8315	49.23	active	2.3798	56.27	Active	3.0000
1e		12.80	active	2.9266	35.21	active	2.3330	35.21	Active	2.8982
1f		9.08	active	2.8237	127.94	inactive	2.2653	28.37	Active	2.8126
1g		70.64	inactive	2.3624	83.49	inactive	2.1981	67.75	None	*
1h		15.36	None	*	25.81	active	0.9075	15.36	None	*
1i		5.89	None	*	15.91	active	0.6191	17.67	None	*
2a		14.41	active	2.9512	28.75	active	2.3623	26.89	active	2.9549
2b		8.81	active	2.9518	17.57	active	2.3152	26.73	active	2.8921
2c		6.49	active	2.9481	17.44	active	2.2927	20.45	active	2.8627
2d		16.16	None	3.0000	57.81	active	2.3170	79.31	inactive	2.8916
2e		4.23	active	2.7896	13.06	active	2.2944	14.53	active	2.8032
2f		5.70	active	2.8770	19.95	active	2.2716	19.54	active	2.5093
2g	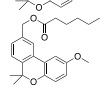	22.80	inactive	2.8537	27.68	active	2.2765	42.34	active	2.7774
2h	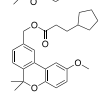	8.36	active	2.5886	122.38	inactive	2.2158	30.92	active	2.7433

2i	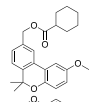	13.14	active	2.6695	24.31	active	2.2505	40.48	active	2.7955
2j		7.40	active	2.9401	5.70	active	2.3034	6.94	active	2.9219
2k		3.84	active	2.9057	12.76	active	2.2247	12.76	active	2.8049
2l	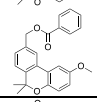	5.88	active	2.8945	21.04	active	2.2408	21.90	active	2.7818
3a		24.23	inactive	2.5657	24.23	active	2.2909	29.82	active	2.6763
3b		21.25	inactive	2.5572	28.33	active	2.2904	43.21	active	2.6654
3c		56.28	inactive	2.3696	65.07	inactive	2.2465	198.73	inactive	2.4836
3d		31.84	inactive	2.5538	18.44	active	2.2902	58.99	active	2.6456
3e		134.47	inactive	2.6114	144.71	inactive	2.3226	120.71	inactive	2.5716
4		33.42	inactive	2.5912	51.98	active	2.2660	51.98	active	2.6445
5a		66.04	inactive	2.0377	248.07	inactive	1.7884	132.08	inactive	2.1576
5b		35.90	inactive	2.2431	156.07	inactive	1.8517	156.07	inactive	2.5056
5c		67.11	inactive	2.3732	128.76	inactive	1.8321	71.79	None	*
5d		125.84	inactive	2.2288	70.79	inactive	1.7638	44.04	None	*
5e		170.28	inactive	2.2326	117.98	inactive	1.8271	80.62	inactive	2.3465
5f		36.99	inactive	2.2572	45.13	None	*	70.28	None	*
5g		51.79	inactive	2.1936	45.87	None	*	71.39	None	*
5h		10.39	active	2.4039	46.92	active	2.2583	36.87	active	2.5782
5i	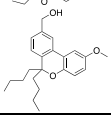	22.85	inactive	2.0281	29.34	active	1.7848	25.39	None	*

6a	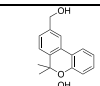	50.77	inactive	2.2084	74.91	inactive	2.4529	91.55	inactive	2.3369
6b		92.48	inactive	2.1944	48.09	active	1.8319	179.78	inactive	1.9887
6c		88.41	inactive	2.5229	37.36	active	2.5700	66.59	active	2.4695
6d	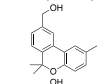	31.46	inactive	2.3457	39.32	active	2.4246	64.88	active	2.4895
6e	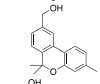	33.03	inactive	2.1414	40.11	active	2.7472	51.90	active	2.1577
6f	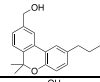	6.44	active	2.1978	16.43	None	*	16.75	active	2.6496
7a	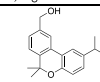	12.39	active	2.5270	18.06	Active	2.4436	15.58	active	2.6377
7b	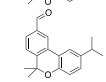	10.70	active	2.5140	12.13	None	*	11.41	active	2.4784
7c	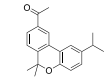	3.40	active	2.5006	8.83	active	2.1406	9.51	active	2.4704
7d	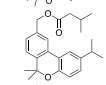	10.91	active	2.6385	272.85	inactive	2.2343	25.92	active	2.4716
7e	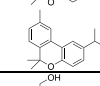	23.65	inactive	2.2265	49.18	None	*	49.55	None	*
8a	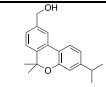	14.17	active	2.3008	19.12	active	3.0000	21.25	active	2.2945
8b	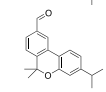	7.13	active	2.0808	17.83	active	2.7757	17.83	active	2.3260
8c	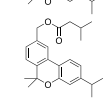	13.64	active	2.3253	63.30	inactive	2.8152	43.66	active	2.2253
8d	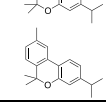	50.30	inactive	2.1138	311.58	inactive	2.5318	236.50	inactive	2.2032
9a	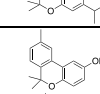	54.93	inactive	1.4595	30.38	active	1.4232	33.29	None	*
9b	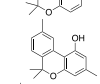	5.90	None	*	15.73	None	*	21.23	None	*
9c	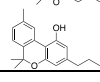	7.41	None	*	10.31	None	*	14.17	None	*

[a] Activity is measured in μM, * Ligands which did not align to the model

3.1.1. Pharmacophore hypothesis developed for T. cruzi

Ten pharmacophore hypotheses were generated, those with the five highest Phase Hypo scores are shown in Table 1, the hypothesis AAHHH_2 was ranked as the best aligned model. From the 54 ligands (27 active and 27 inactive), 50 aligned with AAHHH_2. The pharmacophore model with excluded volumes generated nearby C-6, and close to the hydrogen acceptor sites can be observed in Figure 1. The fitness scores presented in Table 3 as a measure of how well the ligands are aligned to AAHHH_2.

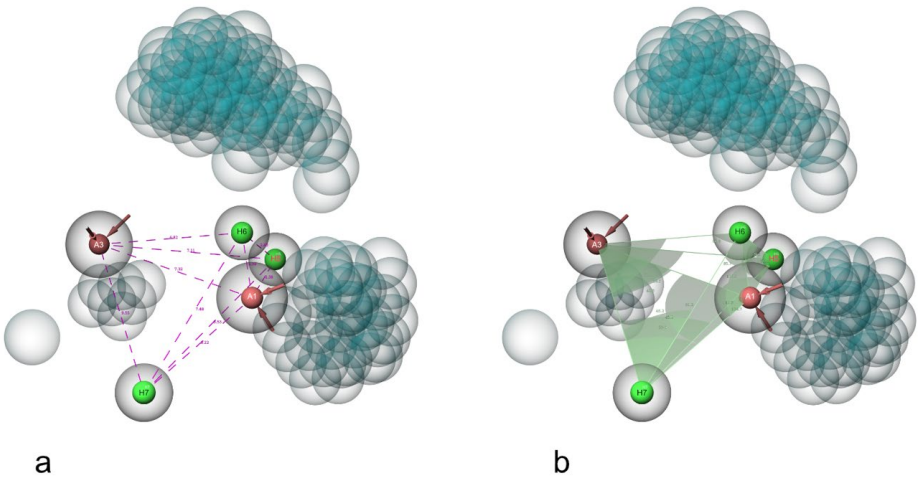

Figure 1. Pharmacophore hypothesis for *T. cruzi* (AAHHH_2). a) inter-site distances, b) inter-site angles.

The highest fitness score was calculated for ester **2d** (fitness score = 3), defined by Phase as the reference ligand. On the other hand, active ligands **9b** and **9c** (cannabinol) did not align with the model, and inactive analogue **9a** showed the lowest fitness score (fitness score = 1. 4595). Most of the inactive analogues showed low fitness scores, for instance neither **5a**, with no hydrophobic features to align with sites H5 and H6, nor **5i**, which appear to clash with the excluded volumes, align well with the model. The only compound from the **5-**series to show a good alignment was **5h**, substituted with two ethyl groups at C-6. Compounds missing other pharmacophoric features also showed low fitness scores, for instance, analogues **6a** and **6b** showed poor overlap with the hydrophobic site H7 (C-ring). Similarly, analogues without HBA in the A-ring showed low fitness scores. The alignment of inactive ligands **1b**, **5a**, **5c**, **5e**, and **6b** is shown in Figure 2.

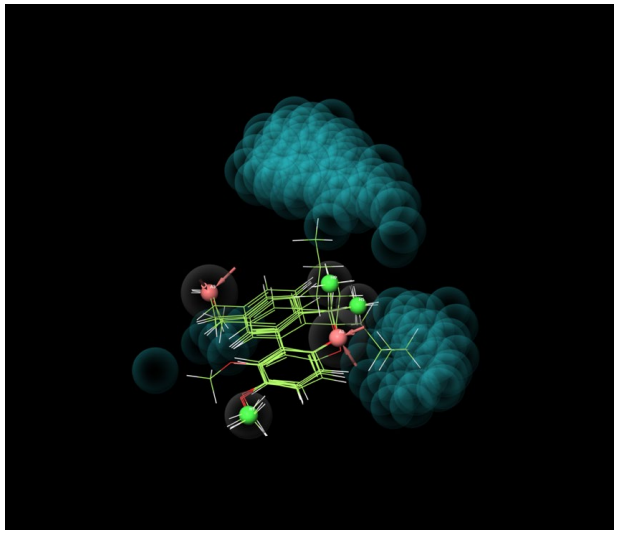

Figure 2. Inactive ligands **1b**, **5a**, **5c**, **5e**, and **6b** aligned to AAHHH_2

The best alignments were shown by the pulchrol esters (**2**-series) and the ethers **1d**, **1e**, and **1f**; but analogue **1d** was not active. The active ligands from the **7**-series had moderately good fitness scores, while the only inactive ligand from the **7**-series fit the model poorly. In contrast, the active amines **1h** and **1i** did not align well with the model. The alignment of active ligands **1a** (pulchrol), **2e**, **5h**, **6f**, and **7c** is shown in Figure 3.

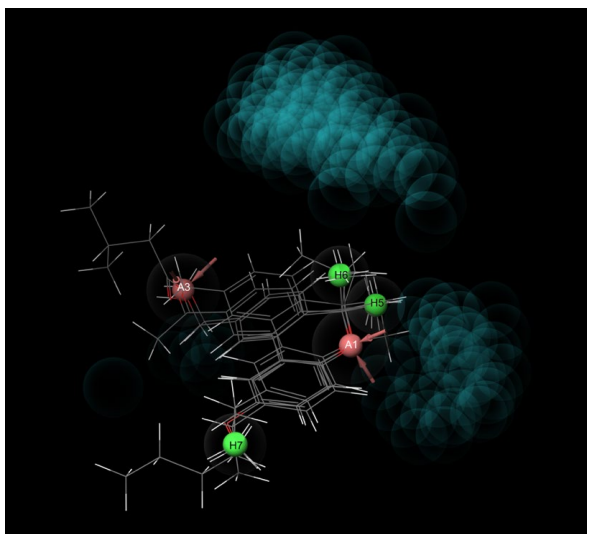

Figure 3. Alignment of the active ligands **1a** (pulchrol), **2e**, **5h**, **6f** and **7c** to AAHHH_2.

3.1.2. Pharmacophore hypothesis developed for L. braziliensis

Nine pharmacophore hypotheses were generated for *L. braziliensis*. The five best Phase Hypo score models are shown in Table 1 and the best ranked hypothesis is AAHHH_6. From the 54 ligands under study (38 active and 16 inactive), 47 aligned with AAHHH_6. The model and the excluded volumes were generated mainly around site A2 (A-ring) as shown in Figure 4.

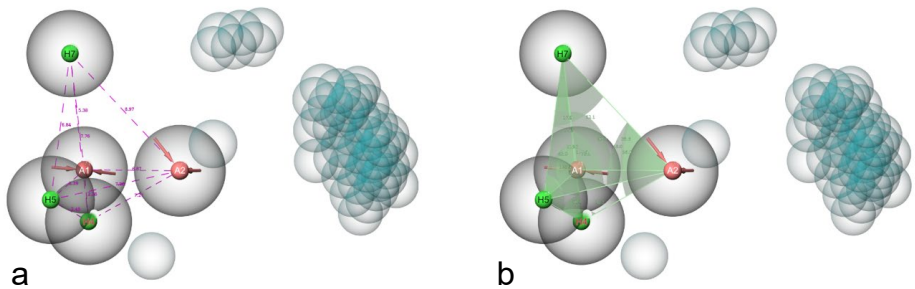

Figure 4. Pharmacophore hypothesis for *L. braziliensis* (AAHHH_6). a) inter-site distances, b) inter-site angles.

The ligand with the best fitness score (Fitness score = 3) was analogue **8a**, substituted with an isopropyl group at C-3 and a benzylic alcohol in the A-ring. In contrast to the model obtained for *T. cruzi*, the highest ranked model for *L. braziliensis* aligned better with ligands that possess substituents at position 3 in the C-ring (**8**-series). The presence of a HBA in the A-ring appears to be more relevant for *L. braziliensis* than was for *T. cruzi*, for instance, analogues **1b**, **1c**, and **9a**, which lack a HBA in A-ring showed low fitting scores. Having said that analogue **1c** and **9a** were active toward *L. braziliensis* and were expected to have a better alignment with the pharmacophore model. In a similar vein, inactive ether **1f** fit the model moderately well, whereas no alignment was expected.

Among the analogues with transformation in the A-ring, none of the protonated amines (**1g** to **1i**) were represented by the pharmacophore model, while the esters (most of them active) showed a moderately good fitting. However, the inactive ester **2h**, should not have fit the model, possibly due to clashing. The analogues with modifications in the B-ring seemed to agree better with the model. However, the most potent ligand from the **5**-series did not align with the model. In contrast to the model obtained for *T. cruzi*, the model for *L. braziliensis* described better the

analogues with substituents at C-3 rather than C-2 in the C-ring. Generally, the pharmacophore model developed for *L. braziliensis* did not manage to clearly distinguish between active and inactive ligands.

Active ligands **2e**, **2i**, **5i** and **7c** alignment to model AAHHH_6 can be observed in Figure 5, and Figure 6 shows the alignment of the inactive ligands **1g**, **3c**, **5a**, **6a** and **8d**.

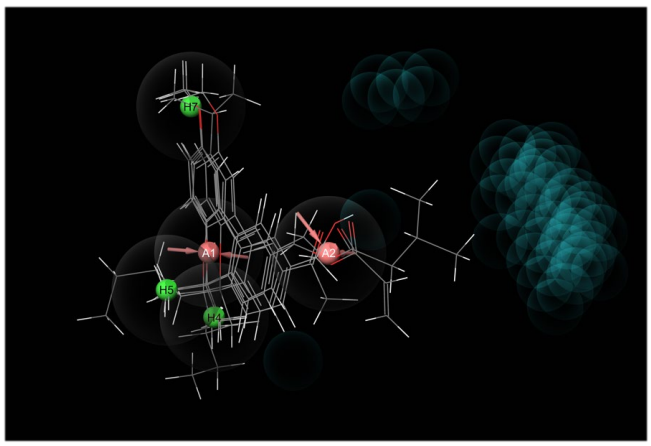

Figure 5. Alignment of active ligands **2e**, **2i**, **5i** and **7c** to model AAHHH_6

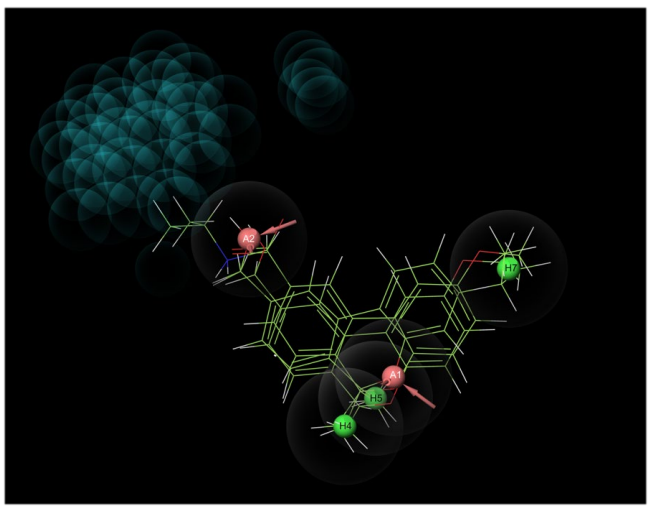

Figure 6. Alignment of inactive ligands **1g**, **3c**, **5a**, **6a** and **8d** to model AAHHH_6

3.1.3. Pharmacophore hypothesis developed for L. amazonensis

As for *L. braziliensis*, nine pharmacophore hypotheses were generated by Phase, the five best ranked hypotheses are shown in Table 1, and the highest Phase Hypo score value was shown by model AAHHH_3. For *L. amazonensis*, 43 ligands were more active than pulchrol and 11 less potent, and just 41 were aligned to the pharmacophore model AAHHH_3 (See Figure 8). As Figure 7 shows, Phase did not generate excluded volumes for AAHHH_3.

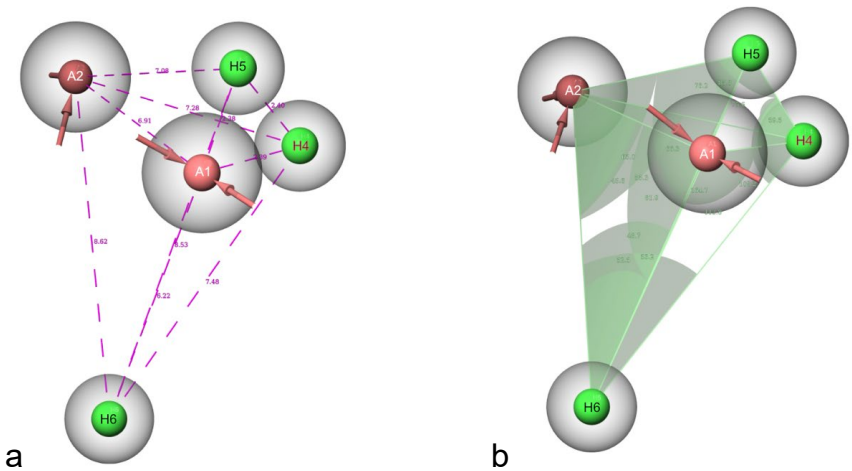

Figure 7. Pharmacophore hypothesis for *L. braziliensis* (AAHHH_6). a) inter-site distances, b) inter-site angles.

Similar to what was observed in the pharmacophore model generated for *L. braziliensis*, the analogues with no HBA substituents in the A-ring aligned poorly to model AAHHH_6. Some analogues with variations in the B-ring did not fit the model either (**5c**, **5d**, **5f**, **5g**, and **5i**). The lowest fitting scored were shown by **5a**, **6b**, **6e**, **8c**, **8d**, but analogues **8c** and **6e** were active and were expected to fit into the model. The best aligned ligands were pulchrol (**1a**), ethers **1d** and **1f**, and most of the esters from the **2**-series. Similar to the model developed for *L. braziliensis*, the best ranked model obtained for *L. amazonensis* doesn't seem to accurately differentiate between actives and inactives, for instance, the inactive analogues **1b**, **3c**, **3e,** and **5b** fit the model moderately well, while active analogues **6e**, **8a**, **8b,** and **8c** showed low fitness score values.

3.2. Qualitative analysis of predicted pharmacologically-relevant descriptors

The pharmacokinetic properties of pulchrol derivatives **1a** to **9c** were analyzed qualitatively using the parameters calculated by QikProp (Schrödinger, 2021-1).

A set containing 51 descriptors with pharmacokinetic importance was obtained after the calculations were performed in QikProp's normal mode. Descriptors with values that vary between ligands, and descriptors contributing to the assessment of oral absorption efficacy are discussed below. A description of the parameters and their recommended range values are presented in Table 4 [20, 21].

Table 4. QikProp descriptors

Descriptor	**Description**	**Range** [a]
#star [b]	Number of descriptor values that fall outside the 95% range of similar values for known drugs. A large number of stars suggest that a molecule is less drug-like than molecules with few stars.	0 - 5
SASA	Total solvent accessible surface area ($Å^2$) using a probe with 1.4 Å radius	300 - 1000
PSA	Van der Waals surface area ($Å^2$)	7 to 200
QPpolarz	Predicted polarizability ($Å^3$)	13 - 70
Lipinski's rule of 5	Number of violations of Lipinski's rule of five (Lipinski)	Maximum 4
MW	Molecular weight	130 - 725
DonorHB	Estimated number of hydrogen bonds that would be donated by the solute to water molecules in aqueous solutions.	0 - 6
AcceptorHB	Estimated number of hydrogen bonds that would be accepted by the solute to water molecules in aqueous solutions.	2 - 20
QPlogPo/w	Predicted octanol/water partition coefficient	-2 - 6.5
Rule of three	Number of violations of Jorgensen's rule of three.	Maximum 3
QPlogS	Predicted aqueous solubility	-6.5 - 0.5
QPPCaco	Predicted apparent Caco-2 cell permeability (nm/s) for non-active transport.	< 25 poor; > 500 great

#metabol	Number of likely metabolic reactions	1 - 8
#rotor	Number of non-trivial (not CX3), non-hindered (not alkene, amide, small ring) rotatable bonds.	0 - 15
Human Oral Absorption	Predicted qualitative human oral absorption. [c]	1 = low, 2 = medium, 3 = high
QPlogKhsa	Prediction of binding to human serum albumin	-1.5 – 1-5
QPlogBB	Predicted brain/blood partition coefficient for orally delivered drugs.	-3.0 - 1.2
CNS	Predicted central nervous activity on a -2 (inactive) to +2 (active) scale.	-2 - +2
QPlogHERG	Predicted IC_{50} value for blockage of HERG K^+ channels	Concern below -5

[a] Recommended value for 95% of known drugs.

[b] Descriptors included in #stars: Molecular weight, dipole moment, ionization potential, electron affinity, total solvent accessible area; hydrophobic, hydrophilic, π and weakly polar components of the SASA, polar surface area , total solvent accessible volume, number or rotatable bonds, hydrogen bond donors, hydrogen bond acceptors, globularity, polarizability, hexadecane/gas partition coefficient, octanol/gas partition coefficient, octanol/water partition coefficient, aqueous solubility, binding to human serum albumin, brain/blood partition coefficient, number of likely metabolic reactions.

A descriptor defined as "#star" was generated by QikProp as an overall ADME score that considers 29 other descriptors (See Table 4). The #star parameter can be used to qualify the pharmacokinetic quality of the ligands. The greater the number of #stars, the less drug-like a compound is predicted to be. A distribution plot of the #star descriptor (see Figure 8) shows that most of the compounds have #star values equal to 0 or 1. Just 8 ligands have #star > 1, indicating that they may not be able to be orally absorbed, among those ligands, we found hydrophobic compounds with methyl substituents at position 9 in the A-ring (**1b**, **7e**, **8c**, **9a**, and **9b**), chlorinated analogue **1c**, ester **2h**, and ether **1f**.

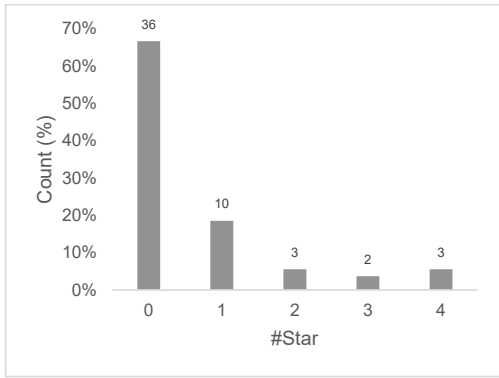

Figure 8. Distribution plot of the #star descriptor

Some properties related to de #star parameter, for instance, the total solvent accessible area (SASA), the total solvent-accessible volume, and the globularity of the compounds showed to be inside the recommended values according to QikProp. Other properties related to the #star descriptor, such as the polar surface are (PSA) and the predicted polarizability (QPpolrz) also showed to be between the recommended ranges (See Table 4).

Another set of parameters used as guidelines to identify orally-absorbed drug candidates are the Lipinski's "Rule of five" (MW < 500 Da, HBD < 5, HBA < 10 and log *P* < 5). According to results generated by QikProp, 70% of the ligands complied with all Lipinski's guidelines, while the other 30% did not meet them [19]. All the ligands had molecular weight (MW) values inferior to 500 Da, less than 5 hydrogen bond donors (HBD) and less than 10 hydrogen bond acceptors (HBA). However, 30% of the compounds showed to have log *P* values above 5 (see Figure 9).

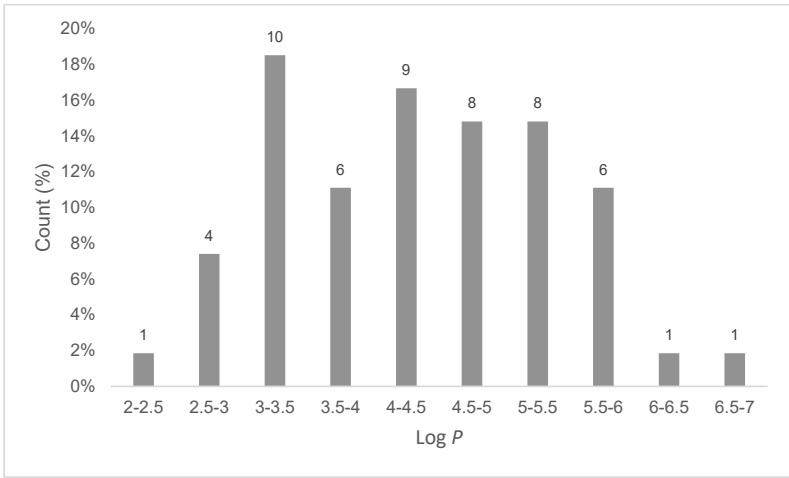

Figure 9. Distribution of log *P* values between the ligands

Relative hydrophilic/hydrophobic properties are crucial for drug's ADME characteristics. Too polar drugs may not be able to cross the cell membranes, bind to plasma protein or be excreted to fast. Too hydrophobic compounds, on the other hand, can get dissolved in fat globules in the gut and not be absorbed in optimal amounts. A log *P* value below 5 may indicate that a favorable hydrophilic/hydrophobic balance exists, as for 70% of the analogues under study (see Figure 11).

The Jorgensen's "Rule of three" is another set of guidelines used to evaluate oral availability considering the predicted aqueous solubility (QPlogS > -5.7), the predicted apparent Caco-2 cell permeability (QPPCaco > 22 nm/s) and the number of likely metabolic reactions (#metab < 7) [20, 21]. The results generated by QikProp showed that 63% of the compounds followed Jorgensen guidelines. All the compounds showed to comply with the expected values of permeability for the Caco-2 cells and all of them showed to likely experience 1 to 3 metabolic reactions. However, 37% of the ligands showed predicted water solubility values below -5.7 (See Figure 11).

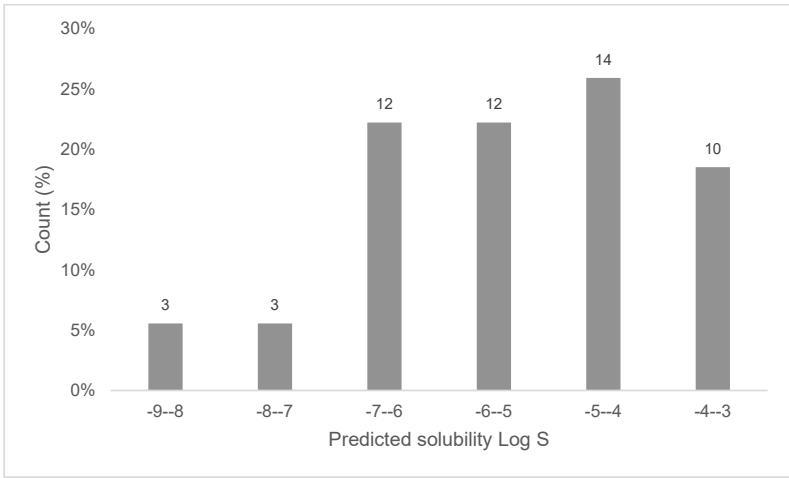

Figure 11. Distribution of the predicted solubility in water.

Another parameter that may affect the absorption is the molecular flexibility. The distribution of the number of non-trivial/non-hindered rotatable bonds (#rotor) is shown in Figure 13.

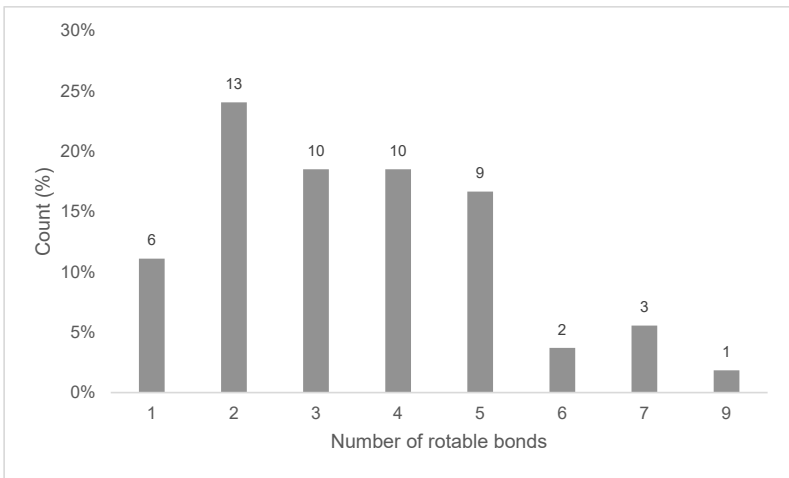

Figure 12. Distribution of rotatable bonds

Molecules with several bonds can lead to a large number of conformations, which can allow them to interact with more than one receptor to produce unwanted biological responses. It can also affect the bioavailability, since molecules with high flexibility are less likely to be orally active. A limit of 7 rotatable bonds is recommended in the literature [13], just four molecules among the 54 pulchrol analogues under study here, had more than 7 rotatable bonds (see Figure

11). The human oral absorption parameter calculated by QikProp also predicted that 72% of our ligands may have high oral absorption, while 28% may have low oral absorption.

The plasma-protein binding was evaluated estimating the binding to human serum albumin (logKhsa), according to the results obtained from QikProp, all the ligands fell in the recommended range, indicating the compounds are likely to circulate freely within the blood stream and hence have access to the target site.

The blood-brain barrier partition coefficient (QPlogBB) expressed in logB/B units was also calculated by QikProp. Figure 12 shows that all ligands are in the recommended range of QPlogBB values. However, according to other authors [26], if QPlogBB ≥ 0.3 then the ligand will penetrate the blood-brain barrier; if 0.3 < QPlogBB < -1 the ligand may still pass the blood-brain barrier; and just if QPlogBB < -1 the ligands will not penetrate the blood-brain barrier.

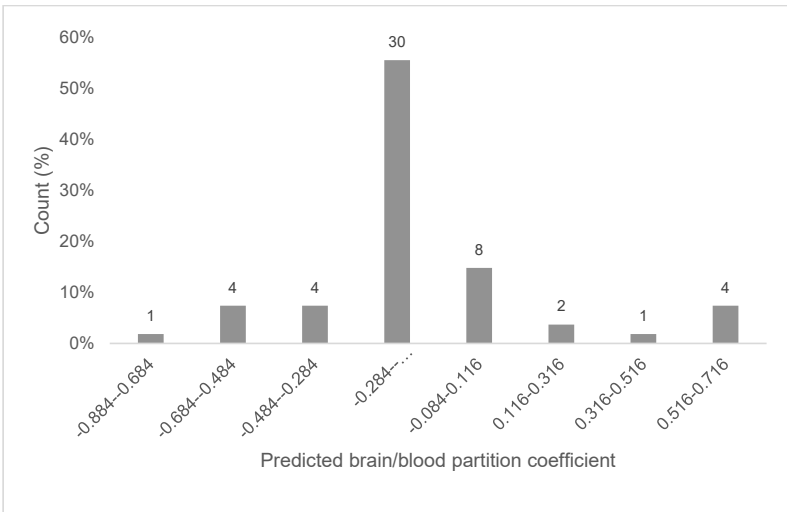

Figure 12. Distribution of the predicted brain/blood partition coefficient

According to the above-mentioned range [26], five analogues will penetrate the brain-blood barrier, while the 49 resting analogues will show less permeability. None of the compounds showed QPlogBB values above. The central nervous system descriptor (CNS) calculated by QikProp predicts the activity in the central nervous system, -2 (inactive) to +2 (active) values were assigned to the ligands. Most of the ligands (80%) had a 0 CNS value, 9 compounds were more likely to be active (CNS > 0) and just 2 to be inactive (CNS < 0).

Finally, the blockage of human ether-a-go-go-related gene potassium (HERG K^+) channel was predicted. The HERG K^+ channels appear to be the target responsible for the cardio-toxicity of a wide range of drugs. Predicted binding affinity to HERG K^+ gives an idea of potential toxicity in the early stages of drug discovery. As it is shown in Figure 13, 70% of the compounds fall on recommended range value for HERG K+ binding.

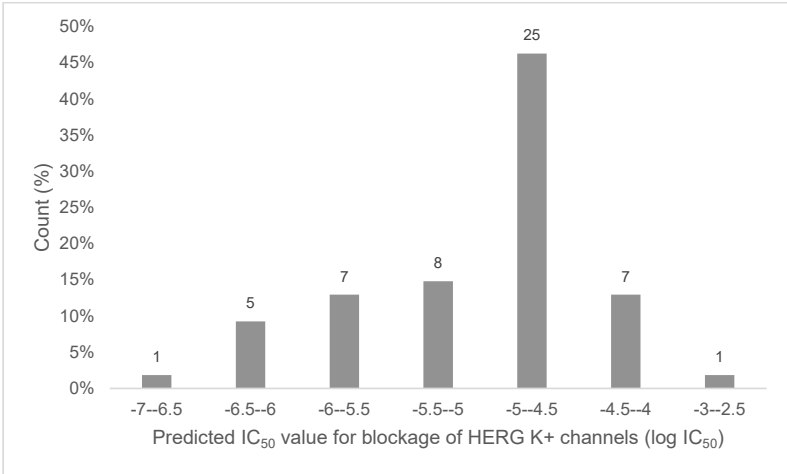

Figure 13. Distribution of the predicted log IC_{50} values for blockage of HERG+ channels

4. Conclusions

A set of pharmacophore hypotheses was developed for each parasite studied in this research (*T. cruzi*, *L. braziliensis* and *L. amazonensis*), and the three best ranked models were evaluated. Additionally, several pharmacologically relevant descriptors were generated and used to qualitatively evaluate the drug-likeness of the 54 pulchrol analogues presented in this study.

Natural compound pulchrol and several synthetic analogues have shown potential activity toward parasites from the family Trypanosomatidae. However, the molecular target to which pulchrol and its analogues bind is unknown. Pharmacophore models were generated in this investigation to visualize the possible surroundings around the ligands and the main pharmacophoric features involved in binding with the active site.

The three best score pharmacophore hypotheses were evaluated, one for each of the parasite. The same pharmacophoric sites were determined for the models, two hydrogen bond acceptor features (one at the benzylic position in the A-ring and the other on heterocycle oxygen in the

B-ring), and three hydrophobic features (one in the C-ring and the other two on the B-ring). However, differences in the inter-site distances and angles between the models were observed, which may indicate that differences exist between the active sites in the different parasites.

The alignment of the ligands to each model was evaluated considering the ligands fitness scores. The model developed for *T. cruzi* seems to explain the activity of the ligands, therefore, further studies are recommended to validate the hypothesis and subsequently develop of 3D-QSAR studies. In contrast, the models developed for the *Leishmania* species could not distinguish between active and inactive ligands, to develop a pharmacophore capable of aligning with the active ligands, a modification in the activity threshold is recommended and the manual addition of excluded volumes to characterize better the surroundings of the molecule, taking into account stearic clashes.

Leishmaniasis and the Chagas disease mainly affect people in tropical and subtropical areas, some of the current treatments are administered parenterally and require supervision or even hospitalization. Many areas in which the above-mentioned diseases are found are underdeveloped and the affected have the need to travel to other cities to be treated. Therefore, orally administered drugs are preferred as treatment.

Several pharmacokinetic-related descriptors were generated for the 54 ligands considered in this study. Most of the molecules complied with the Lipinski's "Rule of five" and the Jorgensen's "Rule of three", but few compounds failed to meet one of the rules for each guideline. The octanol/water partition coefficient and the solubility in water are the properties that were not optimal for some compounds. Most of the ligand outside the recommended values were too hydrophobic, which can negatively affect their absorption. However, a characteristic of the pulchrol scaffold that may result beneficial for absorption is its rigidity, which also reduces the probability of interactions with undesired molecular targets.

Possible binding to plasma-proteins was predicted for human serum albumin and all the ligands fall inside the recommended range of values. The ability of the ligands to penetrate the blood-brain barrier was also predicted and 80% of the ligands showed moderate values for the predicted brain/blood partition coeffect. Most of the compounds showed low binding affinity to the $HERGK^{+}$ channels, however, care should be taken in the design of new analogues and biological assays are recommended to be certain that cardiotoxicity is not a risk.

Overall, more than 80% of the compounds have good pharmacokinetic characteristics for oral administration. However, focus future studies on the least hydrophobic active ligands may prevent issues concerning blood-brain barrier penetration and undesired central nervous system activity.

References

[1] Campos-Ríos, M. G. REVISIÓN DEL GÉNERO Bourreria P. Browne (Boraginaceae) EN MÉXICO. *Polibotánica* **2005**, No.19, 39-103.

[2] Erosa-Rejón, G. J.; Yam-Puc, A.; Chan-Bacab, M. J.; Giménez-Turbax, A.; Salamanca, E.; Peña-Rodríguez, L. M.; Sterner, O. Benzochromenes from the roots of *Bourreria pulchra*. *Phytochem. Lett.* **2010**, *3* (1), 9-12.

[3] World Health Organization Home Page. Chagas disease (American tripanosomiasis). Retrieved from https://www.who.int/chagas/disease/en/ (accessed April 02, 2021).

[4] World Health Organization Home Page. WHO Report on Global Surveillance of Epidemic-prone Infectious Diseases – Leishmaniasis. Retrieved from https://www.who.int/csr/resources/publications/CSR_ISR_2000_1leish/en/ (accessed April 02, 2021).

[5] Pérez-Molina, J. A.; Molina, I. Chagas disease. *The Lancet* **2018,** *391* (10115), 82-94.

[6] Chatelain, E. Chagas disease research and development: Is there light at the end of the tunnel? *Comput. Struct. Biotechnol. J.* **2016,** *15*, 98-103.

[7] Terrazas, P.; Salamanca, E.; Dávila, M.; Manner, S.; Giménez, A.; Sterner, O. SAR:s for the Antiparasitic Plant Metabolite Pulchrol. 1. The Benzyl Alcohol Functionality. *Molecules*. **2020**, 25, 3058.

[8] Terrazas, P.; Salamanca, E.; Dávila, M.; Manner, S.; Giménez, A.; Sterner, O. SAR:s for the Antiparasitic Plant Metabolite Pulchrol. 2. B- and C-ring substituents. *In press, Molecules*.

[9] Terrazas, P.; Salamanca, E.; Dávila, M.; Manner, S.; Giménez, A.; Sterner, O. SAR:s for the Antiparasitic Plant Metabolite Pulchrol. 3. New substituents in A/B-rings and A/C-rings.. *In manuscript*.

[10] Gilbert, I. H. Drug discovery for neglected diseases: molecular target-based and phenotypic approaches. *J Med Chem.* **2013,** *56* (20), 7719-7726.

[11] Reguera, R. M.; Calvo-Álvarez, E.; Álvarez-Velilla, R.; Balaña-Fouce, R. Target-based vs. phenotypic screenings in Leishmania drug discovery: A marriage of convenience or a dialogue of the deaf? Int. J. Parasitol. Drugs Drug Resist. 2014, 4 (3), 355-357.

[12] Kaye, P.; Scott, P. Leishmaniasis: complexity at the host–pathogen interface. Nat. Rev. Microbiol. 2011, 9 (8), 604-615.

[13] Patrick, G. L. An Introduction to Medicinal Chemistry, 5th ed.; Oxford University Press: Oxford, U.K., **2013**; pp 227-265.

[14] Zheng, W.; Thorne, N.; McKew, J. C. Phenotypic screens as a renewed approach for drug discovery. *Drug Discovery Today*. **2013,** 18 (21), 1067-1073.

[15] Al-Ali, H. The evolution of drug discovery: from phenotypes to targets, and back. *Med. Chem. Commun*. **2016,** 7 (5), 788-798.

[16] Field, M. C.; Horn, D.; Fairlamb, A. H.; Ferguson, M. A. J.; Gray, D. W.; Read, K. D.; De Rycker, M.; Torrie, L. S.; Wyatt, P. G.; Wyllie, S.; Gilbert, I. H. Anti-trypanosomatid drug discovery: an ongoing challenge and a continuing need. *Nat. Rev. Microbiol.* **2017,** *15* (4), 217-231.

[17] Weng, H.-B.; Chen, H.-X.; Wang, M.-W. Innovation in neglected tropical disease drug discovery and development. *Infect Dis Poverty*. **2018,** 7 (1), 67.

[18] Croft, S. L.; Sundar, S.; Fairlamb, A. H. Drug resistance in leishmaniasis. *Clin. Microbiol. Rev.* **2006,** *19* (1), 111-126.

[19] Lipinski, C. A. Lead- and drug-like compounds: the rule-of-five revolution. *Drug Discov. Today*: Technologies. **2004**, 1 (4), 337-341.

[20] Jorgensen, W. L.; Duffy, E. M. Prediction of Drug Solubility from Monte Carlo Simulations. *Bioorg. Med. Chem. Lett*. **2000**, 10, 1155-1158.

[21] Jorgensen, W. L.; Duffy, E. M. Prediction of Drug Solubility from Structure. *Adv. Drug Delivery Rev*. **2002**, 54, 355-366.

[22] Duffy, E. M.; Jorgensen, W. L. Prediction of Properties from Simulations: Free Energies of Solvation in Hexadecane, Octanol, and Water. *J. Am. Chem. Soc*. **2000**, 122, 2878-2888.

[23] Winiwarter, S.; Ridderström, M.; Ungell, A. L.; Andersson, T. B.; Zamora, I. 5.22 - Use of Molecular Descriptors for Absorption, Distribution, Metabolism, and Excretion Predictions. In Comprehensive Medicinal Chemistry II; Taylor, J. B.; Triggle, D. J; Eds. Elsevier: Oxford, U.K., **2007**; pp 531-554.

[24] Colmenarejo, G.; Alvarez-Pedraglio, A.; Lavandera, J.-L. Cheminformatic Models To Predict Binding Affinities to Human Serum Albumin. *J. Med. Chem*. **2001**, 44, 4370-4378.

[25] Luco, J. M. Prediction of the Brain-Blood Distribution of a Large Set of Drugs from Structurally Derived Descriptors Using Partial Least-Squares (PLS) Modeling. *J. Chem.*

Inf. Comput. Sci. **1999**, 39, 396-404.

[26] Kunwittaya, S.; Nantasenamat, C.; Treeratanapiboon, L.; Srisarin, A.; Isarankura-Na-Ayudhya, C.; Prachayasittikul, V. Influence of logBB cut-off on the prediction of blood-brain barrier permeability. *Biomedical and Applied Technology Journal*. **2013**, 16-34.

[27] Potts, R. O.; Guy, R. H. Predicting skin permeability. *Pharm. Res*. **1992**, 9, 663–669.

Kelder J.; Grootenhuis, P. D.;Bayada, D.M.; Delbressine, L.P., Ploemen, J.P. Polar molecular surface as a dominating determinant for oral absorption and brain penetration of drugs. *Pharm. Res*. **1999**, 16, 1514–1519.

Supplementary data

The following tables contain the descriptors calculated by QikProp that were discussed in this study.

Table 4. Descriptors calculated by QikProp part 1

Mol	Structure	#stars	#rotor	CNS	MW	SASA	donorHB	acceptHB	QPpolrz	QPlogPo/w	QPlogS
1a		0	3	0	270.327	523.009	1	3.2	29.804	3.429	-4.174
1b		4	1	1	254.328	510.502	0	1.5	30.208	4.081	-5.676
1c		3	1	1	288.773	533.851	0	1.5	31.941	4.898	-6.146
1d		1	3	0	284.354	552.616	0	3.2	32.188	3.825	-4.667
1e		1	4	0	312.408	621.869	0	3.2	36.58	4.422	-6.393
1f		3	7	0	354.488	716.01	0	3.2	41.892	5.483	-8.273
1g	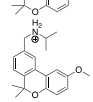	0	4	2	311.423	628.371	1	3	37.092	4.547	-4.759
1h		1	5	2	325.45	662.588	1	3	38.951	4.965	-5.22
1i		0	6	2	339.477	690.642	1	3	40.639	5.294	-5.57
2a		0	3	0	312.365	611.767	0	3.5	35.868	4.25	-5.489
2b		0	4	0	340.418	667.197	0	3.5	39.775	5.147	-6.377
2c		1	4	0	354.445	677.93	0	3.5	41.324	5.413	-6.58
2d		0	5	0	340.418	674.027	0	3.5	39.352	5.112	-6.343
2e		1	5	0	354.445	696.839	0	3.5	41.333	5.48	-6.776
2f		1	5	0	368.472	696.735	0	3.5	42.767	5.726	-6.774
2g		0	7	0	368.472	651.361	0	3.5	39.92	5.409	-5.588

2h		2	7	0	408.536	798.079	0	3.5	47.731	6.681	-8.369
2i	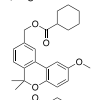	1	4	0	380.483	724.849	0	3.5	44.491	5.897	-7.469
2j		0	4	0	324.376	633.819	0	3.5	37.349	4.616	-5.744
2k		0	4	0	364.397	660.346	0	4	40.937	4.901	-5.985
2l	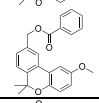	1	4	0	374.435	699.181	0	3.5	44.086	5.684	-6.983
3a		0	2	0	268.312	513.839	0	3.5	29.875	3.061	-3.792
3b		0	2	0	282.338	543.415	0	3.5	31.975	3.576	-4.357
3c		0	2	-1	284.311	521.46	1	3.5	30.395	3.309	-4.326
3d		0	2	0	298.338	571.242	0	3.5	33.71	3.823	-4.884
3e	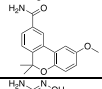	0	2	0	283.326	526.697	2	4	30.772	2.626	-4.156
4	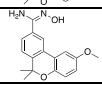	0	5	-1	298.341	546.195	3	4.7	30.384	2.305	-3.578
5a		0	3	0	242.274	468.954	1	3.2	25.651	2.772	-3.22
5b		0	3	0	256.301	495.874	1	3.2	27.762	3.106	-3.694
5c		0	3	0	256.301	495.874	1	3.2	27.762	3.106	-3.694
5d		0	2	0	254.285	486.902	0	3.5	27.84	2.726	-3.286
5e		0	2	0	254.285	486.902	0	3.5	27.84	2.726	-3.286
5f		0	4	0	270.327	514.524	1	3.2	29.053	3.415	-3.861
5g		0	4	0	270.327	515.23	1	3.2	29.043	3.444	-3.873
5h		0	5	0	298.381	564.31	1	3.2	32.129	4.038	-4.587

5i	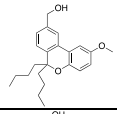	0	9	0	354.488	691.4	1	3.2	39.71	5.645	-6.24
6a		0	2	0	240.301	485.876	1	2.45	27.966	3.321	-3.919
6b		0	3	0	270.327	524.148	1	3.2	30.117	3.477	-4.195
6c		0	3	0	270.327	521.013	1	3.2	29.773	3.426	-4.139
6d		0	2	0	254.328	518.235	1	2.45	29.841	3.634	-4.5
6e		0	2	0	254.328	518.419	1	2.45	29.852	3.636	-4.504
6f	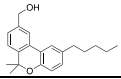	0	6	0	310.435	645.386	1	2.45	36.654	5.159	-6.166
7a		0	3	0	282.382	572.716	1	2.45	33.388	4.306	-5.303
7b		0	2	0	280.366	563.978	0	2.75	33.479	4.025	-5.139
7c		0	2	0	294.393	591.744	0	2.75	35.498	4.532	-5.665
7d		0	5	0	366.499	643.912	0	2.75	41.076	5.765	-6.165
7e		4	1	2	266.382	560.195	0	0.75	33.793	4.971	-7.312
8a		0	3	0	282.382	571.616	1	2.45	33.32	4.327	-5.295
8b		0	2	0	280.366	564.557	0	2.75	33.509	4.03	-5.15
8c		1	5	0	366.499	747.131	0	2.75	44.972	6.459	-8.121
8d		4	1	2	266.382	561.231	0	0.75	33.845	4.984	-7.323
9a		2	1	1	240.301	485.912	1	1.5	28.246	3.657	-4.384
9b		1	1	1	254.328	512.017	1	1.5	29.979	4.062	-4.863
9c	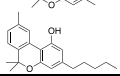	2	5	0	310.435	642.074	1	1.5	36.961	5.597	-6.617

Table 4. Descriptors calculated by QikProp part 2

Mol	Structure	QPlogHERG	QPPCaco	QPlogBB	#metab	QPlogKhsa	PSA	Rule of five	Rule of three	Human oral absorption
1a		-4.64	2961.629	-0.112	2	0.333	38.736	0	0	3
1b		-4.564	9906.038	0.144	2	0.726	15.504	0	0	3
1c		-4.684	9906.038	0.065	2	0.857	15.502	0	1	3
1d		-4.816	9906.038	-0.541	3	0.425	24.228	0	0	3
1e		-5.279	9906.038	-0.395	3	0.751	23.279	0	1	1
1f	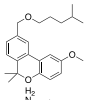	-5.786	9906.038	-0.207	3	1.148	23.173	1	1	1
1g		-6.045	1988.932	0.623	3	0.863	28.997	0	0	3
1h		-6.263	2126.051	0.59	3	0.991	28.634	0	0	3
1i		-6.382	1860.435	0.465	3	1.109	29.855	1	0	3
2a		-5.364	2528.688	-0.24	2	0.612	54.378	0	0	3
2b		-5.583	4107.291	-0.094	3	0.902	50.086	1	1	1
2c		-5.453	4250.4	-0.072	2	1.021	47.482	1	1	1
2d		-5.679	3291.028	-0.266	3	0.875	52.063	1	1	1
2e		-5.754	3797.679	-0.203	3	1.019	50.713	1	1	1
2f		-5.443	3902.786	-0.171	3	1.129	47.874	1	1	1
2g		-4.68	3121.775	-0.345	3	0.946	47.927	1	0	3
2h		-6.236	3229.135	-0.445	3	1.492	52.046	1	1	1

2i	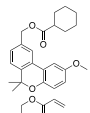	-5.828	3875.897	-0.138	3	1.244	50.219	1	1	1
2j		-5.735	2859.599	-0.255	2	0.689	52.669	0	1	3
2k		-6.218	2697.867	-0.284	3	0.749	61.56	0	1	3
2l	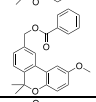	-6.683	3090.242	-0.242	2	1.08	51.076	1	1	1
3a		-4.547	1817.694	-0.242	1	0.173	52.789	0	0	3
3b		-4.723	3144.947	-0.036	1	0.332	44.506	0	0	3
3c		-2.793	252.091	-0.494	1	0.158	64.946	0	0	3
3d		-5.035	2761.584	-0.113	1	0.454	51.895	0	0	3
3e	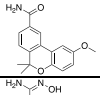	-4.635	870.606	-0.555	2	0.203	68.434	0	0	3
4		-4.797	639.059	-0.884	1	-0.008	74.941	0	0	3
5a		-4.476	2966.165	-0.091	3	0.042	40.063	0	0	3
5b		-4.545	2967.651	-0.1	3	0.19	39.807	0	0	3
5c		-4.545	2967.652	-0.1	3	0.19	39.807	0	0	3
5d		-4.453	1818.418	-0.226	2	0.015	53.853	0	0	3
5e		-4.453	1818.417	-0.226	2	0.015	53.853	0	0	3
5f		-4.464	2968.941	-0.158	3	0.285	39.158	0	0	3
5g		-4.487	3270.305	-0.121	3	0.284	37.839	0	0	3
5h		-4.642	3267.788	-0.2	2	0.508	36.168	0	0	3
5i	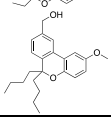	-5.366	3263.224	-0.493	2	1.027	35.7	1	1	1

6a		-4.686	2963.273	-0.036	1	0.311	30.525	0	0	3
6b		-4.656	2969.835	-0.109	2	0.349	35.694	0	0	3
6c		-4.576	2965.884	-0.108	2	0.334	38.706	0	0	3
6d		-4.668	2963.552	-0.054	2	0.472	30.52	0	0	3
6e		-4.67	2963.287	-0.054	2	0.473	30.517	0	0	3
6f	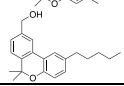	-5.427	3269.985	-0.313	2	0.952	29.185	1	1	3
7a		-4.854	2963.491	-0.136	2	0.731	30.529	0	0	3
7b		-4.779	1817.322	-0.277	1	0.651	44.59	0	0	3
7c		-4.902	3143.054	-0.057	1	0.806	36.314	0	0	3
7d		-4.436	3177.585	-0.206	3	1.234	40.172	1	1	3
7e		-4.786	9906.038	0.635	2	1.203	7.304	0	1	1
8a		-4.842	3269.216	-0.093	2	0.726	29.188	0	0	3
8b		-4.789	1817.919	-0.278	1	0.653	44.569	0	0	3
8c		-5.89	3943.319	-0.202	3	1.499	42.834	1	1	1
8d		-4.805	9906.038	0.635	2	1.206	7.285	0	1	1
9a		-4.509	3007.651	0.03	2	0.523	29.857	0	0	3
9b		-4.441	4288.437	0.164	3	0.673	26.558	0	0	3
9c	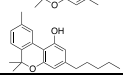	-5.267	4285.355	-0.125	3	1.178	26.557	1	1	1